Protein Phosphatase 6 function and regulation throughout the cell cycle



Josip Ahel

St Edmund Hall

University of Oxford

A thesis submitted for the degree of

Doctor of Philosophy

Trinity term 2018

Abstract

Faithful cell division is a basic requirement for the generation of all living cells. Essential to this task is the correct formation and maintenance of bipolar mitotic spindles, which segregate the duplicated genome in mitosis. This process is dependent on the balanced and concerted activities of Aurora A and PLK1 kinases. Integration of function between these two kinases is partially explained by Aurora A-mediated activation of PLK1. Further regulation is conferred by the heterotrimeric protein phosphatase 6 (PP6), which counteracts Aurora A autoactivation. How the activity of this phosphatase is regulated in space and time remains poorly understood. The results presented here demonstrate that PP6 is functionally stratified into three distinct pools based on the regulatory SAPS subunit, which confers binding-mediated substrate specificity. This property allows only PP6-SAPS2 and PP6-SAPS3 to dephosphorylate Aurora A. Furthermore, SAPS subunits confer unique regulatory properties to the holoenzyme. Uniquely, PLK1 binds to and phosphorylates PP6-SAPS2 in mitosis, inhibiting its activity against Aurora A. The combined action of PP6-SAPS2 and the constitutively active PP6-SAPS3 establishes feedback control between PLK1 and Aurora A activation during mitosis, and during a G2 DNA damage checkpoint. Concordantly, PP6 is important for normal cell cycle progression in non-transformed cells. Thus, this work firmly establishes the features conferring specific properties to PP6 holoenzymes and uncovers the first known mechanism of PP6 activity regulation.

To my family

Karmela, Marijan, Ivan, Tvrtko, Jakov and Juraj

Acknowledgements

Many people have in one way or another helped me to complete my doctorate. I would in particular like to thank my supervisor, Francis Barr, for having faith in a young and inexperienced student, and all of his lessons. Ulrike Grüneberg, my co-supervisor, for her insight and guidance. I am also grateful to Prof Matthew Whitby and Prof Fanni Gergely for assessing the thesis thoroughly. To my brother Ivan for pushing me to apply in the first place. To members of the Barr lab and Grüneberg labs for their practical and theoretical input – especially Ricardo Nunes-Bastos, Michael Cundell and Andreas Gerondopoulos. James, thank you for dealing with my banter on a daily basis. Thank you Corinna, Vanessa and Tara for the fun times in the lab and your contributions. For technical support, the Oxford Advanced Proteomics Facility, Micron Advanced Imaging Facility staff, and all supporting staff of the Biochemistry department. To everyone at St Edmund hall for administrative and welfare support. To Cancer Research UK, for funding my work.

Finally, I thank my parents and brothers. Your unwavering support is a pillar on which I stand. Without you, I would not exist. Without you, I would not develop. Without you, this thesis would never have been made.

And Tvrtko – for making me eat my beans and watching from above.

Table of contents

Chapter 1 Introduction (*Omnis cellula e cellula*)..... 1

1.1 Cell cycle progression is controlled by protein phosphorylation and dephosphorylation 2

1.2 G1-S phase transition and the initiation of DNA replication..... 3

1.3 G2 phase and the switch-like activation of CDK1-cyclin B 8

1.4 A G2 DNA damage checkpoint inactivates mitotic kinases 10

1.5 Chromatin condensation & nuclear envelope breakdown are driven by CDK1, Aurora B and PLK1..... 11

1.6 CDK1-cyclin B, Aurora A & PLK1 promote spindle assembly 13

1.7 The spindle checkpoint prevents cyclin B destruction 18

1.8 Cyclin B destruction permits chromosome segregation..... 21

1.9 Cytokinesis and nuclear envelope reformation 26

1.10 Phosphoprotein phosphatases and cell cycle control..... 28

1.11 Aurora and Polo kinase activation..... 32

1.12 Negative regulation of Aurora A by protein phosphatase 6 37

1.13 Functional and architectural properties of PP6..... 40

1.14 The carcinogenic PP6-Aurora A interplay 41

Chapter 2 Functional characterization of PP6 holoenzymes 44

2.1 Preparation of PP6 holoenzymes 45

2.2 PP6-SAPS2 and PP6-SAPS3 are Aurora A phosphatases..... 49

2.3 PP6-SAPS2 and 3 are required for normal mitotic progression..... 51

2.4 PP6-SAPS3 is the major Aurora A phosphatase in mitosis..... 56

2.5 PP6 holoenzymes are stable throughout the cell cycle 58

2.6 SAPS subunits contribute unique interaction partners 64

2.7 ANKRD subunits interact with all SAPS subunits 66

Chapter 3 Regulation of PP6-SAPS2 by PLK1 69

3.1 Timing the SAPS2-PLK1 interaction – experimental framework 70

3.2 The SAPS2-PLK1 interaction persists through G2 and mitosis 72

3.3 SAPS2 contains a canonical polo-box domain binding motif 79

3.4 The docking site on SAPS2 is phosphorylated by PLK1 *in vivo* 81

3.5 PLK1 inhibits PP6-SAPS2 activity *in vitro* 84

3.6 PLK1 regulates active Aurora A levels via PP6 89

3.7 Bora links timely PLK1 and Aurora A activation 92

3.8 PLK1 regulation of PP6-SAPS2 does not affect bulk Aurora A during an unperturbed cell cycle 93

Chapter 4 PP6 and the DNA-damage checkpoint response 102

4.1 PP6 regulation of Aurora A in DNA-damaged cells 103

4.2 Non-transformed cells arrest in response to the loss of PP6-SAPS2 106

4.3 Targeting PP6-deficient cells by DDR inhibition 113

Chapter 5 Discussion 116

5.1 Functional stratification & specificity of protein phosphatase 117

5.2 PP6-SAPS3 is the major mitotic Aurora A phosphatase 120

5.3 PLK1 negatively regulates PP6-SAPS2 121

5.4 System-level feedback between PLK1 and Aurora A 128

5.5 PP6-SAPS2 and PP6-SAPS3 function in spindle regulation 131

5.6 The interplay of PP6 and the DNA damage response 132

5.7 An expanded view of PP6 function and regulation 138

Chapter 6 Materials and methods 139

6.1 Reagents and antibodies 140

6.2 Cell culture 141

6.3 Molecular cloning 145

6.4 Western blotting 146

6.5 Immune precipitations 146

6.6 Production of phosphatase and substrate complexes 149

6.7 Protein preparation titrations 150

6.8 *In vitro* phosphatase assays 150

6.9 *In vitro* kinase assays 150

6.10 Combined *in vitro* kinase and phosphatase assays 151

6.11 Cell-based biochemical assays 151

6.12 G2 DNA damage cell biochemistry 152

6.13 Immune precipitations for mass spectrometry 153

6.14 Mass spectrometry 154

6.15 Fixed-cell imaging 154

6.16 Live-cell imaging 156

6.17 Clonogenic survival assays 157

6.18 Western blot quantifications 157

6.19 Protein sequence alignment 157

6.20 Figure management 158

Appendix 159

Bibliography 164

List of Figures

Figure 1.1 - The vertebrate cell cycle 4

Figure 1.2 - Biochemical networks controlling the G1-S transition. 6

Figure 1.3 - Biochemical networks regulating the G2/M transition 9

Figure 1.4 - Simplified model of centrosome maturation 14

Figure 1.5 - Mitotic spindle formation 15

Figure 1.6 - The spindle assembly checkpoint 19

Figure 1.7 - Control of anaphase and cytokinesis events in vertebrate cell 22

Figure 1.8 - Chromosome segregation defects in anaphase and their consequences 25

Figure 1.9 - Principles of phosphprotein phosphatase holoenzyme regulation 29

Figure 1.10 - Principles of Aurora and Polo kinase regulation. 33

Figure 1.11 - Protein phosphatase 6 is a cancer-associated AurA T-loop phosphatase from the PP2A family 39

Figure 2.1 - Optimization of PP6 holoenzyme purification using cells stably expressing PPP6C-FLAG 46

Figure 2.2 – Phosphatase and Aurora A purification and titration 47

Figure 2.3 - PP6-SAPS2 and PP6-SAPS3 are AurA T-loop phosphatases 50

Figure 2.4 - Depletion of SAPS3 most closely resembles the PPP6C-null phenotype 53

Figure 2.5 - Depletion of SAPS3 results in pronounced mislocalization of active AurA. 54

Figure 2.6 - PP6-SAPS3 is the major AurA pT288 phosphatase in cells 57

Figure 2.7 - PP6 subunits are stably expressed and differentially phosphorylated throughout the cell cycle 60

Figure 2.8 - PP6 holoenzyme composition is constant throughout the cell cycle 62

Figure 2.9 - Interactome analysis of SAPS subunits 63

Figure 2.10 - Endogenous SAPS2 and PLK1 interact 66

Figure 2.11 - Interactome analysis of SAPS and ANKRD subunits. 68

Figure 3.1 - Synchrony during thymidine release is insufficient to assess the PLK1-SAPS2 interaction timing 71
Figure 3.2 - Double thymidine block-release dramatically improves synchrony 72
Figure 3.3 - SAPS2 interacts with PLK1 consistently through the cell cycle 73
Figure 3.4 - Endogenous SAPS2 interacts with PLK1 consistently through the cell cycle.... 74
Figure 3.5 - SAPS2 interacts with PLK1 consistently throughout the cell cycle 76
Figure 3.6 - The PLK1-SAPS2 interaction during mitotic exit 78
Figure 3.7 - PLK1 docks to 770SSP on SAPS2 via the Polo-box domain..... 80
Figure 3.8 - PLK1 phosphorylates its own docking site on SAPS2 82
Figure 3.9 - Regulation of PP6-SAPS2 activity by PLK1 in vitro 86
Figure 3.10 - PLK1-deficient PP6-SAPS2 is more active than WT 88
Figure 3.11 - PLK1-AurA feedback is established through PP6..... 90
Figure 3.12 - PP6-SAPS2 and PP6-SAPS3 cooperate in PLK1-AurA feedback..... 92
Figure 3.13 - Bora depletion leads to delayed mitotic entry and AurA activation. 94
Figure 3.14 - Depletion of PP6 subunits affects Aurora A, but not CDK1 activation dynamics. 96
Figure 3.15 - PP6-SAPS2 does not limit Aurora A recruitment to centrosomes. 97
Figure 3.16 - SAPS2 does not control Aurora A deactivation during mitotic exit..... 99
Figure 3.17 - PLK1 regulation of SAPS2 does not affect unchallenged cell cycle progression 101
Figure 4.1 - PP6 links the Aurora A activation status to the DDR in late G2 104
Figure 4.2 - p53 induction protects PPP6C-depleted cells from accumulating damage 108
Figure 4.3 - Non-transformed cells mount a p53 response upon depletion of PP6 subunits 109
Figure 4.4 - Cells depleted of PP6-SAPS2 induce a p21 checkpoint response 111
Figure 4.5 - Depletion of PP6-SAPS2 causes a cell cycle arrest 113
Figure 4.6 PP6-depleted cells are sensitive to DDR inhibitors..... 115
Figure 5.1 - Putative mechanisms of SAPS2 inhibition and its relief..... 125

Figure 5.2 - PLK1-PP6-Aurora A feedback in the cell cycle..... 130

Figure 5.3 - Potential gateways for PP6 in checkpoint control..... 137

Figure A1 - PLK1-deficient PP6-SAPS2 is more active than WT……162

List of Tables

Table 6.1 - Inhibitors and selection antibiotics. 140

Table 6.2 - siRNAs used for protein depletion in mammalian cells. 141

Table 6.3 - Accession numbers of PP6 subunit DNA sequences used for cloning..... 143

Table 6.4 - Primers used for cloning and mutagenesis. 144

Table 6.5 - Antibodies used for western blotting, immunofluorescence and immunoprecipitations. 147

Table A1 - Curated list of proteins enriched in SAPS IPs, supporting figure 2.9 160

Table A2 - SAPS2 phosphopeptides detected by mass spectrometry, supporting figure 2.9. 163

List of Abbreviations

APC/C	Anaphase promoting complex/cyclosome
ATP	Adenosine triphosphate
AGC	Automatic gain control
AMPA	α-amino-3-hydroxy-5-methyl-4-isoxazolepropionic acid
ANKRD	Ankyrin repeat containing subunit
ANOVA	Analysis of variance
Arpp19	cAMP-regulated phosphoprotein 19
ATM	Ataxia telangiectasia mutated
ATR	ATM- and Rad3-related protein
AurA	Aurora A
AurB	Aurora B
BAF1	Barrier-to-autointegration factor 1
BLM	Bloom syndrome protein
Bora	Protein Aurora Borealis
BRCA1	Breast cancer antigen 1
BSA	Bovine serum albumin
BUB1	Budding uninhibited by benzimidazoles 1
BUB3	Budding uninhibited by benzimidazoles 3
BUBR1	Budding uninhibited by benzimidazoles related 1
CAK	CDK-activating kinase
CKS	Cyclin dependent kinases regulatory subunit
CBB	Coomassie brilliant blue
CCD	Charge-coupled device
CDC20	Cell division control protein 20
CDC25	Cell division control protein 25

CDH1	CDC20 homologue 1
CDK	Cyclin dependent kinase
CDK5RAP2	CDK5 regulatory subunit-associated protein 2
CDKN1A	Cyclin-dependent kinase inhibitor 1A
CDKN1B	Cyclin-dependent kinase inhibitor 1B
CENP-A	Centromere protein A
Cep192	Centrosomal protein of 192 kDa
ch-TOG	Colonic and hepatic tumor overexpressed gene protein
CHK	Checkpoint kinase
CID	Collision-induced dissociation
CIP2A	Cancerous inhibitor of PP2A
CPC	Chromosomal passenger complex
DAPI	4′,6-diamidino-2-phenylindole
DDR	DNA damage response
DMEM	Dulbecco's modified Eagle medium
DMSO	Dimethyl sulfoxide
DNA	Deoxyribonucleic acid
DNA-PKcs	DNA-dependent kinase catalytic subunit
DSB	Double stranded break
DTT	Dithiothreitol
E2F	Transcription factor E2F
ECT2	Epithelial cell-transforming sequence 2
EDTA	Ethylenediaminetetraacetic acid
EM	Electron multiplication
EM-CCD	Electron-multiplication charge-coupled device
ENSA	Endosulfine-α
FOXO3	Forkhead box O3

GFP	Green fluorescent protein
GTP	Guanosine triphosphate
HEAT	Huntingtin, elongation factor 3, A-subunit of PP2A, TOR1 yeast PI3-kinase
HRP	Horse radish peroxidase
hTERT	Human telomerase reverse transcriptase
HURP	Hepatoma up-regulated protein
INCENP	Inner centromere protein
IP	Immune precipitation
KAP1	KRAB-associated protein 1
KAPβ2	Karyopherin beta 2
KIF18	Kinesin-like protein 18
KIF4A	Chromosome-associated kinesin 4A
KNL1	Kinetochore-null protein 1
KO	Knock-out
LC-MS	Liquid chromatography-mass spectrometry
MAD1	Mitotic arrest deficient 1
MAD2	Mitotic arrest deficient 2
MAP	Mitogen-activated protein
MAPK	Mitogen-activated protein kinase
MASTL	Microtubule-associated serine/threonine-protein kinase-like
MCAK	Mitotic centromere-associated kinesin
MCC	Mitotic checkpoint complex
MDM2	E3 ubiquitin-protein ligase Mdm2
MPS1	Mono-polar spindles 1
mRuby	Monomeric Ruby
MTOC	Microtubule organizing center

MYPT	Myosin phosphatase-targeting subunit 1
Myt1	Membrane-associated tyrosine- and threonine-specific cdc2-inhibitory kinase
NEBD	Nuclear envelope breakdown
NEDD1	Neural precursor cell expressed developmentally down-regulated protein 1
NEK2	NIMA-related kinase 2
NP40	nonyl phenoxypolyethoxylethanol
NuMA	Nuclear mitotic apparatus
NUSAP1	Nucleolar and spindle-associated protein 1
PAGE	Poly-acrylamide gel electrophoresis
PBD	Polo box domain
PBS	Phosphate-buffered saline
PCM	Pericentriolar material
PCNA	Proliferative cell nuclear antigen
PICH	PLK1-interacting checkpoint helicase
PLK	Polo-like kinase
PP1	Protein Phosphatase 1
PP2A	Protein Phosphatase 2A
PP4	Protein phosphatase 4
PP6	Protein phosphatase 6
PPP	Phospho-protein phosphatases
PRC1	Protein regulator of cytokinesis 1
px	Pixel
RACGAP1	Rac GTPase-activating protein 1
RB	Retinoblastoma protein
RBP	RNA-binding protein

ROI	Region of interest
RPE1	Retinal pigmented epithelium 1
RPLC	Reverse phase liquid chromatography
SAC	Spindle assembly checkpoint
SAF	Spindle assembly factor
SEM	Standard error of the mean
SD	Standard deviation
SAPS	SIT4 phosphatase-associated protein
SCF	SKP-Cullin-F box
sCMOS	Scientific complementary metal-oxide-semiconductor
SDS	Sodium dodecyl sulphate
siRNA	Small interfering RNA
TACC3	Transforming acidic coiled-coil-containing protein 3
TCEP	tris(2-carboxyethyl)phosphine
TEAB	Triethylammonium bicarbonate
TFA	Trifluoroacetic acid
TPX2	Targeting proteins for Xklp2
TRIP13	Thyroid hormone receptor interacting protein 13
UV	Ultraviolet
WT	Wild type

Chapter 1 Introduction (*Omnis cellula e cellula*)

1.1 Cell cycle progression is controlled by protein phosphorylation and dephosphorylation

All cells in existence today arose from their ancestors through continued growth, reproduction and heritable adaptation [1]. Fundamentally, these processes are underpinned by complex biochemical networks linked into a cycle which allows the regulated replication of the genetic material and its segregation into two newly formed cells. In eukaryotes, the cell cycle culminates in mitosis, when the spindle apparatus segregates the duplicated genetic material condensed in chromosomes. Correct function of this process is essential, as aberrations result either in death, developmental defects or diseases such as cancer. Researching the cell cycle from a mechanistic standpoint is therefore critical to understand, diagnose and treat these aberrations. Here I will present and discuss known and proposed elements of the cell cycle and the mechanisms that form the basis of the regulatory network controlling it, with a particular focus on kinase and phosphatase regulation and their links to disease.

In eukaryotes, the cell cycle is driven by a series of regulated, switch-like phosphorylations [2], created by the activity of the family of cyclin-dependent serine/threonine kinases (CDKs) (reviewed in [3]). At its core, this system is universally conserved from yeast to humans, but in this work I will focus on metazoans with particular emphasis on the mammalian cell cycle. CDKs are constitutively expressed in mammalian cells, but are inactive until they bind a compatible cyclin [4]. Apart from activating the kinase, cyclins also confer a degree of substrate specificity [5, 6], which is additionally refined by regulatory interactors, the CKS proteins [4]. Unlike the CDK, cyclins are generally not constitutively expressed, but synthesized and destroyed upon specific cues [7].

Different CDK-cyclin combinations define the different cell cycle stages – G1 phase, S phase, G2 phase and mitosis (Figure 1.1). The functions of the different CDK-cyclin modules are integrated with kinases of the Aurora and Polo families which are responsible for executing additional cell cycle stage-specific phosphorylations [8-10]. Cell cycle control is not limited to fluctuating kinase activity alone. Rather, dynamic control is provided through the combined activities of these kinases and their opposing phosphatases [11]. Specific members of the serine/threonine phosphoprotein phosphatase (PPP) family, PP1 and PP2A, are the most prominent cell cycle-regulating phosphatases [11-13]. PPPs have wider roles in addition to cell cycle control, including regulation of metabolism and the interphase cytoskeleton, but these will not be discussed in detail (reviewed in [14]).

1.2 G1-S phase transition and the initiation of DNA replication

The cell cycle starts when a resting cell transitions from the non-proliferating first gap phase (G1) into the growth or synthesis (S) phase. This transition is controlled by the activation of CDK2 by cyclins E and A in response to mitogen stimulation (Figure 1.2A) [15]. The accumulation of these cyclins is regulated at the transcriptional level by the transcription factor E2F, which is inhibited by the retinoblastoma protein (RB) in G1 [16, 17]. S-phase entry is further prevented due to inhibition of CDK2 by its inhibitory binding partner $CDKN1B^{p27}$ [15, 18]. These two inhibitory pathways are silenced by CDK4/6-cyclin D, which are stimulated by growth factor and mitogenic signalling pathways [19]. Cyclin D accumulates in G1, but its association with CDK4/6 is prevented by inhibitory proteins from the INK4 family [20].

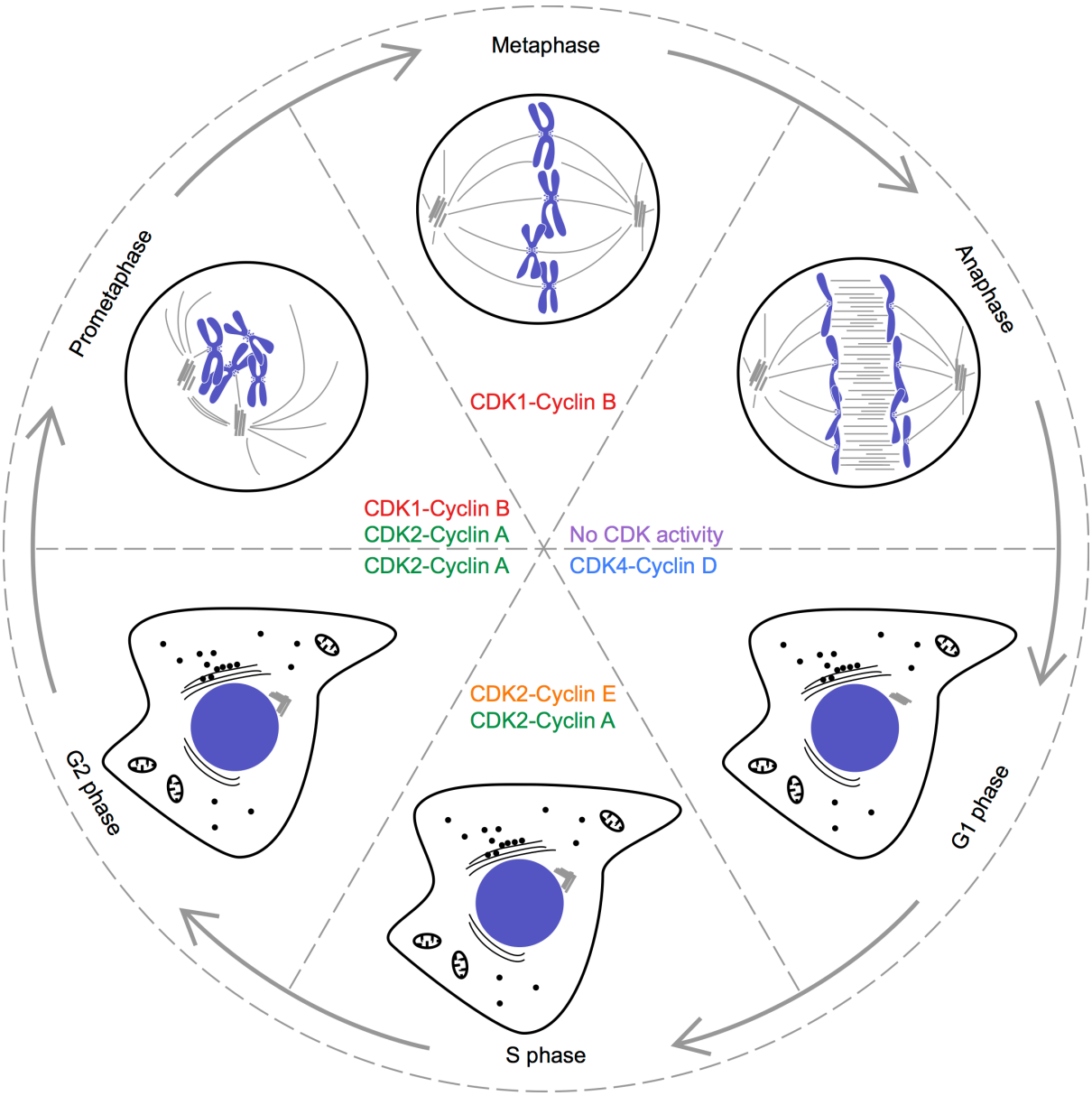


Figure 1.1 - The vertebrate cell cycle. Unique combinations of CDK:cyclin complexes control cell cycle progression and determine the cell cycle phases. CDK4:cyclin D initiates the G1-S transition, allowing the formation of CDK2:cyclin E/A complexes, the combination of which drives DNA replication. Cyclin E is degraded in late S phase and CDK2:cyclin A controls processes associated with G2 phase and contributes to mitotic entry, along with the principal mitotic kinase CDK1:cyclin B. As mitosis progresses, cyclin A is degraded and CDK1:cyclin B maintains the metaphase state exclusively. Degradation of cyclin B triggers chromosome segregation and the re-establishment of the G1 state.

Furthermore, any complexes that do form are inhibited by CDKN1B^{p27} [21]. In the presence of mitogens, both of these inhibitory layers are relieved and CDK4/6

phosphorylate and inhibit RB [19, 22], allowing E2F activation and promoting the synthesis of cyclin E [17]. As the cyclin accumulates, CDK2-cyclin E complex levels rise, phosphorylating CDKN1B^{p27} and targeting it for degradation [15, 23]. This allows for a rapid, switch like activation of CDK2 and irreversible entry into S phase [15]. Further acceleration is provided through inhibition of the E3-ubiquitin ligase cofactor CDH1, which normally targets cyclin A and cyclin E for degradation [24, 25]. Concomitantly, the synthesis of cyclin A begins, allowing it to complex with CDK2 and contributing to CDKN1B^{p27} and CDH1 inhibition [15, 23-25]. Transcription of DNA replication factors is also initiated and from this point onwards the cell is committed to cell cycle completion [15].

However, entry into S phase can be halted by the overriding action of the DNA-damage dependent p53 pathway (Figure 1.2B, reviewed in [26]). Under normal conditions, p53 is rapidly ubiquitinated by MDM2 and its levels kept low by proteasomal degradation [27]. Upon DNA-damage, p53 accumulates owing to a phosphorylation by one of several DNA damage response (DDR) kinases, including ATM, ATR and DNA-PK, which protects it from ubiquitination and hence proteasomal degradation [28]. Stabilised p53 then acts as a transcription factor for CDKN1A^{p21} [29], a potent inhibitor of CDKs including CDK4-cyclin D and CDK2-cyclin A/E [30]. Furthermore, CDKN1A^{p21} halts DNA replication through inhibition of the DNA-polymerase cofactor PCNA [31]. Both the p53 pathway and G1-S transition machinery are very frequently defective in cancers. Loss-of-function mutations or downregulation of p53 are some of the most common drivers of tumorigenesis, and mutations in RB cause childhood retinoblastoma [32].

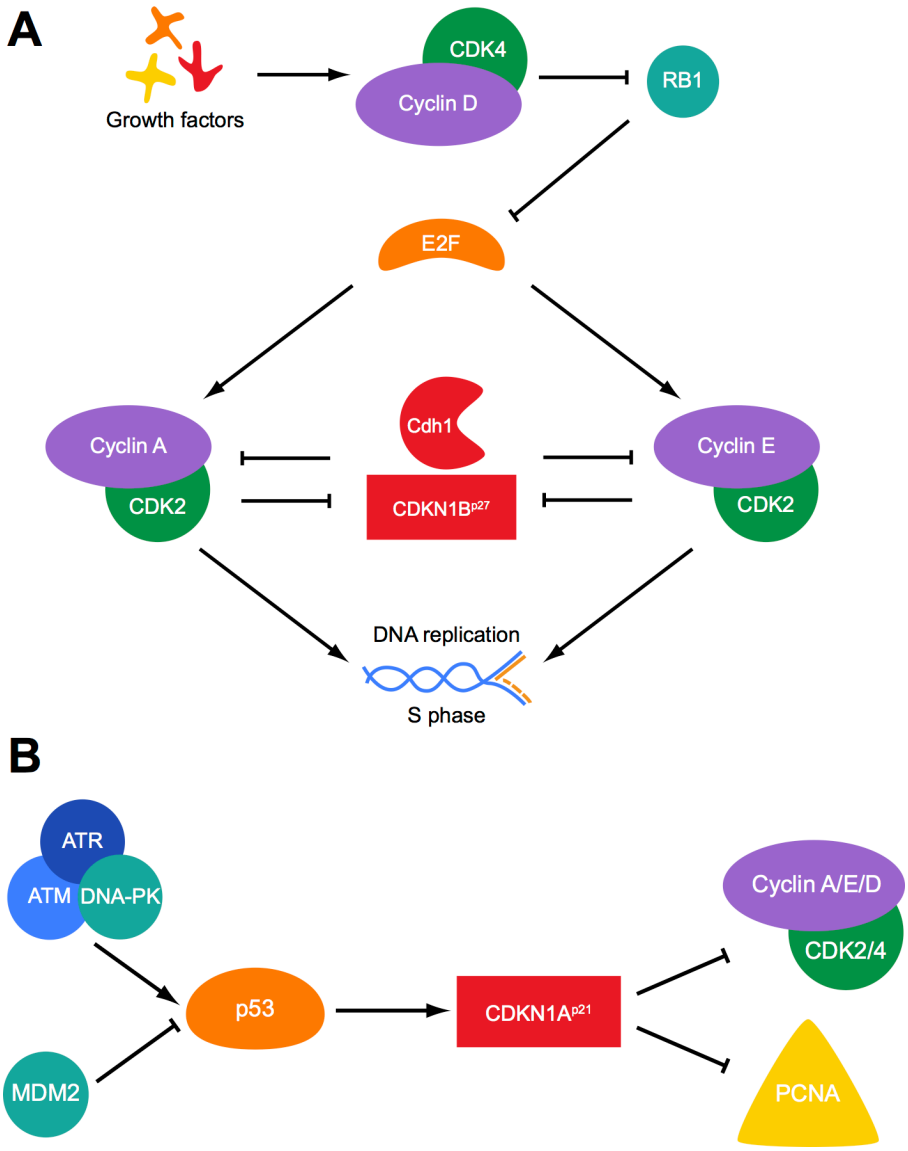


Figure 1.2 - Biochemical networks controlling the G1-S transition. (A) Network controlling the initiation of DNA replication. Growth factors, nutrients and other signals result in the creation of active CDK4:cyclin D complexes, which inhibit RB1. This relieves the inhibition of the transcription factor E2F, driving the synthesis of cyclin A and E, which then associate with and activate CDK2. Rising CDK2:cyclin levels overcome inhibitory inputs from Cdh1 and CDKN1B^{p27}, and in turn directly inhibit the activity of these inhibitors, reaching full activation and driving DNA replication. **(B)** The G1 phase DNA damage checkpoint. Continuous synthesis of p53 is counteracted by MDM2-mediated degradation. This turnover is inhibited through phosphorylation of p53 by DDR kinases, allowing the accumulation of p53, which drives the synthesis of CDKN1A^{p21}. CDKN1Ap21 then efficiently prevents S phase initiation by inhibiting G1-S CDK:cyclin complexes and precludes DNA replication by inhibiting PCNA.

Similarly, the commonly used HeLa cancer cell line is RB- and p53-defective due to HPV-mediated transformation, and thus does not have a functional G1-S checkpoint [33].

Once cells have entered S-phase, the ongoing activities of CDK2-cyclin A/E control DNA replication. The two active CDK2 complexes then have differing roles in this process. CDK2-cyclin E is required for initiation of DNA replication and CDK2-cyclin A is required to maintain it [34]. As S phase progresses, cyclin E is phosphorylated by CDK2-cyclin A and becomes a substrate for the SCF ubiquitin ligase, thus targeting it for proteasomal destruction [35, 36]. Replication is performed by the replisome complex, composed of DNA polymerases, helicases and essential auxiliary factors (reviewed in [37]). A good example of such a factor is PCNA, which associates with the replisome and increases its processivity [38]. Replisomes assemble focally at origins of replication and move across chromatin as replication forks to cover the entire genetic code [37]. Once the process is complete, replisomes dissociate from chromatin and disassemble [37].

During replication, the genome is sensitive to aberrations. In particular, if a replication fork encounters a locus harbouring DNA damage, it will stall until the damage is repaired [39, 40]. In addition, replication itself frequently induces DNA damage due to errors, chemical modifications and nuclease-assisted proofreading [41]. As such, cells in S phase have a higher frequency of detectable DNA damage than in other cell cycle phases [42]. Moreover, DNA replication is sensitive to nucleotide levels, and will reversibly pause if one or more nucleotides is lacking. As a result, depletion of cytidine through inhibition of ribonucleotide reductase by exposure to excess thymidine can be used to reversibly arrest cells in S phase [43].

1.3 G2 phase and the switch-like activation of CDK1-cyclin B

Once DNA replication is complete, the transitionary second gap phase (G2) begins. During this time cells undergo further growth, and synthesise a cohort of factors necessary for mitosis. Key among the factors synthesized in G2 are the Aurora and Polo family kinases [44, 45], mitotic spindle assembly factors (SAFs), and regulators of chromosome structure and cytokinesis [46]. Most importantly, cyclin B, the partner of the principal mitotic kinase CDK1 is made [46]. However, this doesn't cause immediate mitotic entry owing to a multi-layered regulatory system inhibiting CDK1 and restricting its access to key substrates (Figure 1.3A). Firstly, CDK1-cyclin B complexes localize to the cytoplasm, separated from spindle assembly factors which are sequestered in the nucleus [47]. Furthermore, CDK1 is phosphorylated and inhibited by two kinases – Myt1 and Wee1 [48, 49]. These inhibitory phosphorylations on T14 and Y15 prevent ATP binding and thus render the kinase inactive [50]. This inhibition is central to the switch-like activation profile of CDK1 by cyclin B and proper duration of G2 phase. Premature mitotic entry triggered in the absence of Wee1 activity results in defects in virtually every aspect of mitosis, from chromosome condensation and spindle assembly to chromosome segregation [51]. Once a threshold level of cyclin B is reached Wee1/Myt1-mediated inhibition is overcome since CDK1-cyclin B complexes start to inhibit Wee1 and Myt1 and promote the activity of CDC25 (Figure 1.4A) [52, 53]. At this point, CDK1-cyclin B translocates into the nucleus and the Wee1 phosphorylations on CDK1 are removed by three CDC25 phosphatases with overlapping functions (CDC25A, B or C) [11, 47, 54]. In addition, CDK1-cyclin B complexes are phosphorylated and activated by the CDK-activating kinase complex (CAK) [55].

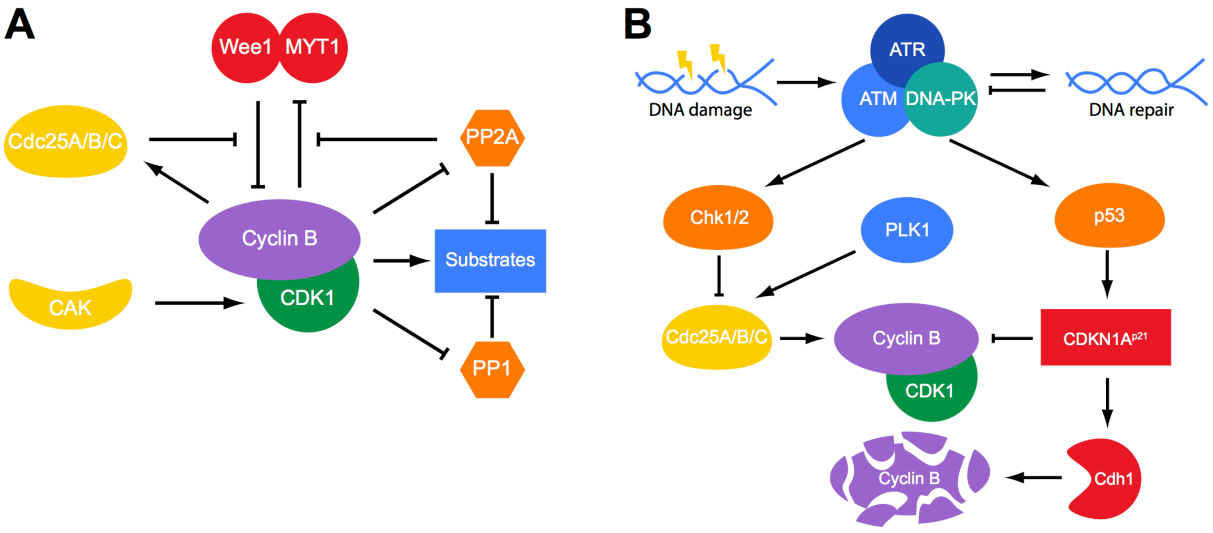


Figure 1.3 Biochemical networks regulating the G2/M transition. (A) Multilayered system regulating the activation of CDK1:cyclin B. CDK1:cyclin B complexes are held inactive through phosphorylations by Wee1 and MYT1, which can be removed by the Cdc25 phosphatases. Once sufficient CDK1:cyclin B complexes have been assembled and activated by CAK, a small pool can escape inhibition and start activating Cdc25 and inhibiting Wee1 and MYT1. This liberates more active CDK1:cyclin B which in turn inhibits two groups of phosphatases - PP1 and PP2A - and acts on downstream targets, triggering mitotic entry. **(B)** DNA damage in G2 can inhibit CDK1:cyclin B. Activated DNA damage kinases activate checkpoint kinases Chk1 and Chk2, which inhibit critical cell cycle factors such as Cdc25 phosphatases, preventing CDK1:cyclin B activation. The reversal of this effect upon the silencing of DNA damage signaling requires the activity of PLK1. Alternatively, terminal cell cycle exit can be triggered by activation of the p53-p21 pathway, resulting in Cdh1-mediated degradation of cyclin B.

Further contribution to CDK1 activation is made by PLK1, which phosphorylates and activates CDC25C [56, 57]. As a consequence of these positive-feedback loops, CDK1 activation is extremely rapid [11, 58]. Once fully activated, active CDK1 is in large excess and triggers nuclear envelope breakdown, making mitotic entry irreversible [11, 59].

Mitotic entry is also regulated by the activity of specific PPPs. Inhibition of PP2A-subfamily phosphatases in G2 cells by the algal toxin okadaic acid (OA) triggers unregulated entry into mitosis [60]. This feature has been largely

attributed to two phosphatases - PP2A-B55 and PP1 [11, 60]. CDK1 activation at the G2-M transition results in the inactivation of these counteracting phosphatases (Figure 1.3A). For PP2A-B55, CDK1 does not do this directly, but rather through activation of the Greatwall kinase (MASTL) [61]. Activated MASTL phosphorylates two small unstructured proteins – Arpp19 and ENSA – which then bind tightly to PP2A-B55 and act as competitive inhibitors or "unfair substrates", leading to a reduction in bulk PP2A-B55 activity [62, 63]. PP2A-B55 is thought to play two key roles. It has been suggested that PP2A-B55 is important to remove phosphorylation created by residual CDK1-activity that escapes Wee1-dependent inhibition in G2 [11, 64]. PP2A-B55 also prevents the inhibition of Wee1 by CDK1 [65], thus lowering CDK1-activity. By contrast, PP1 is proposed to be directly inhibited through CDK1 phosphorylation of T320, reducing general CDK1-counteracting phosphatase activity. Because PP1 dephosphorylates an activating phosphorylation on Greatwall kinase (MASTL), this also indirectly controls PP2A-B55 activity [66, 67].

1.4 A G2 DNA damage checkpoint inactivates mitotic kinases

To safeguard the integrity of the genome, it is imperative that excessive DNA damage is detected and corrected before cell division. Particularly dangerous are double stranded breaks (DSBs) which have to be repaired before irreversible commitment to mitosis, as this would cause catastrophic chromosome breaks [68]. To achieve this, the DDR feeds back onto cell cycle control and prevents CDK1 activation (Figure 1.3B). Once DNA damage has been detected, key signalling kinases DNA-PK, ATM or ATR are activated, depending on the type of damage and cell cycle stage (reviewed in [68]). These kinases initiate DNA repair by activating repair effector proteins, and also activate checkpoint kinases Chk1 and

Chk2 [68]. The checkpoint kinases then inhibit CDC25 phosphatases, preventing CDK1 activation in G2 [69-71]. Furthermore, other mitotic kinases such as PLK1 and Aurora A are kept inactive [72]. The underlying mechanisms are unclear, but they are inhibited either through prevention of their activation, or through deactivation of previously activated kinase complexes. A separate p53-dependent pathway can also be employed. In part, it works in the same way as in G1, wherein p53 stabilisation leads to expression of $CDKN1A^{p21}$ [73-75]. $CDKN1A^{p21}$ then directly and reversibly inhibits CDK1. However, if the cell fails to repair the damage, this G2 checkpoint pathway induces the translocation of cyclin B into the nucleus where it becomes refractory to activation and cannot support mitotic entry [74, 75]. Ultimately, cyclin B is degraded in CDH1-dependent manner and the cell enters senescence [74]. Just prior to mitotic entry, DNA damage-induced cyclin B degradation can also happen directly in the cytoplasm [75]. If the cell is able to overcome the damage, checkpoint signalling is abolished allowing the recovery of cell cycle progression [71, 76]. However, this recovery depends on the activities of Aurora A, PLK1 and CDC25, further integrating it with other components of the cell cycle machinery [71, 76].

1.5 Chromatin condensation & nuclear envelope breakdown are driven by CDK1, Aurora B and PLK1

Once all the conditions have been met, two events occur that mark entry into mitosis. First, the chromatin starts to condense through the concerted action of histone modifications and the activities of condensin I and II (reviewed in [77]). Aurora B, as a part of the chromosomal passenger complex (CPC), is recruited to chromatin due to CDK1-dependent phosphorylation of other components of the complex (reviewed in [78]). It then performs a dual role in chromatin condensation.

Firstly, phosphorylation by Aurora B is required for the recruitment of condensin I to chromosomes, which drives lateral compaction of chromosomes [79, 80]. Secondly, Aurora B phosphorylates Histone 3 on S10. This phosphorylation correlates with chromosome condensation but its contribution to the process is unclear. In some species it is essential, but this seems not to be the case in vertebrates [81, 82]. Condensin II drives axial compaction of chromosomes and is regulated by PLK1 [83]. This requires a priming phosphorylation of condensin II by CDK1, allowing PLK1 binding. PLK1 then hyperphosphorylates condensin II and promotes its DNA supercoiling activity [83]. These processes allow the chromosomes to compact in a regulated fashion, achieving full condensation in metaphase.

In the next critical step, the nuclear envelope breaks down. This event is driven by CDK1-cyclin B and led by rearrangements of two elements – the nuclear lamina and nuclear pore complexes (reviewed in [84]). The nuclear lamina is a meshwork of intermediate fibres composed of lamin A/C dimers and lamin B which serves as mechanical support for the nuclear envelope [85]. Once phosphorylated by CDK1, the lamina is deconstructed, releasing chromatin and destabilizing the nuclear envelope [85, 86]. Nuclear pores are large complexes allowing regulated transport across the nuclear envelope [84, 87]. This transport is enabled by importins, which bind to specific motifs on target proteins and serve as adaptors that are recognized by the pore complex [88]. Once inside the nucleus, Ran-GTP mediates the disassembly of importin-cargo complexes [88]. Importin binding often blocks the functionality of bound cargo proteins, and this feature is exploited for regulation of several factors after nuclear envelope breakdown (NEBD), only allowing their release in the vicinity of chromatin [89, 90]. A notable

example of this is TPX2, which is both a spindle assembly factor and activator for Aurora A [90]. Apart from their role in transport, nuclear pore complexes also serve as structural reinforcement of the nuclear envelope, and are disassembled upon CDK1 phosphorylation [87, 91]. With the loss of both the nuclear lamina and nuclear pores, the structural frame supporting the nuclear envelope is lost and NEBD occurs. Concomitantly with chromatin condensation, CDK1-cyclin B activity also promotes centrosome separation – a key event in preparation for mitotic spindle formation [92]. This is achieved by the activity of the kinesin Eg5, which is directly promoted by CDK1 [92]. Once active, Eg5 slides antiparallel microtubules between the two centrosomes apart, which results in separation [92]. Lastly, cell-cell and cell-surface adhesion is reduced and the cell reshapes into a sphere.

Some evidence suggests that mitotic entry requires CDK2-cyclin A, or that this complex can at least support it in the absence of cyclin B [93]. However, the relative contribution of this complex compared to CDK1-cyclin B is unclear. Regardless, once the cell enters mitosis, cyclin A is degraded and mitosis is maintained exclusively through CDK1-cyclin B activity [2, 94].

1.6 CDK1-cyclin B, Aurora A & PLK1 promote spindle assembly

Following NEBD and chromosome condensation, capture of the chromosomes by spindle microtubules is the next key step in mitosis. At this stage, CDK1-cyclin B complexes become mixed with substrates due to the loss of nuclear-cytoplasmic compartmentalization [47] and overcomes counteracting phosphatase activities [11]. The resultant stable phosphorylation state triggers spindle assembly, activates the spindle assembly checkpoint (SAC) and initiates the dissolution of organelles such as the Golgi apparatus [92, 95, 96].

Mitotic spindle formation initiates in G2 phase when centrosomes are duplicated, followed by growth and compositional alteration in a process called centrosome maturation (Figure 1.4, reviewed in [45]). This process is regulated, most prominently by PLK1 and Aurora A. It begins when PLK1 phosphorylates the scaffolding proteins Cep192 and pericentrin, which then recruit additional factors [44, 97]. Furthermore, interphase-specific centrosomal proteins are removed due to PLK1 activity [98]. Crucially, these initial changes result in the recruitment of NEDD1, which enables the deposition of γ-tubulin in concentric rings around the centrosome, expanding it dramatically [99]. This γ-tubulin ring complex augments the ability of the centrosome to nucleate microtubules, which will support the formation of a dense mitotic spindle [100]. The maturing centrosome recruits the kinase Aurora A through its interaction with Cep192 in mammals or centrosomin, the homologue of CDK5RAP2, in *Drosophila melanogaster* [44, 101]. Aurora A potentiates the maturation process by promoting the activity of PLK1 and other PCM components [102].

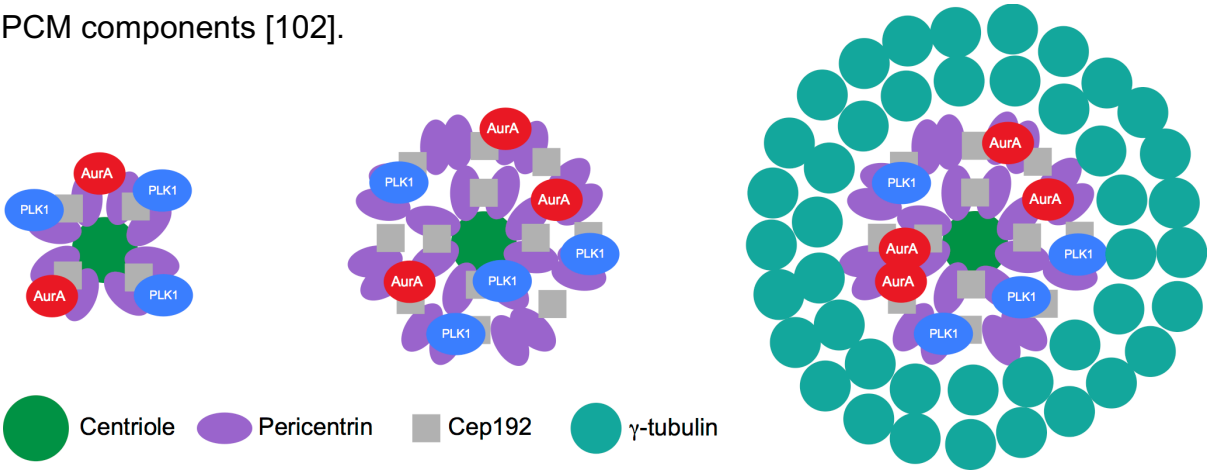
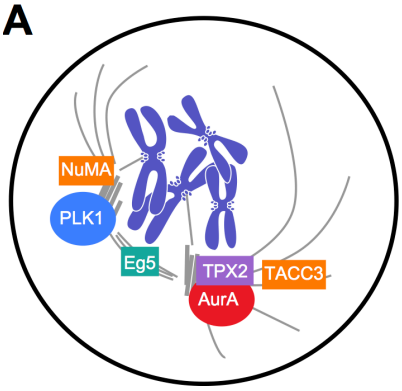


Figure 1.4 - Simplified model of centrosome maturation. In G2 phase, duplicated centrioles start accumulating pericentriolar material. Initial deposition of pericentrin and Cep192 allows the recruitment of PLK1, which promotes further expansion of the PCM and the recruitment of AurA. The two kinases regulate further changes to the centrosome, including the assembly of the γ-tubulin ring complex, which expands the PCM and supports microtubule nucleation in mitosis.

A



B

	Function	Regulated by
Eg5	Spindle pole separation	CDK1 - activation
TPX2	Mitotic spindle organization	Importin - inhibition
NuMA	Spindle pole architecture	AurA, CDK1 - localization
TACC3	Microtubule bundling	AurA - activation

Figure 1.5 - Mitotic spindle formation. (A) Nuclear envelope breakdown liberates a host of spindle assembly factors, which associate with separating centrosomes and forming spindle microtubules. This regulates all aspects of mitotic spindle assembly, from the establishment of bipolarity, through the structure of microtubule bundles and spindle poles to regulation of microtubule dynamics. **(B)** Select spindle assembly factor function and regulation.

Concomitantly with maturation, the parental and daughter centrosomes are detached from one-another due to the activity of NEK2 kinase [103]. Each separated mature centrosome brings about the formation of a spindle pole around it after nuclear envelope breakdown, when spindle assembly factors are released. However, centrosomes themselves are not essential to form spindle poles in vertebrates, but rather seem to only facilitate this process [104]. In line with this, vertebrate oocytes lack centrosomes yet can still form spindle structures from acentriolar microtubule organizing centres (MTOCs) [104]. Although the centrosome is not required for this, the kinase Aurora A is [105, 106]. Intriguingly, injection of Aurora A-coated beads into Xenopus oocytes induces the formation of MTOCs around them [105]. Thus, SAF regulation by Aurora A is a basic requirement for the formation of both mitotic and meiotic spindles [105-107].

The spindle pole is composed of PCM proteins, microtubules and a supporting lattice formed from the protein NuMA and microtubule bundling factors such as TACC3 and NUSAP1 [108]. Once formed, it is the principal point of

microtubule nucleation, provided by microtubule nucleation factors such as TPX2, and the centrosome-associated γ-tubulin ring complexes [99, 109]. These also ensure that the polarity of microtubules is defined – minus-ends are nucleated at the poles and the plus-ends extend towards the cell equator or cortex [110]. Many SAFs are regulated by mitotic kinases (Figure 1.5). CDK1 directly regulates several of them. In addition to the already described phosphorylation of Eg5 [92], these include NuMA and TPX2, whose association with the mitotic spindle is affected by at least one CDK1 phosphorylation (Figure 1.5B, [111-113]. This regulation also integrates the role of CDK1 in spindle assembly with Aurora A and PLK1, which remain associated with spindle poles in mitosis and are required for the maintenance of bipolar spindles (Figure 1.5A). In part, this is achieved by Aurora A-dependent phosphorylation of TACC3 and NuMA, regulating their microtubule bundling activity and localization [114-116]. PLK1, on the other hand, maintains the phosphorylations of PCM components, thus safeguarding the structure of spindle poles [44, 97]. In addition, some reports indicate that PLK1 affects the localization of TPX2 and promotes its function as an Aurora A activator, which can further contribute to the regulation of spindle architecture [117, 118]. Consistent with these important roles, inhibition of Aurora A or PLK1 result in spindle architecture and function defects. In particular, Aurora A inhibition causes a collapse into monopolar spindles, and PLK1 inhibition in the disassembly of spindle poles [106, 119, 120].

Away from spindle poles, microtubules are further stabilised by microtubule bundling proteins such as HURP [121]. Microtubule branching points can also be formed with by the concerted action of TPX2 and the augmin complex [122]. However, this structural stability is insufficient for correct spindle function and has

to be complemented with dynamic regulation. This is achieved through regulated microtubule polymerisation and rapid depolymerisation events termed catastrophe [123, 124]. Microtubule polymerisation can occur spontaneously in the presence of GTP and excess tubulin [125], but in cells this process is accelerated with the aid of SAFs, best characterised for ch-TOG [126, 127]. On the flip side, microtubule catastrophe is also promoted by auxiliary proteins. The kinesin MCAK is considered to be the major catastrophe-promoting factor in mammalian cells, but other kinesins, such as KIF18, may contribute [128, 129]. The activity of MCAK is spatially and temporally regulated through phosphorylation by Aurora kinases, which inhibit its microtubule depolymerase activity [123, 129, 130]. However, the major way microtubules are stabilised in mitosis is not direct kinesin regulation, but end-on attachment to kinetochores [131]. These microtubules are then referred to as kinetochore- or K-fibres [131]. The correct function of K-fibres is a prerequisite for faithful chromosome segregation – the primary role of the mitotic spindle. A K-fibre-specific bridging complex composed of TACC3, ch-TOG and clathrin further stabilizes these microtubules [132]. An additional layer of regulation is added by Aurora A kinase, which promotes the formation of this bridging complex [133]. Additional microtubules emanate from spindle poles away from the cell equator towards the cell cortex, where they anchor [134]. These are called astral microtubules. Dynamic astral microtubules position mitotic spindles within cells, with the aid of the minus-end-directed kinesin dynein which ties them to the cell cortex [135]. Spindle positioning is particularly important for asymmetric cell divisions, wherein it controls where the division plane is ultimately set [136].

In contrast to SAFs, factors regulating anaphase and cytokinesis events are inhibited upon mitotic entry [136]. A well-characterised example is PRC1, a

microtubule-binding protein which stabilizes antiparallel microtubule structures at the central spindle in anaphase [136, 137]. Phosphorylation of PRC1 T481 by CDK1 reduces its affinity for microtubules and is a good marker for prometaphase and metaphase states [137]. The phosphorylation is only removed in anaphase, allowing the protein to promote the correctly timed organisation of central spindle microtubules [137].

1.7 The spindle checkpoint prevents cyclin B destruction

Spindle assembly and chromosome alignment are complex processes that take time to complete. During chromosome alignment, it is essential that each chromosome is attached to the spindle in such a way that sister kinetochores are attached to opposite spindle poles. Chromosome segregation must therefore be delayed until this state can be reached. To do this, cells retain a system to monitor and correct microtubule-kinetochore attachments while delaying sister chromatid separation. This system is called the spindle assembly checkpoint (SAC) (Figure 1.6, reviewed in [138] and [139]). The core purpose of the SAC is for unattached kinetochores to generate a diffusible signal, the mitotic checkpoint complex (MCC), the creation of which is critically dependent on the activity of the kinase MPS1 localized to unattached kinetochores (Figure 1.6A, [138]). MCC is composed of MAD2, BUB3, BUB1 and BUBR1 which bind and sequester CDC20, an activating cofactor of the anaphase promoting complex/cyclosome (APC/C) E3-ubiquitin ligase [138, 140]. With CDC20 bound, the APC/C ligase activity can target two key substrates – cyclin B and securin – for proteasomal degradation [141, 142]. Securin and cyclin B both protect sister chromatid cohesion by inhibiting the cohesin protease separase and thus their degradation is required for the cell to trigger mitotic exit [142-144]. Sequestration of CDC20 by the MCC

precludes ubiquitination of cyclin B and securin by APC/C, preventing mitotic exit [145]. Furthermore, MCC has been proposed to bind and directly inhibit assembled APC/C^{CDC20} complexes, however the exact APC/C inhibition mechanism has not been firmly established [145]. Other factors linked to the SAC also contribute to APC/C inhibition. PLK1 has been shown to bind to BUB1, allowing it to phosphorylate and inhibit CDC20 [146, 147], thus promoting SAC activity. In addition, CDK1-cyclin B directly phosphorylates subunits of the APC/C and modulates its activity [148, 149].

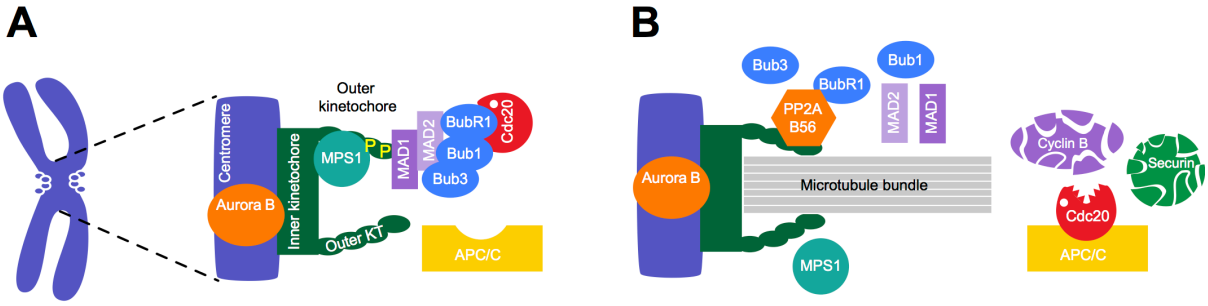


Figure 1.6 - The spindle assembly checkpoint. (A) MPS1 is recruited to unattached kinetochores and phosphorylates a component of the outer kinetochore. MAD1 is recruited to this phosphorylated locus and promotes the assembly of MCC, composed of MAD2, BUB1, BUB3 and BUBR1. The MCC complex binds CDC20, sequestering it from the APC/C. **(B)** Correctly attached kinetochores displace MPS1, allowing PP2A-B56 to turn over MPS1 phosphorylations and resulting in the cessation of MCC production. Pre-existing MCC is disassembled, allowing the association of CDC20 with APC/C, activating it and allowing it to target cyclin B and securin for degradation.

The SAC is integrated with a complementary pathway that allows the correction of erroneous microtubule-kinetochore attachments (reviewed in [150]). These errors manifest in several ways. Syntelic attachments occur when both sister kinetochores attach to microtubules emanating from the same spindle pole. Sister chromatids attached in this way would segregate to the same daughter cell, causing aneuploidy [150]. A second type of erroneous attachment is merotelic. In

this case, one sister kinetochore is linked to one pole, whereas the other binds microtubules from both spindle poles [150]. These attachment types have different geometries to the correct, amphitelic attachments where kinetochores of sister chromatids are attached to microtubules originating from opposite poles. The correction of microtubule-kinetochore attachment errors appears to operate through a mechanism dependent on tension [131]. Syntelic attachments do not generate tension, as a pulling force is applied unidirectionally on both sister kinetochores. This is detected by an Aurora B-dependent pathway which destabilizes the attachment, opening the kinetochore to another attempted attachment event [151]. Correctly attached sister kinetochores are pulled equally towards the opposite spindle poles, spatially distorting the inter-kinetochore material [152]. This increases the distance between Aurora B and its targets on the outer kinetochore, resulting in its inability to destabilize the attachment [152]. Furthermore, PP2A-B56 is required to stabilize microtubule kinetochore attachments by counteracting Aurora B [153]. Depletion of B56 regulatory subunits therefore results in the inability to attach kinetochores to mitotic spindles, resulting in constitutive SAC activation [153, 154]. Once chromosomes are attached to the spindle, two PPPs have been proposed to mediate SAC silencing – PP2A-B56 and PP1 [155]. Both phosphatases have been suggested to counteract Aurora B phosphorylation, and PP2A-B56 additionally removes at least a subset of the critical MPS1 phosphorylation on the outer kinetochore [154, 155]. This system is also regulated by PLK1, which binds and phosphorylates BUBR1 [147]. The PLK1-phosphorylated pool of BUBR1 then recruits PP2A-B56 and promotes its checkpoint silencing activity [156]. In addition, PLK1 activity is required for the formation of stable kinetochore-microtubule attachments [120]. Thus, depending

on context, distinct pools of PLK1 serve both SAC-promoting and SAC-silencing functions.

Merotelic attachments pose a unique problem for this regulatory system, as they do generate tension. For this reason, they sometimes escape detection and the cells progress into anaphase without correcting them [150]. As a consequence, the sister chromatid attached to both poles cannot segregate in anaphase and gets trapped in the middle of the dividing cell [157].

1.8 Cyclin B destruction permits chromosome segregation

Once the bipolar spindle has formed and all of the chromosomes are correctly attached, they are aligned in the middle of the cell. This marks the beginning of metaphase. If all attachments are correctly made, the SAC is silenced, stopping the production of MCC while the previously generated MCC is gradually disassembled (Figure 1.6B, [158]). Once sufficient MCC is removed, APC/C inhibition is relieved and the enzyme can start to ubiquitinate cyclin B and securin, targeting them for degradation [142]. However, the degradation process is gradual and during this time, the cell can still reengage the SAC if attachment defects occur, halting further degradation [159]. Once sufficient cyclin B and securin are degraded, two major events – loss of sister chromatid cohesion and loss of CDK1 activity – trigger anaphase entry [142-144]. Degradation of cyclin B and securin first result in the activation of separase [143, 144]. This protease then cleaves cohesin rings, resulting in the disjunction and separation of sister chromatids [143, 144]. Once the separation has occurred, the cell cannot reengage the SAC or prevent division, due to further degradation of cyclin B, which causes complete deactivation of CDK1 (Figure 1.7A)[160]. PP1 can then overcome inhibition and deactivate MASTL [67]. As a result, the production of phosphorylated ENSA

(pENSA) ceases and PP2A-B55 starts turning over the pre-existing pool of pENSA [11, 137]. This creates a small delay in the activation of the phosphatase which is important to correctly time the events during mitotic exit [137]. Activation of PP2A-B55 allows the turnover of CDK1 phosphorylation, enabling many biochemical and structural rearrangements [137]. However, PP2A-B55 activity does not account for the turnover of all CDK1 sites, and the current view is that PP1 is the second major CDK-counteracting phosphatase in mitotic exit [12].

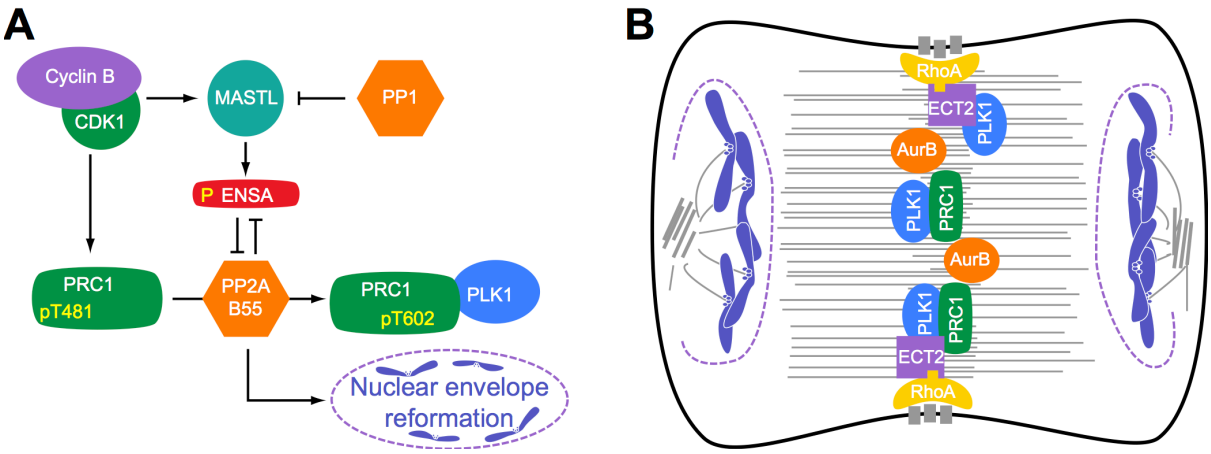


Figure 1.7 - Control of anaphase and cytokinesis events in vertebrate cells.
(A) CDK1:cyclin B prevents chromosome segregation and the activation of cytokinesis factors such as PRC1. Degradation of cyclin B results in the deactivation of CDK1 and the activation of PP1, which in turn inhibits MASTL kinase. The production of phosphorylated ENSA, the inhibitor of PP2A-B55, ceases, and the phosphatase turns over the existing pool, reaching full activity in anaphase. Dephosphorylation of PRC1 pT481, a CDK1 site, allows the phosphorylation of pT602 and binding of PLK1. This complex then organizes the core of the central spindle and regulates the recruitment of other cytokinesis factors. In later stages, PP2A-B55 activity promotes nuclear envelope reformation. **(B)** PLK1 and AurB recruit and regulate numerous cytokinesis factors, including ECT2, the activator of RhoA. Active RhoA then locally alters actin filament dynamics, causing the formation and contraction of the contractile ring, which severs the cells in half.

These general changes in cellular biochemistry result in altered microtubule dynamics, and K fibres are rapidly depolymerised with the assistance of kinesins, driving chromosome segregation [161]. Furthermore, a new microtubule structure – the central spindle – forms between the segregating chromatin masses (Figure 1.7B). The formation of the central spindle is allowed through dephosphorylation of several proteins [113, 137]. Key among these is PRC1. Dephosphorylation of PRC1 pT481 by PP2A-B55 allows PRC1 to be phosphorylated and bound by PLK1, which increases its affinity for microtubules and allows it to organize the antiparallel microtubule structure termed the midzone [136, 137, 162]. This is the core of the central spindle and serves as a recruitment platform for several other factors which regulate central spindle microtubule dynamics and, subsequently, cytokinesis [136]. Many of these factors are regulated by PLK1 and Aurora B, which remain active despite the loss of CDK1 activity [163-165]. PLK1 is affixed to the central spindle via its interaction with PRC1, and Aurora B is transported from the centromeres and recruited to the midzone as part of the chromosomal passenger complex (CPC) [166]. Aurora B then limits microtubule growth by activating the kinesin KIF4A, but this effect is counteracted by PP2A-B56 [167].

Despite the checkpoint surveillance system, some errors persist or only manifest in anaphase during chromosome segregation. These lead to the induction of DNA damage or aneuploidy (reviewed in [168] and [157]) explaining why cells have evolved multiple robust checkpoints and quality control mechanisms prior to commitment to chromosome segregation. Two hallmarks of errors can be observed: chromatin bridges and lagging chromosomes (Figure 1.8A). Chromatin bridges are contiguous DNA strands that connect two segregating chromatin masses. Normally, these are unwound by the concerted

action of the PICH and BLM helicases, and topoisomerases [169, 170]. However, if this system fails due to an impairment of these factors or perturbations of chromosome architecture, a bridge will form. In most cases, bridges are resolved before the completion of cytokinesis, but if they are not, the cleavage furrow will cut through the chromatin, inducing DNA damage [171]. Furthermore, one cell will receive an expanded chromosome while the other will be deficient, altering the genome of both daughter cells [171]. Chromosome bridges also occur when the cell attempts to segregate chromosomes with two centromeres, which can be created by aberrant replication or DNA repair (Figure 1.8A) [157]. In this case, the bridge can only be broken by the cleavage furrow. The term lagging chromosome is used to describe an entire sister chromatid which does not segregate with the rest of the chromatin mass [157]. This is most often caused by two aberrations: uncorrected merotelic attachments, which manifest in a non-segregating chromatid, or a change in microtubule dynamics, which slow segregation [157, 172]. Lagging chromosomes almost always get encased in a separate micronucleus [157]. Micronuclear envelopes are poor in nuclear pore complexes and therefore lack the normal complement of factors present in a main nucleus [173]. As a result, micronuclei are highly aberrant environments and prone to bursting in interphase [173]. The consequences of these differences are dramatic. DNA in micronuclei is highly prone to DNA damage, and chromosomes are often shattered and rearranged in a process termed chromothrypsis [157, 173]. Furthermore, replication of micronuclear DNA is inefficient [173]. Due to these defects, it has an exceedingly high mutation rate [157, 173].

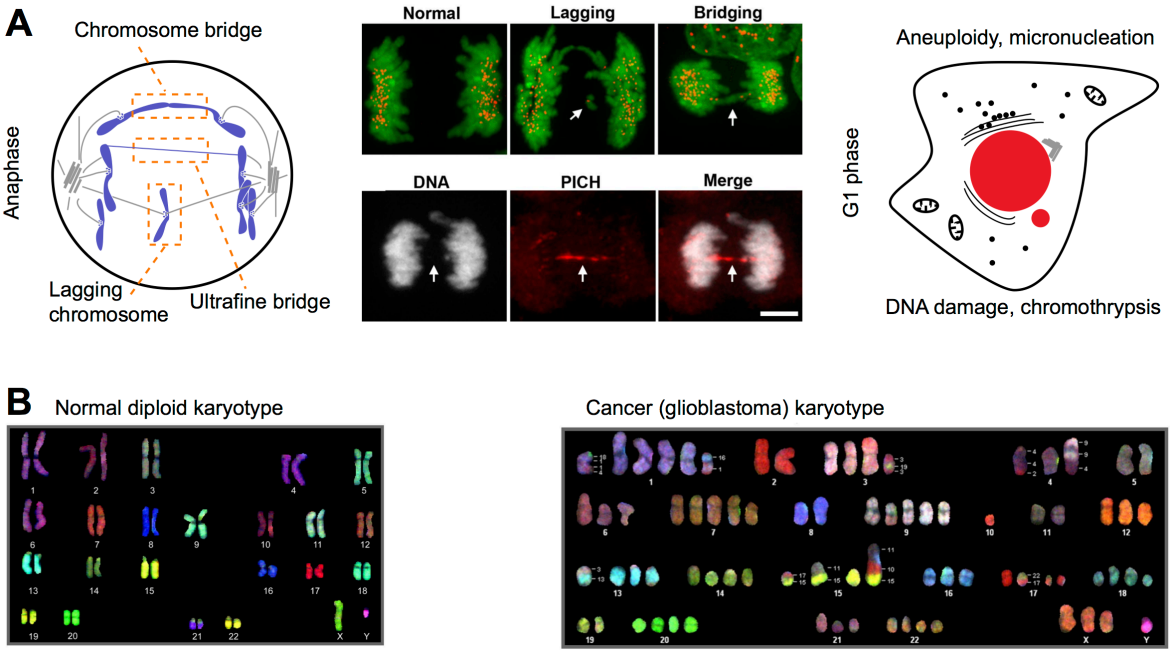


Figure 1.8 - Chromosome segregation defects in anaphase and their consequences. (A) Three types of segregation defects are often observed - chromosome bridges, ultrafine bridges and lagging chromosomes. Chromosome bridges are generated by unresolved sister chromatids. Ultrafine bridges are single DNA strands difficult to visualize with DNA dyes, coated with helicases such as PICH and BLM. Lagging chromosomes are most commonly the result of erroneous kinetochore attachments. These defects promote genome instability through aneuploidy, micronucleation and DNA damage. Further aberrations can result in chromothrypsis - the shattering and rearrangement of entire chromosomes. (images reproduced from [157]) **(B)** Cancers which successively divide with anaphase defects accumulate a large number of changes in their karyotype. (reproduced from [168])

Re-incorporation into the main nucleus after the subsequent cell cycle can then propagate these mutations to daughter cells. Lagging chromosomes may also result in aneuploidy, depending on whether they ultimately end up in the correct daughter cell [157]. Aneuploidy and micronucleation have long been known to be hallmarks of cancer (Figure 1.8B) [157]. Importantly, evidence suggests they are not simply a morphological consequence, but also contribute to cancer formation and adaptability [157].

1.9 Cytokinesis and nuclear envelope reformation

Anaphase and the subsequent events of mitotic exit are highly coordinated in human cells, all of the changes from sister chromatid separation to the initiation of cytokinesis occur within 10min [165]. Cytokinesis is triggered when the guanine exchange factor ECT2 localizes RhoA to the midzone-adjacent cortex and activates it (Figure 1.7B) [174]. This process is spatially and temporally integrated with chromatin segregation via the central spindle. Two kinases, Aurora B and PLK1, are critical for the correct execution of cytokinesis. They directly phosphorylate several proteins which are important for the localization and activity of ECT2 and RhoA [163, 164]. In addition, Aurora B and PLK1 control the structural integrity of the central spindle, affecting the ability of the midzone to support the cytokinesis machinery [162, 165]. The regulated accumulation of active RhoA alters actin dynamics around the spindle midzone, forming the contractile ring [174]. The actin contractile ring then pinches the cell around the midzone, separating it into two daughters [174]. Another consequence of furrow ingression is the compaction of the central spindle midzone into a very dense structure called the midbody. This contains the factors that were previously bound to the midzone and forms a template for the abscission process [136, 175]. The midbody is ultimately taken up by one of the daughter cells and most often degraded [176].

Late in anaphase and telophase, chromosome decondensation occurs and the nuclear envelope reforms around the two segregated chromosome masses [113]. The reformation is in many ways the polar opposite of NEBD. Nuclear pores are reseeded into the reforming nuclear membrane in a regulated fashion and the lamina reassembled (reviewed in [177]). Critical to this process is the activity of

PP2A-B55, which dephosphorylates several nuclear pore components, allowing them to reassemble in a defined order [113]. This contributes to the reformation of the membrane itself, and the resumption of nuclear import in telophase [113, 178]. Several factors are then sequestered into the nucleus, some of which contribute to the establishment of a G1 state or impact on events in the next cell cycle. For instance, Nuclear PLK1 in G1 allows the future deposition of the histone variant CENP-A at centromeres [179]. The spatial control of nuclear envelope reformation is highly regulated, and formation of smooth rounded nuclei is dependent on the compaction of segregating chromatin. Defects in this process result in the formation of either multilobate nuclei or multiple separate nuclei, which then potentially have an altered genomic architecture [180]. Alternatively, chromosomes that have escaped the boundaries of the chromatin mass may be encased in micronuclei [172, 180]. To mitigate this, cells employ DNA-binding kinesins and BAF1, a phosphorylation-regulated protein with a very high affinity for chromatin [180, 181]. During late anaphase and telophase, BAF1 is activated and effectively acts as chromatin glue, closing gaps between chromosomes, compacting the chromatin mass and ensuring smooth nuclear envelope reformation [180].

Cytokinesis marks the end of mitosis. However, many factors that were synthesized in G2 phase are still present in the daughter cells. These are gradually degraded due to the activity of APC/C^{CDH1}. Factors degraded in this way include PLK1 and Aurora kinases [182-185]. APC/C^{CDH1} first becomes active earlier during anaphase and promotes destruction of Aurora A and TPX2 [183, 184], while the Aurora B and PLK1 are only degraded later due to roles in regulating cytokinesis [175, 185]. Therefore, this pathway is important to restore

the cell back to its initial G1 state and ensure completion of a full cell cycle. From this G1 state the cell may differentiate, enter a quiescent state, or initiate a further round of cell growth and division.

1.10 Phosphoprotein phosphatases and cell cycle control

Like cell cycle kinases, serine/threonine phosphatases of the PPP family are important modulators of cell cycle progression and regulated in their own right. The defining feature of this regulation lies in the multi-subunit composition of PPP enzymes [186, 187]. Each functional PPP complex is comprised of a catalytic subunit providing the activity, and at least one other scaffold or regulatory subunit which confers substrate specificity and localization [186-189]. Moreover, additional layers of regulation typically converge on the regulatory subunit of the holoenzyme. Free catalytic subunits that could act non-specifically or in an unregulated fashion are degraded by the cell, as is the case with PP2A-subfamily phosphatases [190]. PPP catalytic subunits are therefore rarely found in isolation. Instead, they are either associated with chaperone proteins or incorporated into holoenzymes [190].The purpose of this system is most likely to limit non-specific activity of monomeric catalytic subunits, which would adversely affect finely balanced protein phosphorylation states.

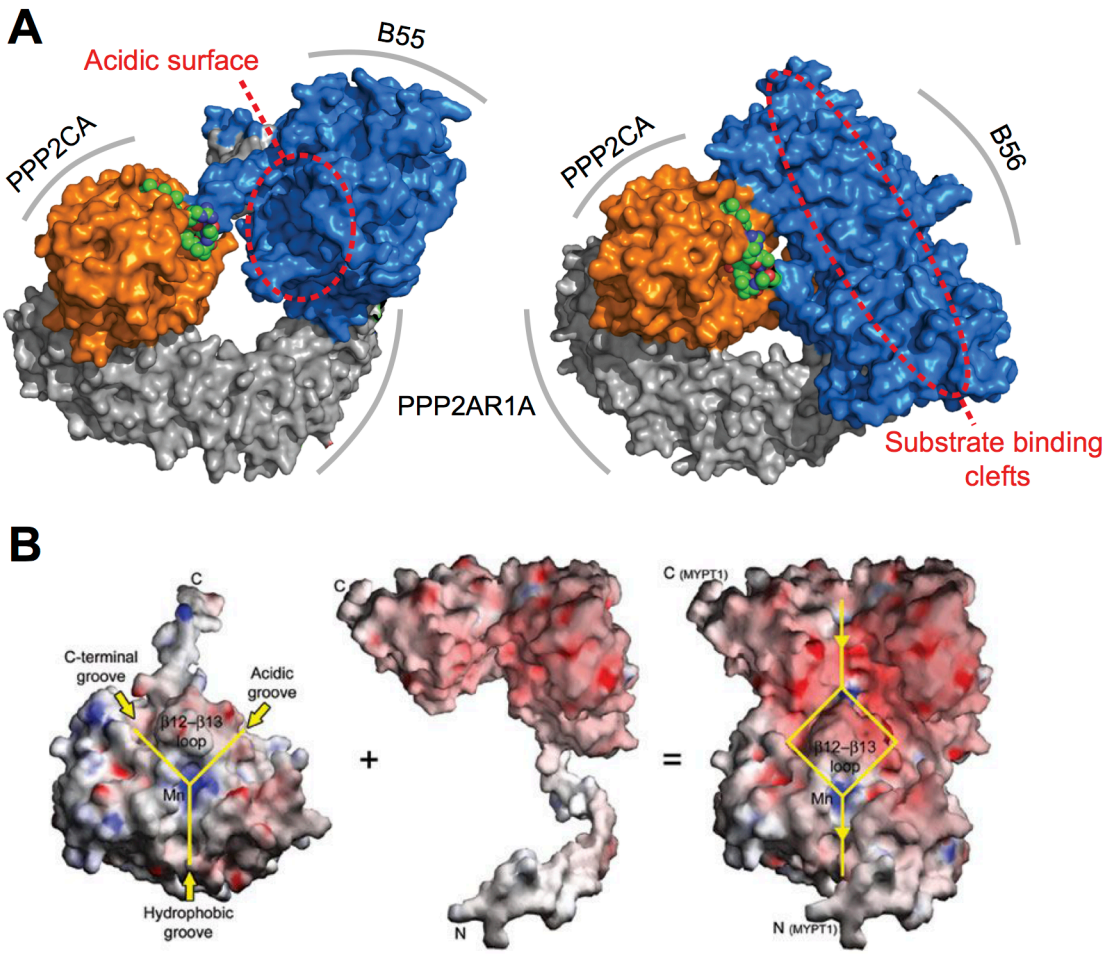


Figure 1.9 - Principles of phosphoprotein phosphatase holoenzyme regulation (A) Structures of PP2A-B55 (PDB ID: 3DW8) and PP2A-B56 (PDB ID: 2IAE) with the active site inhibitor microcystin-LR (spherical model). Architectural differences due to the regulatory B subunit provide varied modes of substrate recognition and recruitment binding partners **(B)** Structure of PPP1Cβ, MYPT1 and their complex, reproduced from [188]. Binding of MYPT1 induces conformational changes to the three substrate binding grooves on PPP1Cβ, which can then specifically accommodate myosin light chain.

The best understood PPPs in terms of the interplay between architecture and regulated function are PP2A and PP1 (Figure 1.9). PP2A holoenzymes are composed of one of two catalytic subunits (PPP2CA/B), one of four regulatory subunits (B55, B56, B'' and B''') and an additional scaffolding subunit (PPP2AR1A) [186]. The structures of two holoenzymes – PP2A-B55 and PP2A-B56 – have been solved and demonstrate well how the regulatory subunit can

affect the properties of the enzyme (Figure 1.9A). The catalytic-scaffolding core is largely unchanged between these two complexes, but the regulatory subunits are architecturally highly diverse [191, 192]. The B56 regulatory subunit is structured into an elongated series of helix-turn-helix HEAT repeats, whereas B55 forms a β-propeller structure [191, 192]. Due to these differences, the surfaces formed upon holoenzyme assembly are distinct and can account for diverse substrate selection and specific regulatory inputs. For instance, the acidic surface of B55 is important for time-resolved substrate selection during mitotic exit, wherein substrate dephosphorylation is ordered based on basicity around the phosphorylation site [113, 192]. This allows PP2A-B55 to first dephosphorylate key anaphase regulators such as PRC1, only later followed by nuclear pore proteins [113]. As a result, nuclear envelope reformation is ensured to occur after chromosome segregation under normal conditions [113]. Conversely, B56 creates an elongated, multi-character surface allowing regulation through localization and stable substrate binding [191, 193]. Two types of stable binding to PP2A-B56 have been described so far. Shugoshin 1 (Sgo1) binds across the regulatory and catalytic subunit and localizes the phosphatase to centromeres in mitosis [194]. There, the activity of PP2A-B56 protects centromeric cohesin from premature cleavage [194]. The second binding mode has been best described for the SAC protein BUBR1 wherein a small {LxxIxE} motif is specifically and stably bound by the regulatory subunit [193, 195]. An equivalent binding mode has been found for KIF4A [167, 195], indicating that this is a general feature of PP2A-B56.

The PP1-subfamily phosphatases have alternate regulatory properties. The catalytic subunit (PP1Cα/β/γ) can associate with up to two hundred different binding partners, with varied consequences [187]. Some, such as the outer

kinetochore component KNL1, have been suggested to localise the phosphatase and thus regulate its function [189], while others directly regulate substrate selection and phosphatase activity. Two well described proteins from the latter group exemplify this concept well – MYPT1 and spinophilin. A PP1 catalytic subunit has three putative substrate binding sites of different characters, which are thought to control substrate selection [188, 196]. Binding of spinophilin to PPP1Cα blocks one of these sites, allowing activity only against its specific substrate – the AMPA receptor (GluR1) [196]. Similarly, MYPT1 specifically binds to PPP1Cβ, obscuring one substrate binding site and additionally altering the phosphatase catalytic site to enhance specific targeting to myosin (Figure 1.9B)[188]. These properties indicate that certain PP1-regulator complexes behave equivalently to PP2A holoenzymes in terms of substrate selection and regulation.

Both PP2A and PP1 phosphatases can also be regulated by other means. Notably, several means of inhibition have been characterized. The ENSA-MASTL inhibitory pathway providing a competitive inhibition mechanism against PP2A-B55 has already been described earlier [62, 137]. In addition, PP2A phosphatases are regulated by other inhibitory stable binding partners. One such protein is CIP2A, which can bind to PP2A-B56 [197]. Similar to ENSA, CIP2A has been proposed to function as an active site competitive inhibitor, but this has not been extensively verified. PP1 can also be inhibited by binding partners. In particular, the disordered protein inhibitor 2 (I-2) binds to PP1 catalytic subunits, blocking several substrate and regulator binding sites and displacing active site metal ions [198]. As a result, the inhibition is highly efficient. It has also been suggested that PP1 is directly inhibited by phosphorylation of T320 [199]. This phosphorylation is

created by CDK1-cyclin B1 upon mitotic entry, allowing temporal control of PP1 activity during the cell cycle [199]. In concert, these pathways allow for the precise regulation of phosphatase activity, which can be deployed upon specific spatial and temporal cues against a wide range of substrates.

1.11 Aurora and Polo kinase activation

Control of CDK activity in the cell cycle is allowed through multi-layered regulation by binding partners, localization and phosphorylation. As already explained, CDKs alone are insufficient to support all cell cycle processes, particularly those revolving around chromatin condensation, mitotic spindle formation and cytokinesis. Rather, these processes require Aurora A and PLK1, which are also controlled by a multi-layer regulatory system.

The major requirement for their activation is the phosphorylation of a structural element called the activation segment or T-loop. This feature is shared with many other kinases, including CDKs and MPS1 (Figure 1.10A) [55, 200]. The structural rearrangements caused by this phosphorylation have been well described for Aurora A and its T-loop residue T288 [201]. X-ray crystallography has revealed that the unphosphorylated T-loop is in an open conformation away from the kinase core [201]. Once phosphorylated, several interactions can be formed between the phosphate and basic residues within the kinase, resulting in the T-loop flipping back to a closed conformation [201]. This movement is proposed to create a substrate binding platform and form the core of the kinase active site that correctly positions the donor ATP molecule [201]. A further critical event is the binding of the activating partner – the microtubule nucleator TPX2.

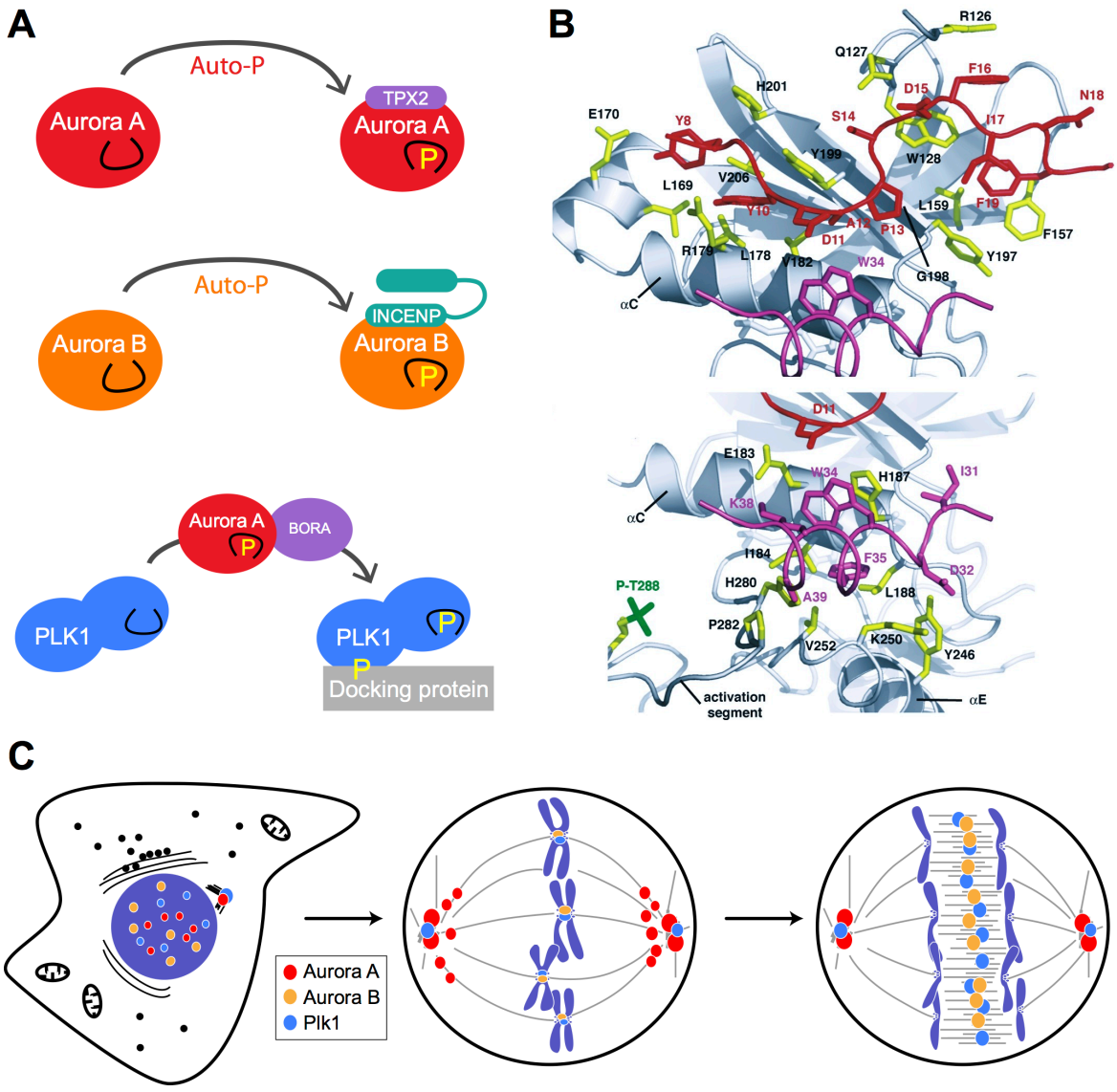


Figure 1.10 - Principles of Aurora and Polo kinase regulation. (A) Aurora A and B autophosphorylate their T-loops, switch to the active conformation and bind the activator proteins TPX2 and INCENP, respectively. The T-loop of PLK1 is phosphorylated by aurora A in the presence of the cofactor Bora. Active PLK1 can then bind to short phosphorylated motifs on docking proteins via its polo-box domain and phosphorylate targets in close proximity. **(B)** Binding interface between T-loop-phosphorylated aurora A (yellow residues) and the N-terminus of TPX2 (red and magenta residues). TPX2 binding stabilizes the closed conformation of the T-loop through two sets of interactions with the kinase. This conformation forms a substrate binding platform, positions the donor ATP and sterically shields AurA pT288 from phosphatases. **(C)** Localization pattern of Aurora kinases and PLK1 changes throughout the cell cycle, reflective of their differential regulation by binding partners.

The N-terminus of TPX2 forms numerous interactions with residues in and close to the Aurora A T-loop, stabilizing the closed conformation (Figure 1.10B)[201]. This serves two purposes: the structural stabilization of the active kinase conformation and protection from phosphatase activity [201]. In the absence of TPX2, the T-loop phosphorylation is highly unstable and a target of phosphatases [201]. Notably, the abundant PP1 has been shown to dephosphorylate monomeric Aurora A pT288 *in vitro*. However, no activity could be detected against a complex of Aurora A and the minimal Aurora A-binding N-terminal fragment of TPX2 [201]. This finding is in good agreement with the structure of this complex, wherein the T-loop phosphorylation is largely inaccessible to approaching proteins due to steric hindrances. The interaction with TPX2 also localizes Aurora A to the mitotic spindle in mitosis, particularly enriching it at spindle poles (Figure 1.10C) [202]. Consistently, only pole-associated Aurora A is pT288-positive under normal conditions [172]. An additional mechanism of Aurora A activation has been described, through binding of TACC3 [114]. This binding occurs at a site distinct from TPX2 and does not cause the T-loop rearrangement into a closed conformation [133]. Consequently, PP1 is able to dephosphorylate the Aurora A T-loop within this complex [114]. However, the binding still promotes Aurora A activity towards TACC3 and other substrates, influencing mitotic spindle assembly, and thus may be relevant for Aurora A regulation in specific circumstances [114].

The paralogous kinase Aurora B has an equivalent system of control, albeit it is channelled to entirely different pathways *in vivo*. It too can auto-activate by phosphorylating its T-loop and associates with an activator protein, INCENP, integrating it into the chromosome passenger complex (Figure 1.10A). INCENP

binding to Aurora B is architecturally different than in TPX2 and Aurora A, but has the same consequence – conformational change of the kinase and protection of the T-loop phosphorylation [203]. Although Aurora B is highly similar to Aurora A in sequence, the difference in binding partners allows it to localise to centromeres in mitosis and to the central spindle in anaphase (Figure 1.10B)[167, 203, 204]. The binding partner is the critical determinant to differential localisation and function of Aurora A and Aurora B, while the kinase itself only makes limited contributions. Mutating G198 in Aurora A to the asparagine found in Aurora B creates a semi-functional, INCENP-associated protein which can localise to centromeres and the central spindle, and partially perform Aurora B functions [205]. This is consistent with the additional finding that Aurora A and Aurora B are able to phosphorylate the same substrates *in vitro* [201, 204, 205]. Due to this reason, differential localization of the two kinases *in vivo* is likely a crucial regulatory mechanism.

Unlike Aurora A and Aurora B, PLK1 does not appear to autophosphorylate its T-loop. Rather, evidence suggests that it is phosphorylated by Aurora A (Figure 1.10A). The T-loop sequence of PLK1 conforms well to the Aurora A phosphorylation consensus motif and depletion or inhibition of Aurora A both reduce the levels of the T-loop phosphorylation on PLK1 T210, which first occurs in G2 phase [76]. However, the reaction is inefficient in the absence of the essential protein Bora, which increases the activity of Aurora A towards PLK1 T210 *in vitro*, although the underlying mechanism is unclear [76, 206]. Furthermore, depletion of Bora results in failure to activate PLK1 through T-loop phosphorylation *in vivo* and delays mitotic entry, in line with the role of PLK1 in CDC25C activation [76, 206]. Once they enter mitosis, cells depleted of Bora

exhibit severe mitotic spindle defects [207]. Activated PLK1 then phosphorylates Bora, targeting it for SCF-mediated degradation [207]. Because of this, mitotic cells do not have an appreciable amount of Bora, but residual amounts have been proposed to promote consistent PLK1 T210 phosphorylation [208].

In contrast to Aurora kinases, T-loop phosphorylated PLK1 does not require stable binding partners to maintain the active state. Instead, PLK1 employs binding partners to control its localization and function (Figure 1.10C). Several such proteins have so far been described, including BUBR1, Bora and CDC25C [56, 147, 207]. These are bound through the specific tandem polo-box domain (PBD) on PLK1 [209]. The PBD domain binds short phosphorylated motifs {S-[pS/pT]-[P/X]}, providing protein and site specificity to the interactions. The basis for specific binding of phospho-sites is provided by two critical residues: H538 and K540, which form a small clamp tightly binding the phosphorylated serine or threonine [210, 211]. Consequently, mutating these residues to alanine prevents the interaction with PBD-mediated binding partners [210, 212]. PLK1 docking-motifs are often target sites for CDKs [162]. Thus, PLK1 function can be controlled through cell-cycle mediated control of PLK1 docking, but in some cases, such as PRC1, PLK1 can phosphorylate its own docking site [162]. Once bound, PBD partners of PLK1 are often also its substrates and this holds true for BUBR1, Bora and CDC25C among others [57, 147, 207, 212]. Thus, PLK1 activity can be targeted through binding, modulating its function.

It has also been observed that ongoing PLK1 activity is required to maintain Aurora A pT288 in mitosis [207]. A model has been proposed wherein PLK1 inhibition results in the stabilisation of Bora, which binds Aurora A and sequesters it from TPX2 [206]. Indeed, *Drosophila* Bora can stably bind Aurora A [213], but

this interaction has proven difficult to detect in mammalian cells [72]. This model would additionally require the continued presence of Bora in mitosis, which is not consistent with the observed SCF-dependent degradation at G2-M [207]. Therefore, the underlying mechanistic properties of this pathway remain poorly understood.

1.12 Negative regulation of Aurora A by protein phosphatase 6

The absolute requirement of the T-loop phosphorylation for activity of Aurora and Polo kinases makes this feature a potential target for regulation. Additional requirements to stabilize the phosphorylation, such as activating binding partners in Aurora kinases, provide a part of it. However, this one-way control is inherently static and irreversible. Dynamic control can only be established by adding the counteracting activity of a phosphatase. Using a combination of biochemical and cell biological analysis, protein phosphatase 6 (PP6) was identified as a specific T-loop phosphatase for Aurora A *in vitro* and in mitotic cells [172]. However, T-loop phosphatases have thus far not been found for Aurora B or PLK1. Uniquely, PP6 has been shown to dephosphorylate Aurora A pT288 in Aurora A-TPX2 complexes both using purified proteins and in cell extracts (Figure 1.11A)[172]. Additionally, loss of PP6 activity by inactivating mutations in cancers or experimental depletion results in higher steady state levels of Aurora A pT288, followed by its spread from spindle poles to other sections of spindle microtubules (Figure 1.11B)[172, 214]. Morphologically, spindles are highly abnormal in these cells with excessive microtubule bundling, spindle positioning defects and intermittent pole fragmentation, consistent with SAF deregulation due to Aurora A hyperactivity (Figure 1.11B)[172]. Furthermore, defects in anaphase can be observed [172]. The chromatin masses do not segregate as compact masses and

lagging chromosomes often occur (Figure 1.11B)[172]. More frequent formation of merotelic attachments would provide the simplest explanation, but direct evidence for this is lacking. However, this scenario is likely, as the aberrant spindles do not function correctly at the kinetochore-microtubule interface, thus being prone to errors [172]. In addition, the altered localization of Aurora A could interfere with the Aurora B-dependent error correction pathway, as the kinases have the potential to target the same substrates. Consistent with kinetochore-microtubule attachment defects and a SAC challenge, mitosis is extended in PPP6C-depleted cells [172]. Altered spindle remodelling dynamics in anaphase due to architectural defects of the spindle and Aurora A deregulation can also contribute to the anaphase defects. As a result, PP6-null melanoma cells have a high incidence of micronucleation compared to those expressing WT PPP6C (Figure 1.11C) [172, 214].

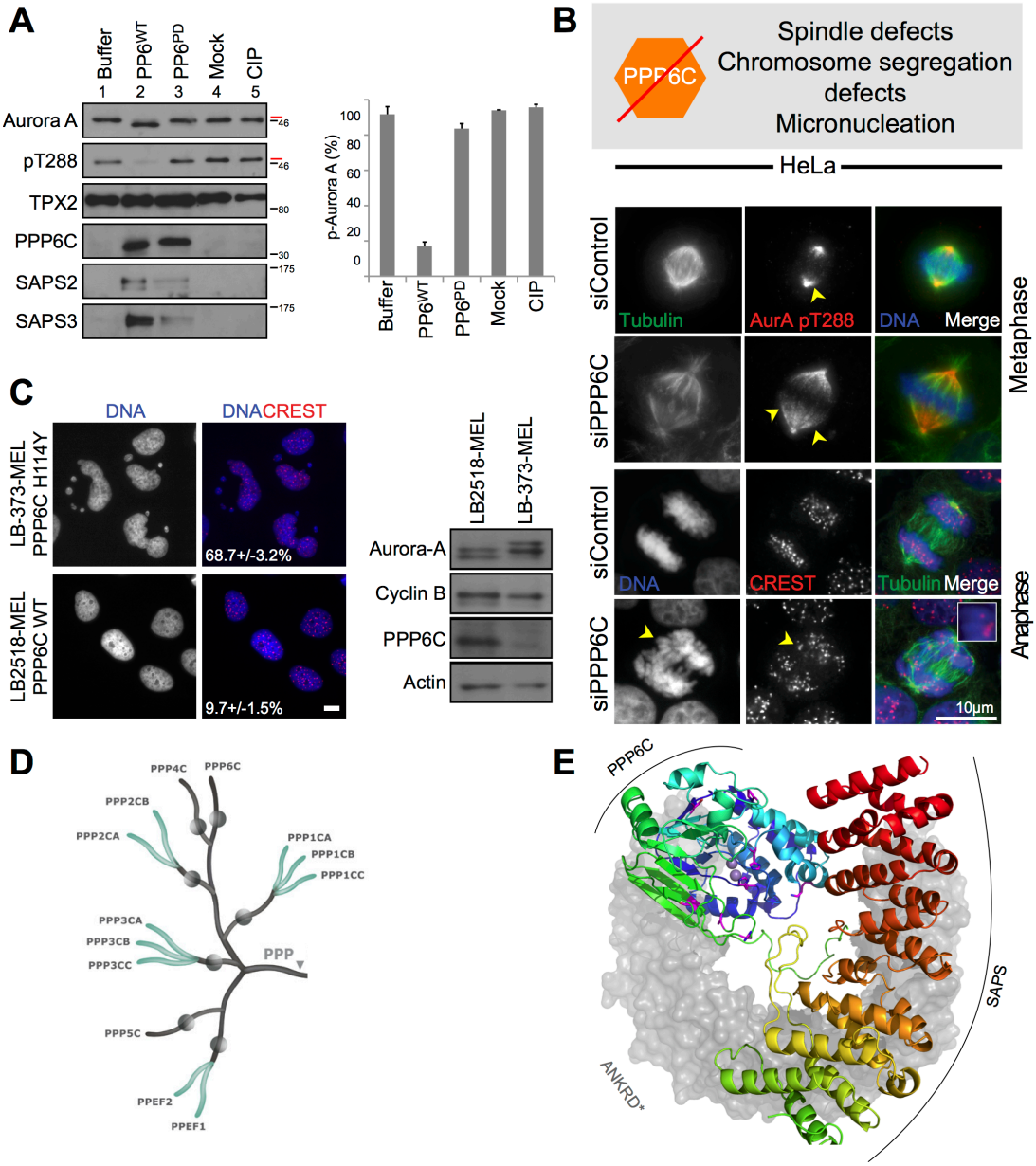


Figure 1.11 - Protein phosphatase 6 is a cancer-associated AurA T-loop phosphatase from the PP2A family. (A) PP6 can dephosphorylate AurA pT288 in complex with TPX2, unlike a broad specificity phosphatase such as calf intestinal phosphatase (CIP). Reproduced from [172] **(B)** PPP6C depletion causes mitotic spindle defects and spread of active AurA on mitotic spindles, followed by defects in chromosome segregation in anaphase. Anaphase images reproduced and adapted from [172] **(C)** Melanoma cells with destabilizing PPP6C mutations exhibit an increased incidence of micronucleation, and an increased ratio of active/inactive AurA compared to canonical, BRAF-mutated patient cells. **(D)** Phylogeny of human PPPs reproduced from [215] (branches not to scale) reveals that PPP6C is associated with the PP2A phosphatase family. **(E)** Computational model of a PP6 holoenzyme, reproduced from [214], resembling a PP2A-B56 holoenzyme.

1.13 Functional and architectural properties of PP6

PP6 is a PP2A family phosphatase (Figure 1.11D). Like PP2A holoenzymes, mammalian PP6 is composed of a catalytic subunit (PPP6C), one of three ankyrin repeat containing subunits (ANKRD28/44/52) and one of three Sit4-associated subunits (SAPS1/2/3) [216-219]. However, little is known about the properties of the PP6 holoenzyme. Predictive structural modelling suggests that SAPS subunits are regulatory, similar to the role of B56 in PP2A (Figure 1.11E)[214]. Consistently, SAPS subunits are predicted to be composed of HEAT repeats and thus may have similar structural properties to B56 [214, 220]. On the other hand, ANKRD subunits, composed of helix-turn-helix ankyrin repeats [218], would perform a scaffolding role, akin to PPP2AR1A. However, this has not been clearly established and different studies in the literature claim either SAPS or ANKRD subunits are regulatory [172, 217, 221]. Indeed, both ANKRD and SAPS subunits appear important for selectivity. ANRKD52 has been proposed to target a subset of PP6 to micro-RNA processing via regulation of Argonaute [222]. SAPS1 was suggested to be important for the DNA damage response, owing to preferential association with DNA-PK, while other studies have suggested that DNA-PK interacts ubiquitously with PP6 holoenzymes [221, 223]. Further literature suggests links to the viral infection response [224], BRCA1-mediated homologous recombination [225] and condensin regulation [226]. However, few of these studies directly validate the proposed substrates or test the contribution of the other subunits in comparison. Thus, currently the only directly validated PP6 substrate is Aurora A pT288.

1.14 The carcinogenic PP6-Aurora A interplay

Aurora A has been extensively described as an oncogene and its amplification has been linked to increased cancer adaptability and poor disease outcomes [227-229]. This can occur in two ways, both of which have been documented in human cancer patients: overexpression of the Aurora A protein or increased kinase activity due to aberrant regulation [214, 230]. Overexpressed Aurora A has been found in a myriad of cancer types, including leukaemia, lung and skin cancer [227, 231, 232]. Because Aurora A auto-activates, this alone may be sufficient to result in amplified kinase activity. On the other hand, point mutations are less commonly observed, but can affect the different properties of Aurora A. In particular, the V174M mutation increases kinase activity compared to WT, while other characterized mutations either inactivate the kinase or alter its regulation by TPX2 [230].

The activation status of Aurora A also increases if PP6 activity is reduced [172]. It is therefore unsurprising that in recent years numerous mutations in PPP6C have been found in human cancers, in particular melanoma [214, 233]. The effects of many of these mutations have been characterised, and they largely cause compromised holoenzyme assembly and/or reduced phosphatase activity [214]. This generates a compounded loss-of-function effect *in vivo*, because monomeric PPP6C is additionally subject to degradation. As a result, cells harbouring mutations that completely compromise holoenzyme assembly, such as H114Y, lack the PPP6C protein (Figure 1.11C)[214]. Loss of PP6 function then translates into Aurora A hyperactivity due to increased steady state T-loop phosphorylation, causing its mislocalization on the mitotic spindle, spindle architecture defects and the formation of micronuclei in these cancers [214]. The

micronuclei become hotspots for DNA damage and genomic rearrangements, and most likely confer an adaptive advantage to the growing tumour [214]. Treating PPP6C-mutated melanoma cells with low dose Aurora A inhibitors results in a reduction in micronucleation frequency, indicating that the observed micronucleation and mitotic defects are Aurora A-dependent [214]. Perturbations in expression of PPP6C have also been discovered with high frequency in several cancer types, including melanoma and ovarian cancer [233]. Due to these observations and its role in suppressing the oncogenic potential of Aurora A, mutations or other perturbations in PP6 are now considered cancer drivers [233]. However, evidence suggests that PP6 mutations are rarely the isolated trigger for cancer formation [234]. Rather, mutations in the MAP kinase pathway or cell cycle regulators such as the p53 response seem to additionally be required [234].

The prevalence and frequency of these Aurora A amplifications suggest that increased and robust Aurora A activity is beneficial for the development or survival of cancer. Aurora A inhibition is therefore considered a viable strategy to treat Aurora A-amplified cancers (The Cancer genome atlas, 2015)[235]. The most promising results were obtained with the specific Aurora A inhibitor MLN8237 (Alisertib), but the success rate is variable. Haematological cancers with high proliferation rates, such as leukaemia, show a significant therapeutic benefit [232, 236]. On the other hand, solid tissue tumours which proliferate more slowly show a limited positive response to the treatment [237, 238]. The most pronounced effects of Aurora A inhibition are observed in mitosis, where it prevents bipolar spindle formation and thus chromosome segregation. Therefore, the differential proliferation rates could explain the variation in efficacy, but this has not been mechanistically demonstrated [238]. An additional limitation presents

itself in patients with overexpressed Aurora A, which have been observed to receive less therapeutic benefit from Aurora A inhibitors [237].

To overcome these limitations and allow the design of more effective cancer treatments, we need to understand the systems regulating Aurora A at the mechanistic level and to inform or devise strategies complementary to Aurora A inhibition. While the activation requirements of Aurora A by TPX2 are well understood, the counteracting phosphatase PP6 is not. In part this is because of the complexity presented by multiple PP6 regulatory and scaffold subunits. The specific aims of this project were therefore to characterize the different isoforms of PP6 present in human cells, to assess the contribution of these different PP6 holoenzymes in Aurora A control, and investigate how these forms are regulated in the context of the cell cycle, finally pinpointing their potential functions in cells.

Chapter 2 Functional characterization of PP6 holoenzymes

2.1 Preparation of PP6 holoenzymes

To directly investigate the determinants of PP6 holoenzyme regulation, direct *in vitro* activity assays were performed. These firstly required active PP6 holoenzymes of defined composition and a good model substrate. Previously, specific and active PP2A-B55 and PP2A-B56 complexes had been purified from mammalian cells [137, 167]. Therefore, a similar approach was adopted, wherein PP6 complexes would be purified from mammalian cells using FLAG-tagged SAPS subunits as bait and assayed against Aurora A-TPX2 complexes purified in a similar fashion. To find optimal purification conditions, a FLAG-based purification procedure was performed on a previously described cell line stably expressing PPP6C-FLAG [172] under varying lysis and elution conditions (Figure 2.1). Lysis with Triton X-100 gave consistently better yields than the commonly used NP40, but elution was less than optimal under these initial buffer conditions (Figure 2.1A). Inclusion of low amounts of Triton X-100 in the elution buffer improved the elution efficiency substantially whereas varying pH did not (Figure 2.1B – compare E1 and AE fractions). Based on this outcome, PP6 holoenzymes were purified using lysis with Triton X-100 and elution at pH7.4 with 0.1% (v/v) Triton X-100 for subsequent experiments.

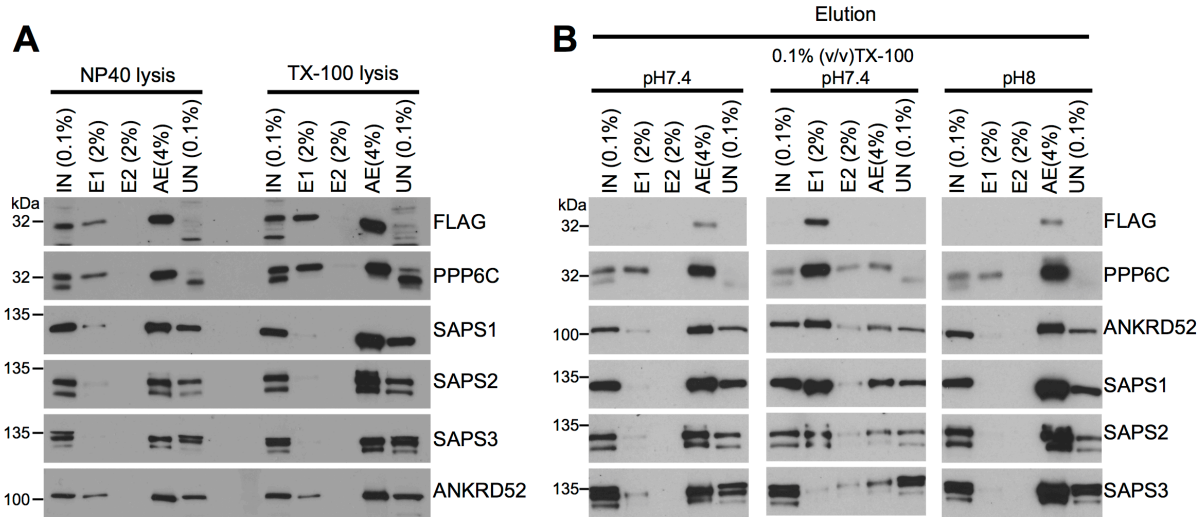


Figure 2.1 - Optimization of PP6 holoenzyme purification using cells stably expressing PPP6C-FLAG. (A) Cells stably expressing PPP6C-FLAG were lysed in buffers as indicated (see materials and methods), followed by a FLAG-based purification procedure and analysis by western blotting. **(B)** Cells were lysed in TX-100 lysis buffer and treated as in (A). Elution was performed with varied buffer conditions as indicated (detailed in materials and methods). IN = input, E1 = elution 1, E2 = elution 2, AE = after elution, UN = unbound

This procedure was then applied to isolate single SAPS-containing enzymes from asynchronous HeLa S3 cells transiently transfected with FLAG tagged SAPS1/2/3 (Figure 2.2A-C). SAPS1 (Figure 2.2A), SAPS2 (Figure 2.2B) and SAPS3 (Figure 2.2C) expressed and remained associated with PPP6C and ANKRD52 during purification under these conditions, indicating that the preparations contained assembled holoenzymes. SAPS3 was expressed at lower levels than either SAPS1 or SAPS2. This behaviour was observed over multiple experiments using different tags at both termini (Figure 2.2, Figure 2.3C, Figure 2.9B), suggesting that SAPS3 has a feature limiting its expression in this system.

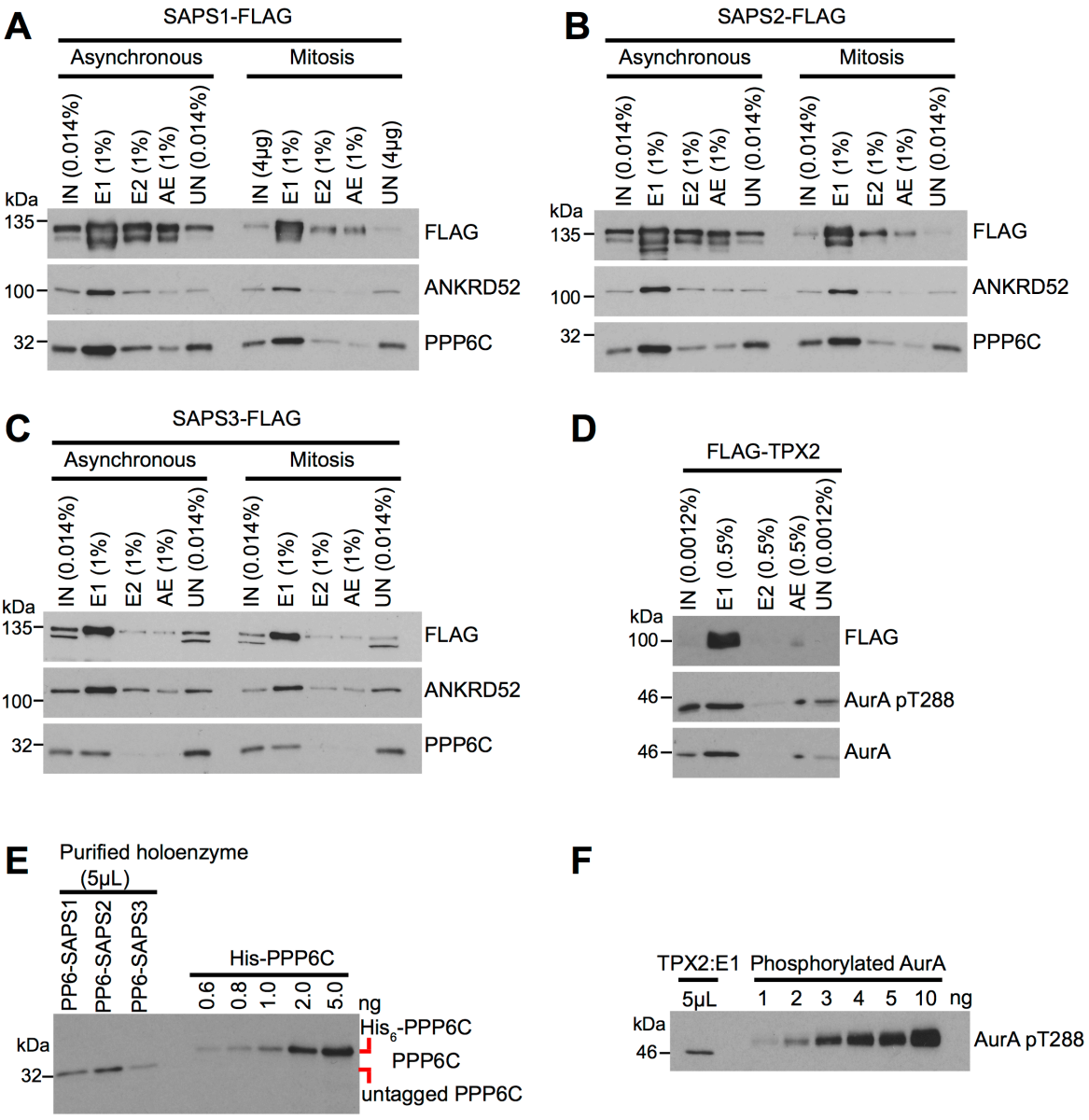


Figure 2.2 – Phosphatase and Aurora A purification and titration. (A-D) HeLaS3 cells were transfected with FLAG tagged proteins as indicated. For AurA purification, cells were arrested in nocodazole and treated with 100nM Calyculin A before harvesting. Protein was purified using a-FLAG-coupled beads and eluted with FLAG peptide. **(E)** The individual PP6 preparations were titrated against a known quantity of PPP6C to extrapolate the molar concentration of assembled complexes. **(F)** The molar quantity of phosphorylated AurA-TPX2 complexes was determined by titration against the previously described recombinant AurA-TPX2 chimera [167] preincubated with ATP for 30min at 30˚C.

Possibly, SAPS3 that is not incorporated into holoenzymes is destabilized and degraded in cells. Alternatively, its expression could be regulated at the post-transcriptional level, but this effect was not explored further. To determine the concentration of catalytic subunit-containing holoenzymes, the different PP6 preparations were titrated against recombinant His_6-PPP6C purified from bacterial cells (Figure 2.2E). The mass concentrations of PPP6C incorporated into holoenzymes were estimated to as follows: PP6-SAPS1 = 0.26ng/µL, PP6-SAPS2 = 0.34ng/µL, PP6-SAPS3 = 0.16ng/µL. These correspond to holoenzyme molar concentrations of [PP6-SAPS1] = 7.99nM, [PP6-SAPS2] = 10.5nM, and [PP6-SAPS3] = 4.52nM. Likewise, Aurora A-TPX2 complexes were purified from nocodazole-arrested cells transiently transfected with FLAG-TPX2 and pre-treated with calyculin A to ensure complete phosphorylation of Aurora A pT288 (Figure 2.2D). Normally, T-loop phosphorylation of Aurora A results in a distinct, slower-moving species on SDS-PAGE (e.g. Figure 2.3A, AurA). Thus, the phosphorylation status of Aurora A can be followed both by its electrophoretic pattern and a specific antibody against Aurora A pT288. Aurora A-TPX2 preparations contained a single Aurora A species which was pT288-positive, providing a natural model substrate for PP6. To determine the concentration, this preparation was titrated against a recombinant Aurora $A^{100-403}$-TPX^{1-42} chimera pre-phosphorylated to completion (Figure 2.2F, [167]), and found to contain 0.6ng/µL T-loop phosphorylated Aurora A, equivalent to a molar concentration of 13.1nM. Importantly, the purification procedure described here yielded preparations that contain only complexed PPP6C. Thus, the risk of non-specific activity from any monomeric phosphatase catalytic subunit is minimised in assays. Similarly, Aurora A is also only found in complex with TPX2, providing a

physiologically relevant substrate for PP6. Conversely, the overexpressed SAPS subunits and TPX2 are found in excess over their binding partners and therefore not fully complexed. This is unlikely to pose a problem, as phosphatase regulatory subunits lack activity in isolation and there is no evidence in the literature that TPX2 alone is a substrate for PP6. Further purification procedures to remove this excess were opted against, as they most likely would have caused losses of material due to the low protein yields. The described workflow was used for all phosphatase and substrate purifications and allowed the *in vitro* activities of the individual enzymes to be measured.

2.2 PP6-SAPS2 and PP6-SAPS3 are Aurora A phosphatases

To test the activities of the PP6 holoenzymes against Aurora A-TPX2, enzyme was diluted in buffer to yield a final reaction concentration of 100pM. Reactions were started by the addition of 4.1nM Aurora A-TPX2 complexes at 30°C and sampled at 10min intervals for 40min (Figure 2.3A-B). Under these conditions, PP6-SAPS2 and PP6-SAPS3 dephosphorylated Aurora A-pT288 faster than the control mock eluate, whereas PP6-SAPS1 did not, achieving full dephosphorylation by the 40min mark (Figure 2.3A-B). This could be followed both by the specific Aurora A pT288 antibody and the downshifting pattern visible from total Aurora A blots (Figure 2.3A, AurA and AurA pT288). The observed difference in activity was not due to different holoenzyme concentrations, as the levels of PPP6C demonstrate those were equal for all conditions and at all timepoints (Figure 2.3A, PPP6C). Furthermore, substrate concentration was equal, as shown by the total Aurora A and the lower band in the FLAG blot, corresponding to TPX2 (Figure 2.3A, FLAG). The upper FLAG band corresponds to the respective SAPS subunit and reflects the difference in expression between SAPS3 and SAPS1/2.

The Aurora A pT288 blots were quantified in replicate experiments and show that PP6-SAPS2 and PP6-SAPS3 have reproducible Aurora A pT288 phosphatase activity while PP6-SAPS1 does not (Figure 2.3B). Equivalent results were obtained from further independent enzyme and substrate preparations.

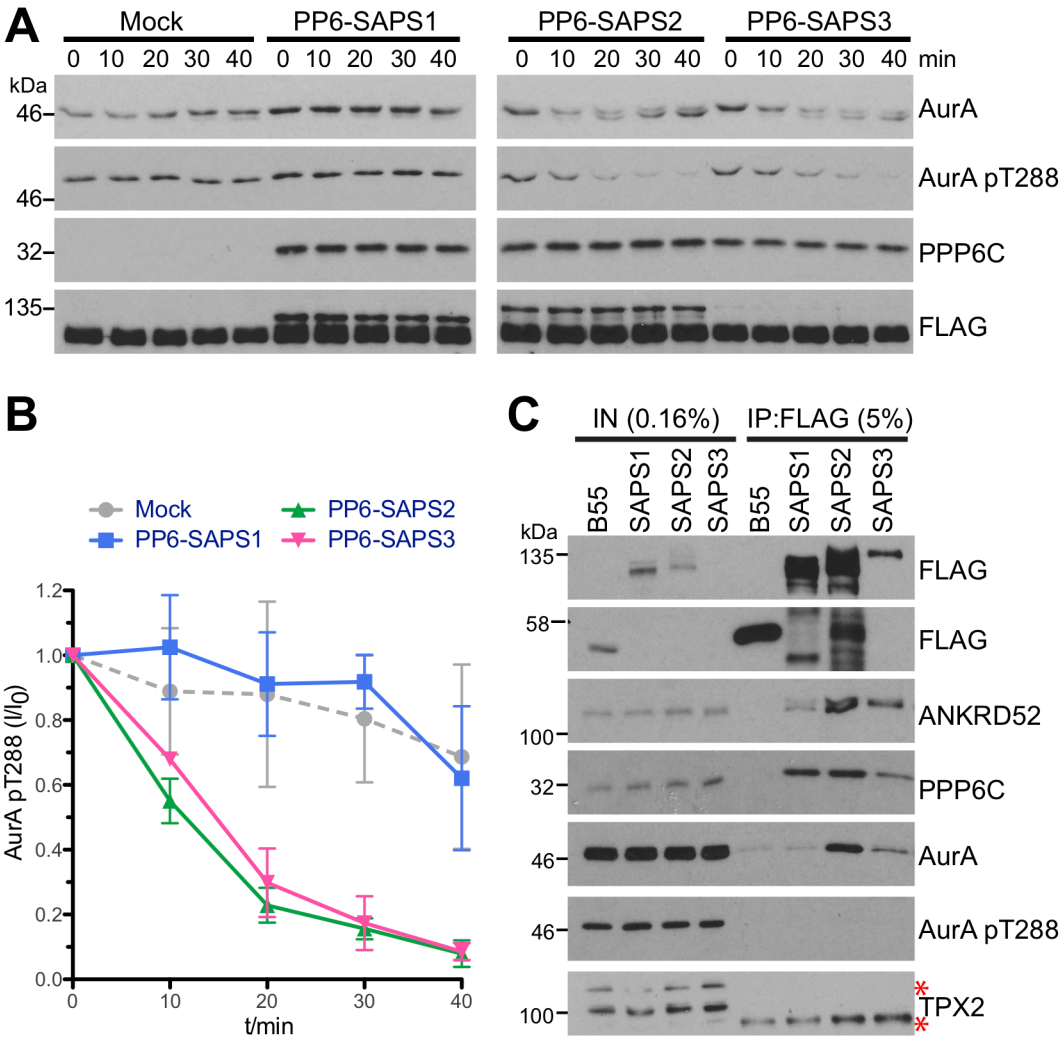


Figure 2.3 - PP6-SAPS2 and PP6-SAPS3 are AurA T-loop phosphatases. (A) Phosphorylated AurA-TPX2 complexes (4.5nM) were incubated with PP6 holoenzymes (100pM) as indicated at 30˚C. **(B)** Densitometric quantification of replicate experiments as in (A) (mean±SEM, n=2). **(C)** HeLaS3 cells were transfected with FLAG-B55 (control), or SAPS1/2/3 as indicated for 36h, arrested in mitosis and subjected to immune-precipitation before western blotting. Non-specific bands are highlighted by asterisks.

As described already, PP6 has to be able to approach the structurally buried Aurora A-pT288 which is inaccessible to other phosphatases such as PP1

[201]. Thus, the feature allowing a PP6 holoenzyme to dephosphorylate the Aurora A T-loop may be stable binding to and dissolution of the Aurora A-TPX2 complex. Therefore, the association between individual SAPS subunits and the substrate, Aurora A-TPX2, was tested. To do this, cells were transfected with FLAG-tagged SAPS subunits, or the related PP2A regulatory subunit B55 which does not stably bind substrates as control (Figure 2.3C). All the SAPS subunits interacted specifically with other holoenzyme components as expected (Figure 2.3C, ANKRD52 and PPP6C). Conversely, increased amounts of Aurora A over control, consistent with specific binding, were only found in SAPS2 and SAPS3 IPs (Figure 2.3C, AurA). The bound Aurora A was not pT288-positive, and no TPX2 was detected in the pulldowns (Figure 2.3C, AurA and TPX2). TPX2 can bind to Aurora A under similar conditions as shown in Figure 2.2D, therefore its absence in this experiment is not a result of technical implications. This suggests that the detected Aurora A was either the dephosphorylated product, or that PP6-SAPS2/3 can bind to the free, inactive Aurora A. Furthermore, this indicates that the primary recognition element of the phosphatase is most likely located on Aurora A, and not TPX2. Additionally, this is consistent with the idea that PP6 binding results in the disassembly of Aurora A-TPX2 complexes. Taken together, these data suggest that the SAPS subunits confer substrate specificity to PP6 through binding-mediated selection.

2.3 PP6-SAPS2 and 3 are required for normal mitotic progression

Loss of PP6 results in pronounced mitotic defects [172, 214]. However, the contribution of the individual PP6 holoenzymes to this phenotype had only been looked at indirectly, via the incidence of micronucleation [172]. To further

characterise the individual contributions, live and fixed-cell imaging was performed. Mitotic progression and spindle morphology were examined by time lapse imaging of previously described cells stably expressing mCherry-H2B and GFP-tubulin [172] upon depletion of different PP6 subunits (Figure 2.4A). Control cells efficiently formed orderly bipolar spindles and aligned the chromosomes at metaphase plates before anaphase initiation (Figure 2.4A, siControl). By comparison, virtually all cells depleted of PPP6C exhibited a phenotype as previously described, with slower and defective spindle formation (Figure 2.4A-B, siPPP6C)[172]. Once formed, the spindles showed frequent pole fragmentation and excessive microtubule bundling. Additionally, spindle positioning was impaired, often resulting in displacement and rotation of the spindle. In anaphase, chromatin masses were less compact and lagging chromosomes could be observed. These effects are consistent with over-activated Aurora A, as described before [172]. All facets of the phenotype were recapitulated by SAPS3 depletion (Figure 2.4A-B, siSAPS3), while SAPS1-depleted cells were indistinguishable from the control (Figure 2.4A-C, siSAPS1). SAPS2 depletion resulted less pronounced spindle defects with intermittent pole fragmentation, and this was observed less frequently than the defects in PPP6C- or SAPS3-depleted cells (Figure 2.4A-B, siSAPS2).

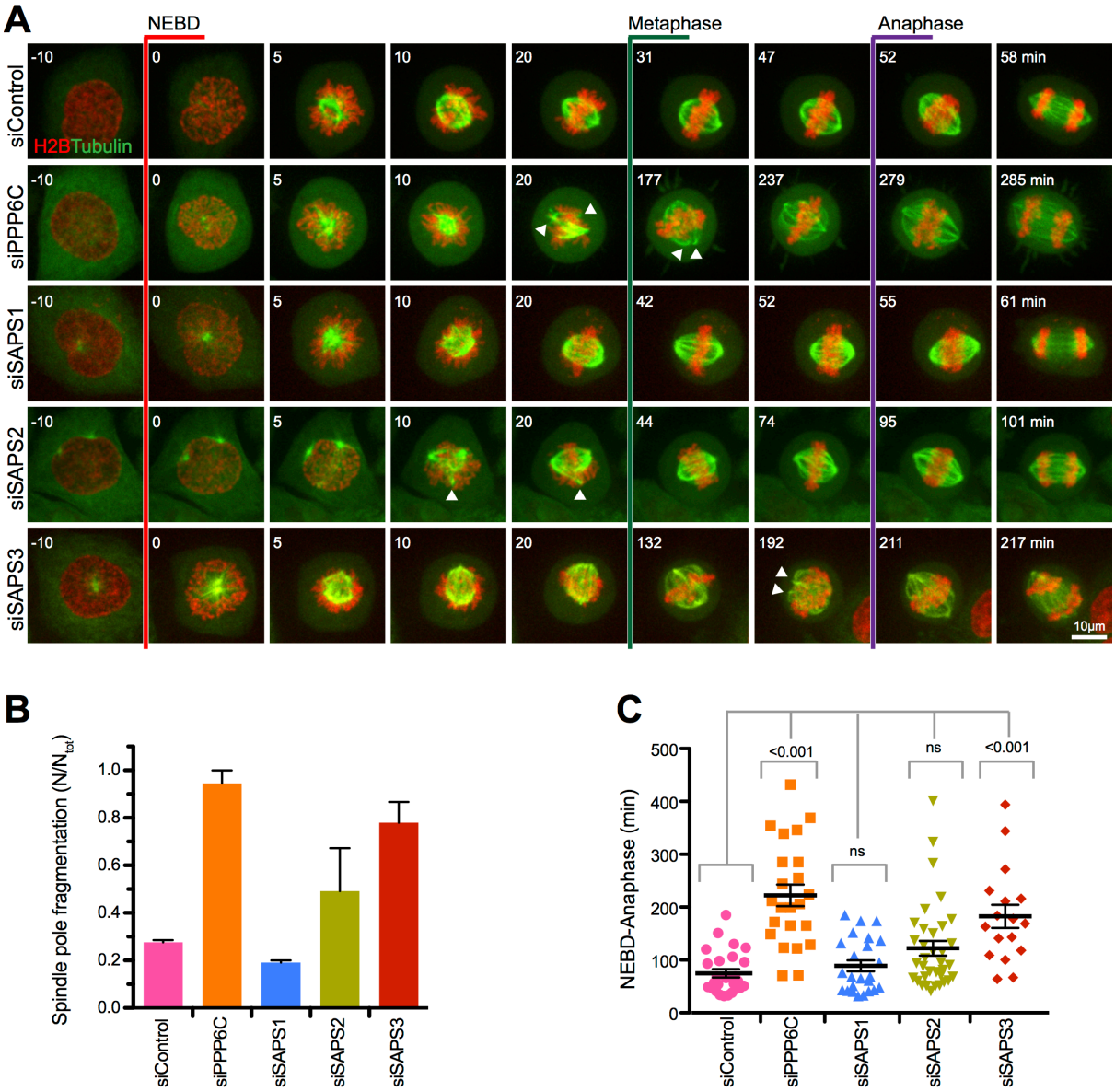


Figure 2.4 - Depletion of SAPS3 most closely resembles the PPP6C-null phenotype
(A) HeLaS3 cells stably expressing mCherry-H2B and GFP-tubulin were depleted as indicated and imaged by time-lapse microscopy. Arrowheads highlight supernumerary microtubule organizing centers or spindle pole fragments. **(B)** Proportion of cells that experience spindle pole fragmentation during a single mitosis was counted from the experiment in (A), N>26 combined from 2-3 biological replicates. **(C)** The required time to progress from nuclear envelope breakdown (NEBD) to anaphase was measured (Mean±SEM, n>15). Significance was determined by a one-way ANOVA test followed by Dunnett's multiple comparison test against siControl. Only cells which entered and exited mitosis during imaging were considered.

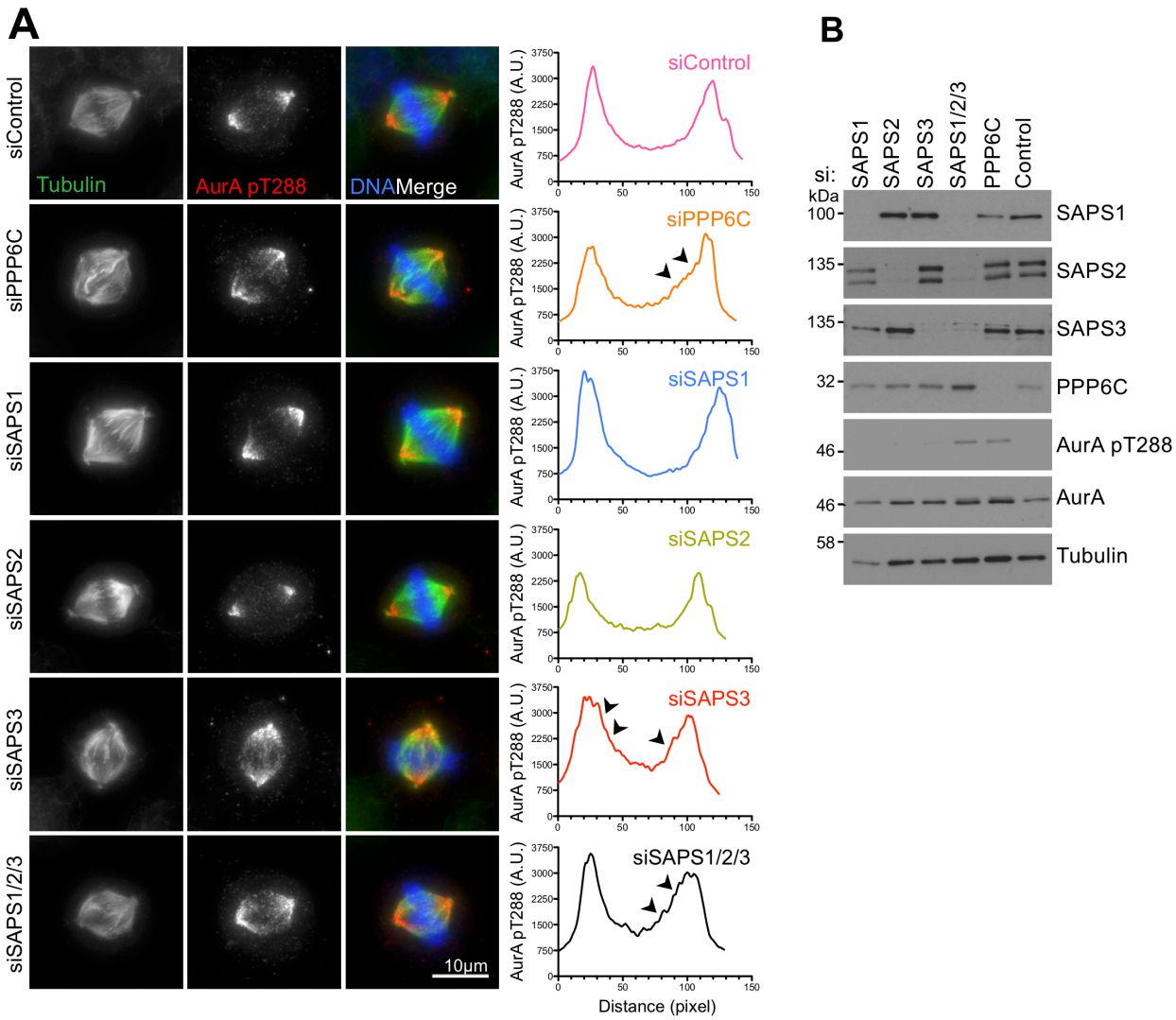


Figure 2.5 - Depletion of SAPS3 results in pronounced mislocalization of active AurA. (A) HeLaS3 cells were treated with siRNA against PP6 subunits for 60h, synchronized by thymidine-release before fixation and staining for factors as indicated. Graphs depict representative pole-pole linear profile plots of AurA pT288 staining corresponding to each condition. Arrowheads highlight non-abrupt AurA pT288 signal transitions **(B)** Cells treated equivalently to those in (A) were lysed in Laemmli sample buffer and analyzed by western blotting.

Reflective of these phenotypes, only cells depleted of PPP6C or SAPS3 had a significantly extended mitosis, defined by the time from nuclear envelope breakdown to anaphase initiation (Figure 2.4C).

Next, the effect of SAPS depletions on the Aurora A activation status and localization was examined (Figure 2.5). Cells were treated with siRNA before thymidine-release synchronization, before fixation and staining (Figure 2.5A). Control cells exhibited focussed Aurora A pT288 at spindle poles, whereas PPP6C depletion resulted in mislocalization of active Aurora A along the mitotic spindle (Figure 2.5A, siControl and siPPP6C) as described before [172]. Depletion of SAPS1 or SAPS2 did not result in mislocalization of Aurora A pT288 or apparent spindle defects under these conditions (Figure 2.5A, siSAPS1 and siSAPS2). By contrast, knockdown of SAPS3 caused both spindle defects and Aurora A pT288 mislocalization, albeit spindle morphology was not affected as strongly as when PPP6C is lost (Figure 2.5A, siSAPS3). Co-depletion of all SAPS subunits was required to fully recapitulate the siPPP6C phenotype in terms of increase in Aurora A pT288 signal on mitotic spindles (Figure 2.5A, siSAPS1/2/3). These effects were additionally tested by western blot analysis of cells generated under the same conditions and lysed in Laemmli sample buffer (Figure 2.5B). This analysis showed that the depletion of PP6 subunits was efficient under all tested conditions (Figure 2.5B, PPP6C, SAPS1-3). Furthermore, Aurora A pT288 is sufficiently stable under during this rapid lysis, allowing the assessment of its amounts at the population level (Figure 2.5B, AurA pT288). The T-loop phosphorylation was readily detectable in PPP6C and SAPS1/2/3-depleted conditions, but could not be observed in others. This suggests that the overall levels of Aurora A pT288 are increased upon the loss of PP6 activity, consistent with findings in the literature and data presented in Figure 2.5A [172]. A further contribution to this increase could be made by protection from dephosphorylation during lysis when PP6 activity is lost. It is also worth noting that detection of

Aurora pT288 by western blotting under these conditions was poor, most likely due to a low mitotic index, even after thymidine-release synchronization.

2.4 PP6-SAPS3 is the major Aurora A phosphatase in mitosis

The requirement for each subunit for Aurora A dephosphorylation was next tested. To do this, a cell extract system was used wherein cells depleted of PP6 subunits were arrested in mitosis and lysed in the presence or absence of microcystin-LR, a potent PPP inhibitor (PP-i) (Figure 2.6A-B). Under these conditions, sites that are dynamically opposed by a phosphatase are turned over when the inhibitor is absent, unless the phosphatase is removed by siRNA. As expected, Aurora A pT288 is turned over in the control condition (Figure 2.6A-B, siCon). However, the phosphorylation is robustly protected when either PPP6C, SAPS3 or all the SAPS in combination are depleted (Figure 2.6A-B, siPPP6C, siSAPS3 and siSAPS1/2/3). By contrast, depletion of SAPS1 or SAPS2 did not confer protection from dephosphorylation (Figure 2.6A-B, siSAPS1 and siSAPS2). Two unexpected additional observations were made from this experiment. Firstly, the amount of SAPS subunits dropped upon PPP6C depletion, suggesting that incorporation into holoenzymes is required to maintain their stability in cells. Secondly, PPP6C depletion resulted in a smeared electrophoretic pattern of SAPS2, which is often observed upon increased phosphorylation.

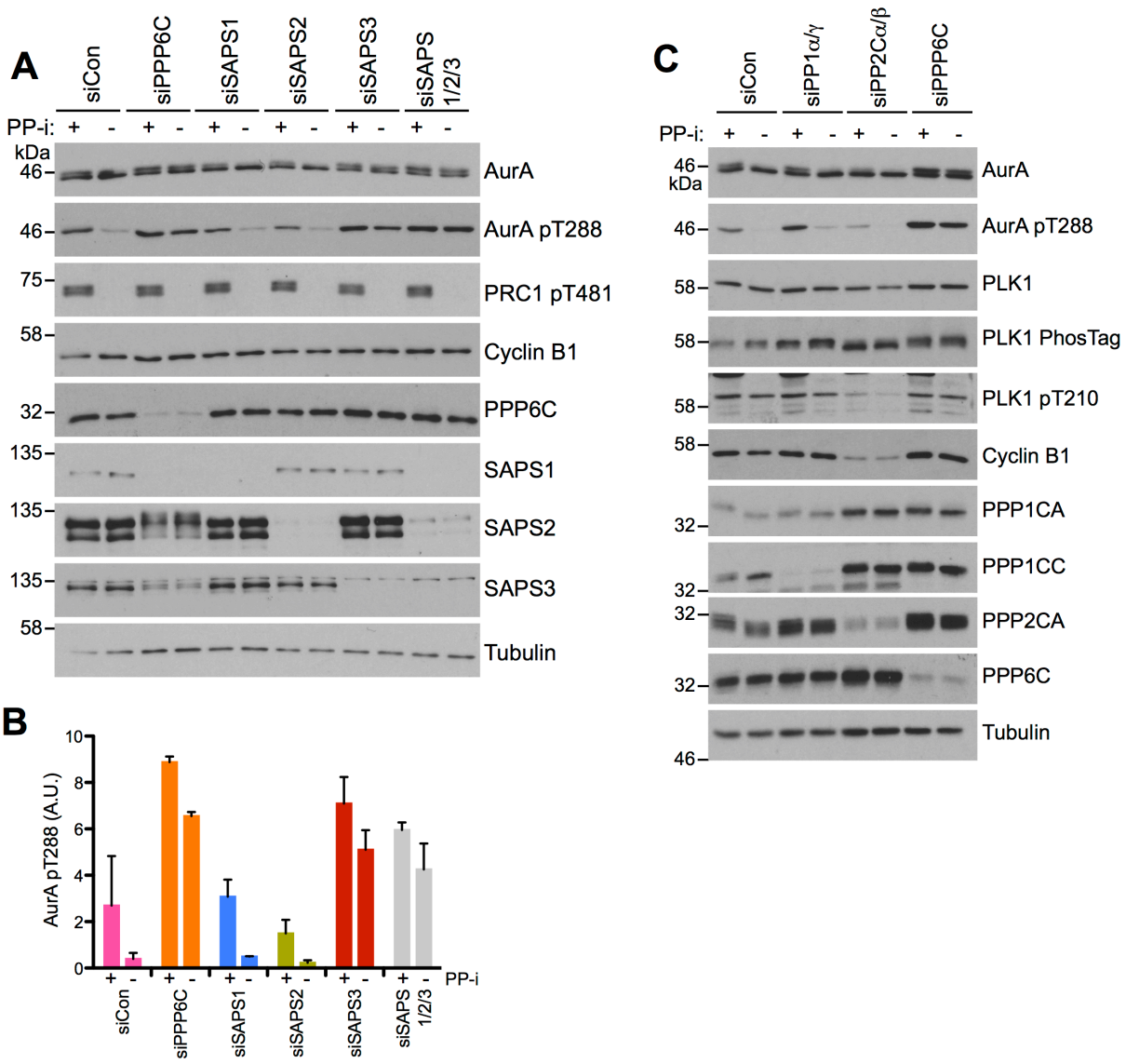


Figure 2.6 - PP6-SAPS3 is the major AurA pT288 phosphatase in cells. (A) Cells were depleted of PP6 subunits for 60h as indicated and arrested with nocodazole, followed by lysis in the presence or absence of 1μM microcystin-LR (PP-i) and western blot analysis. **(B)** Replicate experiments as in (A) were exposure matched for AurA pT288 and subjected to densitometric quantification of AurA pT288 (mean±SEM, n=2). **(C)** An equivalent experiment as in (A) was performed with depletion of other PPPs.

To further validate that other PPPs don't contribute to Aurora A pT288 phosphatase activity, an equivalent experiment was performed depleting the catalytic subunits of other PPPs (Figure 2.6C). Depletion of either PP1 or PP2A did not protect Aurora A pT288 from dephosphorylation (Figure 2.6C, siPP1α/γ and siPP2Cα/β), whereas depletion of PPP6C did (Figure 2.6C, siPPP6C). Intriguingly, another T-loop phosphorylation – pT210 on PLK1 – is stable under the conditions used in this experiment, suggesting that it is not counteracted by a phosphatase that is active under these conditions. It is worth noting that depletion of PP2A catalytic subunits resulted in lower levels cyclin B1 and other factors in the sample. This can be explained by the proposed role of PP2A in counteracting CDK1 activity before mitotic entry; lack of the phosphatase would cause mitotic entry at a lower threshold of cyclin B1, shortening the G2 phase and stopping further synthesis [11, 13].

Together with the *in vitro* results and the *in vivo* analysis, these findings strongly suggest that PP6 is functionally stratified in a manner dependent on the regulatory SAPS subunit. PP6-SAPS1 does not target Aurora A and is dispensable for mitosis. PP6-SAPS3 is the major Aurora A pT288 counteracting phosphatase in mitosis, necessary for normal spindle formation. PP6-SAPS2 can target Aurora A, but it is largely not required for mitotic progression. These observations could be explained if the contribution of PP6-SAPS2 is too small to affect Aurora A and mitosis or by a regulatory mechanism targeting specific PP6 holoenzymes. This hypothetical regulatory system was next explored.

2.5 PP6 holoenzymes are stable throughout the cell cycle

The multi-subunit composition of PP6 provides cells with numerous potential regulatory mechanisms. Firstly, the availability of individual subunits can be

controlled via protein stability or at the level of holoenzyme assembly. Secondly, the holoenzymes can employ regulatory interaction partners, as is the case with PP2A and PP1 [197, 198]. Moreover, the properties of a holoenzyme could be affected by post-translational modifications.

To establish whether PP6 regulatory subunit protein levels change during the cell cycle, cells were arrested at the beginning of S-phase, released and collected in hourly intervals (Figure 2.7A). The protein levels of SAPS2 and SAPS3 were unchanged in the course of the experiment. Equivalent experiments shown later (e.g. Figure 3.4) show the same pattern of behavior for PPP6C. A small drop in the levels of SAPS1 could be observed at 11 and 12h post washout, corresponding to the peak of mitosis indicated by Cyclin B1 levels and presence of the CDK1-dependent phosphorylation PRC1 pT481 (Figure 2.7A). An enriched mitotic population created by nocodazole treatment lacked a SAPS1 signal. The simplest explanation for this is degradation of the SAPS1 protein. However, the major antibody recognition epitope harbours a phospho-acceptor residue conforming to the CDK1-cyclin B consensus motif which, if phosphorylated, may abrogate antibody binding. To test this, mitotic cells treated with control or PPP6C siRNA were lysed in the presence of okadaic acid and incubated with lambda phosphatase (Figure 2.7B). The efficiency of dephosphorylation under this condition was confirmed by the turnover of PRC1 pT481 (Figure 2.7B, λ-PPase +). In the same condition, the SAPS1 signal was downshifted and increased in intensity, demonstrating that the loss of signal in mitosis was most probably due to a phosphorylation-mediated detection effect and not degradation of the protein. A small downshift upon phosphatase treatment was also visible with SAPS3. In a similar fashion, the smearing pattern observed with SAPS2 upon PPP6C depletion

was completely abrogated by lambda phosphatase treatment (Figure 2.7B, siPPP6C λ-PPase + and λ-PPase -), indicating that it was caused by one or more phosphorylations. Inhibition of the lambda phosphatase by Na_3VO_4 mitigated all of the described effects (Figure 2.7B, VO_4^{3-} +). Taken together, these data indicate that PP6 regulatory subunits are expressed constantly during the cell cycle, but are differentially phosphorylated in interphase and mitosis.

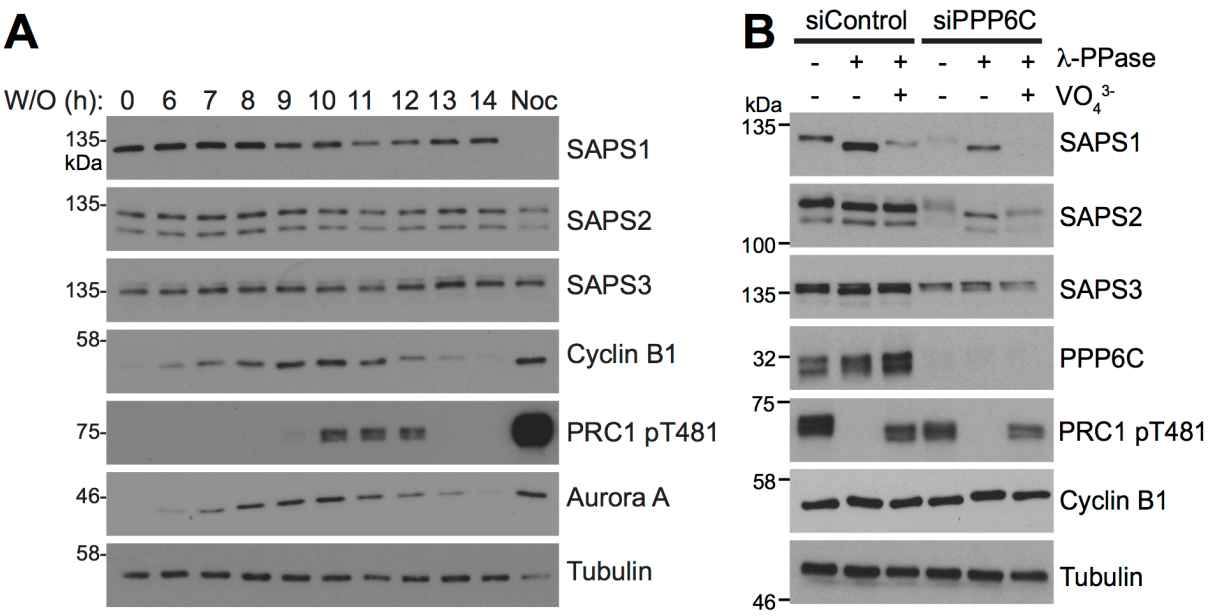


Figure 2.7 - PP6 subunits are stably expressed and differentially phosphorylated throughout the cell cycle. (A) Cells were arrested with thymidine and released or arrested with nocodazole (Noc) before combined harvesting by mitotic shakeoff and treatment with 1mM EDTA in PBS, followed by lysis and western blot analysis as indicated. W/O = washout **(B)** Cells were treated with the indicated siRNAs for 52h before nocodazole arrest, lysed and treated with l-phosphatase in the presence or absence of vanadate as indicated, followed by western blot analysis.

To establish whether holoenzyme composition is altered during the cell cycle, cells stably expressing PPP6C-FLAG were synchronized in S phase, metaphase or anaphase and subjected to immunoprecipitation (Figure 2.8A).

PPP6C associated with all of the SAPS subunits efficiently in all three tested stages which were defined by cyclin B1 levels (Figure 2.8A, S phase, Metaphase and Anaphase). Furthermore, binding to ANKRD28 and ANKRD52 was unaltered by cell cycle stage (Figure 2.8A). As expected, no pulldown was observed in the parental cell controls, either in S phase or metaphase (Figure 2.8A, Control S and Control M). Due to a lack of a high affinity antibody, ANKRD44 could not be followed in this experiment. However, subsequent proteomics analyses showed that it too associated with other holoenzyme components in a similar fashion to ANKRD28 and ANKRD52 (Figure 2.11B-D). The same system was used to test whether depletion of one set of regulatory subunits affects the quantity of holoenzymes assembled with the others. To do this, cells expressing PPP6C-FLAG were treated with siRNA against subunits as indicated, arrested with nocodazole and subjected to immunoprecipitation (Figure 2.8B). All SAPS subunits interacted with PPP6C-FLAG in the control condition (Figure 2.8B, siControl), whereas none of the tested proteins were pulled down in the parental cell line condition (Figure 2.8B, Untagged). Depletion of SAPS2 did not alter the association between PPP6C-FLAG and SAPS1 or SAPS3 (Figure 2.8B, siSAPS2), and co-depletion of SAPS2 with SAPS1 did not change the amount of SAPS3 pulldown (Figure 2.8B, siSAPS1+2). These data indicate that the amounts of individual PP6-SAPS holoenzymes are independent and remain constant under these conditions. In addition, this finding supports the SAPS depletion experiments in Figures 2.4-2.6, indicating that the manipulations affected only the desired holoenzymes, and not the others.

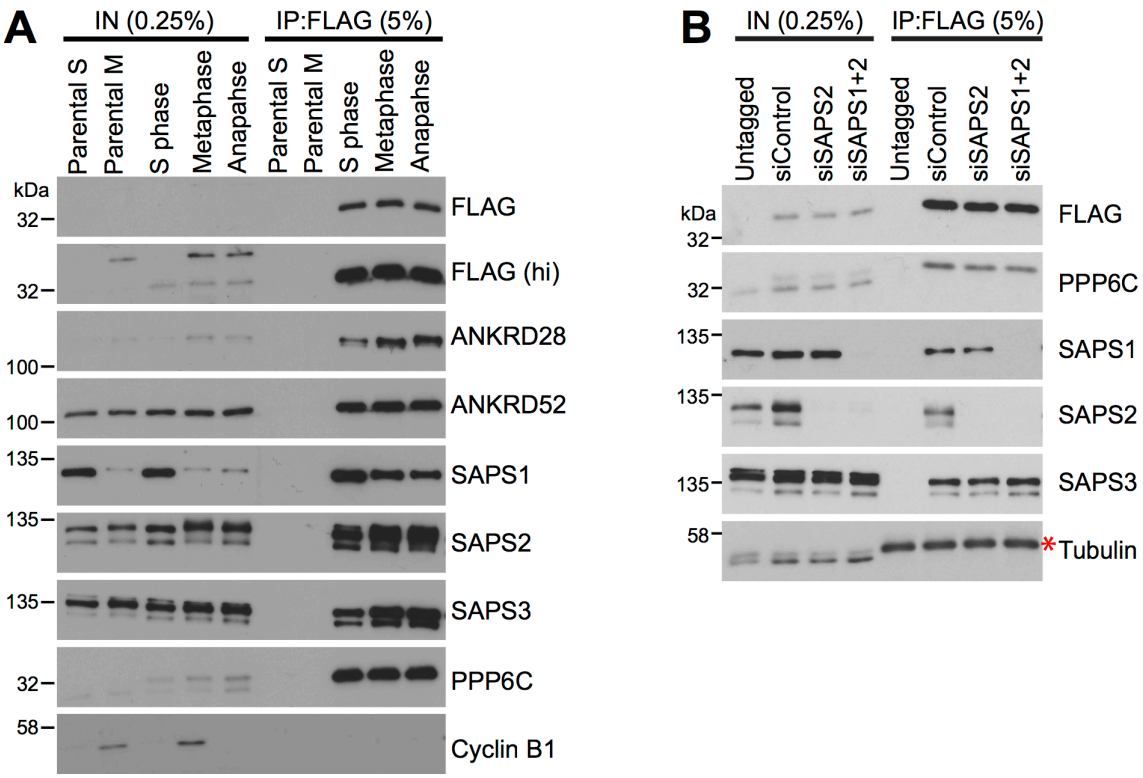


Figure 2.8 - PP6 holoenzyme composition is constant throughout the cell cycle. (A) Parental HeLa S3 cells or HeLa S3 stably expressing PPP6C-FLAG were arrested in S phase, metaphase or anaphase as indicated before lysis and immune precipitation, followed by western blot analysis. S=S phase, M=M phase **(B)** Cells as in (A) were treated with siRNA as indicated and arrested with nocodazole, followed by lysis, immune precipitation and western blot analysis. The asterisk indicates a cross-reactive signal created by the heavy chain of the antibody used for the immunoprecipitation.

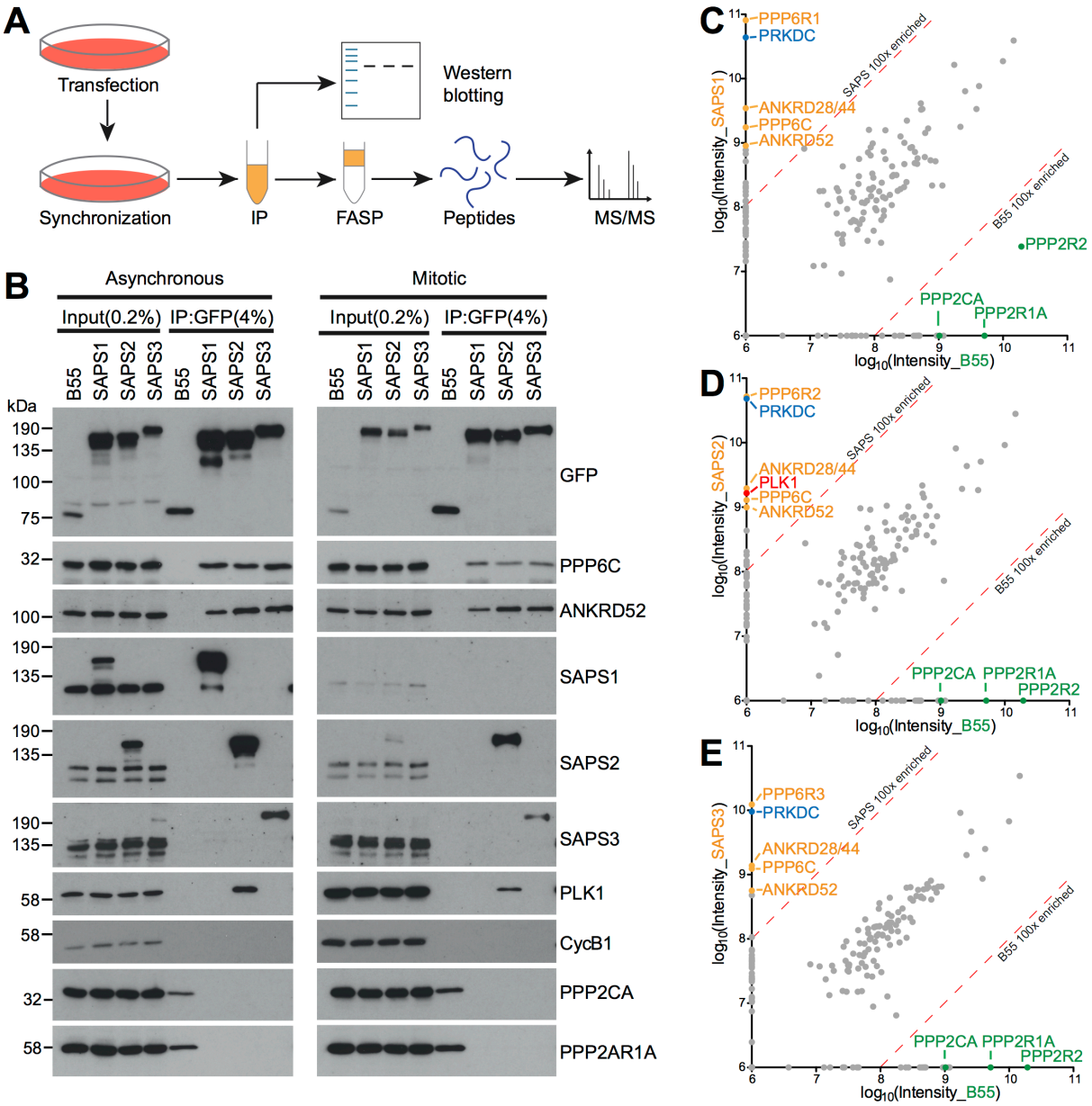


Figure 2.9 - Interactome analysis of SAPS subunits. (A) Schematic of the workflow used to prepare and analyze the interactome screen for SAPS1/2/3. **(B)** Cells were transfected with constructs as indicated for 48h for asynchronous or 36h before nocodazole arrest, followed by lysis and immunoprecipitation. **(C-E)** Samples analyzed in (B) were prepared for mass spectrometry using filter assisted sample preparation before LC/MS-MS. Output data were computationally annotated and protein group intensities found in asynchronous SAPS1/2/3 were compared to the B55 control IP. Note that missing intensity values for assigned protein groups were replaced with a minimal background value of 6. Candidates were defined as specific if enriched more than 100-fold (2 logarithmic units) over the control B55 IP.

2.6 SAPS subunits contribute unique interaction partners

The interactomes of individual PP6 holoenzymes were explored using HeLa S3 cells transfected with GFP-tagged SAPS1/2/3 or B55 as control. These cells were then harvested from either asynchronous cultures or after a nocodazole arrest. Immune precipitation was then performed, and the samples analysed by mass spectrometry and western blotting (Figure 2.9). Core holoenzyme components (PPP6C and ANKRD subunits) bound to all of the SAPS subunits efficiently in interphase and mitosis (Figure 2.9B, Figure 2.9C-E). The ANKRD44 subunit is nearly identical in sequence to ANKRD28 and could not be confidently separated from ANKRD28 by proteomic analysis in this experiment (Figure 2.9C-E, ANKRD28/44). Consistent with previous observations, the signal obtained from the specific SAPS1 antibody was reduced in mitosis, but robust amounts of SAPS1 could be detected by blotting against the GFP tag (Figure 2.9B). A curated list of interactors detected in this experiment can be found in the appendix (Appendix Table A1). All the SAPS subunits pulled down the non-homologous end joining kinase DNA-PK (Figure 2.9C-E). Reports in the literature stated that this interaction was either preferential for SAPS1 or DNA-PK was globally recruited to PP6 holoenzymes [221, 223]. The data presented here agree with the latter. Intriguingly, PLK1 was robustly and specifically detected in SAPS2 IPs, both by mass spectrometry and western blotting. (Figure 2.9B, Figure 2.9D). Furthermore, the interaction could be observed in both asynchronous and mitotic cells (Figure 2.9B). To verify this, reciprocal immune precipitation (IP) experiments targeting endogenous SAPS2 and PLK1 were performed from asynchronous and nocodazole-arrested cells (Figure 2.10). SAPS2 associated with other PP6 subunits in both asynchronous and mitotic samples (Figure 2.10A). PLK1

interacted with SAPS2 strongly in asynchronous and somewhat less efficiently in nocodazole-arrested samples (Figure 2.10A). The SAPS2-PLK1 interaction was most likely direct as other interaction partners of PLK1, such as BUBR1, were not detected in the IP or proteomics analysis (Figure 2.10A, Figure 2.9C-E and Table A1). Immune precipitation of endogenous PLK1 gave an equivalent result wherein PLK1 interacted with SAPS2 more efficiently in the asynchronous sample than in mitosis (Figure 2.10B). Importantly, PPP6C and ANKRD52 were detected in PLK1 IPs (Figure 2.10B), suggesting that PLK1 can bind an assembled PP6 holoenzyme. As expected, previously described interaction partners, BUBR1 and PRC1, readily associated with PLK1 under these conditions (Figure 2.10B).

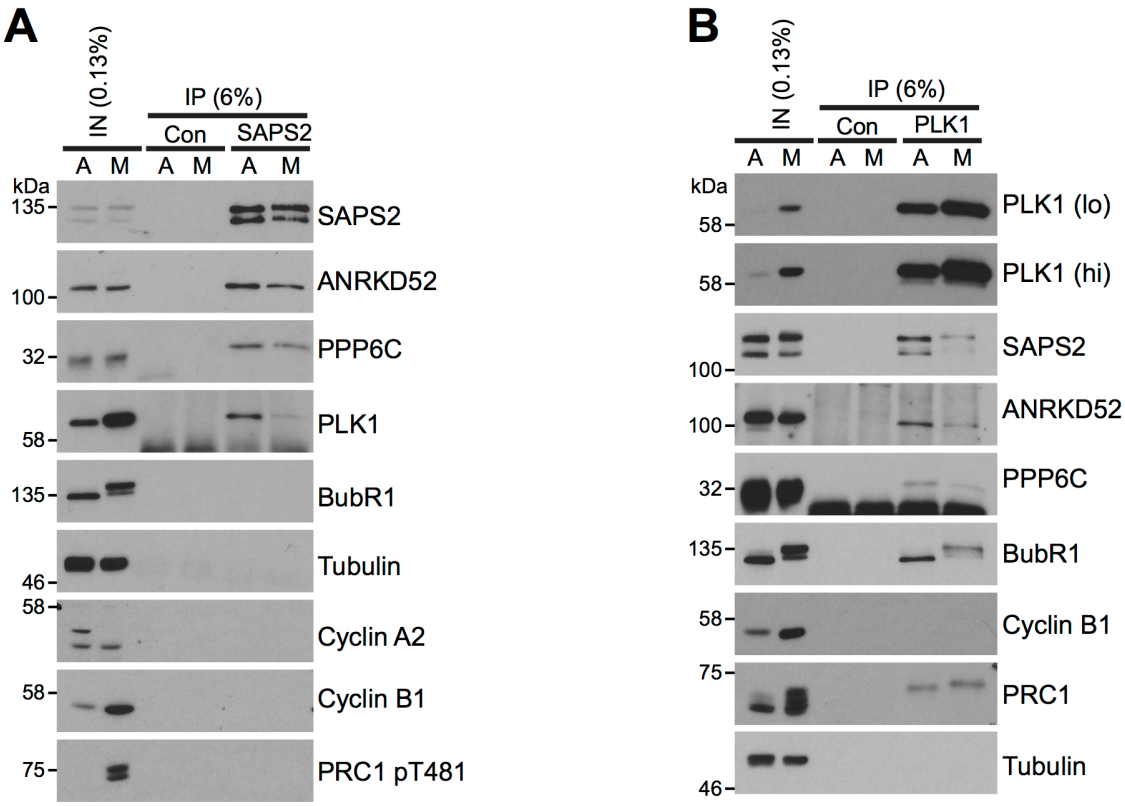


Figure 2.10 - Endogenous SAPS2 and PLK1 interact. (A) Asynchronous or nocodazole-arrested HeLaS3 cells were harvested by treatment with 1mM EDTA in PBS or mitotic shakeoff, respectively, immune precipitated with an antibody against SAPS2 or GFP as non-specific control and analyzed by western blotting. **(B)** Endogenous PLK1 was immune precipitated from interphase or nocodazole-arrested HeLaS3 cells harvested as in (A) and analyzed by western blotting. A = asynchronous, M = nocodazole-arrested mitotic

2.7 ANKRD subunits interact with all SAPS subunits

An equivalent procedure was applied to investigate the interactomes of ANKRD subunits. Asynchronous HeLa S3 cells were transfected with FLAG-ANKRD subunits and harvested before immune precipitation (Figure 2.11) followed by western blot analysis (Figure 2.11A) and mass spectrometry (Figure 2.11B-D). The FLAG antibody failed to detect the ANKRD28 transgene, but it was readily detected by the specific antibody and mass spectrometry (Figure 2.11A and

2.11B). All of the ANRKD subunits could associate equally well with PPP6C and SAPS subunits, shown both by western blotting and mass spectrometry. Furthermore, DNA-PK could be detected in all of the pulldowns by mass spectrometry (Figure 2.11B-D). However, the measured intensities were an order of magnitude lower than with SAPS subunits, suggesting DNA-PK is a second-order interactor of ANRKD subunits. We were unable to detect PLK1 in any of the conditions, indicating that the ANKRD subunits don't directly contribute to the interaction.

Collectively, these results support the conclusion that holoenzyme assembly is not a major pathway used to regulate PP6 and that the composition of PP6 holoenzymes remains relatively unchanged throughout the cell cycle. This suggests regulatory systems are provided by interaction partners and/or post-translational modifications, mediated by the regulatory SAPS subunits. Two candidates were found that are ideally placed to fulfil this role: DNA-PKcs, which binds to all PP6 holoenzymes, and PLK1, a specific interactor of PP6-SAPS2. Concomitantly with our discovery, the SAPS2-PLK1 interaction was detected in two large-scale interactome screens [239, 240]. However, the nature and significance of this interaction was not explained in these studies. PLK1 is essential for mitotic spindle formation and maintenance, and this function overlaps with that of Aurora A. In contrast, DNA-PK has limited influence on mitotic events. Together these observations suggest that PP6-SAPS2 is specifically regulated by PLK1, and may thus contribute to the functional integration between Aurora A and PLK1 kinases. The properties and function of this potential regulatory system were therefore explored further.

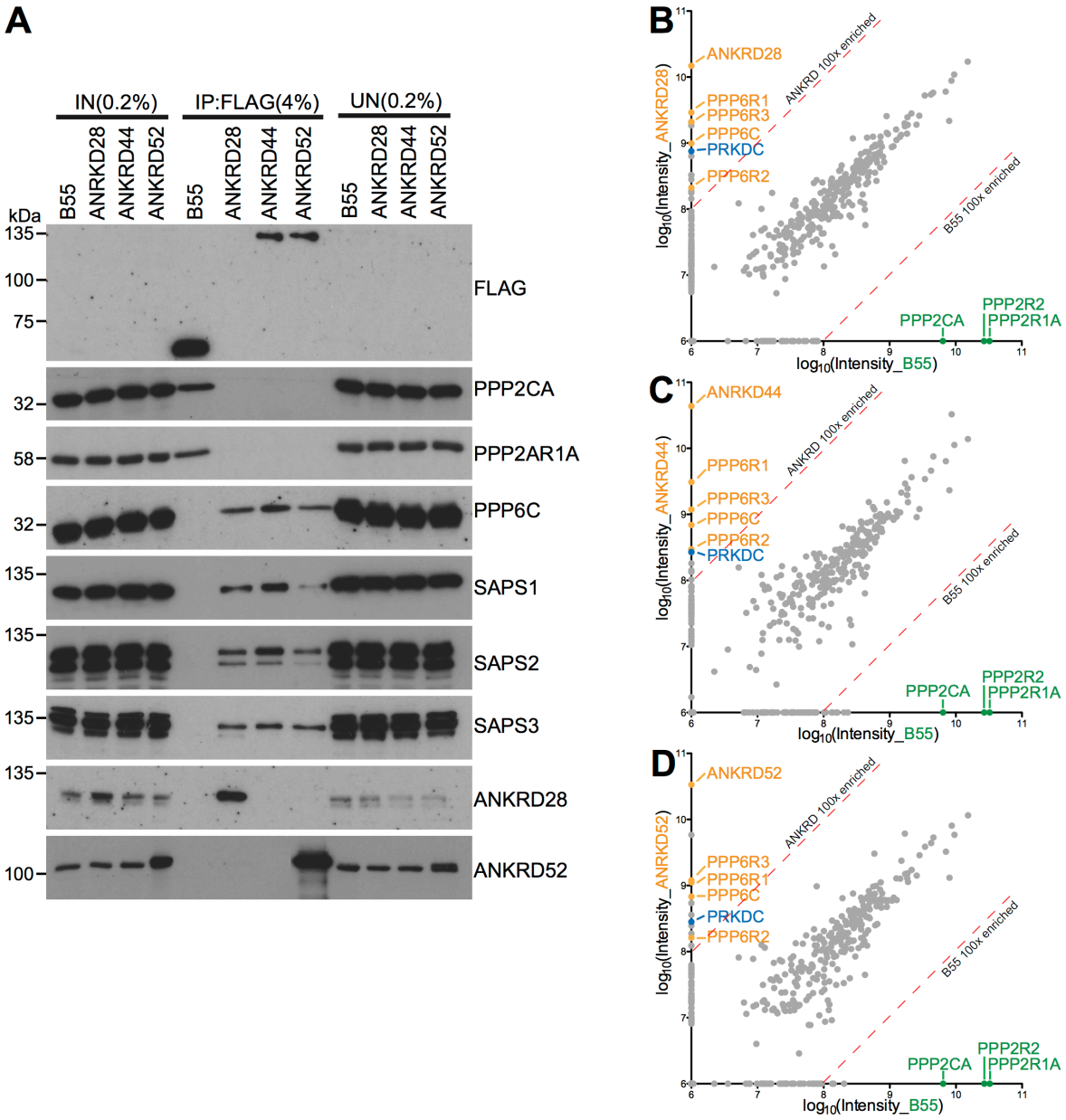


Figure 2.11 - Interactome analysis of SAPS and ANKRD subunits. (A) Asynchronous HeLa S3 cells were transfected with FLAG-ANRKD28/44/52 as indicated and subjected to immune precipitation. They were then treated equally as for the SAPS interactome analysis in in figure 2.9 **(B-D)** Intensity measurements of protein groups found in ANKRD IPs were compared to those in the control B55 condition in the same way as in figure 2.9.

Chapter 3 Regulation of PP6-SAPS2 by PLK1

3.1 Timing the SAPS2-PLK1 interaction – experimental framework

Initial experiments suggested that SAPS2 and PLK1 interact less in mitosis than in interphase, but it was unclear precisely when during the entire cell cycle the interaction is maximal and therefore most likely to establish regulation. To probe this, cells were transfected with SAPS2-GFP, arrested with a thymidine block and released before harvesting in hourly intervals and immune precipitation (Figure 3.1). Under these initial conditions, cell cycle factors such as cyclin A2 and cyclin B1 showed a very gradual build-up, and there was no abrupt increase in PRC1 pT481, indicating that synchrony was poor (Figure 3.1B). Since the experiment was otherwise robust, showing pulldown of other PP6 subunits, PLK1 and Aurora A, this strategy was pursued further with optimized synchronization.

Double thymidine blocks have been shown to give better synchrony than a single block [206]. This approach was applied in our system with optimised synchronization times (Figure 3.2A). The doubling time for cells used in this work is around 18h. Judging from live-cell imaging experiments (not shown), the cells take 10h from the beginning of S-phase to mitotic entry, leaving about 6h of G1 phase after a 1-2h mitosis. Therefore, the first thymidine block was performed for 18h to trap cells in S phase. The thymidine was then washed out, and added again 10h later to ensure most of the cells had completed DNA replication and therefore become refractory to thymidine arrest during the same cell cycle. The second thymidine block was performed for a further 12h to capture the population at the beginning of S-phase before the second washout and harvesting. This method was tested and shown to improve the synchrony of the culture (Figure 3.2B). Cyclin A2, cyclin B1 and Aurora A accumulated more sharply. Furthermore,

CDK1-cyclin B activation was more abrupt, shown by the behaviour of two substrate sites, PRC1 pT481 and PPP1CA pT320.

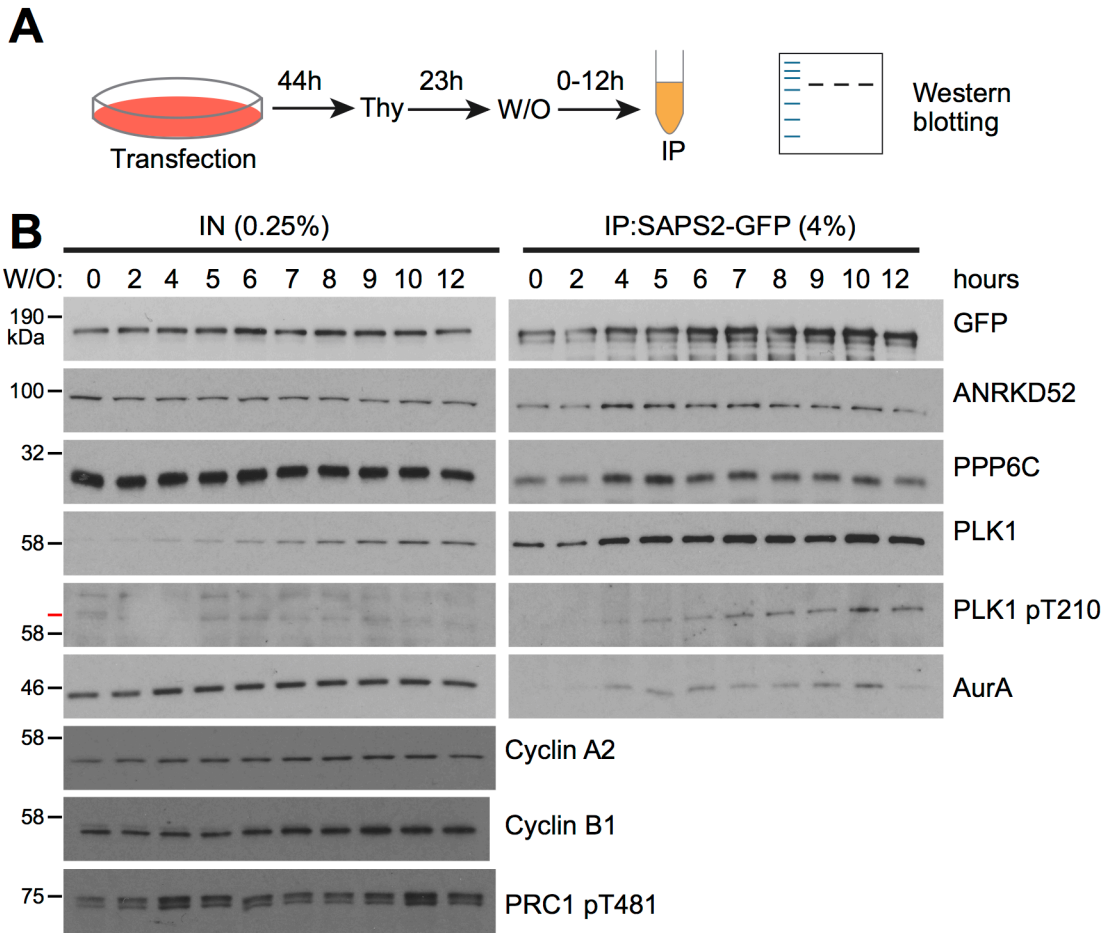


Figure 3.1 - Synchrony during thymidine release is insufficient to assess the PLK1-SAPS2 interaction timing. (A) Schematic of the experimental workflow used. **(B)** Cells were transfected with SAPS2-GFP, arrested with thymidine and released for the indicated time before harvesting by combined mitotic shakeoff and treatment with 1mM EDTA in PBS, followed by immunoprecipitation and western blot analysis. Red line denotes the specific PLK1 pT210 band position. Note the poor synchrony shown by the lack of a sharp buildup of cyclins A2 and B1, and gradual increase in PRC1 pT481. W/O = washout

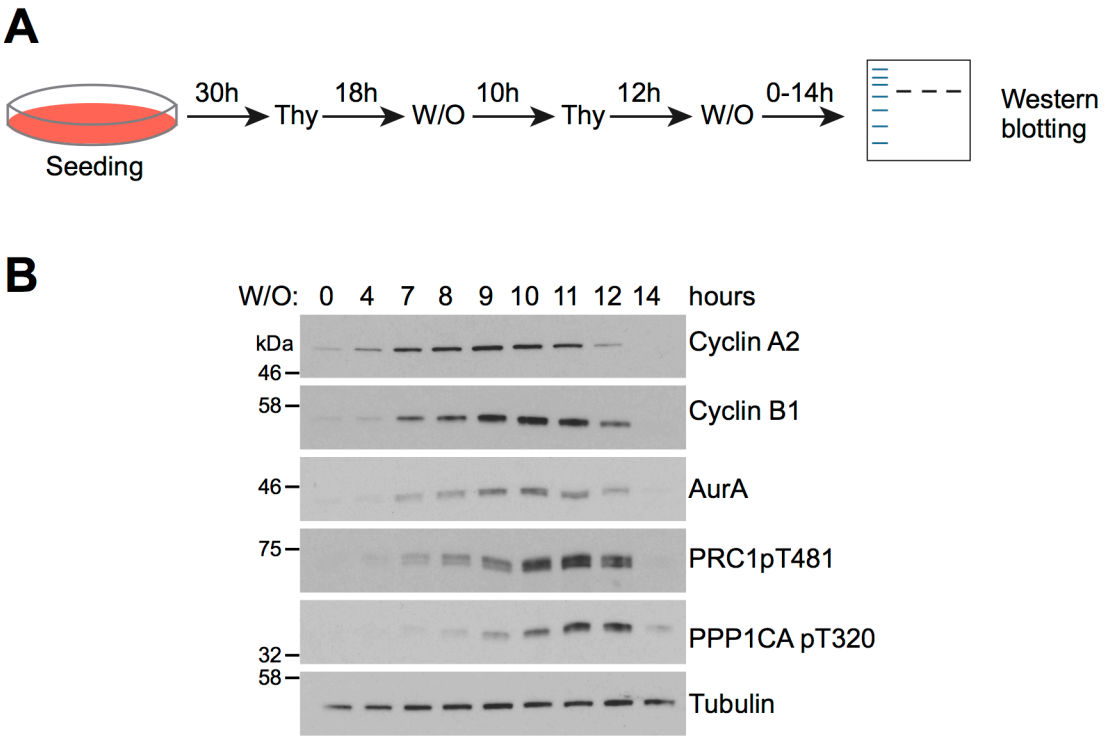


Figure 3.2 - Double thymidine block-release dramatically improves synchrony. (A) Schematic of the experimental workflow used. **(B)** HeLa S3 cells were prepared as outlined in (A), released for the indicated time before harvesting by combined mitotic shakeoff and treatment with 1mM EDTA in PBS, and lysis in Laemmli sample buffer for western blot analysis. Note the abrupt activation of CDK1 indicated by PRC1 pT481 and PPP1CA pT320, indicating improved culture synchrony.

3.2 The SAPS2-PLK1 interaction persists through G2 and mitosis

The analysis of PLK1-SAPS2 interaction timing was then performed with the improved synchronization procedure. To do this, HeLa S3 cells were transfected with SAPS2-GFP 6h before the block procedure and harvested for immune precipitation in hourly intervals up to 15h (Figure 3.3A). The cells entered mitosis 11h after washout demonstrated by an abrupt increase in PRC1 pT481 signal, high cyclin B1 levels and diminishing cyclin A2 (Figure 3.3B). The levels of these

factors also allowed for loose assignment of S phase and G2 states. SAPS2 interacted with other PP6 subunits consistently throughout this experiment (Figure 3.3C), whereas it bound PLK1 robustly starting at 6h after washout. A slight drop in this interaction was observed at the mostly mitotic 12h timepoint, but it recovered later on. The bound PLK1 was active only from 9h post washout, demonstrated by PLK1 pT210 levels, which dropped only after mitosis, when PLK1 degradation and deactivation occur.

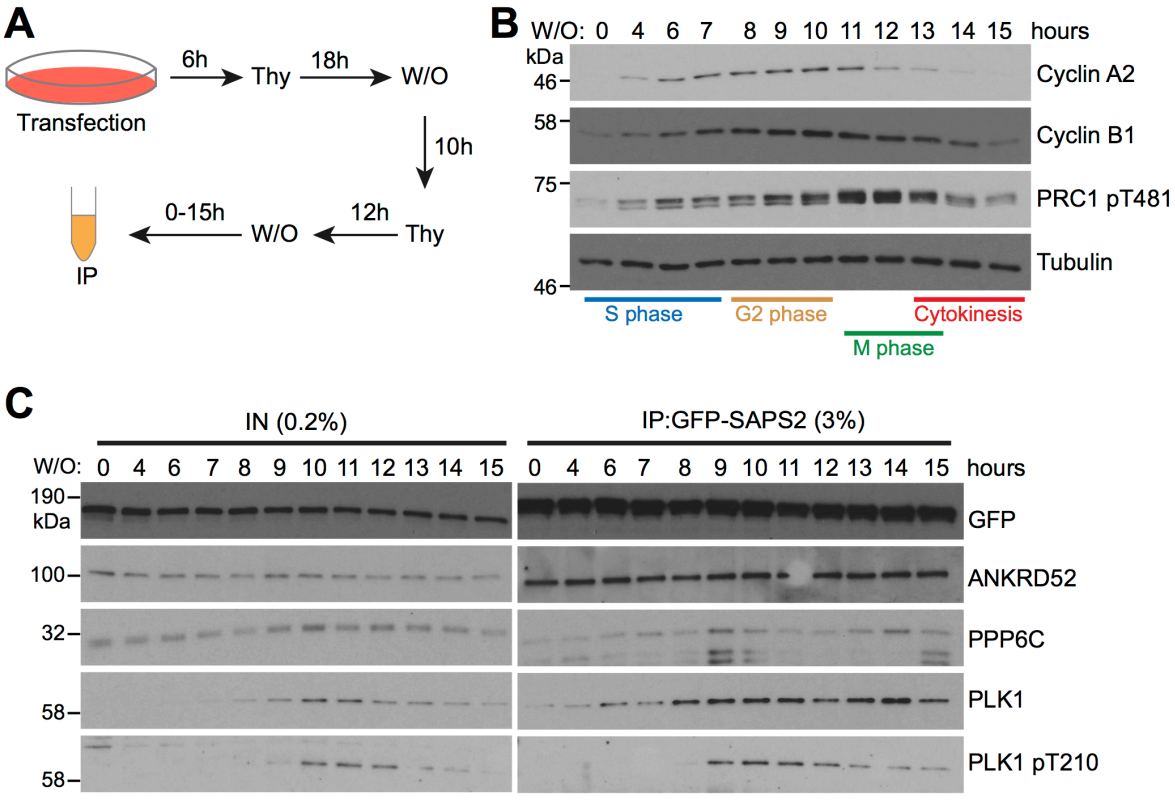


Figure 3.3 - SAPS2 interacts with PLK1 consistently through the cell cycle. (A) Schematic of the experiment workflow used. **(B-C)** HeLa S3 were transfected with SAPS2-GFP and synchronized as indicated in (A), followed by harvesting using combined mitotic shakeoff and 1mM EDTA/PBS treatment. An aliquot was taken out, lysed in Laemmli sample buffer and analyzed by western blotting to verify synchrony (B), while the rest was subjected to immune precipitation (C). W/O = washout.

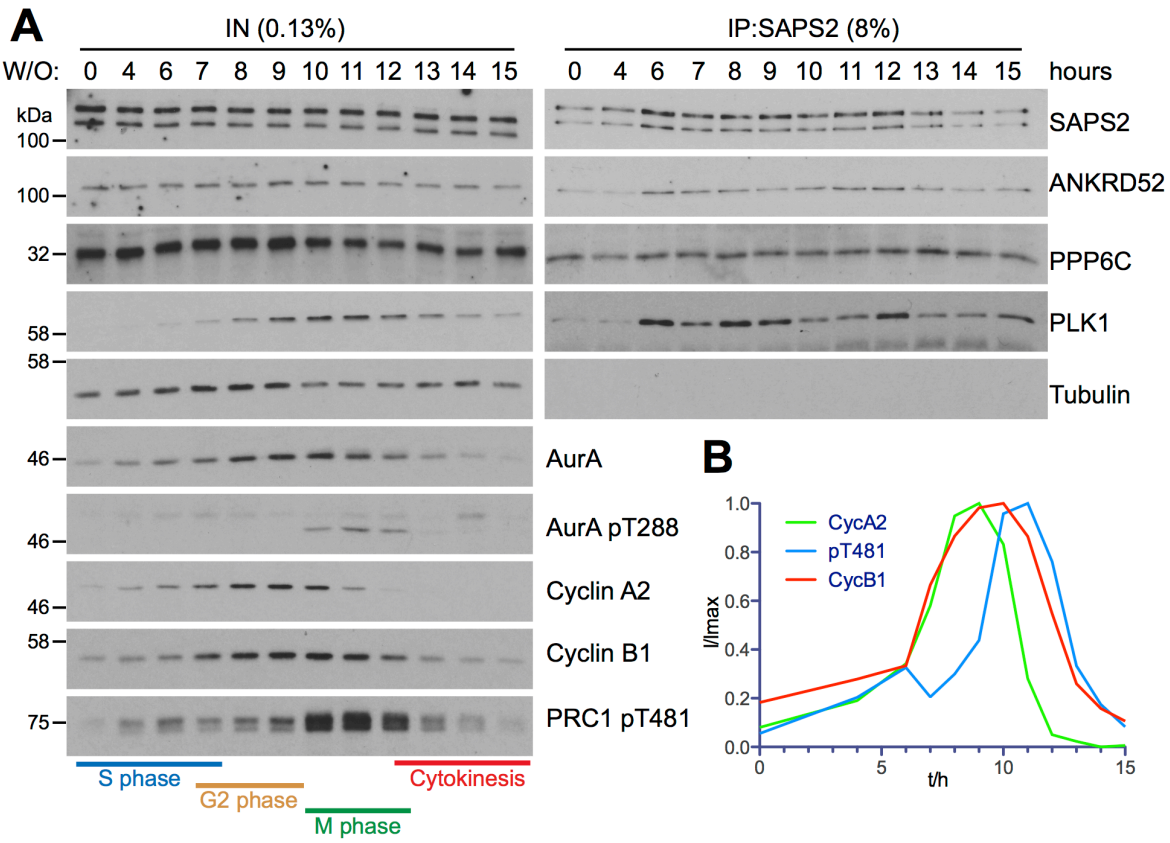


Figure 3.4 - Endogenous SAPS2 interacts with PLK1 consistently through the cell cycle. (A) HeLa S3 cells were arrested with a double thymidine block as in figure 3.2, released and harvested at the indicated times by combined mitotic shakeoff and treatment with 1mM EDTA/PBS before immune precipitation of endogenous SAPS2. The synchrony was verified by western blot analysis of input samples. **(B)** Expression profile of key cell cycle factors, quantified from (A).

The PLK1-SAPS2 interaction timing was further tested using endogenous SAPS2 (Figure 3.4). These cells were not transfected and entered mitosis after 10h, but otherwise behaved equivalently to the previous experiment in Figure 3.3. The levels of Aurora A pT288 were also measured, and only robustly detected once cells entered mitosis. SAPS2 could associate with other holoenzyme constituents as before. The interaction with PLK1 started at 6h after washout, corresponding to the S-G2 phase transition, and exhibited a small drop in the

largely mitotic 10-11h samples. PLK1 pT210 could not be detected in this IP due to the low affinity of this antibody.

An equivalent experiment was then performed pulling down endogenous PLK1 (Figure 3.5). Cells behaved equivalently to the previous experiments in terms of synchrony, entering mitosis abruptly 10h after washout (Figure 3.5, Cyclin A2, Cyclin B1 and PRC1 pT481). Accumulation of PLK1 was observed as cells passed through S-phase into mitosis and was reflected in the amount that was recovered in the IP. Some PLK1 activation occurred earlier in G2, however, most of the T210 phosphorylation occurred between 9 and 10h after washout, corresponding to mitotic entry (Figure 3.5, PLK1 and PLK1 pT210). PLK1 interaction partners showed different temporal patterns of binding. BUBR1 interacted with PLK1 consistently throughout the experiment. On the other hand, PRC1 was only bound when cells were in mitosis, and was particularly enriched 12h after washout, largely corresponding to the metaphase-anaphase transition when cyclin B1 degradation occurs. The bound PRC1 was never pT481-positive, consistent with published data showing this phosphorylation inhibits binding to PLK1 (Figure 3.5, PRC1 and PRC1 pT481) [137]. Uniquely, the PLK1 activation cofactor Bora bound to PLK1 most strongly in G2 phase and at G2-M transition, after which the interaction drops and Bora is degraded (Figure 3.5, Bora(lo) and Bora (hi)). SAPS2 interacted with PLK1 consistently throughout the experiment, similar to BUBR1 (Figure 3.5, SAPS2). The amounts were lower earlier in the cell cycle, mirroring total PLK1 levels. As expected, SAPS1 never interacted with PLK1 (Figure 3.5, SAPS1).

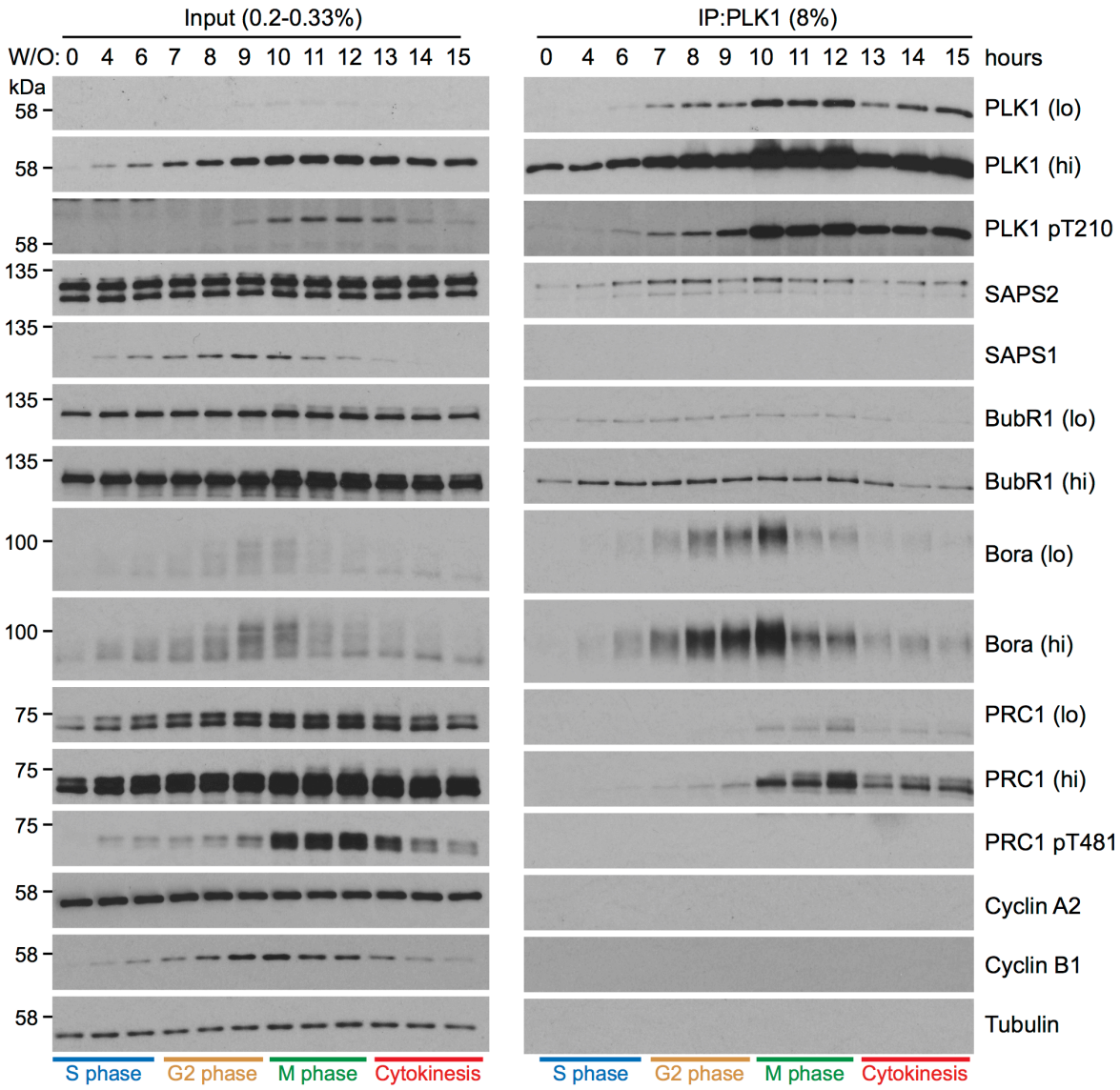


Figure 3.5 - SAPS2 interacts with PLK1 consistently throughout the cell cycle. HeLa S3 cells were arrested with a double thymidine block as in figure 3.2, released and harvested at the indicated times before immune precipitation with an antibody targeting PLK1 and analysis by western blotting. W/O = washout, lo = low exposure, hi = high exposure.

Next, the interaction was examined during synchronous mitotic exit with a previously validated procedure [137]. To do this, cells were transfected with SAPS2-GFP and arrested with nocodazole. They were then released from nocodazole and allowed to build spindles in fresh media. Afterwards, they were

synchronously pushed into anaphase by addition of the MPS1 inhibitor AZ3146 (Mps1-i) and sampled at minute intervals for immune precipitation (Figure 3.6). Under these conditions, cells were in anaphase 30min after AZ3146 addition demonstrated by the lack of cyclin B1 and dephosphorylation of PRC1 pT481 (Figure 3.6 Cyclin B1 and PRC1 pT481). Furthermore, Aurora A inactivation could be followed through collapse into a focused band, and the kinase was also slowly degraded in the later timepoints (Figure 3.6, AurA). PLK1 was more stable than Aurora A under these conditions, and the protein levels of PP6 subunits did not change (Figure 3.6, PLK1, GFP, PPP6C and ANKRD52). Intriguingly, SAPS2-GFP started off with a slightly smeared, phosphorylated band pattern, which was gradually focussed over time (Figure 3.6, GFP). PLK1 binding could be detected at all times, but increased as cells progressed through anaphase from 30 to 50min. Deactivation of PLK1 by PLK1 pT210 dephosphorylation could be observed in later timepoints (60-80min) both in clarified cell lysate, and in the SAPS2-bound pool (Figure 3.6, PLK1 and PLK1 pT210).

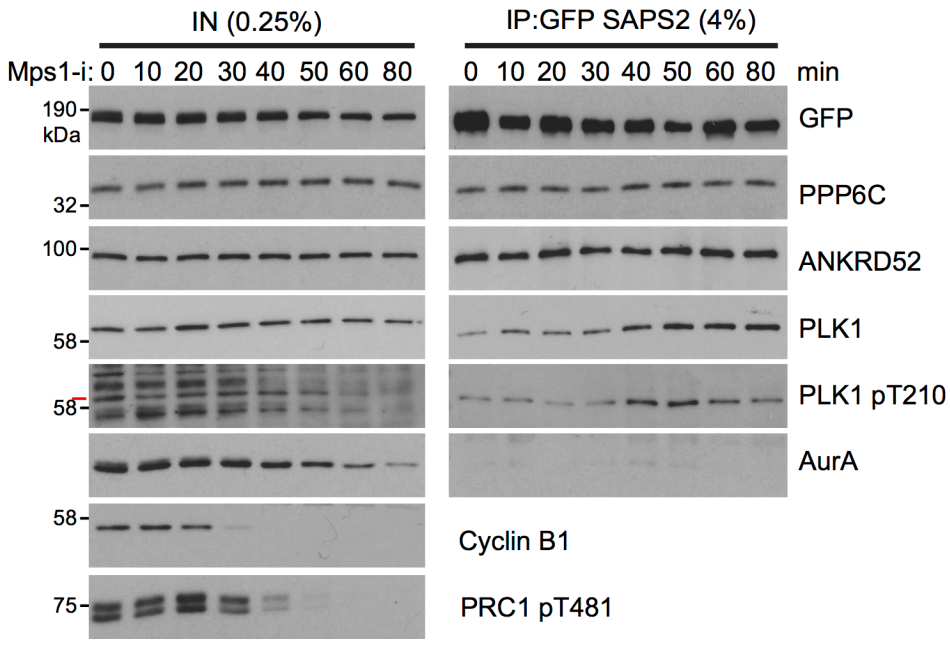


Figure 3.6 - The PLK1-SAPS2 interaction during mitotic exit. HeLa S3 cells were transfected with SAPS2-GFP for 36h before being arrested with nocodazole. Nocodazole was washed out, the cells allowed to rebuild mitotic spindles and synchronously released from mitosis by the addition of the 20μM AZ3146, an MPS1 inhibitor (Mps1-i), for the indicated time before harvesting and immune precipitation.

Collectively, these results narrow down the potential timing and properties of PP6-SAPS2 regulation by PLK1. The PLK1-SAPS2 interaction is itself regulated in time and occurs starting in G2 phase, but the bound PLK1 is largely inactive until late G2 phase. Abrupt bulk activation of PLK1 occurs just before mitotic entry and correlates with the peak of Bora binding, consistent with the role of Bora in the process [76, 206]. Once cells enter mitosis, the level of SAPS2-PLK1 complexes is reduced, possibly due to competition with PLK1 binding partners that become available after nuclear envelope breakdown. Regardless, active PLK1 still binds SAPS2 to an appreciable extent in mitosis and is again increased during mitotic exit, before the kinase is inactivated and degraded. PLK1

most commonly regulates its targets via phosphorylation rather than steric hindrance [147, 207, 212], therefore the most likely window of SAPS2 regulation are late G2 and M phases, when the kinase is active. The properties and consequences of the SAPS2-PLK1 interaction were examined next.

3.3 SAPS2 contains a canonical polo-box domain binding motif

PLK1 generally binds to targets of its regulation via the polo-box domain [10]. This mode of binding specifically recognises short phosphorylated motifs {S-[pS/pT]-P} (Figure 3.7A) [241]. The domain harbours two key residues – H538 and K540 – which binds to the phosphorylated residue [241]. Examination of the sequence of human SAPS2 revealed two candidate sites: ^{724}STP and ^{770}SSP, with the former being poorly conserved and the latter being fully conserved between vertebrates and a species of plants (Figure 3.7B). Invertebrates generally only have one or two forms of SAPS subunits which are usually putatively assigned and uncharacterized. Therefore, they were not considered in this analysis.

To test whether these candidate sites contribute to the interaction, both motifs were mutated to alanine in isolation and combination. Immune precipitation revealed that the ^{770}AAP mutant and the combined ^{724}AAP^{770}AAP mutant were entirely unable to bind PLK1 (Figure 3.7C, ^{770}AA and ^{724}AA^{770}AA). Conversely, the ^{724}AAP mutation in isolation did not affect PLK1 binding compared to WT (Figure 3.7C, ^{724}AA). Crucially, all mutants could associate with PPP6C and ANKRD52, demonstrating they were not deficient for holoenzyme assembly. Next, the requirement for the polo-box domain was tested. To do this, HeLa S3 cells were transfected with either PLK1 WT or H538A/K540A (HK/AA) (Figure 3.7D). The HK/AA mutant was entirely unable to bind SAPS2, whereas the WT was (Figure

3.7D, WT and HK/AA). Taken together, these data show that PLK1 binds to the ^{770}SSP motif on SAPS2 in a polo-box dependent fashion.

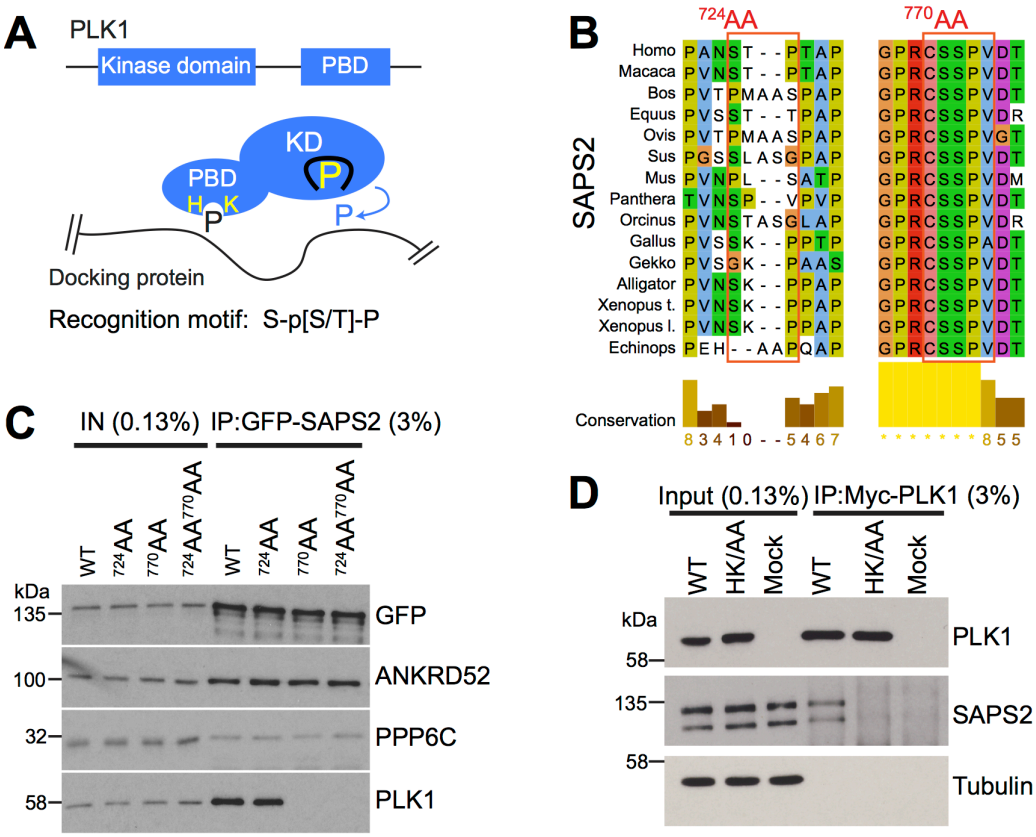


Figure 3.7 - PLK1 docks to 770SSP on SAPS2 via the Polo-box domain. (A) Mechanism of canonical Polo-box domain (PBD)-mediated binding. **(B)** Conservation of two candidate Polo-box recognition motifs on SAPS2. **(C)** Lysates from asynchronously growing HeLaS3 cells were transfected for 48h with GFP tagged B55, SAPS2 WT or mutants for candidate PBD-docking sites as indicated and subjected to immunoprecipitation with an antibody against GFP. The samples were analyzed by western blotting. **(D)** Asynchronously growing HeLaS3 cells were transfected with Myc-tagged PLK1 WT or Polo-box deficient H538A/K540A (HK/AA) and immune-precipitated with an antibody against Myc before western blot analysis. Cells transfected with and empty plasmid were used as control (mock).

3.4 The docking site on SAPS2 is phosphorylated by PLK1 *in vivo*

Polo-box docking partners of PLK1 are often also its substrates [162]. To examine whether this is true for PP6, saturating amounts of PLK1 were mixed with PP6-SAPS preparations from asynchronous HeLa S3 cells and incubated for 30min at 30°C in the presence or γ-[^{32}P]-ATP. Under these conditions, robust phosphorylation of the previously described PLK1 substrate, PRC1, was observed (Figure 3.8A, PRC1). SAPS1 and SAPS3 showed little to no increase in [^{32}P] incorporation (Figure 3.8A, SAPS1 and SAPS3). This indicates that they are not PLK1 substrates with the caveat that SAPS3 could not be loaded to equal amount as the others due to the previously discussed expression problem. Conversely, SAPS2 WT was robustly phosphorylated by PLK1 (Figure 3.8A, SAPS2 WT). On the other hand, no phosphorylation of the SAPS2 docking mutant (^{770}AA) was observed (Figure 3.8A, SAPS2 ^{770}AA). SAPS2 WT showed a small amount of radioactive incorporation in the absence of added PLK1, which was probably due to endogenous PLK1 co-purified with SAPS2. To test this, a sample was left without PLK1 addition and treated with the PLK1 inhibitor BI2536 (PLK1-i) (Figure 3.8B). Treatment with the PLK1 inhibitor resulted in a complete loss of radioactive signal (Figure 3.8B, PLK-i +), indicating that it was generated by the activity of endogenous co-purified PLK1. Furthermore, this suggests that any other potentially co-purified kinases such as DNA-PK or Aurora A don't contribute to the radioactive signal observed on SAPS2 in this experiment.

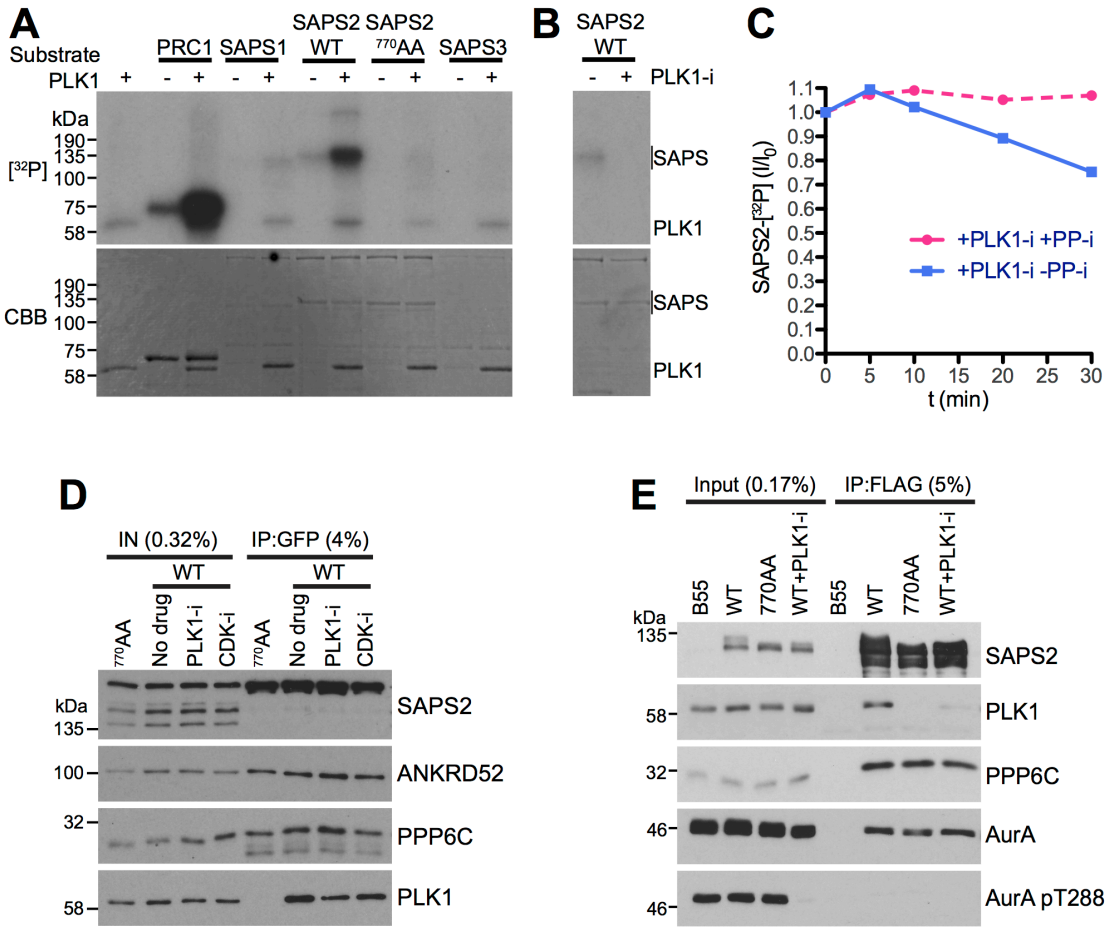


Figure 3.8 - PLK1 phosphorylates its own docking site on SAPS2. (A) PP6 complexes were mixed with PLK1 and γ-[32P]-ATP and incubated at 30˚C for 30min before Coomassie staining and autoradiographic analysis. PRC1 is used as a positive control. **(B)** PP6-SAPS2 WT complexes were incubated with ATP without additional PLK1 in the presence or absence of BI2536 (PLK1-i), using the same procedure as in (A). **(C)** PP6-SAPS2 WT was treated as in (A) before addition of BI2536 (PLK1-i) and incubation at 30˚C in the presence or absence of 1μM okadaic acid (PP-i). The samples were analyzed as in (A), and the autoradiography quantitation given. **(D)** Cells expressing doxycycline-inducible SAPS2 WT or 770AA were synchronized by a double thymidine block and released for 3 hours before a further 3h treatment with 1μM BI2536 (PLK1-i) or 5μM Flavopiridol (CDK-i) before harvesting and immune precipitation. **(E)** HeLaS3 cells were transfected with FLAG-tagged constructs as indicated, arrested in mitosis and harvested. Where indicated, cells were treated with 1μM BI2536 for 100min before harvesting (WT+PLK1-i)

The ability of PP6-SAPS2 to dephosphorylate itself was then tested. To do this, PP6-SAPS2 was phosphorylated as in Figure 3.8A before addition of PLK1 inhibitor and sampling over time in the presence or absence of okadaic acid, a potent PP2A-subfamily inhibitor (PP-i). After exposure, the effect was measured by densitometry. The radioactive signal on SAPS2 was gradually lost over time, reaching ~70% intensity after 30min (Figure 3.8C). Addition of okadaic acid completely abrogated this decay, demonstrating it is due to the activity of a PP2A-subfamily phosphatase. The densitometric quantifications in this experiment were matched by scintillation counts of excised bands (not shown).

These data suggest that PLK1 phosphorylates SAPS2 dependent on the docking site and that the phosphorylation can be opposed by PP6-SAPS2 itself. The docking site requirement for phosphorylation could be caused by two reasons. Firstly, PLK1 may phosphorylate its own docking site. Secondly, efficient phosphorylation of SAPS2 on another site may require stable binding of PLK1 to SAPS2 via docking. These two options, however, are not mutually exclusive. If PLK1 phosphorylates its own docking site, treating cells with a PLK1 inhibitor should result in a reduction in PLK1-SAPS2 binding. To test this, cells expressing inducible GFP-tagged SAPS2 WT or ^{770}AA were arrested with a double thymidine block and released for 3h before treatment with BI2536 for a further 3h. Immune precipitation was then performed and the samples analysed by western blotting. SAPS2 ^{770}AA was entirely unable to bind PLK1 as expected, whereas SAPS2 WT could (Figure 3.8D, ^{770}AA and WT No drug). Treatment with the PLK1 inhibitor resulted in decreased PLK1-SAPS2 binding (Figure 3.8D, WT PLK-i). The contribution of CDK activity was also tested because proline directed phosphorylation sites such as ^{770}SSP are often CDK substrates. Treatment with

the CDK1/2/4/6 inhibitor flavopiridol did not result in decreased PLK1-SAPS2 binding (Figure 3.8D, WT CDK-i) suggesting that these CDKs don't directly contribute to the phosphorylation in cells.

The requirement for PLK1 activity for binding was further examined in mitosis. To do this, HeLa S3 cells were transfected with FLAG-tagged B55, SAPS2 WT or ^{770}AA and subjected to immune precipitation. Where indicated, cells were treated with BI2536 for 100min prior to harvesting (WT+PLK-i). PLK1 inhibition resulted in a marked decrease in PLK1-SAPS2 interaction (Figure 3.8E, WT+PLK-i). Additionally, SAPS2-FLAG WT migrated as a phosphorylated smear which was completely absent in the ^{770}AA mutant and starkly reduced upon PLK1 inhibition (Figure 3.8E, SAPS2). Binding to Aurora A and PPP6C was equivalent in all cases, indicating that holoenzyme assembly and the affinity for the substrate remain unchanged. Curiously, a reduction in Aurora A pT288 in lysate could also be observed upon PLK1 inhibition, in line with a previously published observation [206].

Collectively, these results reveal several important features. Firstly, PLK1 phosphorylates its own docking site on SAPS2 *in vitro* and *in vivo*. Moreover, ongoing PLK1 activity is required to maintain both its own binding and the overall phosphorylation status of SAPS2 in mitosis. These data, along with the previous observation that PPP6C depletion results in increased SAPS2 phosphorylation, strongly suggest the docking site phosphorylation is dynamically opposed by a phosphatase, most likely PP6-SAPS2 itself.

3.5 PLK1 inhibits PP6-SAPS2 activity *in vitro*

The effect of PLK1 on PP6-SAPS2 activity was next examined. To assess whether PLK1 binding affects PP6-SAPS2 activity, PP6-SAPS2 WT complexes

were pre-incubated with varying amounts of added PLK1 in the absence of ATP, ranging from sub-stoichiometric to saturating. These were then incubated with Aurora A-TPX2 (Figure 3.9A). In all cases, equally efficient dephosphorylation could be observed, suggesting that PLK1 binding itself does not affect the activity of PP6-SAPS2 (Figure 3.9A, AurA and AurA pT288), with the caveat that exogenously added PLK1 may not efficiently bind to PP6-SAPS2 complexes under these conditions. The potential effect of phosphorylations on activity was then tested. To do this, phosphatase was mixed with excess PLK1 and incubated in the presence or absence of ATP for 45min at 30°C before addition of Aurora A-TPX2 complexes (Figure 3.9B-C). In order to ensure a complete lack of PLK1 activity without ATP, 1µM BI2536 was also included in those reaction mixtures (Figure 3.9C, -ATP). To prevent re-phosphorylation at T288, Aurora A-TPX2 substrate complexes were pre-treated with the Aurora A inhibitor MLN8237 (Figure 3.9C, all conditions). The amount of phosphatase was titrated such that PP6-SAPS2 WT dephosphorylated 50% of the substrate at T288 after 20min in a standard phosphatase assay (see Figure 2.3A). However, phosphatase activity of both the WT and mutant phosphatase was nearly completely lost in this experiment, independent of ATP (Figure 3.9C, -ATP and +ATP). Two simple possibilities could explain this effect. Firstly, the buffer composition was altered to reflect a compromise between conditions optimal for kinase and phosphatase activities (see materials and methods). While the ionic strength of this buffer was similar to the original used in phosphatase assays, an effect of one of the components on PP6-SAPS2 activity cannot be excluded. Secondly, the phosphatase could be inactivated during the initial incubation with the kinase.

Regardless, since this effect was observed in multiple replicate experiments, alternative strategies were explored.

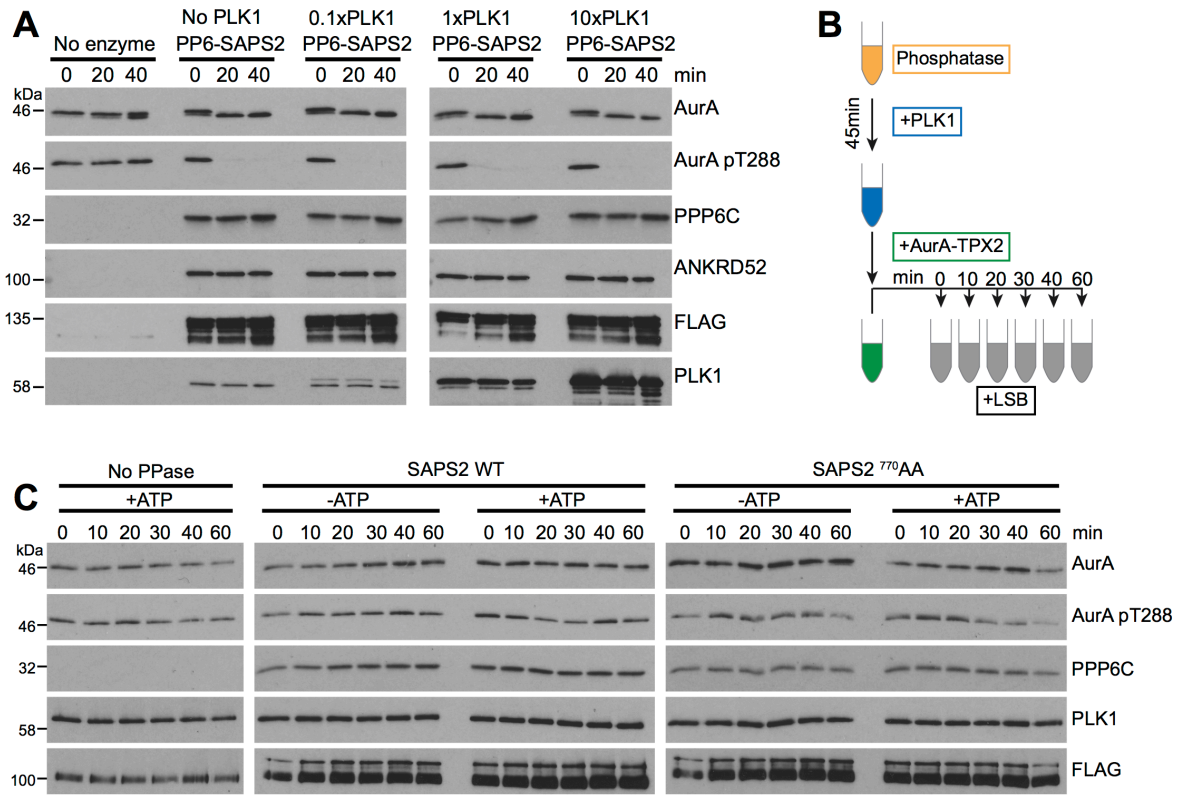


Figure 3.9 - Regulation of PP6-SAPS2 activity by PLK1 in vitro. (A) PLK1 and phosphatase were mixed in varying ratios and incubated 15min on ice. AurA-TPX2 was then added and sampled at indicated times before western blotting. 0.1xPLK1 = 0.68nM 1xPLK1 = 6.8nM, 10xPLK1 = 68nM. **(B)** Workflow schematic describing the experiment in (C). **(C)** PLK1 and phosphatase were mixed with or without ATP and incubated 45min at 30˚C. Samples without added ATP also contained 1μM BI2536 to prevent any phosphorylation by contaminating PLK1. AurA-TPX2 premixed with MLN8237 (1μM final) to prevent rephosphorylation of the kinase was added and samples taken out at indicated times.

To circumvent these difficulties, an alternate approach was developed wherein the state of PP6-SAPS2 from cells would be conserved during purification. Phosphatase purifications are generally done without the inclusion of phosphatase inhibitors in order to prevent the inactivation of the purified enzyme. However, this is problematic if the preservation of phospho-sites on the phosphatase holoenzyme is desired. Therefore, an excess of the reversible competitive phosphatase inhibitor β-glycerolphosphate was included during the majority of the amended procedure (Figure 3.10A). The inhibitor was then removed by several consecutive wash steps and the phosphatase eluted as before, in the presence of the PP2A/PP6 catalytic cofactor, Mn^{2+} (Figure 3.10A). This was applied to purify SAPS2 WT or ^{770}AA in parallel (Figure 3.10B). In both instances, PPP6C was equally efficiently bound, whereas PLK1 bound only to SAPS2 WT as expected. Furthermore, a smeared pattern was again visible for SAPS2 WT which was retained during lysis and in the eluate, indicating that the mitotic phosphorylation state was at least partially maintained (Figure 3.10B, FLAG). Conversely, SAPS2 ^{770}AA was a sharply focussed more rapidly migrating band as before (Figure 3.8E). These preparations were titrated against recombinant PPP6C as in Figure 2E (not shown), before being assayed *in vitro* against Aurora A-TPX2 (Figure 3.10C-D). To do this, 50pM PP6-SAPS2 WT or ^{770}AA were incubated with 3nM T288 phosphorylated Aurora A-TPX2 complexes at 30°C and sampled in 10min intervals. Under these conditions, PP6-SAPS2 WT showed low activity towards Aurora A pT288 whereas PP6-SAPS2 ^{770}AA was considerably more active (Figure 3.10C). Replicate experiments were performed and the dephosphorylation quantified, revealing that SAPS2 WT dephosphorylated ~30% of T288 after 60min while the ^{770}AA mutant unable to

bind PLK1 completely dephosphorylated T288 after 30-40min (Figure 3.10D). These results were qualitatively reproducible across multiple phosphatase and substrate preparations, although the difference in activity varied in magnitude (appendix Figure A1). This finding indicates that PLK1 acts as an inhibitor to PP6-SAPS2, most likely through binding and phosphorylation of the SAPS2 protein.

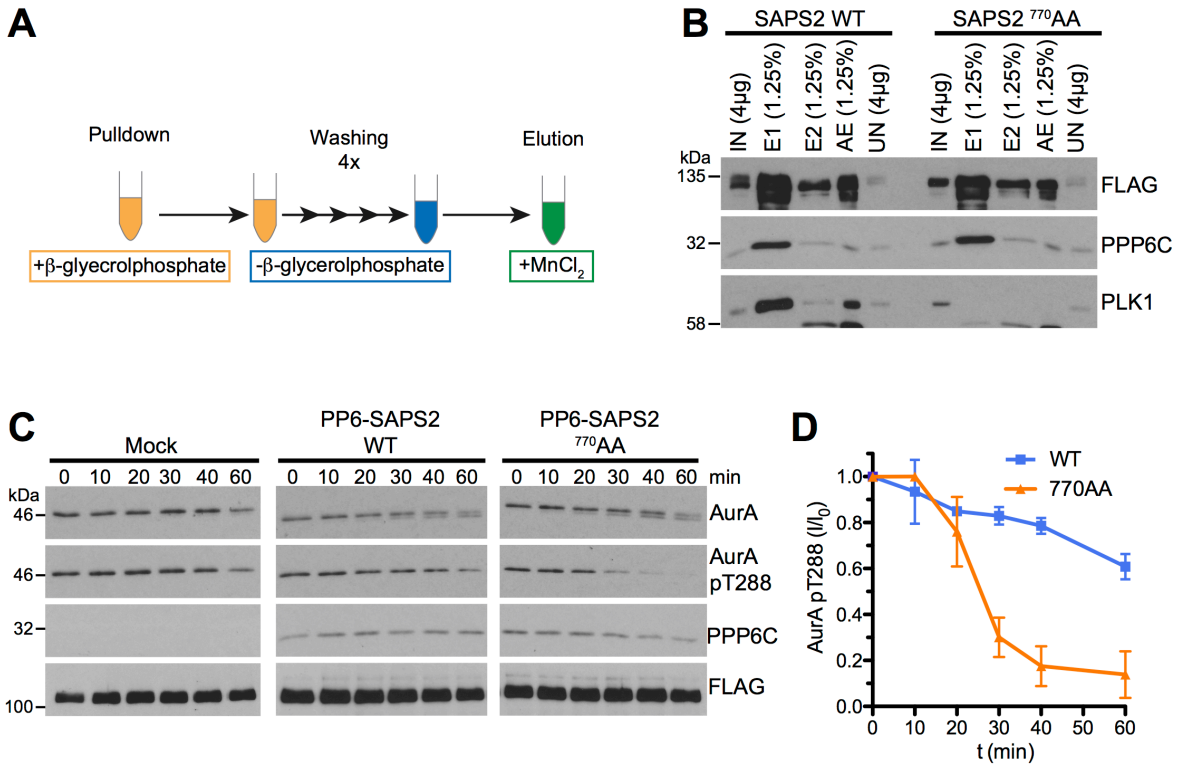


Figure 3.10 - PLK1-deficient PP6-SAPS2 is more active than WT. (A) An altered workflow used to purify PLK1-phosphorylated PP6-SAPS2. Cells were transfected with SAPS2-FLAG for 48h. They were then lysed and incubated with a-FLAG beads in the presence of saturating amounts of β-glycerolphosphate, followed by extensive washing and elution without the inhibitor. **(B)** Eluted PP6-SAPS2 WT or ^{770}AA were analyzed by western blotting. Note the smeared band pattern in the WT input and AE fractions. **(C)** PP6-SAPS2 WT or 770AA complexes (50pM) purified as in (A-B) were assayed against AurA-TPX2 complexes (3nM) at 30˚C. **(D)** Quantification of replicate experiments as in (A). Mean±SEM, n=2.

3.6 PLK1 regulates active Aurora A levels via PP6

Inhibition of PP6-SAPS2 by PLK1 ideally places this Aurora A phosphatase as a potential integrator of Aurora A and PLK1 activities in cells and may explain the observation that PLK1 inhibition results in deactivation of Aurora A [206]. If PP6 mediates this process, the observed deactivation of Aurora A should be abrogated by depletion of PPP6C or the appropriate SAPS subunit. Furthermore, in order for this feedback to be effective for mitotic regulation *in vivo*, it should respond within the timeframe of mitosis – roughly one hour or less. To test whether PP6 activity is required for PLK1-Aurora A feedback, cells treated with non-specific control or PPP6C siRNA were arrested in mitosis before treatment with 1µM BI2536 (PLK1-i) or solvent control for up to 30min (Figure 3.11A). Aurora A pT288 was stable under control-treated condition, whereas PLK1 inhibition resulted in its dephosphorylation within 15min (Figure 3.11A, siControl PLK1-i). Depletion of PPP6C prevented this dephosphorylation (Figure 3.11A, siPPP6C PLK1-i). None of the conditions caused gross changes in overall cell biochemistry, as cyclin B1 was stable and CDK1 activity reflected in PRC1 pT481 was unchanged (Figure 3.11A, all conditions). This suggests that the observed effects are largely limited to the explored PLK1-PP6-Aurora A system and not caused indirectly. Further analysis was performed by immunofluorescence microscopy. To do this, control- or PPP6C-depleted cells were synchronized by thymidine-release and treated with BI2536 or solvent control for 15min before fixation and staining (Figure 3.11B). Control cells exhibited orderly bipolar spindles and robust focussed Aurora A pT288 staining on spindle poles. Inhibition of PLK1 changed spindle morphology, in particular spindle poles, and resulted in a significant reduction of Aurora A pT288 staining (Figure 3.11C). Depletion of PPP6C caused a mislocalization of

Aurora A pT288 along the mitotic spindle and prevented its loss from spindles upon PLK1 inhibition (Figure 3.11B and 3.11C).

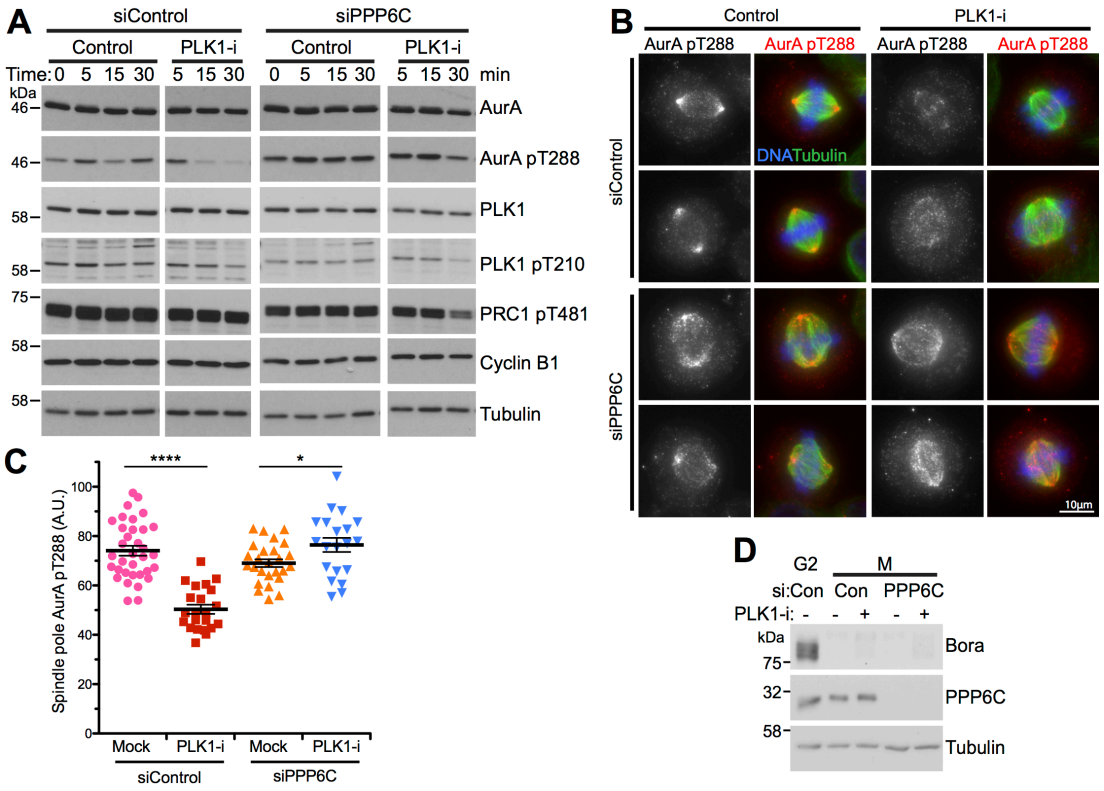


Figure 3.11 - PLK1-AurA feedback is established through PP6. (A) HeLaS3 cells were treated with siRNA as indicated, arrested in mitosis and treated with either DMSO (control) or 1μM BI2536 (PLK1-i) for up to 30min. After harvesting, rapid lysis was performed with Laemmli sample buffer and samples analyzed by western blotting. **(B)** HeLaS3 cells were depleted as indicated, synchronized by thymidine-release and treated with 1μM BI2536 or solvent control for 15min before fixation and immunofluorescent staining. **(C)** Quantification of AurA pT288 signal around mitotic spindle poles, mean±SEM given (n>20). Vertices indicate significance of 1-way ANOVA followed by Bonferroni's multiple comparison test. **(D)** Cells were treated with siRNAs as indicated and synchronized to G2 or M phase before treatment with 1μM BI2536 for 30min.

Importantly, Bora was not stabilized under any of the conditions (Figure 3.11D). This demonstrates that the previously proposed mechanism for PLK1-Aurora A feedback, wherein Bora sequesters Aurora A [207], cannot account for the experimental observations. Therefore, PP6 activity, not Bora, is required to establish functional feedback between PLK1 and Aurora A.

The contribution of the two Aurora A phosphatase complexes, PP6-SAPS2 and PP6-SAPS3, was next tested. Cells were depleted of PP6 subunits as indicated and arrested in mitosis before treatment with the PLK1-inhibitor BI2536 (Figure 3.12). Control cells showed gradual dephosphorylation of Aurora A pT288 (Figure 3.12, siControl +PLK-i). Depletion of PPP6C or SAPS3 resulted in stabilization Aurora A pT288 dephosphorylation when PLK1 was inhibited, and depletion of SAPS2 also mitigated this effect (Figure 3.12, siPPP6C, siSAPS2 and siSAPS3 +PLK1-i). On the other hand, inhibition of Aurora A itself resulted in very rapid dephosphorylation under control conditions (Figure 3.12, siControl +AurA-i), suggesting that Aurora A autophosphorylation is under control of a highly active phosphatase. This dephosphorylation was markedly slowed when either PPP6C or SAPS3 were depleted (Figure 3.12, siPPP6C and siSAPS3 +AurA-i), suggesting PP6-SAPS3 contributes a constitutive baseline Aurora A pT288 counteracting activity. Depletion of SAPS2 did not show the same effect (Figure 3.12 siSAPS2 +AurA-i), in excellent agreement with earlier observations in Figure 2.6A, where SAPS2 did not contribute Aurora A pT288 phosphatase activity in cell extracts. Depletion of PPP6C did not result in full stabilization of Aurora A pT288 upon Aurora A inhibition (Figure 3.12, siPPP6C +AurA-i). The remaining 10% of PPP6C after depletion, estimated from western blotting in this experiment (data not shown), may account for the observed activity. Alternatively, inhibition of

Aurora A may destabilize Aurora A-TPX2 complexes, resulting in some degree of dephosphorylation of free Aurora A by PP1 [201]. Moreover, Aurora A-TPX2 complexes may be undergoing natural assembly-disassembly cycles which depend on Aurora A activity. Collectively, these data demonstrate that PP6-SAPS2 is a PLK1-regulated Aurora A phosphatase *in vivo* and works in concert with the constitutively active PP6-SAPS3 to establish full feedback between PLK1 and Aurora A.

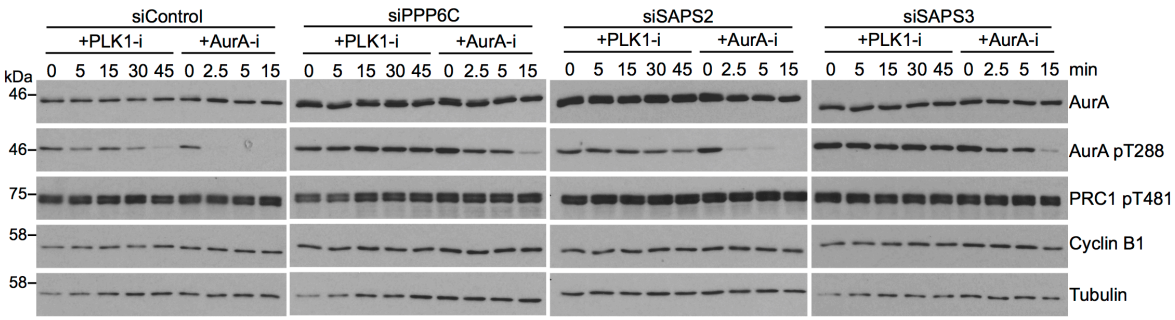


Figure 3.12 – PLK1-Aurora A feedback is controlled by PP6-SAPS2 and PP6-SAPS3. HeLa S3 cells were transfected with siRNA duplexes against PP6 subunits as indicated for 55h, arrested with nocodazole and treated with either 1μM BI2536 (PLK1-i) or 500nM MLN8237 (AurA-i). Aliquots of cells were taken in indicated minute intervals, washed, and lysed rapidly by addition of Laemmli sample buffer and analyzed by western blotting.

3.7 Bora links timely PLK1 and Aurora A activation

The requirement for PLK1 activity in Aurora A control was then further examined by perturbing PLK1 activation. To do this, cells were arrested with a double thymidine block and depleted of Bora to prevent PLK1 activation. Since loss of Bora has highly adverse effects on mitosis [207], the siRNA treatment was performed only during the second thymidine block. This was sufficient for complete depletion, but prevented the accumulation of defects before harvesting, which could have impacted the results. Under these conditions, control cells progressed through S phase and G2 and entered mitosis abruptly 10h after

washout, as demonstrated by the sharp rise in PRC1 pT481 (Figure 3.13, siControl). Bora became increasingly modified during the progression and degraded upon mitotic entry. At this time, the bulk of Aurora A pT288 and PLK1 pT210 was created. These were inactivated during mitotic exit, at the 14h timepoint. Bora depletion resulted in delayed mitotic entry, which only occurred appreciably by 14h after washout (Figure 3.13, siBora), in agreement with previously published data [206, 207]. This delay resulted in prolonged synthesis of cell cycle factors, including cyclins A2 and B1, PLK1 and Aurora A, which accumulated to higher levels. PLK1 activation was inefficient even after this extended time and PLK1 pT210 was barely detectable (Figure 3.13, siBora 14 hours). At the time of mitotic entry, Aurora A was activated, but this was proportionally less to the total Aurora A pool when compared to control cells (Figure 3.13, siBora 14 hours). This reduction in proportional Aurora A pT288 steady state levels could be explained by increased PP6-SAPS2 activity, due to the inability of Bora-depleted cells to activate PLK1.

3.8 PLK1 regulation of PP6-SAPS2 does not affect bulk Aurora A during an unperturbed cell cycle

The data presented so far support the view that PLK1-mediated inhibition of SAPS2 happens in mitosis. Because, the initial activation of both PLK1 and Aurora A occurs in late G2 phase, it was therefore hypothesized that depletion of SAPS2 would lead to premature activation of Aurora A in G2 and conversely, loss of PLK1-mediated regulation would delay Aurora A activation in G2. This could further cause altered PLK1 activation dynamics, as the PLK1 T-loop is phosphorylated by Aurora A [76, 206].

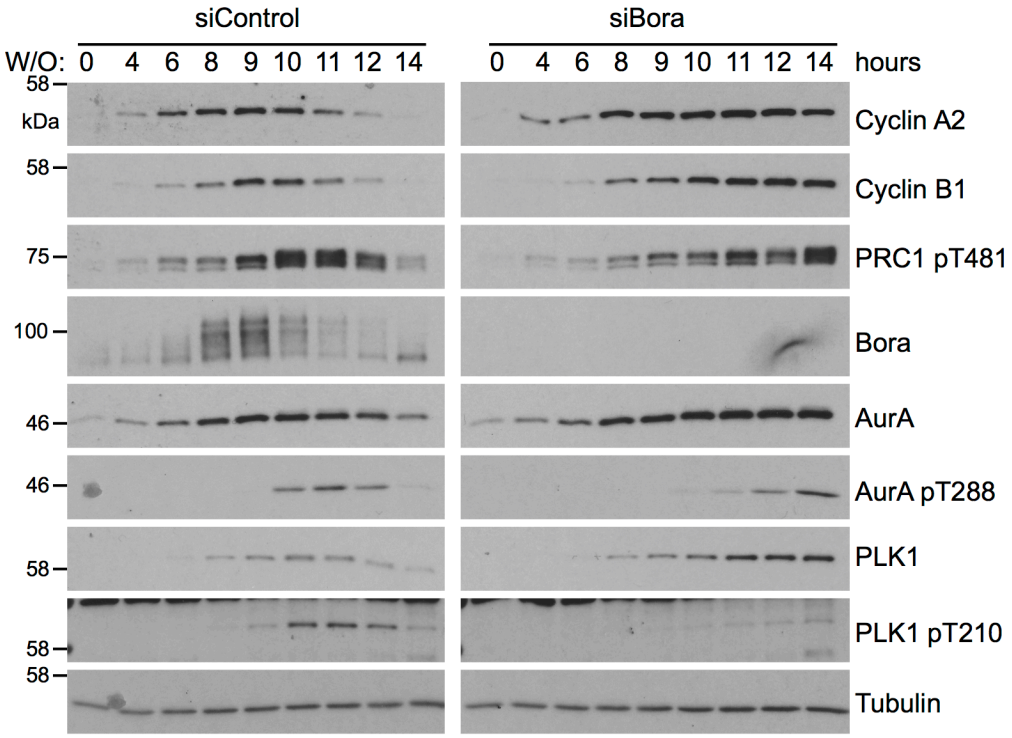


Figure 3.13 - Bora depletion leads to delayed mitotic entry and Aurora A activation. HeLa S3 cells were arrested with a double thymidine block as before, treated with siRNA during the second thymidine block and released. Samples were harvested by combined mitotic shakeoff and treatment with 1mM EDTA in PBS, before rapid lysis in Laemmli sample buffer and western blot analysis.

To test this hypothesis, cells were arrested with a double thymidine block and depleted of PP6 subunits as indicated before release into media containing taxol (Figure 3.14A). Taxol was included to prevent mitotic exit, allowing isolated examination of the biochemical status during mitotic entry. Depletion of all targets was highly efficient with this procedure (Figure 3.14B). Under these conditions, control cells gradually entered mitosis starting from 11h after washout, indicated by the levels of cyclin B1 and CDK1 activity, demonstrated by its substrate, PRC1 pT481 (Figure 3.14A, siControl). At this time, cyclin A2 degradation starts, further supporting the assigned time of mitotic entry. Low levels of Aurora A pT288 could be detected 1-2h before bulk mitotic entry and rose sharply when cells entered mitosis. Loss of Aurora A pT288 could be observed nearing the end of the

experiment, even though mitotic exit did not occur (Figure 3.14A, siControl 13hrs). The dynamics of Aurora A pT288 were unaltered between control and SAPS2 depletion (Figure 3.14A, siSAPS2; Figure 3.14C), but the level of Aurora A pT288 was increased and detected earlier when PPP6C (Figure 3.14A, siPPP6C; Figure 3.14C) or SAPS1/3 in combination were depleted (Figure 3.14A, siSAPS1/3; Figure 3.14C). The observed differences in the behaviour of the Aurora A and PLK1 T-loop phosphorylation was not caused by differential cell cycle progression, as the build-up of cell cycle factors, including Aurora A and PLK1, was equivalent, and PRC1 T481 was phosphorylated equally between the conditions (Figure 3.14D). Interestingly, although the total level of PLK1 was the same as in the control, the peak signal for PLK1 pT210 in mitosis (10-11hrs) was reduced in PPP6C depleted cells (Figure 3.14A). Although unexpected, this result does support the view that PLK1, PP6 and Aurora A activities are interlinked. This effect might be explained by changes in the behaviour of the Aurora A and PLK1 regulator Bora. However, under all conditions, Bora was increasingly modified during the course of the experiment under all conditions, and was degraded upon mitotic entry with similar kinetics (Figure 3.14A). These data suggest that PP6-SAPS2 activity does not appreciably suppress Aurora A activation during mitotic entry, and that this function is largely provided by PP6-SAPS3.

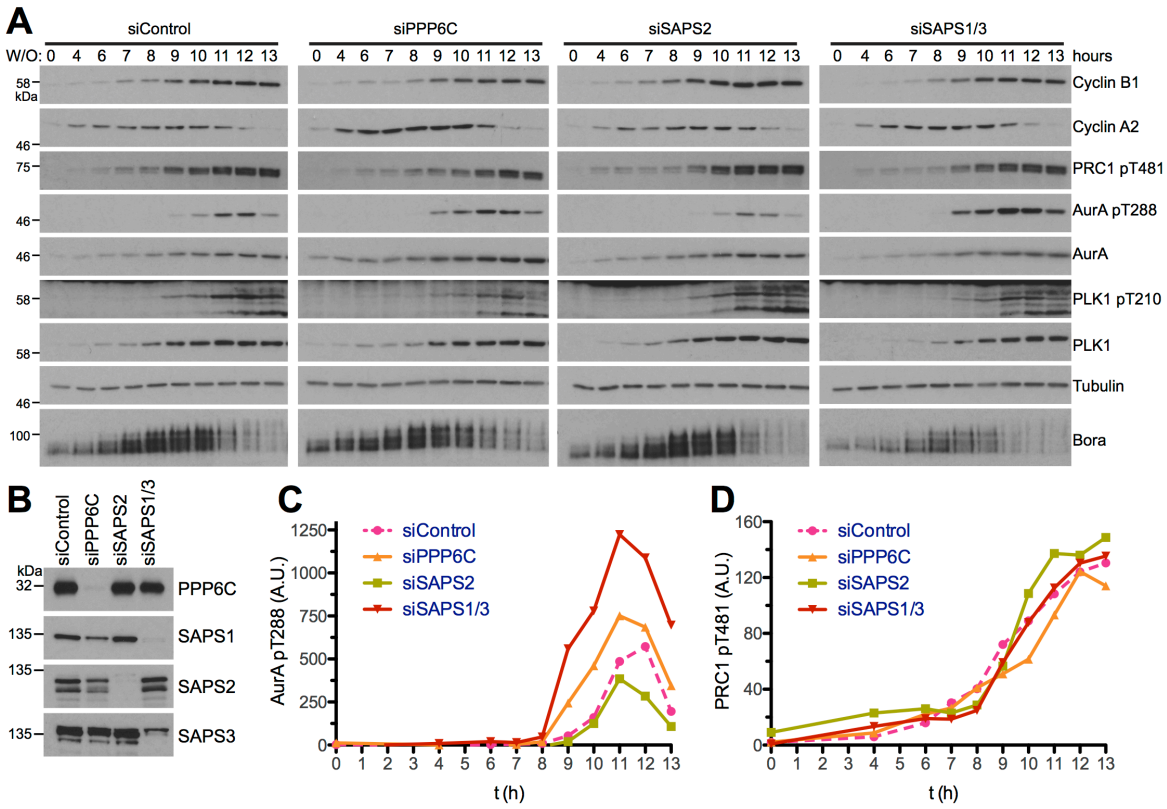


Figure 3.14 - Depletion of PP6 subunits affects Aurora A, but not CDK1 activation dynamics. (A) HeLa S3 cells were depleted of PP6 subunits as indicated, arrested with a double thymidine block and released. Taxol (100nM) was added after 6h to prevent cells from exiting mitosis and cells harvested as indicated by combined mitotic shakeoff and 1mM EDTA/PBS treatment. **(B)** Samples collected 13h after washout were used to test the depletion efficiency by western blotting. **(C-D)** Densitometric quantitation of AurA pT288 (B) and PRC1 pT481 (C) from (A). For contrast, the control curves are dashed.

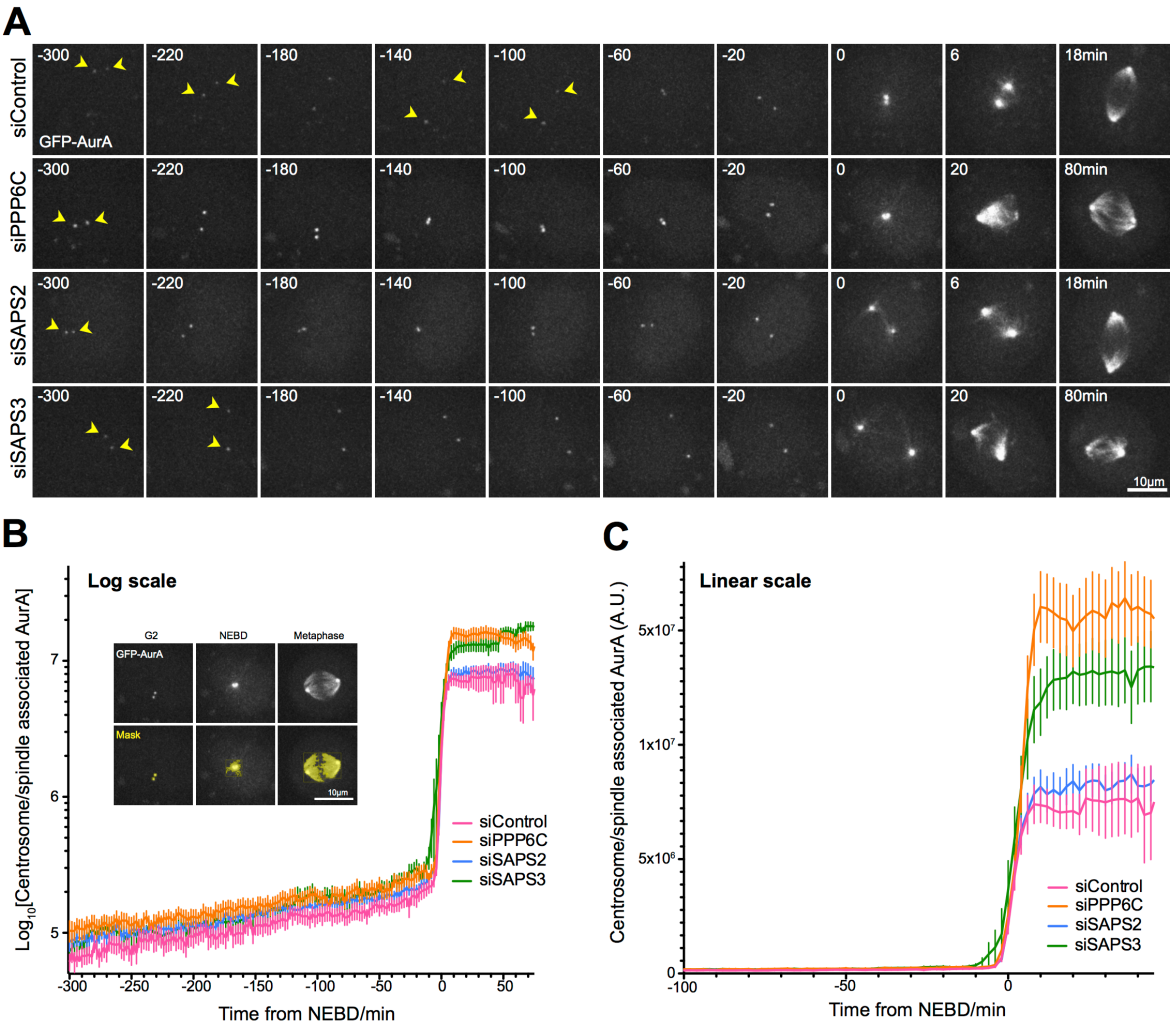


Figure 3.15 - PP6-SAPS2 does not limit Aurora A recruitment to centrosomes. (A) Heterozygous HeLa S3 cells expressing GFP-AurA under the endogenous promoter were treated with siRNA as indicated for 50h, synchronized with a thymidine arrest, released and imaged by time-lapse microscopy. Times are given relative to NEBD. Arrowheads indicate the location of centrosomes. **(B)** Measurement of centrosome/spindle associated GFP-AurA from G2 into mitosis. Insets demonstrate the measured objects at 3 different stages. Note the logarithmic scale. Mean±SEM given (n>13 combined from 2 biological replicates, n=11 from 1 replicate for siSAPS3). **(C)** Data from (B) recalibrated to the window of mitotic entry on a linear scale, highlighting the rapid association of GFP-AurA with mitotic spindles and the level differences upon depletion of PP6 subunits.

To assess how PP6 affects Aurora A function in G2 and mitosis, the intensity of Aurora A associated with the centrosome and the mitotic spindle was measured by volumetric object detection. In G2 phase, the amounts of Aurora A

recruited to centrosomes behaved similarly between all conditions, although a small but consistent increase could be observed when PPP6C was depleted (Figure 3.15A-B). In these cells, the amount of Aurora A recruited to the spindle after nuclear envelope breakdown increased two-fold over control or SAPS2 depletion (Figure 3.15C, siPPP6C). This mitotic effect was also observed in cells depleted of SAPS3, albeit to a slightly smaller extent. (Figure 3.15C, siSAPS3). These findings further support the view that the primary phosphatase limiting centrosome- and spindle-associated Aurora A is the constitutively active PP6-SAPS3 and not PP6-SAPS2.

The contribution of PP6-SAPS2 to Aurora A deactivation during mitotic exit was next examined. Cells expressing inducible SAPS2 WT were depleted of SAPS2 and rescued with SAPS2-GFP before nocodazole arrest. Nocodazole was then washed out and the cells allowed to rebuild mitotic spindles before induction of synchronous mitotic exit by treatment with AZ3146 (Mps1-i) as in Figure 3.6. These were harvested in minute intervals and analysed by western blotting (Figure 3.16). Anaphase entry occurred 20min after MPS1 inhibition, demonstrated by cyclin B1 degradation and PRC1 pT481 dephosphorylation (Figure 3.16, siControl). Concomitantly, Aurora A pT288 was dephosphorylated, and the kinase degraded in later time-points. Depletion of SAPS2 did not slow this dephosphorylation, and it was also unaltered when the depletion was rescued (Figure 3.16, siSAPS2 and Rescue). Neither cyclin B1 degradation nor PRC1 pT481 dephosphorylation were affected by the depletion or rescue, indicating that the biochemical network controlling mitotic exit was unaltered.

The effect of SAPS2 deregulation on cell cycle progression was then tested. To do this, cells inducible for either SAPS2 WT or ^{770}AA were treated with

either control or SAPS2 siRNA duplexes, rescued where indicated and arrested with a double thymidine block. They were then released and followed over time by western blotting (Figure 3.17A). Depletion was efficient in this experiment, and SAPS2 WT and ^{770}AA induced at equivalent levels (Figure 3.17B). Under all conditions the peak of cells in mitosis indicated by both CDK-phosphorylation of PRC1 T481 and the mitotic index was observed 10-11h after washout (Figure 3.17A, 3.17C and 3.17D). These counts included cells in all stages of mitosis, including anaphase and telophase. Biochemical corroboration was obtained by examining cyclin B1 and cyclin A2 levels, and the amount of PRC1 T481 phosphorylation. Furthermore, the inhibitory CDK1 phosphorylation on Y15 was removed at the assigned time of mitotic entry, in line with previous reports [11].

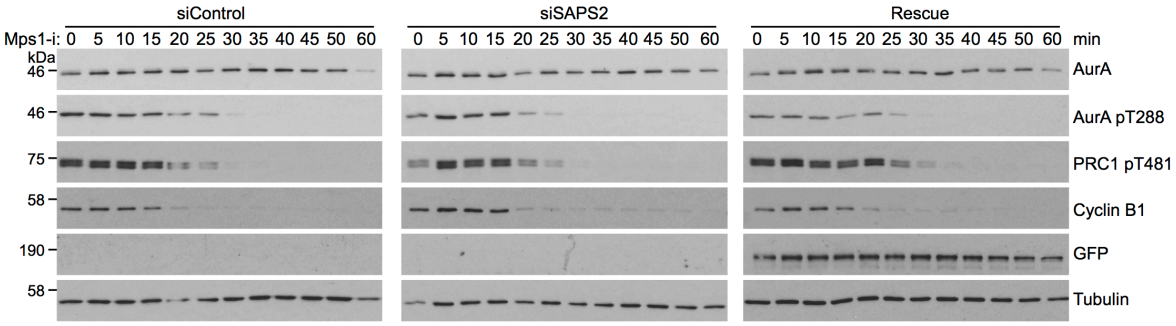


Figure 3.16 - SAPS2 does not control Aurora A deactivation during mitotic exit. Cells expressing inducible SAPS2 WT were treated with siRNA for 62h and induced for 48h to rescue as indicated before nocodazole arrest. The nocodazole was then washed out and the cells allowed to rebuild mitotic spindles, before induction of synchronous mitotic exit by inhibition of MPS1 (Mps1-i). Cells were harvested at the indicated times, lysed in Laemmli sample buffer and analyzed by western blotting.

Aurora A pT288 behaved similarly between all conditions, with low levels visible 9h after washout, and peaked 10h after washout in all conditions, regardless of whether SAPS2 WT or ^{770}AA was expressed.

Taken together, the results presented here suggest that PLK1 regulation of PP6-SAPS2 does not affect unperturbed progression through the cell cycle and doesn't appreciably impact on Aurora A activation and deactivation in an unchallenged cell cycle. However, PP6-SAPS2 may require additional inputs or work in concert with other regulatory systems to establish control of Aurora A in G2. Good candidates for this are other PLK1-controlled pathways such as the regulation of cell cycle progression by the DNA-damage response. These were therefore explored further.

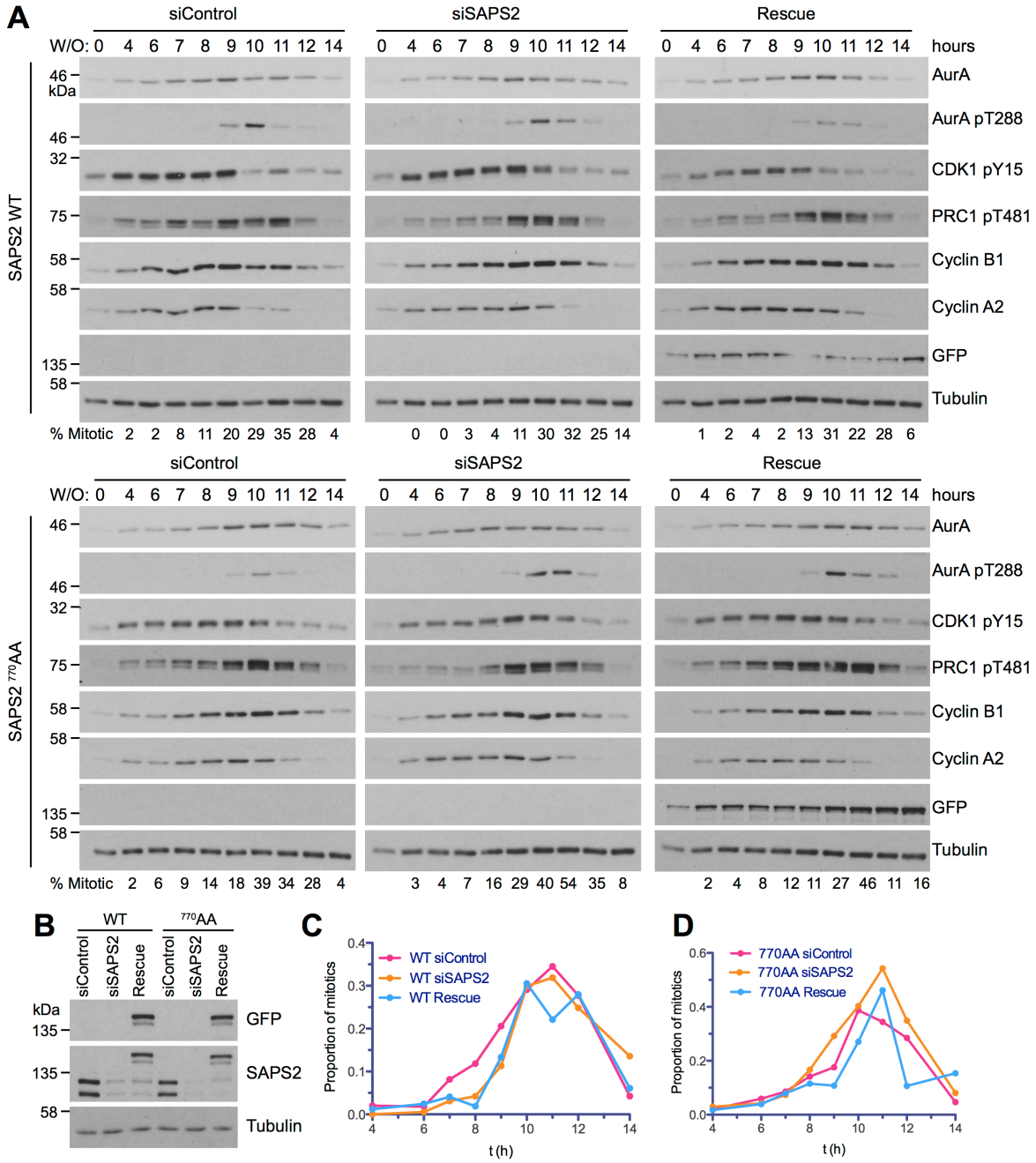


Figure 3.17 - PLK1 regulation of SAPS2 does not affect unchallenged cell cycle progression. (A) Cells expressing inducible SAPS2 WT or ^{770}AA were treated with siRNA and rescued for 48h where indicated. After a double thymidine block, they were released and harvested at the indicated times by combined mitotic shakeoff and treatment with 1mM EDTA/PBS before lysis in Laemmli sample buffer. The proportion of cells in mitosis was counted for every timepoint. **(B)** Depletion and induction were verified by western blotting. **(C-D)** Graphical representation of the proportion of mitotic cells for the respective conditions.

Chapter 4 PP6 and the DNA-damage checkpoint response

4.1 PP6 regulation of Aurora A in DNA-damaged cells

The contribution of PP6 in DNA damage-mediated control of Aurora A and PLK1 activation was first examined in the context of a G2 checkpoint arrest. To do this, HeLa S3 cells were depleted of PP6 subunits, synchronized with a double thymidine block and released for 7h (Figure 4.1A). They were then treated with 30µg/mL phleomycin (Figure 4.1A, Phleo +), a potent DNA-damaging agent, for a further 2h, while control samples were left untreated (Figure 4.1A, Phleo -). Untreated control cells showed no DNA damage signal judged by γ-H2A.X phosphorylation at 7h or 9hrs, corresponding to early or late G2 phase, respectively (Figure 4.1A, Phleo -, siCon). Phleomycin induced DNA damage over untreated cells, demonstrated by the early DDR phosphorylation γ-H2A.X (Figure 4.1A, Phleo +, all conditions). Cells largely do not enter mitosis under any of the conditions, indicated by the lack of a pronounced PRC1 pT481 signal and cyclin A2 stability. These G2 cells exhibited Aurora A and PLK1 activation, demonstrated by the respective T-loop phosphorylations. PLK1 pT210 was unaffected by induction of DNA damage, whereas Aurora A activation was reduced (Figure 4.1A, Phleo +, all conditions). This reduction was less pronounced when PPP6C was depleted, but was not affected by SAPS2 or SAPS3 depletion, although the steady state levels were increased upon SAPS3 depletion (Figure 4.1A, siPPP6C; Figure 4.1B).

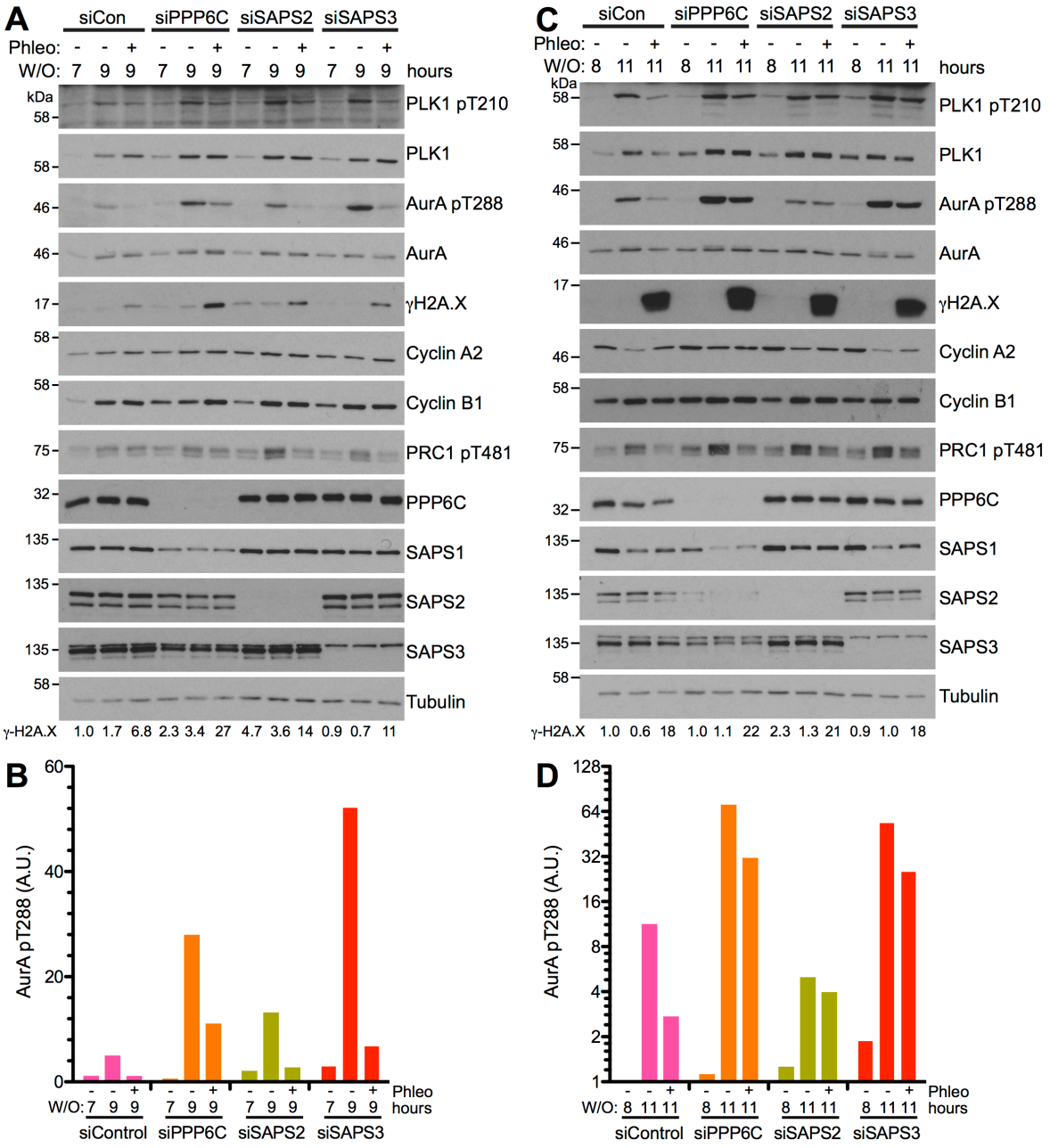


Figure 4.1 - PP6 links the AurA activation status to the DDR in late G2. (A) HeLa S3 cells were treated with siRNA as indicated, arrested with a double thymidine block and released for 7h before treatment with 30µg/mL Phleomycin for a further 2h and lysis. Quantification of the γ-H2A.X signal normalized to the 7h siControl sample is shown underneath. **(B)** Raw densitometric measurements of AurA pT288 corresponding to (A). **(C)** Cells were treated as in (A), with altered release timing as indicated to observe mitotic entry and phleomycin addition at 8h post washout. Quantification of the γ-H2A.X signal normalized to the 8h siControl sample is shown underneath. **(D)** Raw densitometric measurements of AurA pT288 corresponding to (C). Note the logarithmic scale on the graph.

The degree of Aurora A and PLK1 activation under a G2 DNA damage checkpoint arrest compared to mitotic cells was then examined. This was achieved by arresting siRNA-treated HeLa S3 cells with a double thymidine block before release for 8h. At this, point phleomycin was added and the cells incubated for a further 3h (Figure 4.1C). The timing of phleomycin addition was altered to allow untreated cells to enter mitosis. Induction of damage was highly effective and cells initiated the DDR by creating the γ-H2A.X phosphorylation (Figure 4.1C, Phleo +). Undamaged cells entered mitosis by the 11h timepoint, indicated by an increase in PRC1 pT481 and reduction of cyclin A2 due to destruction in prometaphase (Figure 4.1C, Phleo - 11 hours; [94]). PLK1 and Aurora A were also activated by this time, compared to early G2 cells at 8h after washout which lacked T-loop phosphorylation signals. Induction of damage in control cells prevented them from entering mitosis and resulted in decreased Aurora A pT288 and PLK1 pT210 compared to the untreated samples (Figure 4.1C, siCon Phleo +; Figure4.1D). By contrast, cells depleted of PPP6C, SAPS2 or SAPS3 were able to activate the kinases to an appreciable extent under damaged conditions, even though mitotic entry was prevented under in all three cases (Figure 4.1C, Phleo +; Figure 4.1D). PPP6C and SAPS3 depletions also resulted in increased levels of Aurora A pT288 levels in mitosis, whereas SAPS2 depletion did not (Figure 4.1D).

The results presented here indicate that DNA damage in late G2 phase results in decreased activation of Aurora A and PLK1, which is contributed to by PP6. However, loss of PP6 activity does not override the checkpoint to allow mitotic entry under these conditions.

4.2 Non-transformed cells arrest in response to the loss of PP6-SAPS2

PP6 loss-of-function has been extensively linked to several forms of cancer [233], and it mostly coincides with mutations in p53 or the MAP kinase pathway, which abrogate several cell cycle checkpoints [234]. The experiments presented thus far were performed in cells where these checkpoints are suppressed. To test their interplay with PP6, the non-cancer diploid cell line hTERT-RPE1 was therefore treated with PPP6C siRNA and examined. Depletion was found not to be efficient in these cells, but even this partial effect resulted in the stabilization of p53, indicating that they may have arrested the cell cycle (Figure 4.2E). By immunofluorescence, stable nuclear p53 could be detected in around 60% of PPP6C-depleted cells compared to ~15% under control conditions (Figure 4.2A, Figure 4.2C). PPP6C depletion on its own did not result in increased incidence micronucleation (Figure 4.2A-B). This indicates that the mitotic phenotype had not developed. I hypothesized that this was due to the p53-mediated arrest and therefore a comparison was made to co-depletion of p53 and PPP6C. This resulted in no p53 induction as expected and full PPP6C depletion could thus be achieved (Figure 4.2C, Figure 4.2E). Furthermore, the incidence of micronucleation was increased over control (Figure 4.2B). Interestingly, p53 depletion on its own also resulted in the induction micronucleation, albeit less pronounced. The cells were also stained for γ-H2A.X and the frequency of damage-positive nuclei showed the same trend as micronucleation frequency (Figure 4.2D). These data suggest that PP6-dependent defects are detected by the p53 pathway, which may prevent the development of further aberrations.

To assess whether this induction of p53 results in a cell cycle arrest, a homozygous endogenously tagged cyclin B1-GFP hTERT-RPE1 cell line (generously provided by Dr Tatiana Alfonso Perez) was depleted of PPP6C and analysed by immunofluorescence (Figure 4.3A, 4.3C). Furthermore, the contribution of the major and minor Aurora A phosphatases, PP6-SAPS3 and PP6-SAPS2, was examined. Efficient depletion of all subunits was achieved under these conditions (Figure 4.3B). Imaged cells were categorized based on the association of cyclin B1-GFP with the centrosome [cyclin B1(±)] which indicated they had proceeded into G2 phase, and their p53 status [p53(±)]. As before, depletion of PPP6C resulted in p53 induction in ~60% of cells, increased over control (Figure 4.3C, siPPP6C CycB1(-) p53(+)). A corresponding drop was observed in the proportion of cyclin B1(+) cells, and in cells lacking either centrosomal cyclin B1 or nuclear p53, which reflect a sum of non-arrested G1 cells and S phase cells (Figure 4.3C, CycB1(-) p53(-)). Similarly, depletion of SAPS2 resulted in an increase in the proportion of p53-positive cells, albeit to a smaller extent (Figure 4.3C). Preliminary data suggest that SAPS3 depletion also results in an increase in the number of p53-positive cells as SAPS2 depletion (Figure 4.3C). SAPS2 and SAPS3 depletions also caused a small decrease in non-arrested G1/S phase cells (Figure 4.3C, CycB1(-) p53(-)). Finally, the observed incidence of p53 induction was qualitatively matched by population p53 levels detected by western blotting in PPP6C and SAPS2 depletions (Figure 4.3B, siPPP6C; siSAPS2). Although a similar number of cells stabilize p53 upon SAPS3 depletion as after SAPS2 silencing, p53 levels are overall higher in this condition, indicating that larger amount of p53 is stably expressed on a per-cell basis (Figure 4.3B, siSAPS3).

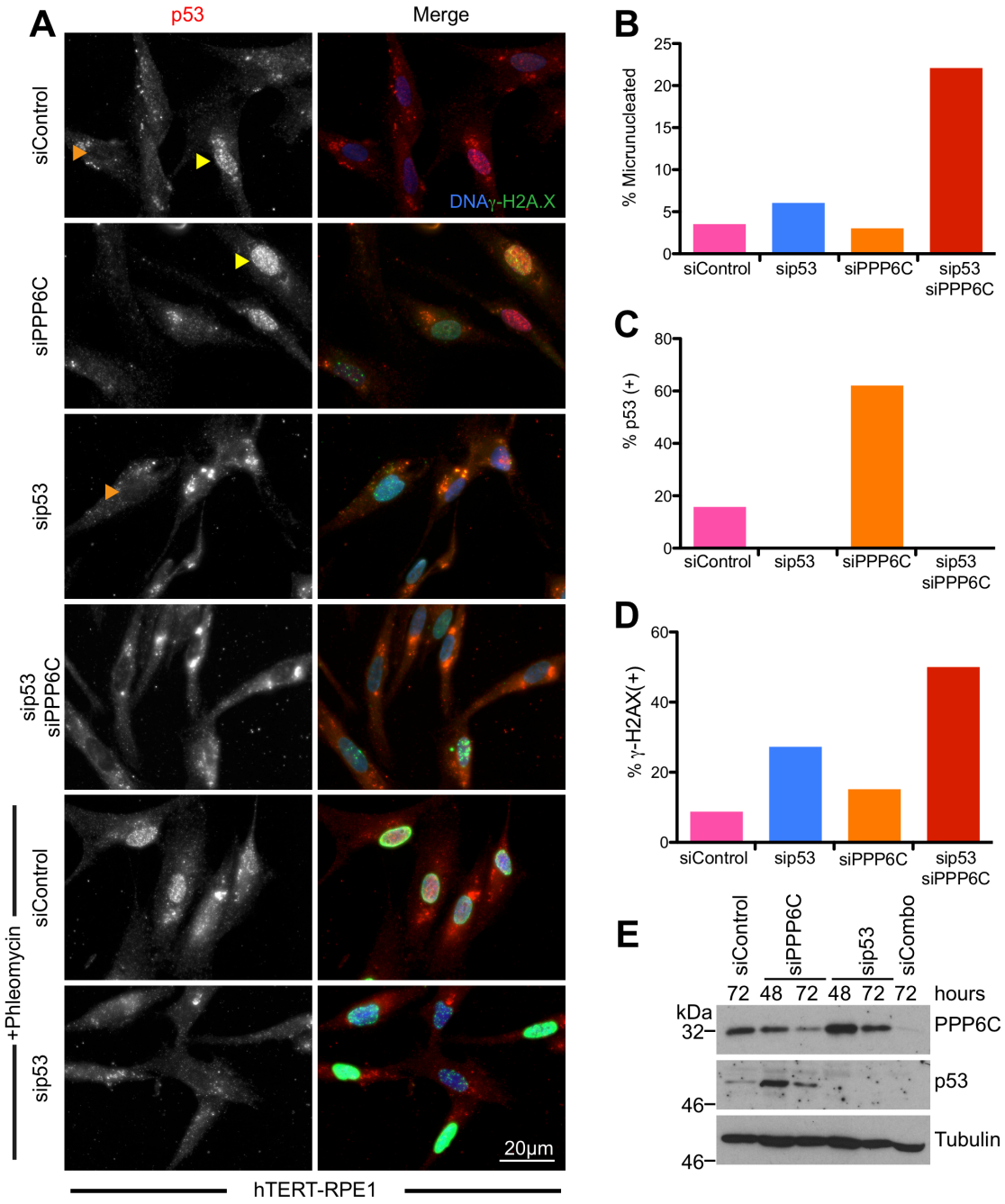


Figure 4.2 - p53 induction protects PPP6C-depleted cells from accumulating damage. (A) hTERT-RPE1 cells were treated with siRNA as indicated and fixed before IF staining. Where shown, cells were treated with phleomycin (60μg/mL) for 2h to induce saturating amounts of DNA damage. Examples of p53 positive and negative nuclei are highlighted by arrows. **(B-D)** Phenotype quantifications from the experiment in (A), showing micronucleation incidence (B), fraction of p53-positive nuclei (C), and fraction of nuclei positive for γ-H2A.X (D). Single biological replicate shown, 57-88 cells analyzed per condition. **(E)** Western blot analysis of hTERT-RPE1 cells treated with siRNAs for varying lengths of time as indicated and lysed in Laemmli sample buffer. siCombo = siPPP6C+sip53

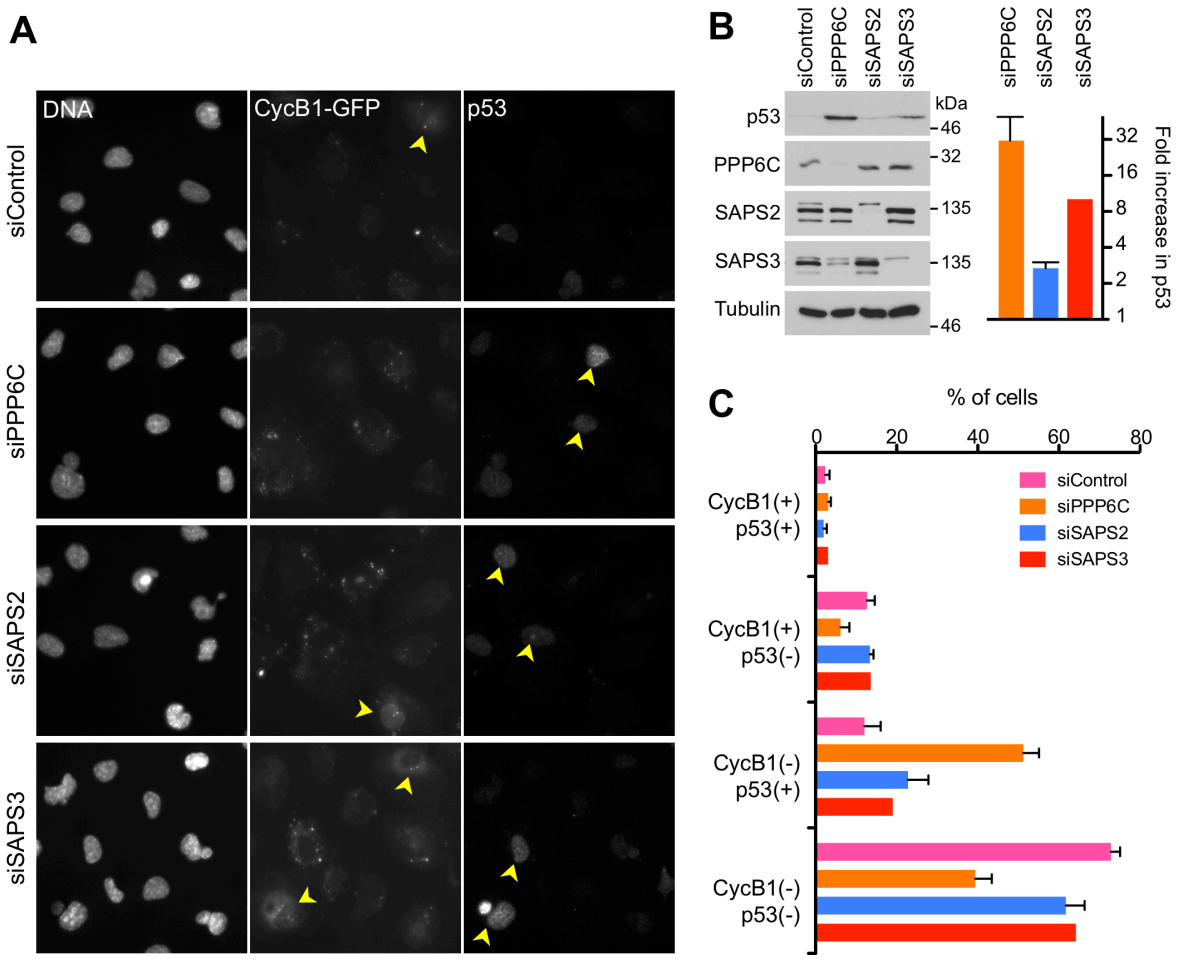


Figure 4.3 - Non-transformed cells mount a p53 response upon depletion of PP6 subunits. (A) hTERT-RPE1 cells expressing Cyclin B1-GFP at the endogenous level were treated with siRNA for 72h, fixed and stained as indicated. Arrowheads indicate examples of Cyclin B1- and p53-positive cells. **(B)** Cells treated as in (A) were rapidly lysed in Laemmli sample buffer and analyzed by western blotting. The graph represents the average fold increase in p53 levels upon depletion, determined by western blotting. (Mean±SEM, n=2. siSAPS3 n=1). **(C)** Cells as in (A) were categorized based on Cyclin B and p53 status (Mean±SEM, n=3. siSAPS3 n=1)

To further address whether a canonical p53-p21 checkpoint response is mounted under these conditions, previously described hTERT-RPE1 cells expressing p21-GFP and mRuby-PCNA under their endogenous promoters ([31], generously provided by Dr Alexis Barr) were treated with siRNA for 70h, fixed and stained (Figure 4.4A-B). They were then scored for replication, assigned by the presence of PCNA foci – corresponding to S phase cells – and their p21 status (Figure 4.4B, PCNA(+); p21(+)). Furthermore, their DNA damage status was assessed by γ-H2A.X staining to assess whether the arrest correlates with increased DNA damage incidence (Figure 4.4A-B). Depletion of PPP6C resulted in highly penetrant increased induction of p21 and a reduction in PCNA-positive replicating cells (Figure 4.4B, siPPP6C). Similarly, SAPS2 depletion caused a smaller increase in the incidence of p21-positive cells and a slight decrease in cells positive for PCNA foci (Figure 4.BA, siSAPS2). By contrast, preliminary data show that SAPS3 depletion completely impairs p21 induction and only a meagre reduction in PCNA-positive cells is observed (Figure 4.4B). γ-H2A.X staining did not correlate with p21 induction, but rather followed the same trend as the PCNA status, reduced upon PPP6C or SAPS2 depletion (Figure 4.4B, γ-H2A.X). On average, over 85% of PCNA-positive cells also contained γ-H2A.X foci and the shrinkage of this population accounts for the majority of the fluctuation in γ-H2A.X incidence between conditions. Therefore, the trend can be explained by a difference in replication-induced DNA damage due to the cell cycle arrest.

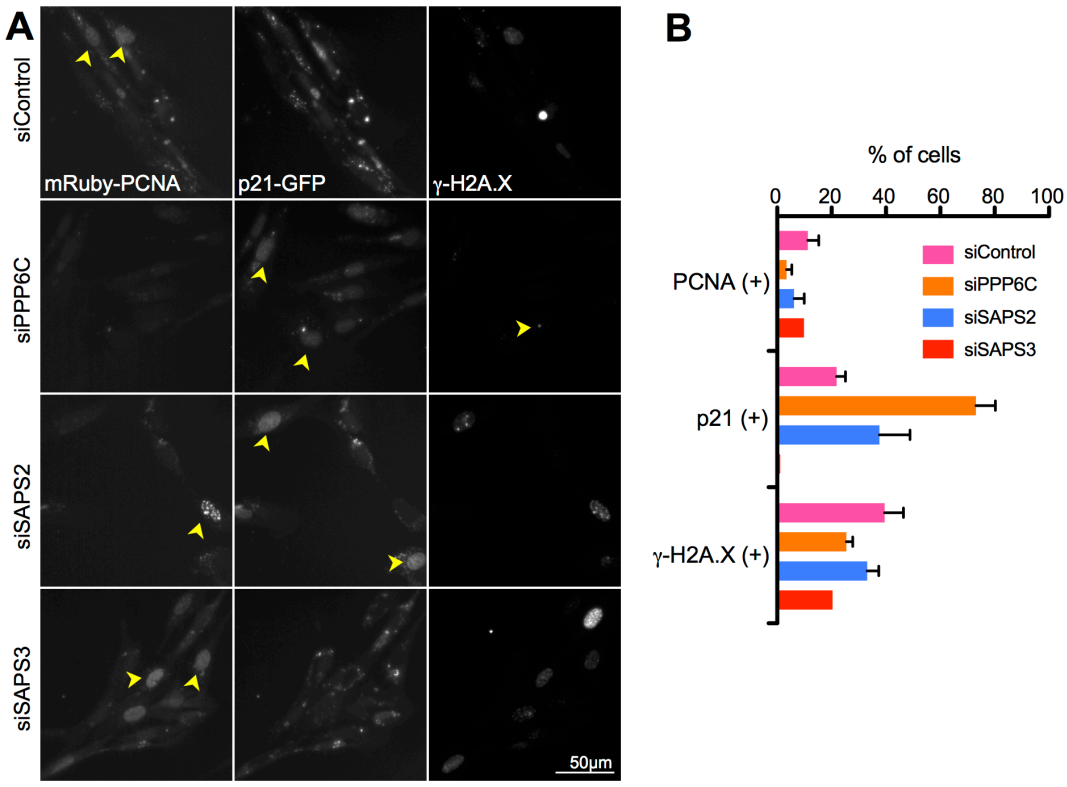


Figure 4.4 - Cells depleted of PP6-SAPS2 induce a p21 checkpoint response. (A) hTERT-RPE1 cells expressing p21-GFP and mRuby-PCNA from their endogenous loci were treated with siRNA for 72h, fixed and stained. Arrowheads highlight PCNA-, p21- and γ-H2A.X-positive cells. **(B)** Cells as in (A) were categorized based on PCNA, p21 and γ-H2A.X status. (Mean±SEM, n=3 for p21 and PCNA. n=2 for γ-H2A.X. n=1 for all siSAPS3 categories)

To assess the extent of the arrest and pinpoint which cell cycle stage it occurs at, live cell time-lapse imaging was employed. Cyclin B1-GFP hTERT-RPE1 cells were depleted of PPP6C, SAPS2 or SAPS3, imaged for 24h, and categorized based on their fate during the course of the experiment (Figure 4.5A-B). Cells which failed to accumulate any cyclin B1 during the entirety of the experiment were categorized as quiescent (Figure 4.5A, Quiescence), and cells which went through mitosis were categorized as dividing (Figure 4.5A, Division). A third group of cells accumulated cyclin B1 but then degraded either in the

cytoplasm or after nuclear import (Figure 4.5A, G2 arrest)[74, 75]. These can conclusively be categorized as arresting in G2 (Figure 4.5B, G2 arrest). It is worth noting that the quiescent category (Figure 4.5A-B, Quiescence) is the sum of cells arrested in G1 and cells which degraded cyclin B in G2 phase prior to imaging. Any cells which accumulated cyclin B, but neither entered mitosis or degraded the cyclin during the course of the experiment were unassigned (Figure 4.5B, Unassigned). Depletion of PPP6C resulted in an increased frequency of quiescence and an equivalent decrease in the population of dividing cells, indicating that a cell cycle arrest is occurring (Figure 4.5B, siPPP6C). This trend was also followed by SAPS2-depleted cells, although fewer quiescent cells were observed (Figure 4.5B, siSAPS2). In addition, SAPS2 depletion resulted in an increased G2 arrest incidence than in either of the other depletion conditions (Figure 4.5B, siSAPS2). This could be explained if defects associated with loss of SAPS2 escape initial detection in G1 more frequently than in PPP6C-depleted cells, and are subsequently picked up by the G2 checkpoint. Alternatively, it could relate to a specific function in S/G2 phase. SAPS3 depletion resulted in a smaller increase in quiescence than either PPP6C or SAPS2 silencing, and a mildly decreased proportion of dividing cells. The frequency of a G2 arrest was not affected under this condition (Figure 4.5B, siSAPS3).

Taken together, these results support the conclusion that PP6 loss-of-function causes detrimental changes in normal diploid cells, the gravity of which is stifled by the p53 checkpoint pathway. The cause of this arrest is separable from the mitotic role of PP6-SAPS3 in Aurora A regulation, suggesting that it is mediated by interphase-specific roles of PP6 holoenzymes.

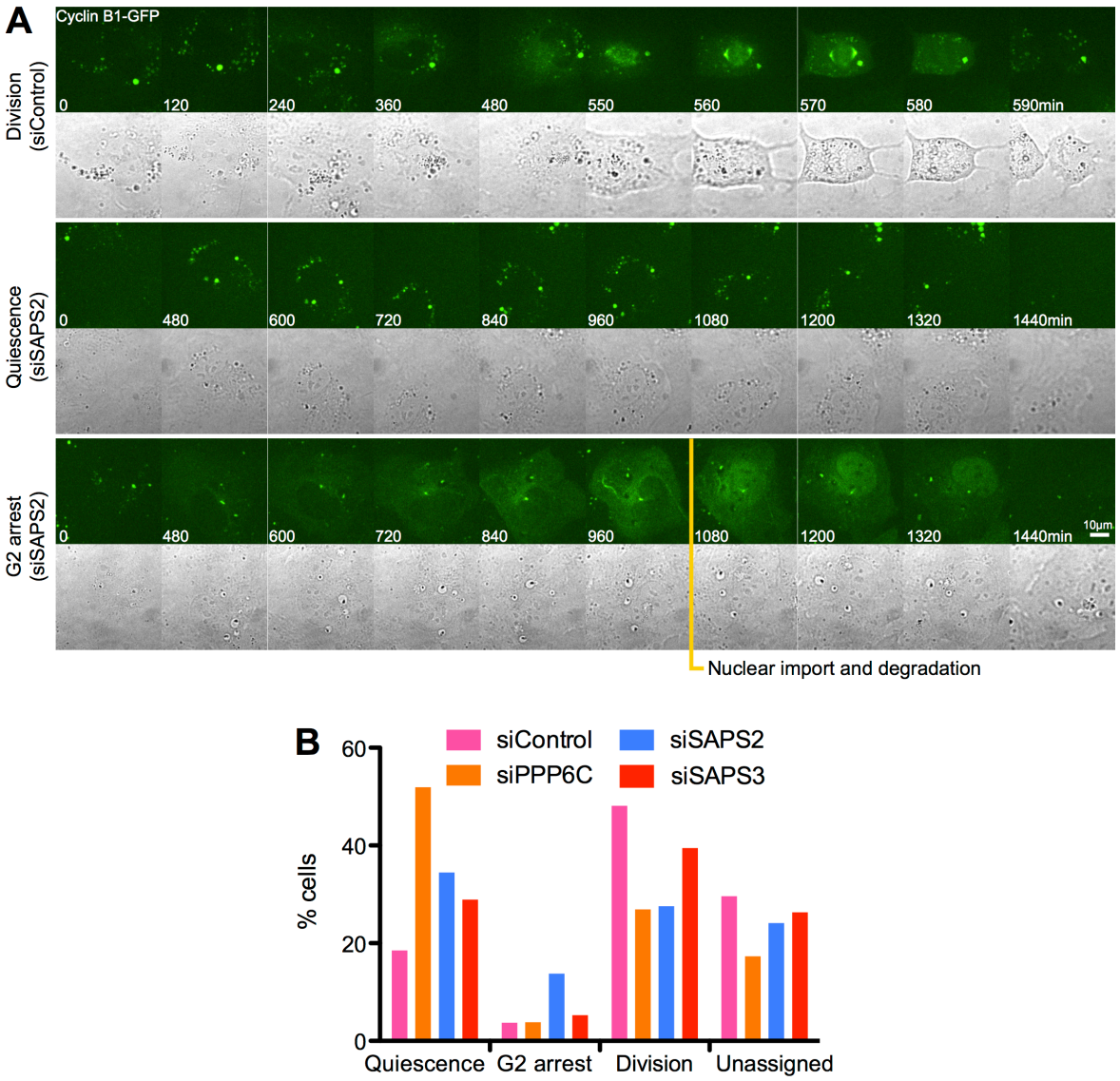


Figure 4.5 - Depletion of PP6-SAPS2 causes a cell cycle arrest. (A) hTERT-RPE1 cells expressing cyclin B1-GFP were treated with siRNA as indicated before time-lapse imaging in 5min intervals for 24h. Stills depict representative cells for each phenotype class. **(B)** Cells from (A) were categorized based on fate and counted (N>27, 1 biological replicate, 2 replicates combined for siPPP6C).

4.3 Targeting PP6-deficient cells by DDR inhibition

Aberrations acquired from successive divisions without PP6 activity may cause additional damage in cancer cells, which most often do not have functional cell cycle checkpoints. A particularly detrimental outcome would be the acquisition of

double-stranded breaks, which are generally lethal if not repaired. The predominant pathway used for repair of these breaks in cells is non-homologous end joining, which is dependent on the activity of DNA-PK [68]. If this idea is correct, then inhibition of DNA-PK when PP6 is depleted should lead to reduced viability. HeLa S3 cells were depleted of PP6 subunits as indicated before plating at limiting concentration in the presence or absence of the DNA-PK inhibitor NU7441 until colonies formed. These colonies were then fixed, stained and scored for survival (Figure 4.6A-C). PPP6C depletion resulted in fewer colonies than in control, indicating that on its own it adversely affects cell survival (Figure 4.6B). Inhibition of DNA-PK resulted in slightly reduced viability in control cells and showed an additive effect with PPP6C depletion (Figure 4.6A-D, +PRKDC-i). The depletion of individual SAPS subunits didn't show as high an impact on cell viability as loss of PPP6C (Figure 4.6A-B, 4.6D, siSAPS1; siSAPS2; siSAPS3). Treatment with the DNA-PK inhibitor most adversely affected cells depleted of SAPS1, whereas SAPS2- or SAPS3-depleted cells were only mildly affected. These results suggest that inhibition of non-homologous end joining may be used to reduce the viability of PP6-impaired cells with limited efficacy. One caveat is that these experiments were done with transient depletion, giving the cells only a short-term insult. The effects may be more pronounced in cells constitutively lacking the phosphatase and experiencing recurring challenges to DNA repair. Further experiments with cells with a constitutive loss of PP6 function, such as PP6-null cancer patient cell lines, will be required to test this strategy more thoroughly.

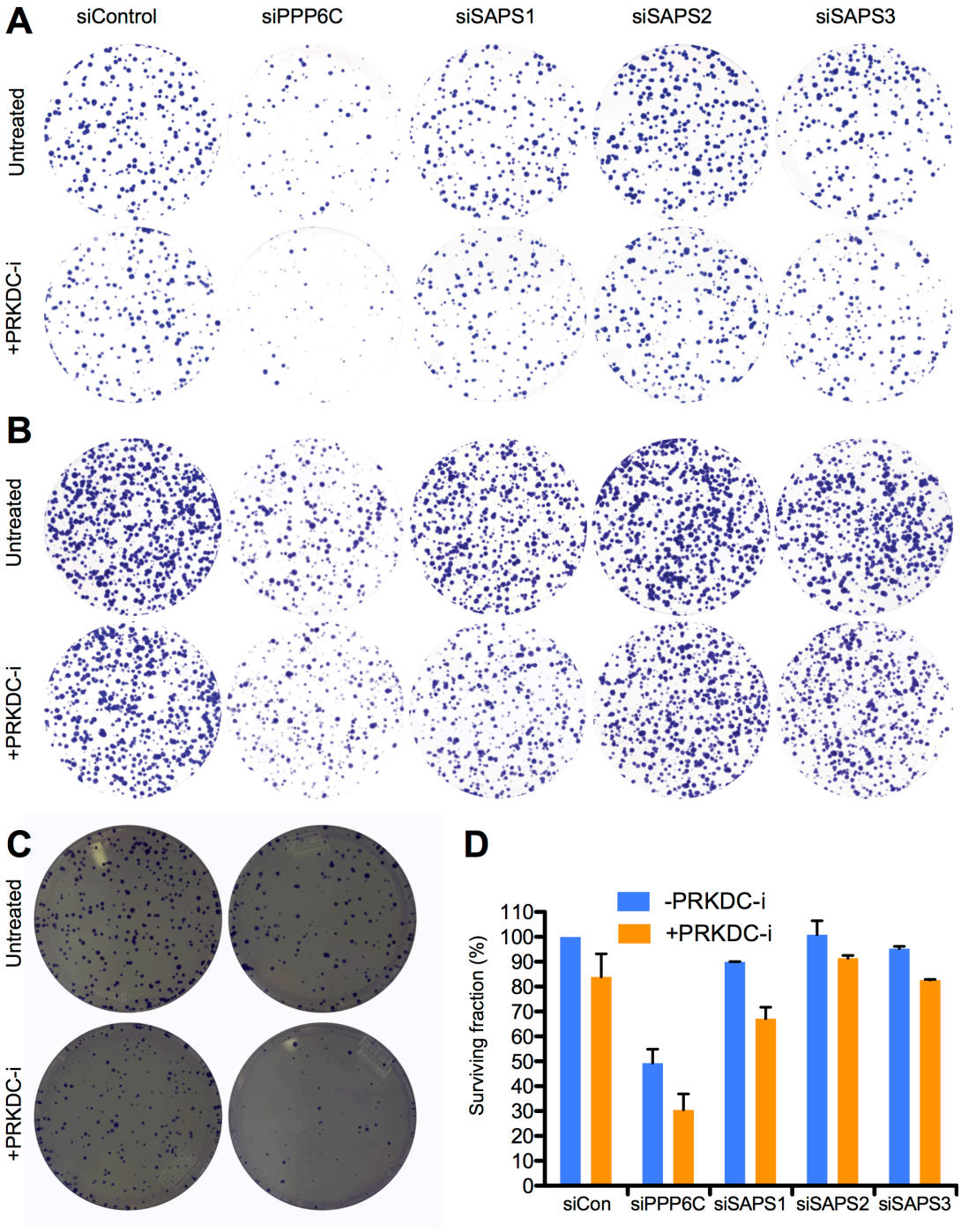


Figure 4.6 PP6-depleted cells are sensitive to DDR inhibitors. (A-C) HeLa S3 cells were treated with siRNA for 72h before plating at limiting density (500-750 cells per 6cm dish) in the presence or absence of 1μM NU7441 (PRKDC-i) and fixation and staining with Crystal Violet. Three replicate experiments shown. **(D)** Surviving fraction was calculated from colony numbers in the three replicate experiments shown in (A-C), normalized to the untreated control dish in each replicate. Mean±SEM given, n=3 for Control and PPP6C depletion, n=2 for SAPS depletions.

Chapter 5 Discussion

5.1 Functional stratification & specificity of protein phosphatases

Mutations in the catalytic subunit of protein phosphatase 6 (PP6) act as drivers for a number of cancers, most notably UV-induced malignant melanoma [214, 231, 234, 242]. Previous studies have shown that these mutations result in loss of phosphatase activity and destabilisation of the catalytic subunit [214]. This previous work treated PP6 as a single entity, however the presence of 3 putative regulatory subunits (SAPS1-3) thought to play a role in substrate recognition suggested a more complex picture. Data presented here directly demonstrate that PP6 cannot be considered as one functional unit, in terms of either substrate recognition or regulation. Rather, it can be stratified into three major forms based on the SAPS subunit incorporated into the heterotrimeric holoenzyme. There is little evidence to support the idea that ANKRD subunits specifically modulate the behaviour of PP6, as discrete holoenzyme preparations with a single SAPS subunit but mixed composition of ANKRD subunits have unique patterns of behaviour. Additionally, all ANKRD subunits interact equivalently with all SAPS subunits. Furthermore, all organisms that express PP6 also possess a SAPS protein, whereas obligatory co-evolution with ANKRDs is not observed [218]. For instance, yeasts do not express ANKRD subunits and form functional heterodimeric PPP6C-SAPS holoenzymes [219]. In addition, using chimeric SAPS1-SAPS2 constructs, an Aurora A binding site could be broadly mapped to the C-terminal half of SAPS2, indicating that it is indeed direct (Dr Elena Poser and Prof Francis Barr, personal communication). Together, these findings indicate that it is the SAPS subunits that provide the primary governance of holoenzyme properties. I therefore propose that individual PP6 holoenzymes should be

referred to as PP6-SAPS1/2/3, akin to the annotation of PP2A holoenzymes. However, it is possible that additional ANKRD-mediated properties are important in specific tissues or under particular growth or stress conditions.

One of the unique properties conferred by SAPS subunits is substrate specificity, and in the case of Aurora A, specificity for the active pool of the enzyme associated with TPX2. PP6-SAPS1 is unable to dephosphorylate Aurora A-TPX2 complexes *in vitro*, while PP6-SAPS2 and PP6-SAPS3 have Aurora A pT288 activity, and this is reflected in their contribution to mitotic spindle architecture in cells. Structural and biochemical studies have demonstrated that TPX2 binding sterically shields Aurora A pT288 from incoming phosphatases [201]. For dephosphorylation to occur, this limitation must be overcome, which can be achieved in in one of two ways. Firstly, dynamic association-dissociation cycles could be exploited by a phosphatase to dephosphorylate uncomplexed Aurora A. Monomeric Aurora A is dephosphorylated by PP1 [201], but this is not sufficient to establish correct regulation in mitosis [172]. Moreover, this model alone cannot account for the differences in activity *in vitro* where protein concentrations are low and the equilibrium is biased towards the dissociated state. By inference, spontaneous complex disassembly is unlikely to be rapid or long-lived enough to support robust control of Aurora A. More likely, effective Aurora A pT288 phosphatases have a feature allowing them to wrestle Aurora A free from Aurora A-TPX2 complexes. Indeed, PP6-SAPS2 and PP6-SAPS3 can stably bind Aurora A in immune precipitations. This binding may be strong enough to overcome the Aurora A-TPX2 interaction and allow dephosphorylation of the T-loop. If this hypothesis is correct, SAPS2 and SAPS3 are specific protein complex

disaggregases, and their addition to Aurora A-TPX2 might be sufficient to dissociate the complex.

Binding-mediated complex dissolution has previously been described in several other systems. One relevant example is the disassembly of the mitotic checkpoint complex. This process is initiated when $p31^{Comet}$ binds to MAD2 and recruits it to the TRIP13 ATPase [243]. The binding induces a conformational change, which inserts a portion of MAD2 into the ATPase pore, allowing it to be passed through upon ATP hydrolysis, thus causing disassembly of the entire MCC [243]. In a similar fashion, binding of SAPS2/3 to Aurora A may induce conformational changes in the kinase, abolishing the TPX2 binding interface, and favouring the release of Aurora A. In this model, any positive change in Gibbs free energy could also be offset by dephosphorylation of the T-loop in the follow-up reaction, equivalent to ATP hydrolysis. Induced complex disassembly can also happen passively. Recently, the importin KAPβ2 has been demonstrated to disassemble pathological aggregates of a variety of nuclear RNA-binding proteins (RBPs) [244]. Initially, the binding occurs via the nuclear localization sequence on the RBPs [244]. This locally concentrates the importin and promotes secondary interactions with low complexity elements in RBPs, inducing disassembly of RBP aggregates [244]. This mechanism is particularly intriguing due to two reasons. First, it is a two-step process inducing a change in poorly structured features, which could be considered similar to the Aurora A T-loop. Furthermore, KAPβ2 is composed of a series of a-helical repeats [245], similar to the predicted structure of SAPS subunits [214]. Such an elongated surface can provide a large number of interaction sites, the sum of which may be sufficient to displace other binding partners.

If SAPS subunits act as Aurora A-TPX2 disaggregases, pT288 dephosphorylation by a phosphatase such as PP1 might be possible in the presence of excess SAPS2/3, with the caveat that SAPS subunits in isolation may not be sufficient for the dissociation. *In vivo*, where protein concentrations are higher, spontaneous and induced dissociation likely function cooperatively. Transient dissociation of Aurora A-TPX2 complexes could be specifically extended by the SAPS2/3-Aurora A interaction to allow PP6-mediated dephosphorylation, but remain too short for phosphatases which lack the binding feature. Similar binding-mediated substrate retention has been demonstrated for PP2A-B56 with its substrates RacGAP1 and FOXO3, although the purpose of this binding is not complex dissociation, but more efficient substrate targeting and dephosphorylation [195].

5.2 PP6-SAPS3 is the major mitotic Aurora A phosphatase

The functional distinction between PP6-complexes revealed that PP6-SAPS3 is responsible for the majority of Aurora A phosphatase activity in mitosis. This is demonstrated well by PP6-SAPS3-dependent dephosphorylation of Aurora A pT288 in mitotic extracts. Furthermore, the activity of this specific phosphatase is required to effectively dephosphorylate the Aurora A T-loop after inhibition of its autophosphorylation. Reflective of this function, depletion of SAPS3 is sufficient to recreate the mitotic defects seen upon PPP6C depletion, accompanied by expanded localization of active Aurora A along the mitotic spindle. It is thought that these spindle defects are caused by altered spatial regulation of SAFs, owing to the increased and partially mislocalised Aurora A activity [172]. Consistently, multiple facets of the phenotype correlate with the known effects Aurora A has on some SAFs. For instance, excessive microtubule bundling may be a result of

increased activity of TACC3, a known Aurora A target [246]. In addition, the positional instability of spindles can be explained by aberrant regulation of NuMA, which is important for anchoring astral microtubules at the cell cortex [115]. However, it is not entirely clear which defects contribute most to the chromosome segregation errors in anaphase. The classical way these occur is an increased incidence of erroneous microtubule-kinetochore attachments. One mechanism by which this could happen is altered regulation of Aurora B-dependent attachment error correction. The system is thought to be based on spatial distancing of Aurora B substrates, which is very sensitive to the activity gradient of the kinase [152]. Upon PP6-SAPS3 depletion, this fine regulation could be perturbed by delocalized Aurora A activity, as both Aurora A and B are able to phosphorylate the same substrates [201, 247]. This would result in less stable microtubule-kinetochore attachments, compromising chromosome congression and prolonging mitosis. Ultimately, this model predicts that aberrant error correction in conjunction with poor microtubule structure may increase the frequency of microtubule-kinetochore attachment errors when PP6-SAPS3 is lost. Testing it will require methods of direct observation, such as super resolution microscopy able to resolve the architecture of individual microtubule-kinetochore attachments.

5.3 PLK1 negatively regulates PP6-SAPS2

The functional stratification of PP6 holoenzymes also allows for regulation of specific pools of PP6, most notably PP6-SAPS2. This regulation is established through association with PLK1 via a canonical polo-box mediated binding, reminiscent of other PLK1-regulated proteins, such as PRC1 and BUBR1 [147, 212]. Peaking in mitosis, PLK1 phosphorylates PP6-SAPS2 and inhibits its activity. Since PLK1 inhibition in both G2 phase and mitosis compromises the

PLK1-SAPS2 interaction, one of the *in vivo* phosphorylation sites is likely the polo-box motif. In addition, PLK1 is entirely unable to phosphorylate a docking site-mutated SAPS2, which indicates either that the docking site is the only PLK1-dependent phosphorylation on SAPS2, or that it is required for hierarchical phosphorylation steps. It is somewhat unclear where and when this regulation is fully established. Immunoprecipitations demonstrate that the binding persists throughout the lifetime of PLK1 in the cell, but based on electrophoretic patterns, SAPS2 does not get appreciably phosphorylated before mitosis. Low PLK1 activity due to the lack of PLK1 T210 phosphorylation in interphase could explain this observation. However, inactive PLK1 would also fail to phosphorylate the docking site on SAPS2. Alternatively, these phosphorylations are opposed by a phosphatase that is highly active in interphase, but inactive in mitosis, such as PP2A-B55 or PP1 [11].

One caveat to the argument that the docking phosphorylation is created by PLK1 in interphase is the localization of PLK1 and SAPS2 in interphase cells. Most PLK1 is sequestered in the nucleus and only a small portion associates with centrosomes [248], while PP6-SAPS2 localizes to the cytoplasm and is excluded from the nucleus [172]. This also draws the question of why an interaction between the two proteins could be observed at all before nuclear envelope breakdown. A possible explanation is that the procedure used to prepare the immunoprecipitates breaks the nuclear envelope allowing the formation of PLK1-SAPS2 complexes in solution. This is consistent with the fact that DNA-PKcs is also detected as an interactor under these conditions, even though the protein is nuclear [223]. Binding during extract preparation could explain why the phosphorylation status of SAPS2 in G2 phase is low, but not how the docking site

is primed. The obvious candidates to perform this function, CDK2 and CDK1, do not appear to affect the interaction between SAPS2 and PLK1. An intriguing possibility is that the docking site phosphorylation is phosphorylated by another Polo kinase, such as PLK4, which controls centrosome duplication in S and G2 phases [249]. This event would also create cross-talk between centrosome maturation and centrosome duplication, as PLK4 would regulate indirectly Aurora A in early G2 phase. The bulk of PLK4 is degraded later in G2 due to autophosphorylation-mediated targeting by the SCF ubiquitin ligase, but at that point there could be sufficient PLK1 activity to maintain the interaction [250]. The inhibitory potential of BI2536 was only systematically tested against PLK1, PLK2 and PLK3 [119]. Thus, it is possible that it also inhibits PLK4, which could then explain the reduced PLK1-SAPS2 complex formation in interphase upon BI2536 treatment. It is also possible that the docking site phosphorylation on SAPS2 is only created in mitosis by PLK1 and retained in interphase from a previous cell cycle. However, this is unlikely, as PLK1 inhibition in mitosis results in the dissociation of the PLK1-SAPS2 complex, indicating that the phosphorylation is dynamically opposed by phosphatase activity at this stage. *In vitro*, PP6-SAPS2 appears to be able to turn over phosphorylations created by PLK1, although data presented here do not precisely determine which sites are being turned over under those conditions. Regardless, the simplest and therefore most consistent explanation for the observed dissociation is that PP6-SAPS2 autodephosphorylates the PLK1-docking motif.

This observation has interesting implications on the potential mechanism of PP6-SAPS2 inhibition and its relief (Figure 5.1). The simplest mechanism, wherein binding or phosphorylation by PLK1 prevents Aurora A binding seems unlikely, as

both WT and PLK1-deficient SAPS2 appear to bind Aurora A to the same extent in IPs. However, the caveat to this observation is that the bound Aurora A is not pT288-positive, and hence not the actual substrate of PP6-SAPS2. This binding can still serve as a proxy measurement of affinity for pT288-positive Aurora A, but does not provide direct proof. Biophysical tests such as isothermal titration calorimetry with recombinant proteins may provide a more accurate account. In addition, these IPs were done with overexpressed SAPS2, creating an artificial excess of monomeric regulatory subunits and potentially masking slight differences in Aurora A binding. Regardless, PLK1 may still sterically affect dephosphorylation of Aurora A by occluding the phosphatase active site, rather than preventing stable substrate binding. Alternatively, binding or phosphorylation by PLK1 may result in conformational change in the holoenzyme, restricting access to the catalytic site. This might not cause gross changes in the affinity for the substrate, provided that the major Aurora A binding site is unchanged by either event. However, this mechanism does not easily explain how PLK1 phosphorylations on SAPS2 are turned over.

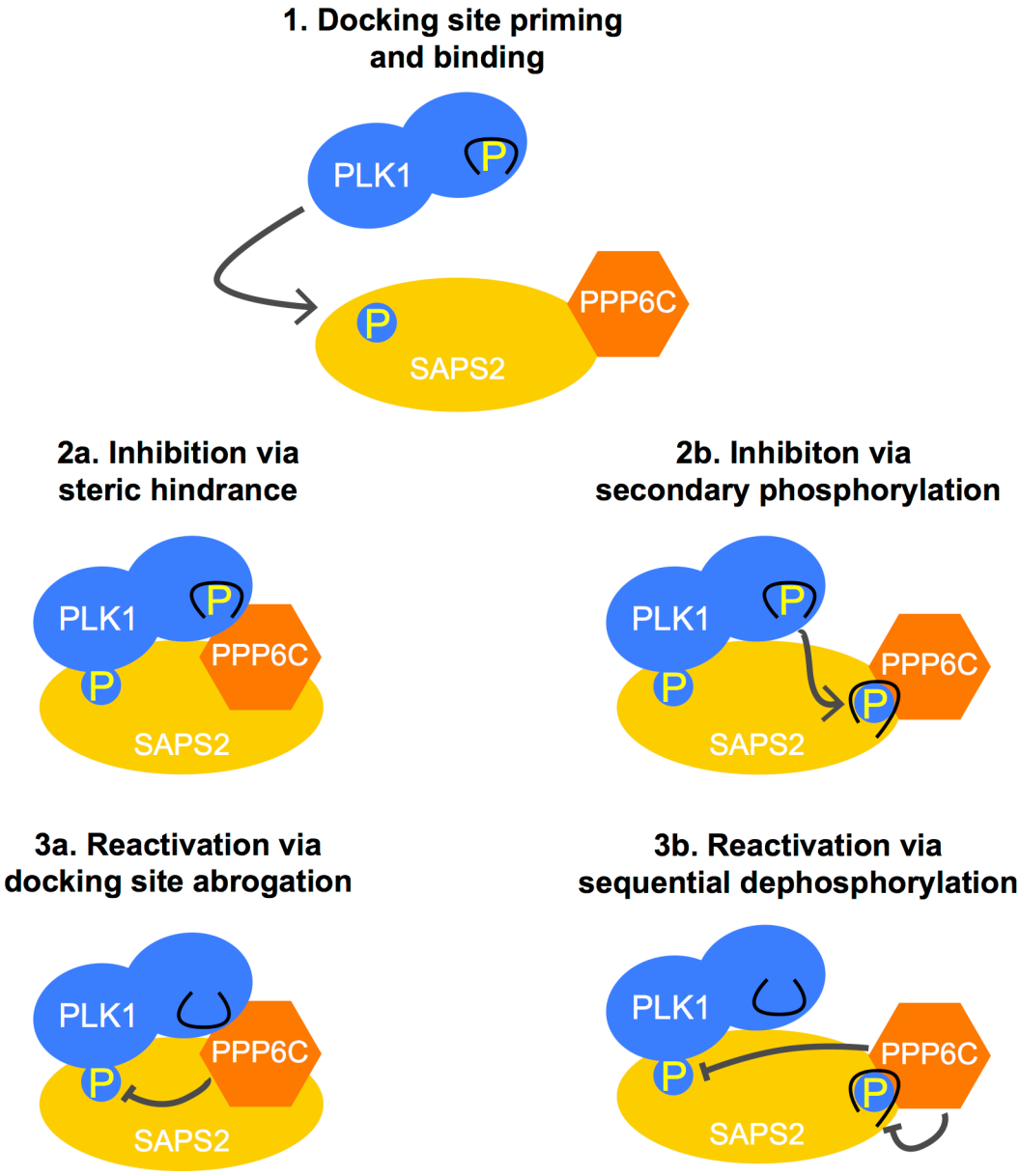


Figure 5.1 - Putative mechanisms of SAPS2 inhibition and its relief. First, active PLK1 primes its own docking site and binds to PP6-SAPS2 holoenzymes. This establishes inhibition either sterically, or through direct inhibition of catalysis via a secondary phosphorylation, which can occupy the phosphatase active site. Inactivation of PLK1 allows the inhibition to be relieved through autodephosphorylation of the docking motif, or by sequential dephosphorylation of the secondary phosphorylation followed by the PLK1 docking site.

An alternate possibility is that PP6-SAPS2 can inhibit itself by an autoinhibitory motif created by the unstructured PLK1-phosphorylated loop (Figure 5.1). The loop could be inserted into the phosphatase active site, analogous to the mechanism by which the unstructured phosphorylated protein ENSA inhibits PP2A-B55 [113]. This mechanism has several features which are consistent with data presented here. Firstly, it provides efficient phosphorylation-dependent inhibition of the enzyme. Furthermore, this mechanism would allow PP6-SAPS2 to turn over its own inhibitory phosphorylation, reminiscent of how PP2A-B55 overcomes inhibition by ENSA [137]. The inhibitory loop could be provided either intramolecularly (*cis*), or from a second SAPS2 molecule (*trans*). These two options can be tested by allowing PP6-SAPS2 to dephosphorylate itself *in vitro* at different concentrations. A zero-order, concentration independent reaction would confirm the *cis* model, whereas higher order reactions would indicate that the dephosphorylation happens in *trans*. Identifying both the biochemical mechanism and the exact site is important, as these properties have implications on the potential efficiency of inhibition. Although theoretically possible, the *trans* mechanism is unlikely, as this would limit the efficiency of inhibition in cells due to the low concentration of PP6-SAPS2. In *cis*, if the loop is also the PLK1 docking site, PLK1 binding would compete with inhibition, thus limiting the efficiency. The final option, where docked PLK1 phosphorylates another loop on SAPS2 which then folds back into the active site, has the greatest inhibitory potential. In this case, the phosphorylation could be replenished after every dephosphorylation cycle, due to the binding-mediated increase in effective concentration of PLK1. This cycle would be terminated upon mitotic exit, when PLK1 is degraded. Mass spectrometry analysis of SAPS2-GFP IPs indicates that SAPS2 is phosphorylated

on multiple other sites and that the occupancy of these increases in mitosis. The most notable of these were T10, S289 and S803 (Appendix Table A2), although further characterization of these sites is necessary to understand their effect on SAPS2 function.

In a recent study, Kettenbach and colleagues also found that PLK1 inhibits PP6-SAPS2 [251]. They attributed this property to phosphorylation on either T10, S289 or S823 based on *in vitro* activity assays guided by mass spectrometry [251]. This is consistent with the model of inhibition via hierarchical phosphorylation, dependent on PLK1 docking. However, there are several findings in the Kettenbach study which are inconsistent with data presented here. Firstly, the authors propose that PLK1 preferentially binds a specific PP6-SAPS2-ANKRD28 holoenzyme, whereas no discrimination was found in experiments presented here [251]. This could be borne out of the methodology used to estimate protein quantities – Kettenbach and colleagues estimated the difference by peptide numbers (a measure of detection efficiency), whereas averaged peak intensities, which more accurately reflect protein abundance, were compared in this work. Secondly, the PLK1 docking site on SAPS2 is proposed to be phosphorylated by CDK1. This conclusion was drawn from *in vitro* binding assays, where phosphorylation of SAPS2 by CDK1-cyclin B promoted the PLK1-SAPS2 interaction [251]. It is possible that this does indeed happen *in vitro*, but *in vivo* experiments with PLK1 and CDK inhibitors presented here suggest CDKs make little to no contribution to docking. In addition, the docking phosphorylation is said to be stable and not opposed by phosphatases, based on interactome analyses after inhibition of kinase activity for 30min. [251] By contrast, data presented here demonstrate PLK1 inhibition results in the dissociation of PLK1-SAPS2

complexes. This could be explained by the duration of kinase inhibitor treatment, which was longer (>100min) in this work.

Based on these collective findings, it is now clear that PP6-SAPS2 is inhibited by PLK1 in a cell cycle dependent fashion. In order to unpick the sub molecular mechanism of this inhibition, detailed structural studies coupled with biochemical tests will be required. Regardless, this demonstrates that PP6 can be regulated, opening a new paradigm in the understanding of this phosphatase and raising the possibility of other regulatory systems integrated with different cellular processes.

5.4 System-level feedback between PLK1 and Aurora A

Thus, cells have two pools of Aurora A T-loop phosphatases – the constitutively active PP6-SAPS3 and the regulated PP6-SAPS2. This might explain some of the Aurora A spatiotemporal activation profile during cell cycle progression (Figure 5.2A). As cells enter into G2 phase and start synthesizing Aurora A, its autoactivation in the nucleus is prevented by sequestration of TPX2. In the cytoplasm, Aurora A associates with centrosomes, but is suppressed by the activity of PP6-SAPS2 and PP6-SAPS3. PLK1 levels rise in parallel with Aurora A, and low-level Aurora A activity due to transient activation gradually phosphorylates the PLK1 T-loop. This activated pool of PLK1 can then associate with, phosphorylate and inhibit PP6-SAPS2, reducing Aurora A pT288 phosphatase activity. The resultant increase in Aurora A activity then promotes further PLK1 activation. Once a threshold level is reached in late G2 phase, PP6-SAPS2 is completely inhibited and active Aurora A levels rise further. Upon NEBD, TPX2 inhibition is relieved and the pool of Aurora A sequestered in the nucleus is released, allowing high levels of Aurora A activation to be achieved. However,

these levels are lower than the theoretical maximum due to the activity of PP6-SAPS3, preventing aberrant spindle assembly factor regulation. When cells exit mitosis, Aurora A can be inactivated by a combination of dissociation from TPX2, and degradation of both Aurora A and TPX2 by APC/C^{CDH1} [183].

This modular system provides a safe way to regulate Aurora A, wherein its activity is always sufficiently suppressed to prevent spindle defects and tumorigenesis, but more counteracting activity can be deployed when necessary. Moreover, it integrates the functions of PLK1 and Aurora A beyond the previously described activation of PLK1 by Aurora A [76, 206]. The concerted activity of PP6-SAPS2 and PP6-SAPS3 is required for this feedback, at least in mitosis, as depletion of either pool prevents the dephosphorylation of Aurora A pT288 upon PLK1 inhibition. The PLK1-Aurora A feedback also creates a net-positive feedback loop for Aurora A autoactivation, as Aurora A activates the inhibitor (PLK1) of its inhibitor (PP6-SAPS2) (Figure 5.2B). Small increases in the amount of Aurora A or PLK1 can therefore cause a larger or faster increase in Aurora A activation, which might explain why cancer patients with Aurora A amplification receive less clinical benefit from Aurora A inhibitor therapy [237]. If this is correct, supplementing Aurora A inhibitor treatment with PLK1 inhibitors may improve the efficacy (Figure 5.2B).

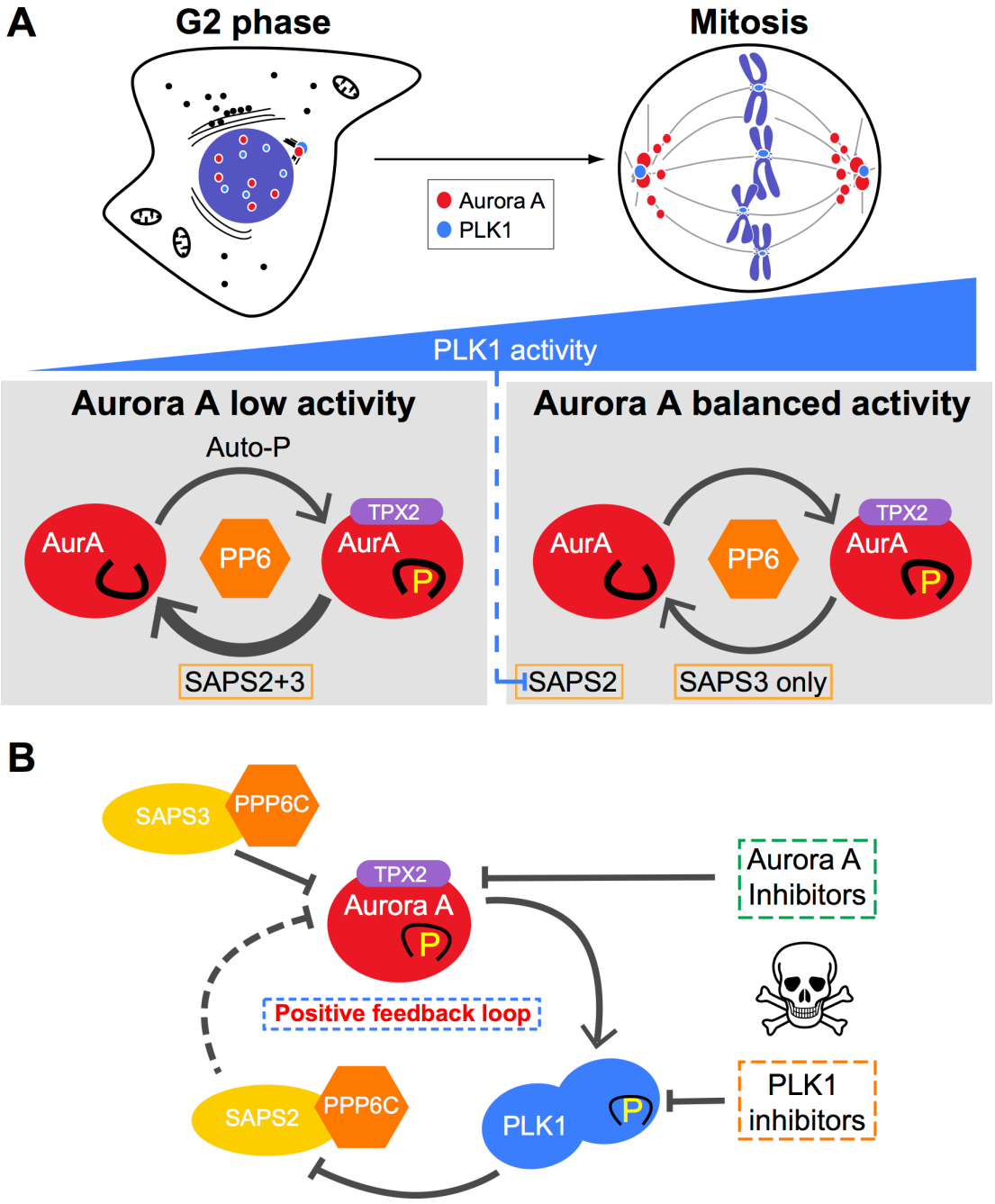


Figure 5.2 - PLK1-PP6-Aurora A feedback in the cell cycle. (A) In interphase, Aurora A autophosphorylation is kept in check by the summed activity of PP6-SAPS2 and PP6-SAPS3. As cells progress through G2 phase, PLK1 levels rise and the kinase starts getting activated, allowing it to inhibit PP6-SAPS2. Upon mitotic entry, this inhibition is maximal, and the cell is left only with PP6-SAPS3 activity, allowing balanced Aurora A activation. **(B)** PP6-SAPS2 closes a positive feedback loop between Aurora A and PLK1, because Aurora A activates the inhibitor of its inhibitor. Because of this, amplification of the Aurora A protein may cause a large increase in its overall activation status. Supplementing Aurora A-inhibitor chemotherapy with PLK1 inhibitors may increase the efficacy of Aurora A-amplified tumour targeting.

As discussed before, PLK1 has other essential functions which are not related to Aurora A, such as the regulation of cytokinesis [248]. Global inhibition of PLK1 is therefore likely to induce additional toxicity in all dividing cells. In a more specific approach, the PLK1-SAPS2 interaction could be targeted directly to break this positive feedback loop. However, it is questionable whether completely specific compounds interfering with the interaction could even be developed, because the mechanism of binding is shared with a multitude of other PLK1 partners. Further mechanistic and structural understanding of the interplay is therefore critical to resolving these issues.

5.5 PP6-SAPS2 and PP6-SAPS3 function in spindle regulation

While a clearer picture of the roles for the different PP6-SAPS holoenzymes emerges from this work, a number of questions remain about their functions at different times in the cell cycle. The data presented her indicate that the majority of Aurora A phosphatase activity is contributed by PP6-SAPS3, reflected in its contribution to the maintenance of spindle architecture. However, some defects can be observed in the absence of SAPS2, most notably an increased tendency towards spindle pole fragmentation. This indicates that SAPS2 may make a small but important contribution to the suppression of Aurora A activity in mitosis. One way this could occur is by local dephosphorylation of select pools of Aurora A, such as the one associated with TACC3. Alternatively, PP6-SAPS2 could act on other substrates including NuMA, which is required for spindle pole stability. However, there is currently no evidence to support these views. By contrast, data presented here and elsewhere clearly establish a role for PP6-SAPS2 in PLK1-Aurora A feedback. However, this is not critical for global regulation of Aurora A activation during unperturbed cell cycles. Depletion of SAPS2 or replacement of

the WT protein with the unregulated docking site mutant does not significantly alter Aurora A activation and deactivation timings or the association of Aurora A with centrosomes and mitotic spindles.

While the role of SAPS2 in the regulation of somatic cell spindles is not pronounced, it is essential during development. Knockout mice for either PPP6C or SAPS2 are not viable (IMPC 6.1, [252]). This could be explained by aberrant regulation of Aurora A, which initiates and regulates the formation of acentriolar microtubule-organizing centres of oocyte meiotic spindles [105]. Oocytes are much larger than somatic cells, and thus require a more rigorous mechanism controlling the location and timing of spindle formation. A key regulatory system controlling this is the sequestration of TPX2 by importins, which is only released by Ran GTPase proximal to chromatin [90]. This affects microtubule nucleation directly and through activation of Aurora A. However, the function of Aurora A in meiotic spindle formation has to be further integrated with PLK1. Thus, PP6-SAPS2 may ensure that Aurora A can only get consistently activated adjacent to active pools of PLK1. This would coordinate Aurora A and PLK1 and provide a failsafe mechanism ensuring robust spindle assembly during early embryonic divisions.

5.6 The interplay of PP6 and the DNA damage response

Although key details relating to the role of PLK1-regulation need to be elucidated, as argued above PP6-SAPS2 is clearly an essential gene. Biochemical studies with purified proteins also show that PLK1 inhibits PP6-SAPS2, but the significance of this regulation for cell cycle control is less clear. Indeed, rather than regulated association with PLK1 triggering PP6 inactivation, PP6-SAPS2 appears to be continuously associated with PLK1 through the cell cycle and thus

constitutively inhibited. This raises the question of when and how PLK1-mediated inhibition is overcome, and PP6-SAPS2 becomes activated. One input that could mediate this activation is the DNA damage response, which triggers a reversible checkpoint response in G2 cells, preventing the activation of CDK1, Aurora A and PLK1 [76]. Depletion of either PP6-SAPS2 or PP6-SAPS3 allows the cells to activate Aurora A and PLK1 in late G2, even under a checkpoint challenge. This indicates that the concerted activity of these two phosphatases suppresses Aurora A autoactivation under these conditions. Aurora A and PLK1 activities are essential for recovery from a DNA-damage induced arrest in G2, but CDK1 activation is still prevented in the absence of PP6-SAPS2 or PP6-SAPS3 and the cells do not enter mitosis. This suggests that the role of PP6 is limited to Aurora A/PLK1 regulation and does not extend to additional mechanisms regulating CDK1 activation in the context of a G2 arrest. It is unclear whether Aurora A autophosphorylates first, followed by deactivation, or it is prevented from being appreciably activated in the first place. These two scenarios have different implications for the extent of the role of PP6 in the process. In the latter option, PLK1 will also be suppressed since Aurora A activity is required to phosphorylate the PLK1 T-loop. However, if both T-loops are initially phosphorylated and subsequently quenched, the cells must have another mechanism to dephosphorylate PLK1 pT210. Previous efforts in the literature to conclusively identify a PLK1 T-loop phosphatase were unsuccessful [72], and data presented in this thesis suggest that PP2A, PP1 and PP6 do not do this job in mitosis. Whether any of these phosphatases are able to do this in G2 phase is unclear, and the cell could employ other enzymes to perform this function.

Further evidence links PP6 to the integration of the DDR and cell cycle progression. Cells lacking PPP6C or SAPS2 arrest the cell cycle in a p53-dependent fashion. This arrest primarily occurs in G1 phase through induction of p21, but escaping cells can also terminally exit the cell cycle in G2 by degrading cyclin B. Preliminary data suggest this arrest is separable from the mitotic role of PP6. Depletion of PP6-SAPS3, the major Aurora A phosphatase, does not result in p21 induction or a pronounced cell cycle arrest, although p53 stabilization is observed. However, further experiments will be required to validate and expand on these findings. Furthermore, it is noteworthy that the effects of individual SAPS2 or SAPS3 depletions are not sufficient to explain the striking incidence of cell cycle arrest upon PPP6C depletions. This suggests that the arrest may be caused by a synergistic defect caused by the loss of multiple PP6 holoenzymes. Alternatively, the effect could primarily be contributed to by the untested PP6-SAPS1. On the whole, this early response safeguards cells from further aberrations, as cells without a functional p53 response and depleted of PPP6C accumulate micronuclei. However, it is unclear what defect sets the pathway off when PP6 is silenced. The primary trigger for the p53 cell cycle arrest is DNA damage (Figure 5.3)[28]. An increase in DNA damage incidence in PP6-deficient cells is therefore one possible explanation for the arrest, but it could also be caused by a failure to silence checkpoint signalling after naturally-occurring DNA damage. An increase in DNA damage could be a consequence of mitotic defects, as poorly segregated chromosomes are often damaged by the cleavage furrow or encapsulated in micronuclei, which are known DNA damage hotspots [157, 214]. However, obvious mitotic defects, including in anaphase, are not observed in SAPS2-depleted cells. In addition, SAPS3 depletion, which causes the most

severe defects at this stage doesn't concordantly trigger a cell cycle arrest. Therefore, this phenotype is unlikely to be a major contributor. Accumulation of DNA damage could also occur if PP6 has a direct role in promoting DNA repair. The stable interaction with DNA-PKcs provides further indications that PP6 may be involved in this process. A study by Douglas and colleagues reports that the dissolution of repair foci after ionizing radiation is slower in PPP6C-depleted cells [223]. This effect was not attributed to a single regulatory subunit, although PP6-SAPS1 – the non-Aurora A phosphatase – was the most promising candidate in biochemical assays [223]. However, prolonged DNA damage was not observed in comet assays upon depletion of PPP6C or SAPS1, suggesting these cells are not deficient in DNA repair [223]. Therefore, checkpoint-proficient cells more likely arrest due to a defect in checkpoint silencing.

Multiple steps in the p53 cell cycle checkpoint are promoted by phosphorylation, and compromised dephosphorylation of any of those could cause sustained checkpoint firing (Figure 5.3)[26]. One possibility is that PP6 is required to deactivate one or more DDR kinases, such as ATM or DNA-PK, once the damage lesions have been repaired. Sustained activity of these kinases would lead to prolonged generation of the γ-H2A.X signal, leading to retention of DNA repair factors such as 53BP1, consistent with observations made by Douglas and colleagues [223]. In addition, ATM phosphorylates S15 on p53, which results in protection from MDM2-mediated ubiquitination (Figure 5.3)[28]. Consistent activity of DDR kinases can thus lead to an increased and sustained DNA damage response and an overactive p53 checkpoint. An intriguing mechanism by which this could occur is deficiency in dephosphorylation of the kinase T-loops. However, this feature hasn't been well assigned in either ATM or DNA-PK and it is

unclear whether it is regulated by phosphorylation in these two proteins. Rather, DNA-PK is functionally regulated by a cluster of phosphorylation around T2609 [253], and ATM is regulated through dissolution of inactive dimers due to DNA-damage dependent autophosphorylation on S1981 [254]. Intriguingly, the ATM S1981 phosphorylation is turned over by Wip1, but is also a target for okadaic acid-sensitive phosphatases [255]. It is therefore plausible that one or more PP6 holoenzymes target this site under some conditions (Figure 5.3). Shaltiel and colleagues identified PP4, another PP2A-family phosphatase, as an important cell cycle checkpoint regulator in G1 phase [256]. PP4 does so by dephosphorylating an inhibitory phosphorylation on KAP1, a transcription repressor targeting p21, among other genes [256]. PP6 was not identified in their screen. However, this was performed with checkpoint recovery after combined Chk2 and MAPK inhibitor treatment, and is therefore geared to probe events downstream of these two kinases [256]. Thus, it is possible that upstream events, such as the deactivation of p53-stabilizing kinases ATM and DNA-PK, are controlled by PP6. Consistently, the authors note that depletion of PP4 does not delay p53 degradation upon checkpoint recovery [256]. An alternate possibility is that PP6 is one of the phosphatases able to control p53 function directly. The S15 phosphorylation has been shown to be a target for Wip1, but loss of Wip1 by depletion or KO does not appreciably perturb S phase entry [256]. Conversely, Wip1 is critical to limit the potential of p53 to trigger the degradation of Cyclin B during a G2 checkpoint response [256]. Thus, it is possible that the phosphorylation is targeted by another phosphatase at specific cell cycle stages. In addition, other phosphorylation sites on p53 regulate its transcription factor activity, which is critical for its checkpoint function [26]. The inability to dephosphorylate these could therefore lead to an

overly sensitive response to naturally occurring DNA damage. Furthermore, a p53 phosphorylation on S376 controls its association chaperones that enhance its DNA binding, and is a target of an unidentified ATM-activated phosphatase (Figure 5.3)[26]. These regulatory elements provide another potential mechanism by which PP6 could affect the G1 arrest. All of these possibilities can be initially tested with *in vitro* activity assays. This approach would also narrow down candidate specific PP6 holoenzymes, but would need to be complemented with *in vivo* experiments.

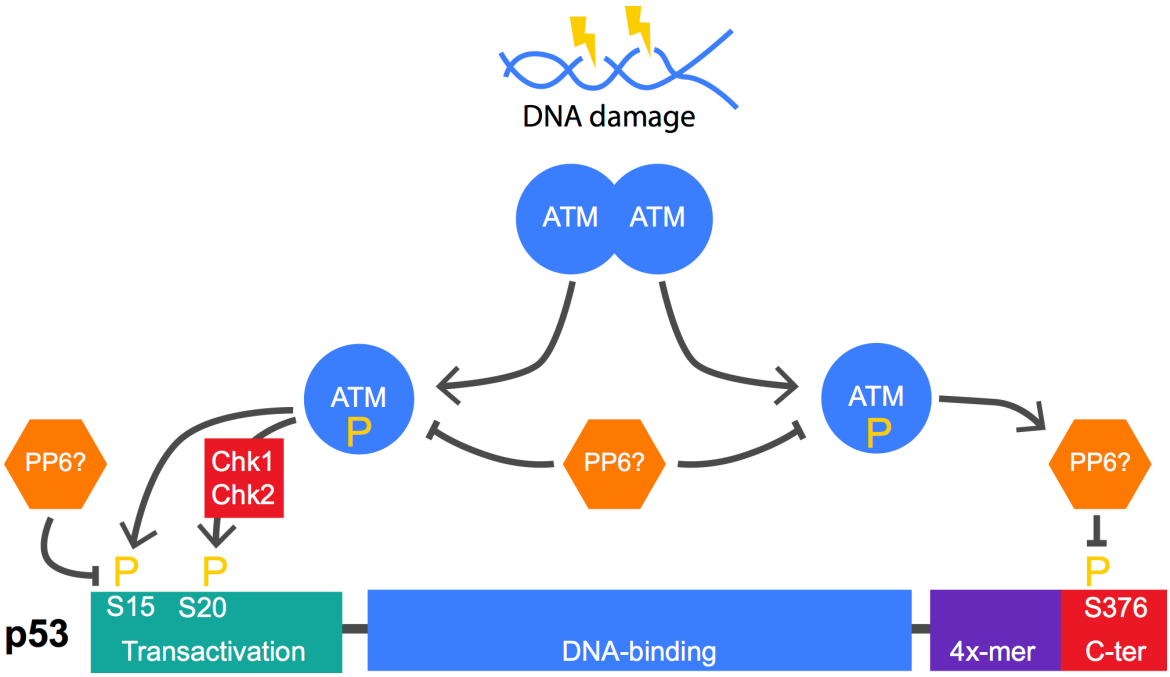


Figure 5.3 - Potential gateways for PP6 in checkpoint control. DNA damage results in the activation of checkpoint kinases such as ATM. ATM is activated by autophosphorylation-mediated dimer disassembly and phosphorylates p53 on S15, protecting it from MDM2-mediated degradation. Chk kinases are also activated by ATM, allowing them to phosphorylate p53 on a secondary site and promote its stability. An okadaic acid phosphatase is further activated by ATM to promote dephosphorylation of the C terminus of p53, promoting its association with auxiliary proteins. Dephosphorylation of either S15 or the activatory ATM phosphorylation may shut down the checkpoint.

Whether PP6 plays a role in these interphase processes or others, expanding on the better described mitotic role of PP6 will be important to understand its role and therapeutic potential.

5.7 An expanded view of PP6 function and regulation

In conclusion, the findings presented here paint a more complete picture of the different roles PP6 plays in the cell cycle, and the ways in which these roles are achieved. Globally, PP6 safeguards the genomic integrity of the cell, both through its mitotic function and additional interphase mechanisms. These diverse roles are fulfilled by functionally distinct holoenzymes, defined by the regulatory SAPS subunits, which serve as a substrate binding platform and hub for regulatory inputs. The next critical step in dissecting the individual roles of these PP6 phosphatases will be a systematic and unbiased search for substrates. Importantly, the findings from such a high throughput approach should be backed by direct *in vitro* assays and *in vivo* methods, and assign the specific PP6 holoenzyme responsible. This should result in a greater understanding of pathways affected by these tumour suppressor phosphatases and allow us to better predict, diagnose and treat cancers associated to these pathways.

Chapter 6 Materials and methods

6.1 Reagents and antibodies

Common laboratory reagents and consumables were bought from Sigma-Aldrich, Thermo Fisher Scientific and VWR. Inhibitors were obtained from Tocris (Flavopiridol, AZ3146), Selleckchem (MLN8237, NU7441, Phleomycin), Axon MedChem (BI2536), CalBiochem (Nocodazole, Taxol). Selection antibiotics were obtained from Invivogen (Blasticidin, hygromycin gold, puromycin). The pcDNA5-FRT-TO vector system with varying tags was used for mammalian cell expression. A list of antibodies, primers, siRNAs and protein sequence accession numbers used for cloning is given in Tables 6.1, 6.2, 6.3, 6.4 and 6.5. An Eppendorf 5702R centrifuge was used for lower speed centrifugation of larger vessels. An Eppendorf 5417R centrifuge was used for all other purposes.

Table 6.1 Inhibitors and selection antibiotics.

Chemical	Solvent	Stock concentration
Flavopiridol	DMSO	5mM
AZ3146	DMSO	20mM
MLN8237	DMSO	10mM
NU7441	DMSO	10mM
Phloemycin-sulphate	DMSO	10mM
BI2536	DMSO	1mM
Nocodazole	DMSO	2µg/mL
Taxol	DMSO	5mg/mL
Blasticidin	Water	10mg/mL
Hygromycin gold	Water	100mg/mL
Puromycin	Water	1mg/mL
Thymidine	Water	100mM

Table 6.2 - siRNAs used for protein depletion in mammalian cells.

siRNA	siRNA code/sequence
SAPS2 SMARTpool	L-021331-01
SAPS2-09	J-021331-09
SAPS1 SMARTpool	L-020420-01
SAPS3 SMARTpool	L-014646-01
SAPS3-09	J-014646-09
PPP6C	GUUUGGAGACCUUCACUUA
Bora SMARTpool	L-014458-00
PPP1CA	CAUCUAUGGUUUCUACGAU
PPP1CC	GCGGAGAGUUUGACAAUGC
PPP2CA	L-003598-01
PPP2CB	L-003599-00
GL2 (control)	CGUACGCGGAAUACUUCGAUU

6.2 Cell culture

HeLa S3 cells were grown in Dulbecco's modified eagle medium (DMEM) supplemented with 10% foetal bovine serum, and RPE1 cells in DMEM-F12 HAM with 10% foetal bovine serum and GlutaMax. All cells were incubated at 37°C, 5% CO_2. Plasmids were transfected using LT1 (Mirus Bio, LLC), at 35% confluency for 48h transfections and at 50% for 24h transfections. To do this, LT1 was diluted in OptiMEM and left to stand for 5min at room temperature before the addition of a mixture of target plasmids and non-expressing pBluescript as a filler. The reactions were mixed gently by tapping and inverting the tubes and incubated at room temperature for 30min. Afterwards, the transfection mixtures were added to cultures dropwise while mixing. For 6-well plate format transfections, 200μL of OptiMEM, 3μL of LT1 and a total amount of 0.8μg of plasmid DNA. The ratio of

target and filler plasmid was altered for specific applications based on the desired expression level. For transfections for immunofluorescence or live-cell imaging, 200ng of target-containing pcDNA5 was used with 600ng of pBluescript. Transfections of larger dishes were done equivalently, but the amounts were scaled up. For 10 cm dishes, 1mL of OptiMEM, 15μL of LT1 and 4μg total plasmid DNA was used. For 15cm dishes, 1mL of OptiMEM, 30μL of LT1 and 8μg total plasmid DNA was used. For these larger scale transfections, which were used exclusively for IPs and enzyme preparations, the ratio between pcDNA5 and pBluescript was 1:1. RNA interference was performed by siRNA transfections using either Oligofectamine (Mirus Bio, LLC) for HeLa cells or Transit-X2 (Mirus Bio, LLC) for RPE1 cells. For transfections in a 6-well plate format, 3μL of transfection reagent was added into 200μL OptiMEM, mixed and left to rest for 5min. Afterwards, 60pmol siRNA was added and the reaction gently mixed before a 30min incubation at room temperature. If combinations of siRNAs were used, these amounts were altered. To combine two siRNAs, 4μL of transfection reagent and 40pmol of each siRNA was used. For triple depletions, 4.5μL of transfection reagent and 30pmol of each siRNA was used. Afterwards, the mixtures were added dropwise into cultures while mixing. Depletions were done for varying amounts of time, tailor made for specific genes and applications, as indicated in the individual figure legends. For depletions in concert with a double thymidine block, cells were transfected 6h before the first block and retreated 1h after the first thymidine washout. In all other cases, only one round of siRNA transfection was used.

Single thymidine synchronizations were performed by addition of 2.5mM thymidine for 16-20h, as indicated for individual experiments. Optimized double

thymidine blocks were performed by a 16h initial treatment with 2.5mM thymidine, followed by a 10h washout, and a second, 12h long treatment with 2.5mM thymidine. Mitotic arrests were done with 100ng/µL nocodazole for 20h. Synchronized mitotic exit in Figure 3.6 and Figure 3.16 was induced by a previously validated procedure [137]. Nocodazole-arrested cells were harvested by mitotic shakeoff, pelleted ($200g_{av}$, 5min, 37°C) and washed thrice with PBS and twice with DMEM, with centrifugations between each wash ($200g_{av}$, 5min, 37°C). Cells were resuspended in DMEM and allowed to rebuild mitotic spindles for 25min under incubator conditions, before the addition of 20µM AZ3146 (MPS1 inhibitor) and sampling at intervals indicated in the relevant figures. Sampling was performed by extracting aliquots of the cell suspension into vessels containing a 2-fold excess of PBS, followed by centrifugation ($400g_{av}$, 5min, 37°C) and snap-freezing.

Table 6.3 - Accession numbers of PP6 subunit DNA sequences used for cloning.

Protein	Accession number
SAPS1	NM_014931.3
SAPS2	NM_001365836.1
SAPS3	NM_001164161.1
ANKRD28	NM_015199.3
ANKRD44	NM_001195144.1
ANKRD52	NM_173595.3

Table 6.4 - Primers used for cloning and mutagenesis.

Primer	Sequence	Purpose
SAPS2_S723A_T724A_F	gatgagccagcgaacGcaGcgcccacagcccc agga	Mutagenesis - ST724AA
SAPS2_S723A_T724A_R	tcctggggctgtgggcgCtgCgttcgctggctcatc	Mutagenesis - ST724AA
SAPS2_S770A_S771A_F	tcagggcccaggtgCGCCGCTccggtggaca cagaa	Mutagenesis - SS770AA
SAPS2_S770A_S771A_R	ttctgtgtccaccggAGCGGCGcacctgggcc ctga	Mutagenesis - SS770AA
SAPS2_Nt_BglII_F	GAGATCTCCatgttctggaagtttgac	Cloning
SAPS2_seq_550	cactggctgaatgaagagaag	Sequencing
SAPS2_seq_1100	ggctcaacacgatggacttac	Sequencing
SAPS2_seq_1650	ggtgctttccctaacgagc	Sequencing
SAPS2_seq_2200	gacgtgggttccagtgtg	Sequencing
SAPS2 Ct_NS_XhoI_R	GCTCGAGcactgggccatttaag	Cloning - C-terminal tagging
SAPS2_siJ09res_F2	ggcaatctcattgcaagaaaaaCGGAGCAA GTCATAACCtTTttgaagaagaaggacaagt tc	Mutagenesis - resistance to siRNA SAPS2-09
SAPS2_siJ09res_R2	gaacttgtccttcttcttcaaAAaGGTTATGAC TTGCTCCGtttttcttgcaatgagattgcc	Mutagenesis - resistance to siRNA SAPS2-09
SAPS3_Nt_BamHI_F	GGGATCCCCatgttttggaaatttgatc	Cloning
SAPS3_seq_550	gaattggttaaatgaggag	Sequencing
SAPS3_seq_1100	ggagctgaatagcattgg	Sequencing
SAPS3_seq_1650	ccaattttattgaccagtttgg	Sequencing
SAPS3_NS_Ct_XhoI_R	GCTCGAGtacagggccattcac	Cloning - C-terminal tagging
SAPS1_Nt_BglII_F	GAGATCTCCatgttttggaagtttgacC	Cloning
SAPS1_seq_550	atgttgtcaattggctcaac	Sequencing
SAPS1_seq_1100	gtgccctgagcgccaatg	Sequencing
SAPS1_seq_1650	gtgctgcagcaggccttc	Sequencing
SAPS1_Ct_XhoI_R	GCTCGAGttgggagcctggg	Cloning - C-terminal tagging
ANKRD28_Nt_BamHI_F	GGGATCCCCatggcgttcctcaaac	Cloning
ANKRD28_seq_700	gatatgaatgaaccaaatgcc	Sequencing
ANKRD28_seq_1400	caggagcaagtgtgaatgacc	Sequencing
ANKRD28_BamHI_mut_F	cgatgcaaatccaggTatccgtgataagca	Mutagenesis - removal of internal BamHI site
ANKRD28_BamHI_mut_R	tgcttatcacggatAcctggatttgcatcg	Mutagenesis - removal of internal BamHI site
ANKRD28_seq_2100	gaaggacagcgttgcatagag	Sequencing

ANKRD28_Ct_NS_SalI_R	CGTCGACgtaggtctcagaatcgg	Cloning - C-terminal tagging
ANKRD44_Nt_BamHI_F	GGGATCCCCatggcagtgctcaaac	Cloning
ANRKD44_seq_700	ggagattgatgaaatcaatg	Sequencing
ANRKD44_seq_1400	ccaacgttaatgaaacagatga	Sequencing
ANKRD44_seq_2100	gaaaaggaagccaacgtagac	Sequencing
ANKRD44_Ct_NS_XhoI_R	GCTCGAGttcttctttttgtacagc	Cloning - C-terminal tagging
ANKRD52_Nt_BglII_F	GAGATCTCCatggggatcctcag	Cloning
ANKRD52_seq_700	gagatcgatgaacccaatgc	Sequencing
ANKRD52_seq_1400	cactgcactatgcagctgct	Sequencing
ANKRD52_seq_2100	cactgatgctggccatcatg	Sequencing
ANKRD52_Ct_NS_XhoI_R	GCTCGAGctcagagtagcag	Cloning - C-terminal tagging

6.3 Molecular cloning

All PCR reactions were performed with Pfu-HotStart polymerase (Agilent Technologies) with 0.2mM dNTPs, 4μM primers and 20ng of template DNA. For mutageneses, 50ng of template DNA and 2.5μM primers were used. Annealing temperatures were set at 5°C less than the lowest primer melting temperature in the reaction, and a 2min elongation per 1kb at 68°C was allowed. PCR products were analysed by agarose gel electrophoresis after which they were extracted using a commercial kit (Qiagen). As standard, the purified product was A-tailed using Taq polymerase (New England Biolabs) and ligated into the pSC-A vector (Agilent Technologies). For restriction digests, 1-3μg DNA was incubated at 37°C with the appropriate endonuclease for 1-3h before analysis by agarose gel electrophoresis. Products were gel-extracted and ligated into 50-100ng vector at a 3:1 insert/vector molar ratio using T4 DNA ligase (New England Biolabs). Plasmids were transformed into XL1-blue Rb^{+}-Ca^{2+} competent bacteria and

isolated using commercially available kits of varying scale (Miniprep, Maxiprep - Qiagen).

6.4 Western blotting

Protein samples in Laemmli sample buffer were separated by standard SDS-PAGE (Mini-PROTEAN, BioRad). The contents of resolving gels were transferred onto nitrocellulose membranes using a semi-dry transfer procedure (TransBlot Turbo, BioRad) with transfer parameters: 2.5A, 25V, 10min for two gels. The nitrocellulose membranes were blocked in 5% cow's milk (Fortified skimmed milk powder, Tesco) dissolved in phosphate buffered saline+0.1% v/v Tween-20 (PBST). Antibody incubations were performed with antibodies diluted in blocking solution to empirically determined concentrations for a minimum of 1h up to a maximum of 24h. When re-probing, 1mM NaN_3 was included in the primary antibody solution. Between each antibody incubation, the membranes were washed for 1h in PBST with a minimum of 4 buffer exchanges. The horseradish peroxidase-ECL system (GE Healthcare), coupled with film-based detection was used to visualize protein bands.

6.5 Immune precipitations

One or two 15cm dishes of cells per condition were transfected (4µg plasmid with target plus 4µg of empty pBluescript per dish) or induced with 1µg/mL doxycycline at 40% confluency. After 36h the cells were treated with 100ng/mL nocodazole or left untreated. If cells were synchronized by a double thymidine block, induction or transfection were done 6h before the first block and redone after the first washout. For nocodazole arrests, cells were harvested by mitotic shakeoff and gently centrifuged ($200g_{av}$, 5min). For double thymidine-release synchronized or

Table 6.5 - Antibodies used for western blotting, immunofluorescence and immunoprecipitations.

Target	Manufacturer	Reference
α-Tubulin	Sigma-Aldrich	T9026
ANKRD28	Abcam	ab137091
ANKRD52	Bethyl Laboratories, Inc.	A302-372A
Aurora A	Cell Signaling Technology	4718S
Aurora A pT288	Cell Signaling Technology	3079
Bora	Cell Signaling Technology	12109S
BUBR1	Bethyl Laboratories, Inc.	A300-368A
CDK1 pY15	Cell Signaling Technology	4539S
Cyclin A2	Abcam	ab32498
Cyclin B1	Millipore	05-373
FLAG	Sigma-Aldrich	F7425
GFP	Barr lab	[172]
γH2A.X	Milipore	05-636
p53	Cell Signaling Technology	2527S
PLK1	Santa Cruz	SC-17783
PLK1	Barr lab	[257]
PLK1 pT210	BD Transduction laboratories	558400
PPP1CA	Bethyl Laboratories, Inc.	A300-904A
PPP1CA pT320	Abcam	ab62334
PPP1CC	Santa Cruz	sc-6108
PPP2AR1A	Santa Cruz	sc-6112
PPP2CA	BD Transduction laboratories	610556
PPP6C	Abcam	ab131335
PRC1	Barr lab	[137]
PRC1 pT481	Abcam	ab62366
SAPS1	Bethyl Laboratories, Inc.	A300-968A

SAPS2	Bethyl Laboratories, Inc.	A300-969A
SAPS3	Bethyl Laboratories, Inc.	A300-972A
TPX2	Abcam	ab32795
α-sheep 2°-HRP	Jackson immunoresearch	713-035-147
α-mouse 2°-HRP	Jackson immunoresearch	715-035-150
α-rabbit 2°-HRP	Jackson immunoresearch	711-035-152

asynchronous cells, the medium was combined with cells detached by a 10min treatment with 1mM EDTA in PBS at 37°C before centrifugation (200g_{av}, 5min). Cells were washed once in warm PBS and snap frozen. Pellets were lysed in NP40 lysis buffer supplemented with phosphatase inhibitors (20mM Tris-HCl pH7.4, 150mM NaCl, 1% (v/v) Igepal CA-630, 0.1% (v/v) sodium deoxycholate, protease inhibitors, 100nM okadaic acid, 40mM β-glycerolphosphate, 10mM NaF, 0.3mM Na_3VO_4) for 20min on ice and cleared by centrifugation at 4°C (20,000g_{av}, 20min). Protein concentration in the lysates was determined by Bradford assay against BSA and 1-3.5mg protein-lysate equivalent was loaded onto 10-20µL of bead slurry (Protein A or G-coupled sepharose or M2-FLAG-coupled agarose, Sigma Aldrich) prewashed twice with lysis buffer. For GFP IPs, 2µg of antibody was added per 1mg of protein. For endogenous IPs, 1µg of antibody was used per 1mg of protein. Beads were incubated with lysate for 2h at 4°C, washed twice with lysis buffer and twice with wash buffer (20mM Tris-HCl pH7.4, 150mM NaCl, 0.1% (v/v) Igepal CA-630 (NP40), 40mM β-glycerolphosphate, 10mM NaF, 0.3mM Na_3VO_4) before resuspension in 3x Laemmli sample buffer. All bead centrifugations were done at 2000g_{av}, 2min, 4°C.

6.6 Production of phosphatase and substrate complexes

Cells were transfected with FLAG tagged proteins of interest (SAPS subunits or TPX2) or empty vector for mock transfections and prepared as for immune precipitation experiments. The quantity was scaled up to a maximum of ten 15cm dishes. For Aurora A-TPX2 preparations, cells were arrested with nocodazole and pretreated for 30min with 100nM Calyculin A before harvesting. In the final conditions, lysis was performed with TX100 lysis buffer (20mM Tris-HCl pH7.4, 150mM NaCl, 1% (v/v) Triton X-100) for 20min on ice and centrifuged (20000g_{av}, 20min) at 4°C. For Aurora A-TPX2 purification the lysis buffer was supplemented with 1µM microcystin-LR and 100nM okadaic acid, and for SAPS2 WT/^{770}AA purification with 40mM β-glycerolphosphate. All of the lysate was loaded onto 15-100µL of M2-FLAG beads (Sigma-Aldritch) and incubated for 3h at 4°C. The beads were then washed twice with lysis buffer, four times with wash buffer (20mM Tris-HCl pH7.4, 150mM NaCl, 0.1% (v/v) Triton X-100) and once in elution buffer (20mM Tris-HCl pH7.4, 150mM NaCl, 0.1% (v/v) Triton X-100, 1mM $MnCl_2$). The beads were then transferred into a smaller vessel and 2 elutions performed at room temperature for 30min with 200µg/mL FLAG peptide in elution buffer. 10% glycerol and 0.1mM DTT were added and the first eluate aliquoted, snap frozen and stored at -80°C. Buffer conditions tested in Figure 2.1 are as follows: NP40 lysis buffer (20mM Tris-HCl pH7.4, 150mM NaCl, 1% (v/v) Igepal CA-630, 0.1% (w/v) sodium deoxycholate), TX100 lysis buffer (20mM Tris-HCl pH7.4, 150mM NaCl, 1% (v/v) Triton X-100), elution buffer pH7.4 (20mM Tris-HCl pH7.4, 150mM NaCl, 1mM $MnCl_2$), elution buffer pH7.4+TX100 (20mM Tris-HCl pH7.4, 150mM NaCl, 1mM $MnCl_2$, 0.1% (v/v) Triton X-100), elution buffer pH8 (20mM Tris-HCl pH8, 150mM NaCl, 1mM $MnCl_2$).

6.7 Protein preparation titrations

The Aaronase mini kinase has been described previously [167]. To achieve maximal phosphorylation, Aaronase in 5mM $MgCl_2$ and 0.1mM ATP was incubated for 30min at 30°C. This was titrated against the Aurora A-TPX2 preparations by western blotting as shown. The PP6 holoenzyme preparations were titrated against recombinant hexahistidine-tagged PPP6C which was a generous gift from the Grüneberg lab.

6.8 *In vitro* phosphatase assays

Phosphatase preparations were diluted to the desired concentration in phosphatase reaction buffer (20mM Tris-HCl pH7.4, 150mM NaCl, 0.1% (v/v) Triton X-100, 1mM $MnCl_2$, I_c=346mM) on ice. Reactions were started by addition of substrate and transferring to 30°C. Aliquots were taken immediately after reaction start and every 10min thereafter and mixed into Laemmli sample buffer before boiling and western blot analysis. Assessment of the effect of PLK1 binding on PP6-SAPS2 activity in Figure 3.9A was done by mixing varying amounts of PLK1 with constant amounts of phosphatase, followed by incubation on ice for 30min to allow time for complex formation. Dephosphorylation reactions were started by the addition of Aurora A-TPX2 and allowed to proceed at 30°C with sampling every 20min up to a maximum of 40min.

6.9 *In vitro* kinase assays

For PLK1 phosphorylation, 100ng PP6-SAPS2 enzyme preparations were mixed with 250ng recombinant PLK1 then diluted in kinase buffer (50mM Tris-HCl pH7.4, 50mM KCl, 10mM $MgCl_2$, 20mM β-glycerolphosphate, 15mM EGTA, 1μM MCLR) to a final volume of 20μL after ATP addition. Reactions were started by adding hot

ATP mix (final 0.1mM ATP, 1mM DTT, 1µCi γ-[^{32}P]-ATP) and incubated for 30min at 30°C. Reactions were stopped by addition on Laemmli sample buffer, resolved by SDS-PAGE and stained with Coomassie brilliant blue. The gels were then dried and exposed to films with the aid of an MS intensifying screen (Kodak).

6.10 Combined *in vitro* kinase and phosphatase assays

PP6-SAPS2 was diluted in kinase-phosphatase buffer (50mM Tris-HCl pH7.4, 50mM KCl, 10mM $MgCl_2$, 1mM $MnCl_2$, 0.1% (v/v) Triton X-100, I_c=266mM) and mixed with an estimated 100-fold excess PLK1. Phosphorylation reactions were started by the addition of 0.1mM ATP or water supplemented with 1µM (final) BI2536 as negative control and incubated at 30°C for 45min. Dephosphorylation reactions were started by addition of the Aurora A-TPX2 substrate supplemented with 1µM (final) MLN8237 to prevent rephosphorylation of Aurora A T288 and performed at 30°C for up to 60min with sampling every 10min. The addition of Aurora A-TPX2 changed the buffer composition to the final values of: 38.92mM Tris-HCl pH7.4, 55.38mM NaCl, 31.5mM KCl, 6.3mM $MgCl_2$, 1mM $MnCl_2$, 0.1% (v/v) Triton X-100, I_c=295mM. For the radioactive phosphorylation/dephosphorylation assay in Figure 3.8C, the phosphorylation reaction was done as described above with the addition of 1µCi γ-[^{32}P]-ATP. Dephosphorylation was allowed under unchanged buffer conditions after addition of 1µM BI2536 in the presence or absence of 1µM okadaic acid and evaluated by autoradiography of dried SDS-PAGE gels as described for naïve kinase assays.

6.11 Cell-based biochemical assays

Cells were treated with siRNA for the appropriate time before a synchronization with nocodazole (100ng/mL, 20h), single thymidine block or double thymidine

block release. If rescues were performed, doxycyline was added or plasmids transfected 30h before the addition of nocodazole, or after the first thymidine washout for double thymidine block synchronizations. Mitotic cells were harvested by vigorous pipetting, followed by gentle centrifugation (200g_{av}, 5min) at 37°C, and interphase cells by treatment with 1mM EDTA in PBS for 10min at 37°C. For experiments assessing the behaviour or total populations these fraction were combined. For figure 3.11A and figure 3.12, 1μM BI2536 or 500nM MLN8237 were prediluted in warm media and added for up to 30min where shown before harvesting. The 0min timepoints were taken before drug addition. Harvested cells were resuspended in warm PBS and pelleted (200g_{av}, 5min) at 37°C before snap freezing or rapid lysis with 1.5x Laemmli sample buffer followed by boiling. For extract-based experiments, frozen pellets were resuspended in ice-cold NP40 lysis buffer (20mM Tris-HCl pH7.4, 150mM NaCl, 1% (v/v) Igepal CA-630) at 1μL/3000cells and incubated on ice for 60min. Where indicated 1μM microcystin-LR was included. Reactions were stopped by addition of Laemmli sample buffer and boiling. The λ-phosphatase (New England Biolabs) treatment in Figure 2.7B was performed by adding 800U of phosphatase into 100μL of NP40 cell lysates supplemented with 1mM $MgCl_2$ and PMP buffer (New England Biolabs) in the presence or absence of 1mM Na_3VO_4 for 30min at 30°C.

6.12 G2 DNA damage cell biochemistry

HeLa S3 cells were treated with siRNA and arrested with a double thymidine block before release and addition of 30μg/mL Phleomycin-sulphate as indicated in Figure 4.1. After the indicated time of treatment, the media was collected and attached cells harvested by treatment with 1mM EDTA/PBS for 10min at 37°C. These two fractions were combined and centrifuged (200g_{av}, 5min 37°C), washed

once with PBS, centrifuged again (200g_{av}, 5min 37°C) and lysed rapidly in Laemmli sample buffer.

6.13 Immune precipitations for mass spectrometry

Immune precipitates were prepared as normal. Bound protein was eluted from beads in two rounds using 100mM glycine pH2.6 for 30min at room temperature and the elutions combined. The mixtures were neutralized with Tris-HCl pH8.5 and 2M urea added before snap freezing before a previously described filter assisted samplre preparation [258], peformed as follows. Eluates were loaded onto 10kDa cutoff filters (Sartorius) prewashed with 200µL wash buffer 1 (50% acetonitrile, 0.1% TFA in water). All centrifugations were peformed at 16000g_{av} for 30min at room temperature. After sample loading, filters were washed twice with 200µL 8M urea in 100mM TEAB pH8. Peptides were then reduced for 30min in 200µL reduction buffer (8M urea, 100mM TEAB pH8, 20mM TCEP) and centrifuged, before alkylation in 200µL alkylation buffer (8M urea, 100mM TEAB pH8, 50mM iodoacetamide) for 30min at room temperature and centrifugation. Filters were then washed twice in 200µL wash buffer 2 (1M urea, 50mM TEAB pH8) and transferred to clean collection tubes with centrifugations after every wash. Peptide digests were performed with 200µL of trypsinization buffer (1M urea, 50mM TEAB pH8, trypsin gold (Promega)). A trypsin/protein (w/w) ratio of 1% was used. To estimate the amount of trypsin needed, an assumption was made that 1% (w/w) of total lysate protein was recovered in IPs, thus requiring 0.1µg of trypsin per 1mg of lysate. Trypsinization was done overnight at 37°C with gentle shaking (200rpm) and digested peptides passed through the filter by centrifugation. Filters were further washed with 200µL 0.1% (v/v) TFA/water, centrifuged and washed again with 200µL 50% (v/v) acetonitrile, 0.1% (v/v)

TFA/water, before the final centrifugation. These combined eluates were dried in a reduced pressure centrifuge (Concentrator plus, Eppendorf) at 37°C for a variant time required to fully lyophilize the samples (normally about 6h), which were then resuspended in 5% (v/v) formic acid, 5% (v/v) DMSO/water and processed by mass spectrometry.

6.14 Mass spectrometry

Samples for mass spectrometry prepared as described already were processed by the Oxford Advanced Proteomics facility. Breifly, liquid chromatography was performed using an EASY-nano-LC 1000 system (Proxeon) with a 75μm internal diameter guard column packed with Reprosil-Gold 120 C18, 3μm, 120Å pores (Dr. Maisch GmbH) in solvent A (0.1% (v/v) formic acid/water) using a constant pressure of 500bar. Peptides were separated on a 45°C heated EASY-Spray column (50cm × 75μm ID, PepMap RPLC C18, 2μm; Thermo Fisher Scientific) using a linear 8–30% (v/v) acetonitrile gradient and constant 200nL/min flow rate. Peptides were introduced via an EASY-Spray nano-electrospray source into a Q Exactive Hybrid Quadropole Orbitrap (Thermo Fisher Scientific) on a 60min gradient. Spectra were acquired with a resolution of 30,000, m/z range 350–1,500, AGC target 106, maximum injection time 250ms. The 20 most abundant peaks were fragmented using CID (AGC target 5 × 103, maximum injection time 100 ms). MS data were processed, interpreted and analyzed using MaxQuant [259] and Perseus [260].

6.15 Fixed-cell imaging

Cells were grown on No. 1.5 coverslips and treated with siRNA as indicated in each experiment before treatment with 2.5mM thymidine for 18h. Thymidine was

washed out and 8-10h later depending on cell line and cells fixed. hTERT-RPE1 cells were not synchronized. In Figure 4.2A, 60µg/mL Phleomycin was added 2h before fixation. All cells analysed by immunofluorescence in this work were done with methanol for 5min at -20°C and washed 3 times with PBS. Methanol-fixed cells were stained with the appropriate dilution of primary antibody for 1h, followed by labelling with secondary antibodies coupled to Alexa Fluor dyes of various excitation/emission properties (Life Technologies) for 1h. DAPI (1µg/mL) or Hoechst 33258 (1µg/mL) were included with the secondary antibodies to label DNA. Three successive washes with PBS were performed after each antibody incubations. Stained coverslips were mounted onto droplets of Mowiol 4-88 (CalBiochem) mounting medium and allowed to set overnight.

Imaging was performed on glass slides using a 40x 0.75 NA air objective or a 60x 1.35 NA oil immersion objective, on an Olympus BX61 microscope system equipped with DAPI, EGFP/Alexa Fluor 488, Alexa Fluor 555, Alexa Fluor 568 and Alexa Fluor 647 filters. Images were captured either using a 1392x1040px Photometrics CoolSnap HQ2 CCD camera with a 14bit depth, or a 2048x2048px Photometrics Prime sCMOS with a 16bit depth. For presentation, single channel outputs were rescaled to levels most appropriate to represent the signal intensity range for each individual staining combination. These were kept constant within each experiment where quantitative comparisons were made, but rescaled in individual images appropriately for morphology markers such as tubulin and DNA staining. Quantitations of fixed cell images were done in Fiji (ImageJ) on the full bit depth raw data, projected using maximum intensity. Linear profiles of Aurora A pT288 staining in Figure 2.5 were measured using the standard inbuilt profile plotting algorithm within a straight 30px width line manually drawn through the two

spindle poles. The intensity values were extracted and reprocessed in GraphPad Prism for presentation. For Aurora A pT288 measurements in Figure 3.11C, circular 30px ROIs were centered around spindle poles determined as points of microtubule convergence and measured for intensity. Equal ROIs were measured outside of the cell and used to perform background subtraction.

6.16 Live-cell imaging

Cells were grown in 35mm dishes using a 14mm No. 0 thickness coverglass window (MatTek Corporation) and otherwise treated equivalently to those prepared for fixed-cell imaging. Live-cell imaging was carried out in a 37°C and 5% CO_2 environment chamber (Tokai Hit) on an Olympus IX81 inverted microscope with a 60x 1.42NA oil immersion objective with an Ultraview Vox spinning disk confocal system (Perkin Elmer). Images were captured with a 512x512px C9100-13 EM-CCD camera (Hamamatsu Corporation), at a 200x EM gain for fluorescence acquisition, a 100x EM gain for brightfield imaging and a 16bit depth. Exposure times ranged from 50 to 150ms for all markers using up to 6% laser power for 488nm and 561nm lasers. Volocity (Perkin Elmer) was used to capture, project and export live-cell images. Acquired data was assembled into movies rescaled to 8bit 1024x1024px images for presentation. GFP-Aurora A intensities in figure 3.15 were measured using automated object detection in Volocity with empirically determined intensity thresholds and a minimum object size restriction between 0.22 and 0.3μm^2. This was coupled to object tracking using an inbuilt algorithm, with track detection based on the shortest travel path and a maximum distance between timepoints set at 8μm. The tracking was used to filter the output object list to contain only objects that corresponded to centrosomes/mitotic spindle structures. The signal intensity values for all valid

objects within a cell at a certain timepoint were then summed and plotted for analysis.

6.17 Clonogenic survival assays

HeLa S3 cells were treated with siRNA 24h after seeding and allowed to deplete for 72h, before trypsinization and counting. The cell suspension was diluted to 100000cells/mL and, depending on experimental replicate, either 500 or 750 cells were seeded per 6cm dish, with six replicate dishes per condition. Colonies were allowed to form for 10-14 days, until clearly visible, washed with PBS, and simultaneously fixed and stained with 25% (v/v) methanol containing 5% (w/v) Crystal Violet for 30min at room temperature. The staining soulution was drained and the dishes rinsed by gentle immersion into lukewarm water, before air-drying at room temperature. Dishes were photographed and the colonies counted automatically by thresholded object detection in Volocity with empirically determined signal minima. These automated counts were verified by cross-comparison to manual colony counts for randomly selected dishes.

6.18 Western blot quantifications

Grayscale images of scanned films exposed within the dynamic range were imported into ImageJ, and intensity measured in 65px by 25px rectangular ROIs around bands. Equal ROIs adjacent to each band were used to perform background subtraction.

6.19 Protein sequence alignment

Global sequence alignments were performed on cannonical Uniprot sequences using ClustalΩ [261] with default settings apart from the output sequence order,

which was set to be retained as input, rather than as aligned by the algorithm. Output alignments were manually curated to filter out poorly annotated protein sequences and visualized using JalView [262]. The SAPS2 protein sequences used for the alignment in Figure 3.7B are as follows: O75170.2, XP_005566963.1, XP_024848648.1, XP_023486840.1, XP_011965353.1, NP_001193301.1, Q8R3Q2.1, XP_019302856.1, XP_004279711.1, XP_015134329.1, XP_015270999.1, XP_014455479.1, XP_012815511.1, NP_001085816.1, XP_004700670.

6.20 Figure management

Figures were processed and assembled using Volocity, Metamorph, ImageJ, Adobe Photoshop CS4 and Adobe Illustrator CS4. All graphs and statistical analyses were prepared with GraphPad Prism (GraphPad Software) and Microsoft Excel.

Appendix

Table A1 - Curated list of proteins enriched in SAPS IPs, supporting figure 2.9

	log10[Intensity]								Peptides								
Gene names	B55A	B55M	SAPS1A	SAPS1M	SAPS2A	SAPS2M	SAPS3A	SAPS3M	B55A	B55M	SAPS1A	SAPS1M	SAPS2A	SAPS2M	SAPS3A	SAPS3M	Enriched in
ABCD3	6	6	8.88939	7.35274	7.98188	7.7988	7.60858	6	0	0	10	1	3	2	2	0	SAPS1
ACTA1;ACTC1;ACTG2;ACTA2	6	6	6	6	6	7.58143	6	8.26071	8	9	5	12	7	8	6	12	SAPS3
ACTN4;ACTN1	6	6	6	6	6	6	6	8.39889	0	0	0	0	0	0	0	4	SAPS3
ALDOA	6	6	6	7.51247	6	6	6	8.75054	0	0	0	2	0	0	0	6	SAPS3
ANKRD28;ANKRD44	6	6	9.54125	9.13021	9.29161	9.55238	9.14067	9.03238	0	0	31	22	23	29	25	19	All SAPS
ANKRD52	6	6	8.9575	8.20556	8.99818	9.0886	8.75173	8.41375	0	0	15	5	14	20	10	6	All SAPS
ANXA1	6	6	6	7.25484	6	6	6	8.6995	0	0	0	1	0	0	0	9	SAPS3
ATAD3B;ATAD3A	6	6	6	6	8.14164	6	6	6	0	0	0	0	5	0	0	0	SAPS2
ATP5B	6	6	7.44573	7.31479	6	6	6	8.55466	0	0	1	1	0	0	0	6	SAPS3
ATP5C1	6	6	8.30777	6	7.97713	6	6	6	0	0	6	0	3	0	0	0	SAPS1
CALML3	6	6	6	6	6	6	6	8.52052	0	0	0	0	0	0	0	4	SAPS3
CALML5	6	6	6	8.49745	6	6	6	9.06126	0	0	0	4	0	0	0	10	SAPS1
CASP14	6	6	6	6	6	7.65967	6	8.42766	0	0	0	0	0	2	0	6	SAPS3
CLTC	6	6	6	6	6	6	6	8.16444	0	0	0	0	0	0	0	5	SAPS3
CTSD	6	6	6	6	6	6	6	8.2977	0	0	0	0	0	0	0	4	SAPS3
DSP	6	6	7.85539	7.83141	6	7.74708	6	8.91937	0	0	4	5	0	2	0	21	SAPS3
EIF5A	6	6	6	8.34412	6	6	7.33746	7.74735	0	1	0	4	0	0	2	2	SAPS1
FABP5	6	6	6	7.04618	6	6	6	8.58658	0	0	0	1	0	0	0	4	SAPS3
GAPDH	6	8.13213	7.92888	8.7916	8.25734	8.01607	8.02796	9.31825	0	3	2	9	4	3	3	11	SAPS3
HIST1H4A	7.71113	6	6	7.77248	8.41736	6	7.18887	8.87775	2	0	0	1	3	0	1	5	SAPS3
HSPD1	8.10857	6	7.80274	8.27075	6	7.69314	7.10527	8.00061	3	0	1	5	0	1	1	3	SAPS1/3
JUP	6	6	7.39067	7.36998	6	8.09223	6.87363	8.85112	0	0	1	2	0	4	1	11	SAPS3
LDHA	6	6	7.32091	8.3133	7.48075	7.42602	7.41747	8.46117	0	1	1	4	2	2	2	5	SAPS1/3
LGALS7	6	6	6	7.55242	6	7.41629	6	9.2448	0	0	0	2	0	1	0	7	SAPS3
MYH9	6	6	6	7.81717	6	6	6	8.67633	0	0	0	2	0	0	0	9	SAPS3

PGAM1;PGAM2;PGAM4	6	6	6	6	6	6	6	8.28809	0	0	0	0	0	0	0	4	SAPS3
PGK1	6	6	7.26288	7.87622	6	6	6	8.15881	0	0	1	2	0	0	0	5	SAPS3
PKM	6	7.82995	6	8.59935	8.10061	7.64732	7.57489	9.13988	0	2	0	11	3	1	1	17	SAPS3
PLK1	6	6	6	6	9.21719	8.84268	6	6	0	0	0	0	21	11	0	0	SAPS2
POLRMT	6	6	6	6	8.16923	7.58002	6	6	0	0	0	0	6	1	0	0	SAPS2
PPP6C	6	6	9.24391	8.79181	9.11049	9.16809	9.09177	9.05196	0	0	10	9	9	9	8	8	All SAPS
PPP6R1	6	6	10.9096	10.3125	7.43006	8.21569	7.46569	7.96982	0	0	46	33	2	4	3	2	SAPS1
PPP6R2	6	6	6	6	10.7161	10.329	7.22456	6	0	0	0	0	53	45	1	0	SAPS2
PPP6R3	6	6	6	6	6	6	10.092	9.83206	0	0	0	0	0	0	42	27	SAPS3
PRKDC	6	6	10.6429	9.88721	10.6819	10.2474	9.98201	9.17447	0	0	189	106	194	132	120	40	All SAPS
PSMA5	6	6	8.10013	7.26862	6	6	6	6	0	0	4	1	0	0	0	0	SAPS1
PSMA7;PSMA8	6	6	8.37814	6	6	6	6	6	0	0	4	0	0	0	0	0	SAPS1
PSMC5	6	6	8.24277	6	6	6	6	6	0	0	4	0	0	0	0	0	SAPS1
PSMD2	6	6	8.09889	6	7.27928	6	6	6	0	0	4	0	1	0	0	0	SAPS1
S100A7;S100A7A	6	6	6	8.62102	6	7.52503	6	9.14835	0	0	0	4	0	1	0	5	SAPS1/3
S100A8	6	6	6	8.82096	6	7.72648	6	9.57545	0	0	0	7	0	2	0	9	SAPS1/3
S100A9	6	6	6	9.35044	6	8.67846	6	10.0977	0	0	0	5	0	2	0	8	SAPS1/3
SERPINB3	6	6	6	7.56005	6	6	6	9.04478	0	0	0	2	0	0	0	11	SAPS3
SERPINB4	6	6	6	6	6	6	6	8.50857	0	0	0	2	0	0	0	8	SAPS3
SFN	6	6	6	7.13117	6	6	6	8.35845	0	1	0	2	0	1	1	6	SAPS3
SLC25A10	6.91026	6	8.91129	7.87026	8.44028	7.77921	7.60483	7.10199	1	0	8	3	4	1	1	1	SAPS1
SLC25A13	6	6	8.83099	7.58865	8.09656	6	6	6	0	0	10	2	3	0	0	0	SAPS1/2
TECR	6	6	8.32932	6	7.33516	6	6	6	0	0	5	0	1	0	0	0	SAPS1
TGM1	6	6	6	6	6	6	6	8.41368	0	0	0	0	0	0	0	6	SAPS3
TPI1	6	6	6	6	6	6	6	8.3591	0	0	0	0	0	0	0	4	SAPS3
VCP	6	6	6	6	6	6	6	8.36631	0	0	0	0	0	0	0	5	SAPS3

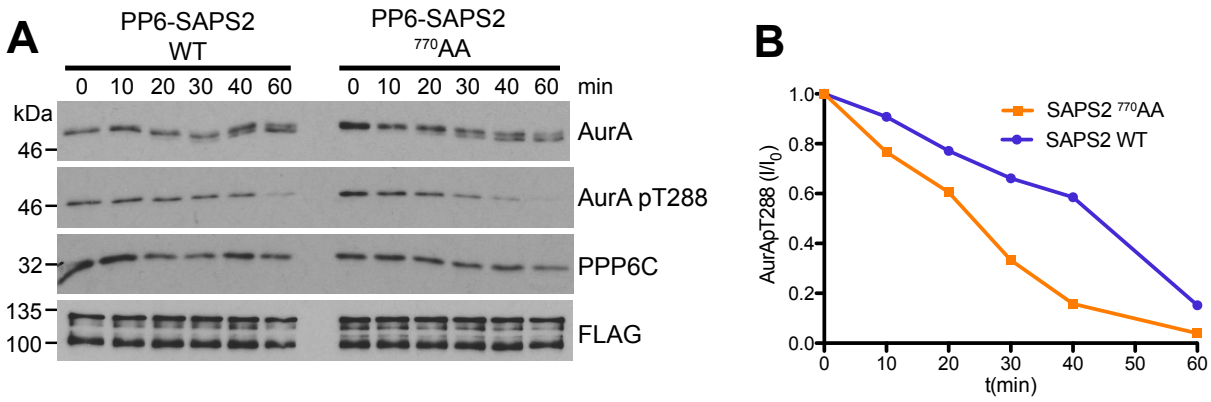


Figure A1 - PLK1-deficient PP6-SAPS2 is more active than WT. (A) PP6-SAPS2 WT or 770AA complexes were assayed against AurA-TPX2 complexes as in Figure 3.10 and analyzed by western blotting. **(B)** Densitometric quantification of AurA pT288 from the western blot in (A).

Table A2 - SAPS2 phosphopeptides detected by mass spectrometry supporting figure 2.9.

Gene names	Number of Phospho (STY)	Phospho (STY) Probabilities	Ratio phospho/base B55_A	Ratio phospho/base B55_M	Ratio phospho/base SAPS2_A	Ratio phospho/base SAPS2_M	Position
PPP6R2	1	AS(0.001)QAS(0.02)YFAVS(0.014)PAS(0.964)PCAWNVCVTR	NaN	NaN	0.022704	0.37169	803
PPP6R2	1	RVGTEGLVDS(1)FSQGLER	NaN	NaN	0.021736	0.30901	289
PPP6R2	1	LLS(1)PACPAPK	NaN	NaN	0.01229	0.26822	877
PPP6R2	1	GRWES(1)FVEETLTETNRR	NaN	NaN	0.094378	0.15434	517
PPP6R2	1	FDLNT(0.009)T(0.839)S(0.152)HVDK	NaN	NaN	0.0098331	0.10572	10
PPP6R2	1	EAPPVEGDSEGAMWT(0.001)AVFDEPANS(0.244)T(0.676)PT(0.078)APGVVR	NaN	NaN	0.0015634	0.075669	724
PPP6R2	1	S(0.988)LET(0.012)PQPAASLPDNTMVTHLFQK	NaN	NaN	0.018336	0.032572	427
PPP6R2	1	S(0.22)LET(0.78)PQPAASLPDNTMVTHLFQK	NaN	NaN	0	0.030518	430

Bibliography

1. Cavalier-Smith, T., *Cell evolution and Earth history: stasis and revolution.* Philosophical Transactions of the Royal Society B-Biological Sciences, 2006. **361**(1470): p. 969-1006.

2. Novak, B. and J.J. Tyson, *Numerical analysis of a comprehensive model of M-phase control in Xenopus oocyte extracts and intact embryos.* J Cell Sci, 1993. **106 (Pt 4)**: p. 1153-68.

3. Nigg, E.A., *Cyclin-dependent protein kinases: key regulators of the eukaryotic cell cycle.* Bioessays, 1995. **17**(6): p. 471-80.

4. Morgan, D.O., *Principles of CDK regulation.* Nature, 1995. **374**(6518): p. 131-4.

5. Loog, M. and D.O. Morgan, *Cyclin specificity in the phosphorylation of cyclin-dependent kinase substrates.* Nature, 2005. **434**(7029): p. 104-8.

6. Swaffer, M.P., et al., *CDK Substrate Phosphorylation and Ordering the Cell Cycle.* Cell, 2016. **167**(7): p. 1750-1761 e16.

7. Murray, A.W., M.J. Solomon, and M.W. Kirschner, *The role of cyclin synthesis and degradation in the control of maturation promoting factor activity.* Nature, 1989. **339**(6222): p. 280-6.

8. Glover, D.M., et al., *Mutations in aurora prevent centrosome separation leading to the formation of monopolar spindles.* Cell, 1995. **81**(1): p. 95-105.

9. Golsteyn, R.M., et al., *Cell cycle analysis and chromosomal localization of human Plk1, a putative homologue of the mitotic kinases Drosophila polo and Saccharomyces cerevisiae Cdc5.* J Cell Sci, 1994. **107 (Pt 6)**: p. 1509-17.

10. Golsteyn, R.M., et al., *Cell cycle regulation of the activity and subcellular localization of Plk1, a human protein kinase implicated in mitotic spindle function.* J Cell Biol, 1995. **129**(6): p. 1617-28.

11. Domingo-Sananes, M.R., et al., *Switches and latches: a biochemical tug-of-war between the kinases and phosphatases that control mitosis.* Philos Trans R Soc Lond B Biol Sci, 2011. **366**(1584): p. 3584-94.

12. Barr, F.A., P.R. Elliott, and U. Gruneberg, *Protein phosphatases and the regulation of mitosis.* J Cell Sci, 2011. **124**(Pt 14): p. 2323-34.

13. Hunt, T., *On the regulation of protein phosphatase 2A and its role in controlling entry into and exit from mitosis.* Adv Biol Regul, 2013. **53**(2): p. 173-8.

14. Wera, S. and B.A. Hemmings, *Serine/threonine protein phosphatases.* Biochem J, 1995. **311 (Pt 1)**: p. 17-29.

15. Barr, A.R., et al., *A Dynamical Framework for the All-or-None G1/S Transition.* Cell Syst, 2016. **2**(1): p. 27-37.

16. Ohtani, K., J. DeGregori, and J.R. Nevins, *Regulation of the cyclin E gene by transcription factor E2F1.* Proc Natl Acad Sci U S A, 1995. **92**(26): p. 12146-50.

17. Geng, Y., et al., *Regulation of cyclin E transcription by E2Fs and retinoblastoma protein.* Oncogene, 1996. **12**(6): p. 1173-80.

18. Toyoshima, H. and T. Hunter, *p27, a novel inhibitor of G1 cyclin-Cdk protein kinase activity, is related to p21.* Cell, 1994. **78**(1): p. 67-74.

19. Ladha, M.H., et al., *Regulation of exit from quiescence by p27 and cyclin D1-CDK4.* Mol Cell Biol, 1998. **18**(11): p. 6605-15.

20. Roussel, M.F., *The INK4 family of cell cycle inhibitors in cancer.* Oncogene, 1999. **18**(38): p. 5311-7.

21. Aktas, H., H. Cai, and G.M. Cooper, *Ras links growth factor signaling to the cell cycle machinery via regulation of cyclin D1 and the Cdk inhibitor p27KIP1.* Mol Cell Biol, 1997. **17**(7): p. 3850-7.

22. Tsutsui, T., et al., *Targeted disruption of CDK4 delays cell cycle entry with enhanced p27(Kip1) activity.* Mol Cell Biol, 1999. **19**(10): p. 7011-9.

23. Sheaff, R.J., et al., *Cyclin E-CDK2 is a regulator of p27Kip1.* Genes Dev, 1997. **11**(11): p. 1464-78.

24. Lukas, C., et al., *Accumulation of cyclin B1 requires E2F and cyclin-A-dependent rearrangement of the anaphase-promoting complex.* Nature, 1999. **401**(6755): p. 815-8.

25. Keck, J.M., et al., *Cyclin E overexpression impairs progression through mitosis by inhibiting APC(Cdh1).* J Cell Biol, 2007. **178**(3): p. 371-85.

26. Lakin, N.D. and S.P. Jackson, *Regulation of p53 in response to DNA damage.* Oncogene, 1999. **18**(53): p. 7644-55.

27. Kubbutat, M.H., S.N. Jones, and K.H. Vousden, *Regulation of p53 stability by Mdm2.* Nature, 1997. **387**(6630): p. 299-303.

28. Shieh, S.Y., et al., *DNA damage-induced phosphorylation of p53 alleviates inhibition by MDM2.* Cell, 1997. **91**(3): p. 325-34.

29. Eckner, R., *p53-dependent growth arrest and induction of p21: a critical role for PCAF-mediated histone acetylation.* Cell Cycle, 2012. **11**(14): p. 2591-2.

30. Xiong, Y., et al., *p21 is a universal inhibitor of cyclin kinases.* Nature, 1993. **366**(6456): p. 701-4.

31. Barr, A.R., et al., *DNA damage during S-phase mediates the proliferation-quiescence decision in the subsequent G1 via p21 expression.* Nat Commun, 2017. **8**: p. 14728.

32. Giacinti, C. and A. Giordano, *RB and cell cycle progression.* Oncogene, 2006. **25**(38): p. 5220-7.

33. Goodwin, E.C. and D. DiMaio, *Repression of human papillomavirus oncogenes in HeLa cervical carcinoma cells causes the orderly reactivation of dormant tumor suppressor pathways.* Proc Natl Acad Sci U S A, 2000. **97**(23): p. 12513-8.

34. Coverley, D., H. Laman, and R.A. Laskey, *Distinct roles for cyclins E and A during DNA replication complex assembly and activation.* Nat Cell Biol, 2002. **4**(7): p. 523-8.

35. Clurman, B.E., et al., *Turnover of cyclin E by the ubiquitin-proteasome pathway is regulated by cdk2 binding and cyclin phosphorylation.* Genes Dev, 1996. **10**(16): p. 1979-90.

36. Singer, J.D., et al., *Cullin-3 targets cyclin E for ubiquitination and controls S phase in mammalian cells.* Genes Dev, 1999. **13**(18): p. 2375-87.

37. Leman, A.R. and E. Noguchi, *The replication fork: understanding the eukaryotic replication machinery and the challenges to genome duplication.* Genes (Basel), 2013. **4**(1): p. 1-32.

38. Prelich, G., et al., *Functional identity of proliferating cell nuclear antigen and a DNA polymerase-delta auxiliary protein.* Nature, 1987. **326**(6112): p. 517-20.

39. Calzada, A., et al., *Molecular anatomy and regulation of a stable replisome at a paused eukaryotic DNA replication fork.* Genes Dev, 2005. **19**(16): p. 1905-19.

40. Labib, K. and B. Hodgson, *Replication fork barriers: pausing for a break or stalling for time?* EMBO Rep, 2007. **8**(4): p. 346-53.

41. Zeman, M.K. and K.A. Cimprich, *Causes and consequences of replication stress.* Nat Cell Biol, 2014. **16**(1): p. 2-9.

42. Ensminger, M., et al., *DNA breaks and chromosomal aberrations arise when replication meets base excision repair.* J Cell Biol, 2014. **206**(1): p. 29-43.

43. Xeros, N., *Deoxyriboside control and synchronization of mitosis.* Nature, 1962. **194**: p. 682-3.

44. Joukov, V., J.C. Walter, and A. De Nicolo, *The Cep192-organized aurora A-Plk1 cascade is essential for centrosome cycle and bipolar spindle assembly.* Mol Cell, 2014. **55**(4): p. 578-91.

45. Conduit, P.T., A. Wainman, and J.W. Raff, *Centrosome function and assembly in animal cells.* Nat Rev Mol Cell Biol, 2015. **16**(10): p. 611-24.

46. Whitfield, M.L., et al., *Identification of genes periodically expressed in the human cell cycle and their expression in tumors.* Mol Biol Cell, 2002. **13**(6): p. 1977-2000.

47. Yang, J., et al., *Control of cyclin B1 localization through regulated binding of the nuclear export factor CRM1.* Genes Dev, 1998. **12**(14): p. 2131-43.

48. McGowan, C.H. and P. Russell, *Human Wee1 kinase inhibits cell division by phosphorylating p34cdc2 exclusively on Tyr15.* EMBO J, 1993. **12**(1): p. 75-85.

49. Booher, R.N., P.S. Holman, and A. Fattaey, *Human Myt1 is a cell cycle-regulated kinase that inhibits Cdc2 but not Cdk2 activity.* J Biol Chem, 1997. **272**(35): p. 22300-6.

50. Marcote, M.J., et al., *A three-dimensional model of the Cdc2 protein kinase: localization of cyclin- and Suc1-binding regions and phosphorylation sites.* Mol Cell Biol, 1993. **13**(8): p. 5122-31.

51. Aarts, M., et al., *Forced mitotic entry of S-phase cells as a therapeutic strategy induced by inhibition of WEE1.* Cancer Discov, 2012. **2**(6): p. 524-39.

52. Kim, S.Y. and J.E. Ferrell, Jr., *Substrate competition as a source of ultrasensitivity in the inactivation of Wee1.* Cell, 2007. **128**(6): p. 1133-45.

53. Trunnell, N.B., et al., *Ultrasensitivity in the Regulation of Cdc25C by Cdk1.* Mol Cell, 2011. **41**(3): p. 263-74.

54. Russell, P. and P. Nurse, *cdc25+ functions as an inducer in the mitotic control of fission yeast.* Cell, 1986. **45**(1): p. 145-53.

55. Larochelle, S., et al., *Requirements for Cdk7 in the assembly of Cdk1/cyclin B and activation of Cdk2 revealed by chemical genetics in human cells.* Mol Cell, 2007. **25**(6): p. 839-50.

56. Kumagai, A. and W.G. Dunphy, *Purification and molecular cloning of Plx1, a Cdc25-regulatory kinase from Xenopus egg extracts.* Science, 1996. **273**(5280): p. 1377-80.

57. Roshak, A.K., et al., *The human polo-like kinase, PLK, regulates cdc2/cyclin B through phosphorylation and activation of the cdc25C phosphatase.* Cell Signal, 2000. **12**(6): p. 405-11.

58. Lindqvist, A., V. Rodriguez-Bravo, and R.H. Medema, *The decision to enter mitosis: feedback and redundancy in the mitotic entry network.* J Cell Biol, 2009. **185**(2): p. 193-202.

59. Gavet, O. and J. Pines, *Activation of cyclin B1-Cdk1 synchronizes events in the nucleus and the cytoplasm at mitosis.* J Cell Biol, 2010. **189**(2): p. 247-59.

60. Picard, A., et al., *Involvement of protein phosphatases 1 and 2A in the control of M phase-promoting factor activity in starfish.* J Cell Biol, 1989. **109**(6 Pt 2): p. 3347-54.

61. Yu, J., et al., *Greatwall kinase participates in the Cdc2 autoregulatory loop in Xenopus egg extracts.* Mol Cell, 2006. **22**(1): p. 83-91.

62. Gharbi-Ayachi, A., et al., *The substrate of Greatwall kinase, Arpp19, controls mitosis by inhibiting protein phosphatase 2A.* Science, 2010. **330**(6011): p. 1673-7.

63. Mochida, S., et al., *Greatwall phosphorylates an inhibitor of protein phosphatase 2A that is essential for mitosis.* Science, 2010. **330**(6011): p. 1670-3.

64. Lorca, T., et al., *An okadaic acid-sensitive phosphatase negatively controls the cyclin degradation pathway in amphibian eggs.* Mol Cell Biol, 1991. **11**(2): p. 1171-5.

65. Mochida, S., et al., *Regulated activity of PP2A-B55 delta is crucial for controlling entry into and exit from mitosis in Xenopus egg extracts.* EMBO J, 2009. **28**(18): p. 2777-85.

66. Grallert, A., et al., *A PP1-PP2A phosphatase relay controls mitotic progression.* Nature, 2015. **517**(7532): p. 94-8.

67. Rogers, S., et al., *PP1 initiates the dephosphorylation of MASTL, triggering mitotic exit and bistability in human cells.* J Cell Sci, 2016. **129**(7): p. 1340-54.

68. Jackson, S.P., *Sensing and repairing DNA double-strand breaks.* Carcinogenesis, 2002. **23**(5): p. 687-96.

69. Furnari, B., N. Rhind, and P. Russell, *Cdc25 mitotic inducer targeted by chk1 DNA damage checkpoint kinase.* Science, 1997. **277**(5331): p. 1495-7.

70. Donzelli, M. and G.F. Draetta, *Regulating mammalian checkpoints through Cdc25 inactivation.* EMBO Rep, 2003. **4**(7): p. 671-7.

71. van Vugt, M.A., A. Bras, and R.H. Medema, *Polo-like kinase-1 controls recovery from a G2 DNA damage-induced arrest in mammalian cells.* Mol Cell, 2004. **15**(5): p. 799-811.

72. Bruinsma, W., et al., *Inhibition of Polo-like kinase 1 during the DNA damage response is mediated through loss of Aurora A recruitment by Bora.* Oncogene, 2017. **36**(13): p. 1840-1848.

73. Bunz, F., et al., *Requirement for p53 and p21 to sustain G2 arrest after DNA damage.* Science, 1998. **282**(5393): p. 1497-501.

74. Krenning, L., et al., *Transient activation of p53 in G2 phase is sufficient to induce senescence.* Mol Cell, 2014. **55**(1): p. 59-72.

75. Feringa, F.M., et al., *Hypersensitivity to DNA damage in antephase as a safeguard for genome stability.* Nat Commun, 2016. **7**: p. 12618.

76. Macurek, L., et al., *Polo-like kinase-1 is activated by aurora A to promote checkpoint recovery.* Nature, 2008. **455**(7209): p. 119-23.

77. Antonin, W. and H. Neumann, *Chromosome condensation and decondensation during mitosis.* Curr Opin Cell Biol, 2016. **40**: p. 15-22.

78. Carmena, M., et al., *The chromosomal passenger complex (CPC): from easy rider to the godfather of mitosis.* Nat Rev Mol Cell Biol, 2012. **13**(12): p. 789-803.

79. Lipp, J.J., et al., *Aurora B controls the association of condensin I but not condensin II with mitotic chromosomes.* J Cell Sci, 2007. **120**(Pt 7): p. 1245-55.

80. Tada, K., et al., *Condensin association with histone H2A shapes mitotic chromosomes.* Nature, 2011. **474**(7352): p. 477-U105.

81. Wei, Y., et al., *Phosphorylation of histone H3 at serine 10 is correlated with chromosome condensation during mitosis and meiosis in Tetrahymena.* Proceedings of the National Academy of Sciences of the United States of America, 1998. **95**(13): p. 7480-7484.

82. Shintomi, K., et al., *Mitotic chromosome assembly despite nucleosome depletion in Xenopus egg extracts.* Science, 2017. **356**(6344): p. 1284-1287.

83. St-Pierre, J., et al., *Polo Kinase Regulates Mitotic Chromosome Condensation by Hyperactivation of Condensin DNA Supercoiling Activity.* Molecular Cell, 2009. **34**(4): p. 416-426.

84. Kutay, U. and M.W. Hetzer, *Reorganization of the nuclear envelope during open mitosis.* Curr Opin Cell Biol, 2008. **20**(6): p. 669-77.

85. Beaudouin, J., et al., *Nuclear envelope breakdown proceeds by microtubule-induced tearing of the lamina.* Cell, 2002. **108**(1): p. 83-96.

86. Peter, M., et al., *In vitro disassembly of the nuclear lamina and M phase-specific phosphorylation of lamins by cdc2 kinase.* Cell, 1990. **61**(4): p. 591-602.

87. Lenart, P., et al., *Nuclear envelope breakdown in starfish oocytes proceeds by partial NPC disassembly followed by a rapidly spreading fenestration of nuclear membranes.* J Cell Biol, 2003. **160**(7): p. 1055-68.

88. Gorlich, D. and U. Kutay, *Transport between the cell nucleus and the cytoplasm.* Annu Rev Cell Dev Biol, 1999. **15**: p. 607-60.

89. Wiese, C., et al., *Role of importin-beta in coupling Ran to downstream targets in microtubule assembly.* Science, 2001. **291**(5504): p. 653-6.

90. Gruss, O.J., et al., *Ran induces spindle assembly by reversing the inhibitory effect of importin alpha on TPX2 activity.* Cell, 2001. **104**(1): p. 83-93.

91. Laurell, E., et al., *Phosphorylation of Nup98 by multiple kinases is crucial for NPC disassembly during mitotic entry.* Cell, 2011. **144**(4): p. 539-50.

92. Smith, E., et al., *Differential control of Eg5-dependent centrosome separation by Plk1 and Cdk1.* EMBO J, 2011. **30**(11): p. 2233-45.

93. Gong, D., et al., *Cyclin A2 regulates nuclear-envelope breakdown and the nuclear accumulation of cyclin B1.* Curr Biol, 2007. **17**(1): p. 85-91.

94. Pines, J. and T. Hunter, *Human cyclin A is adenovirus E1A-associated protein p60 and behaves differently from cyclin B.* Nature, 1990. **346**(6286): p. 760-3.

95. D'Angiolella, V., et al., *The spindle checkpoint requires cyclin-dependent kinase activity.* Genes Dev, 2003. **17**(20): p. 2520-5.

96. Lowe, M., et al., *Cdc2 kinase directly phosphorylates the cis-Golgi matrix protein GM130 and is required for Golgi fragmentation in mitosis.* Cell, 1998. **94**(6): p. 783-93.

97. Lee, K. and K. Rhee, *PLK1 phosphorylation of pericentrin initiates centrosome maturation at the onset of mitosis.* J Cell Biol, 2011. **195**(7): p. 1093-101.

98. Casenghi, M., F.A. Barr, and E.A. Nigg, *Phosphorylation of Nlp by Plk1 negatively regulates its dynein-dynactin-dependent targeting to the centrosome.* J Cell Sci, 2005. **118**(Pt 21): p. 5101-8.

99. Gomez-Ferreria, M.A., et al., *Novel NEDD1 phosphorylation sites regulate gamma-tubulin binding and mitotic spindle assembly.* J Cell Sci, 2012. **125**(Pt 16): p. 3745-51.

100. Kollman, J.M., et al., *Microtubule nucleation by gamma-tubulin complexes.* Nat Rev Mol Cell Biol, 2011. **12**(11): p. 709-21.

101. Terada, Y., Y. Uetake, and R. Kuriyama, *Interaction of Aurora-A and centrosomin at the microtubule-nucleating site in Drosophila and mammalian cells.* Journal of Cell Biology, 2003. **162**(5): p. 757-763.

102. Conduit, P.T., et al., *A molecular mechanism of mitotic centrosome assembly in Drosophila.* Elife, 2014. **3**: p. e03399.

103. Fry, A.M., P. Meraldi, and E.A. Nigg, *A centrosomal function for the human Nek2 protein kinase, a member of the NIMA family of cell cycle regulators.* Embo Journal, 1998. **17**(2): p. 470-481.

104. Khodjakov, A., et al., *Centrosome-independent mitotic spindle formation in vertebrates.* Curr Biol, 2000. **10**(2): p. 59-67.

105. Tsai, M.Y. and Y. Zheng, *Aurora A kinase-coated beads function as microtubule-organizing centers and enhance RanGTP-induced spindle assembly.* Curr Biol, 2005. **15**(23): p. 2156-63.

106. Barr, A.R. and F. Gergely, *Aurora-A: the maker and breaker of spindle poles.* J Cell Sci, 2007. **120**(Pt 17): p. 2987-96.

107. Bury, L., et al., *Plk4 and Aurora A cooperate in the initiation of acentriolar spindle assembly in mammalian oocytes.* J Cell Biol, 2017. **216**(11): p. 3571-3590.

108. Prosser, S.L. and L. Pelletier, *Mitotic spindle assembly in animal cells: a fine balancing act.* Nat Rev Mol Cell Biol, 2017. **18**(3): p. 187-201.

109. Gruss, O.J., et al., *Chromosome-induced microtubule assembly mediated by TPX2 is required for spindle formation in HeLa cells.* Nat Cell Biol, 2002. **4**(11): p. 871-9.

110. Neumayer, G., et al., *TPX2: of spindle assembly, DNA damage response, and cancer.* Cell Mol Life Sci, 2014. **71**(16): p. 3027-47.

111. Kotak, S., C. Busso, and P. Gonczy, *NuMA phosphorylation by CDK1 couples mitotic progression with cortical dynein function.* Embo Journal, 2013. **32**(18): p. 2517-2529.

112. Shim, S.Y., et al., *Phosphorylation of Targeting Protein for Xenopus Kinesin-like Protein 2 (TPX2) at Threonine 72 in Spindle Assembly.* Journal of Biological Chemistry, 2015. **290**(14): p. 9122-9134.

113. Cundell, M.J., et al., *A PP2A-B55 recognition signal controls substrate dephosphorylation kinetics during mitotic exit.* J Cell Biol, 2016. **214**(5): p. 539-54.

114. Burgess, S.G., et al., *Aurora-A-Dependent Control of TACC3 Influences the Rate of Mitotic Spindle Assembly.* Plos Genetics, 2015. **11**(7).

115. Gallini, S., et al., *NuMA Phosphorylation by Aurora-A Orchestrates Spindle Orientation.* Curr Biol, 2016. **26**(4): p. 458-69.

116. LeRoy, P.J., et al., *Localization of human TACC3 to mitotic spindles is mediated by phosphorylation on Ser558 by Aurora A: a novel pharmacodynamic method for measuring Aurora A activity.* Cancer Res, 2007. **67**(11): p. 5362-70.

117. De Luca, M., P. Lavia, and G. Guarguaglini, *A functional interplay between Aurora-A, Plk1 and TPX2 at spindle poles - Plk1 controls centrosomal localization of Aurora-A and TPX2 spindle association.* Cell Cycle, 2006. **5**(3): p. 296-303.

118. Eckerdt, F., et al., *Phosphorylation of TPX2 by Plx1 enhances activation of Aurora A.* Cell Cycle, 2009. **8**(15): p. 2413-2419.

119. Steegmaier, M., et al., *BI 2536, a potent and selective inhibitor of polo-like kinase 1, inhibits tumor growth in vivo.* Curr Biol, 2007. **17**(4): p. 316-22.

120. Lenart, P., et al., *The small-molecule inhibitor BI 2536 reveals novel insights into mitotic roles of polo-like kinase 1.* Current Biology, 2007. **17**(4): p. 304-315.

121. Koffa, M.D., et al., *HURP is part of a Ran-dependent complex involved in spindle formation.* Curr Biol, 2006. **16**(8): p. 743-54.

122. Petry, S., et al., *Branching microtubule nucleation in Xenopus egg extracts mediated by augmin and TPX2.* Cell, 2013. **152**(4): p. 768-77.

123. Zhang, X., S.C. Ems-McClung, and C.E. Walczak, *Aurora A phosphorylates MCAK to control ran-dependent spindle bipolarity.* Mol Biol Cell, 2008. **19**(7): p. 2752-65.

124. Braun, A., et al., *Rac1 and Aurora A regulate MCAK to polarize microtubule growth in migrating endothelial cells.* J Cell Biol, 2014. **206**(1): p. 97-112.

125. Voter, W.A. and H.P. Erickson, *The kinetics of microtubule assembly. Evidence for a two-stage nucleation mechanism.* J Biol Chem, 1984. **259**(16): p. 10430-8.

126. Widlund, P.O., et al., *XMAP215 polymerase activity is built by combining multiple tubulin-binding TOG domains and a basic lattice-binding region.* Proc Natl Acad Sci U S A, 2011. **108**(7): p. 2741-6.

127. Gergely, F., V.M. Draviam, and J.W. Raff, *The ch-TOG/XMAP215 protein is essential for spindle pole organization in human somatic cells.* Genes & Development, 2003. **17**(3): p. 336-341.

128. Helenius, J., et al., *The depolymerizing kinesin MCAK uses lattice diffusion to rapidly target microtubule ends.* Nature, 2006. **441**(7089): p. 115-9.

129. Tanenbaum, M.E., et al., *A complex of Kif18b and MCAK promotes microtubule depolymerization and is negatively regulated by Aurora kinases.* Curr Biol, 2011. **21**(16): p. 1356-65.

130. Ems-McClung, S.C., et al., *Aurora B inhibits MCAK activity through a phosphoconformational switch that reduces microtubule association.* Curr Biol, 2013. **23**(24): p. 2491-9.

131. Akiyoshi, B., et al., *Tension directly stabilizes reconstituted kinetochore-microtubule attachments.* Nature, 2010. **468**(7323): p. 576-9.

132. Booth, D.G., et al., *A TACC3/ch-TOG/clathrin complex stabilises kinetochore fibres by inter-microtubule bridging.* Embo Journal, 2011. **30**(5): p. 906-919.

133. Burgess, S.G., et al., *Mitotic spindle association of TACC3 requires Aurora-A-dependent stabilization of a cryptic alpha-helix.* Embo Journal, 2018. **37**(8).

134. Tame, M.A., et al., *Astral microtubules control redistribution of dynein at the cell cortex to facilitate spindle positioning.* Cell Cycle, 2014. **13**(7): p. 1162-70.

135. Dunsch, A.K., et al., *Dynein light chain 1 and a spindle-associated adaptor promote dynein asymmetry and spindle orientation.* J Cell Biol, 2012. **198**(6): p. 1039-54.

136. Barr, F.A. and U. Gruneberg, *Cytokinesis: placing and making the final cut.* Cell, 2007. **131**(5): p. 847-60.

137. Cundell, M.J., et al., *The BEG (PP2A-B55/ENSA/Greatwall) pathway ensures cytokinesis follows chromosome separation.* Mol Cell, 2013. **52**(3): p. 393-405.

138. Musacchio, A. and E.D. Salmon, *The spindle-assembly checkpoint in space and time.* Nat Rev Mol Cell Biol, 2007. **8**(5): p. 379-93.

139. Musacchio, A., *The Molecular Biology of Spindle Assembly Checkpoint Signaling Dynamics.* Curr Biol, 2015. **25**(20): p. R1002-18.

140. Sudakin, V., G.K. Chan, and T.J. Yen, *Checkpoint inhibition of the APC/C in HeLa cells is mediated by a complex of BUBR1, BUB3, CDC20, and MAD2.* J Cell Biol, 2001. **154**(5): p. 925-36.

141. Peters, J.M., *The anaphase promoting complex/cyclosome: a machine designed to destroy.* Nat Rev Mol Cell Biol, 2006. **7**(9): p. 644-56.

142. Chang, D.C., N. Xu, and K.Q. Luo, *Degradation of cyclin B is required for the onset of anaphase in Mammalian cells.* J Biol Chem, 2003. **278**(39): p. 37865-73.

143. Uhlmann, F., et al., *Cleavage of cohesin by the CD clan protease separin triggers anaphase in yeast.* Cell, 2000. **103**(3): p. 375-86.

144. Stemmann, O., et al., *Dual inhibition of sister chromatid separation at metaphase.* Cell, 2001. **107**(6): p. 715-26.

145. Izawa, D. and J. Pines, *The mitotic checkpoint complex binds a second CDC20 to inhibit active APC/C.* Nature, 2015. **517**(7536): p. 631-4.

146. Jia, L., B. Li, and H. Yu, *The Bub1-Plk1 kinase complex promotes spindle checkpoint signalling through Cdc20 phosphorylation.* Nat Commun, 2016. **7**: p. 10818.

147. Elowe, S., et al., *Tension-sensitive Plk1 phosphorylation on BubR1 regulates the stability of kinetochore microtubule interactions.* Genes Dev, 2007. **21**(17): p. 2205-19.

148. Golan, A., Y. Yudkovsky, and A. Hershko, *The cyclin-ubiquitin ligase activity of cyclosome/APC is jointly activated by protein kinases Cdk1-cyclin B and Plk.* J Biol Chem, 2002. **277**(18): p. 15552-7.

149. Zhang, S., et al., *Molecular mechanism of APC/C activation by mitotic phosphorylation.* Nature, 2016. **533**(7602): p. 260-264.

150. Lampson, M.A. and E.L. Grishchuk, *Mechanisms to Avoid and Correct Erroneous Kinetochore-Microtubule Attachments.* Biology (Basel), 2017. **6**(1).

151. Hauf, S., et al., *The small molecule Hesperadin reveals a role for Aurora B in correcting kinetochore-microtubule attachment and in maintaining the spindle assembly checkpoint.* J Cell Biol, 2003. **161**(2): p. 281-94.

152. Liu, D., et al., *Sensing chromosome bi-orientation by spatial separation of aurora B kinase from kinetochore substrates.* Science, 2009. **323**(5919): p. 1350-3.

153. Foley, E.A., M. Maldonado, and T.M. Kapoor, *Formation of stable attachments between kinetochores and microtubules depends on the B56-PP2A phosphatase.* Nat Cell Biol, 2011. **13**(10): p. 1265-71.

154. Espert, A., et al., *PP2A-B56 opposes Mps1 phosphorylation of Knl1 and thereby promotes spindle assembly checkpoint silencing.* J Cell Biol, 2014. **206**(7): p. 833-42.

155. Nijenhuis, W., et al., *Negative feedback at kinetochores underlies a responsive spindle checkpoint signal.* Nat Cell Biol, 2014. **16**(12): p. 1257-64.

156. Suijkerbuijk, S.J.E., et al., *Integration of Kinase and Phosphatase Activities by BUBR1 Ensures Formation of Stable Kinetochore-Microtubule Attachments.* Developmental Cell, 2012. **23**(4): p. 745-755.

157. Ganem, N.J. and D. Pellman, *Linking abnormal mitosis to the acquisition of DNA damage.* J Cell Biol, 2012. **199**(6): p. 871-81.

158. Eytan, E., et al., *Disassembly of mitotic checkpoint complexes by the joint action of the AAA-ATPase TRIP13 and p31(comet).* Proc Natl Acad Sci U S A, 2014. **111**(33): p. 12019-24.

159. Kuijt, T.E., et al., *Conditional targeting of MAD1 to kinetochores is sufficient to reactivate the spindle assembly checkpoint in metaphase.* Chromosoma, 2014. **123**(5): p. 471-80.

160. Rattani, A., et al., *Dependency of the spindle assembly checkpoint on Cdk1 renders the anaphase transition irreversible.* Curr Biol, 2014. **24**(6): p. 630-7.

161. Maney, T., et al., *Mitotic centromere-associated kinesin is important for anaphase chromosome segregation.* Journal of Cell Biology, 1998. **142**(3): p. 787-801.

162. Neef, R., et al., *Choice of Plk1 docking partners during mitosis and cytokinesis is controlled by the activation state of Cdk1.* Nat Cell Biol, 2007. **9**(4): p. 436-44.

163. Neef, R., et al., *Cooperation between mitotic kinesins controls the late stages of cytokinesis.* Curr Biol, 2006. **16**(3): p. 301-7.

164. Petronczki, M., et al., *Polo-like kinase 1 triggers the initiation of cytokinesis in human cells by promoting recruitment of the RhoGEF Ect2 to the central spindle.* Dev Cell, 2007. **12**(5): p. 713-25.

165. Nunes Bastos, R., et al., *Aurora B suppresses microtubule dynamics and limits central spindle size by locally activating KIF4A.* J Cell Biol, 2013. **202**(4): p. 605-21.

166. Gruneberg, U., et al., *Relocation of Aurora B from centromeres to the central spindle at the metaphase to anaphase transition requires MKlp2.* J Cell Biol, 2004. **166**(2): p. 167-72.

167. Bastos, R.N., M.J. Cundell, and F.A. Barr, *KIF4A and PP2A-B56 form a spatially restricted feedback loop opposing Aurora B at the anaphase central spindle.* J Cell Biol, 2014. **207**(6): p. 683-93.

168. Orr, B., K.M. Godek, and D. Compton, *Aneuploidy.* Curr Biol, 2015. **25**(13): p. R538-42.

169. Spence, J.M., et al., *Depletion of topoisomerase IIalpha leads to shortening of the metaphase interkinetochore distance and abnormal persistence of PICH-coated anaphase threads.* J Cell Sci, 2007. **120**(Pt 22): p. 3952-64.

170. Ke, Y., et al., *PICH and BLM limit histone association with anaphase centromeric DNA threads and promote their resolution.* EMBO J, 2011. **30**(16): p. 3309-21.

171. Janssen, A., et al., *Chromosome segregation errors as a cause of DNA damage and structural chromosome aberrations.* Science, 2011. **333**(6051): p. 1895-8.

172. Zeng, K., et al., *Protein phosphatase 6 regulates mitotic spindle formation by controlling the T-loop phosphorylation state of Aurora A bound to its activator TPX2.* J Cell Biol, 2010. **191**(7): p. 1315-32.

173. Hatch, E.M., et al., *Catastrophic nuclear envelope collapse in cancer cell micronuclei.* Cell, 2013. **154**(1): p. 47-60.

174. Yuce, O., A. Piekny, and M. Glotzer, *An ECT2-centralspindlin complex regulates the localization and function of RhoA.* J Cell Biol, 2005. **170**(4): p. 571-82.

175. Bastos, R.N. and F.A. Barr, *Plk1 negatively regulates Cep55 recruitment to the midbody to ensure orderly abscission.* J Cell Biol, 2010. **191**(4): p. 751-60.

176. Pohl, C. and S. Jentsch, *Midbody ring disposal by autophagy is a post-abscission event of cytokinesis.* Nat Cell Biol, 2009. **11**(1): p. 65-70.

177. De Magistris, P. and W. Antonin, *The Dynamic Nature of the Nuclear Envelope.* Curr Biol, 2018. **28**(8): p. R487-R497.

178. Schmitz, M.H.A., et al., *Live-cell imaging RNAi screen identifies PP2A-B55 alpha and importin-beta 1 as key mitotic exit regulators in human cells.* Nature Cell Biology, 2010. **12**(9): p. 886-893.

179. McKinley, K.L. and I.M. Cheeseman, *Polo-like kinase 1 licenses CENP-A deposition at centromeres.* Cell, 2014. **158**(2): p. 397-411.

180. Samwer, M., et al., *DNA Cross-Bridging Shapes a Single Nucleus from a Set of Mitotic Chromosomes.* Cell, 2017. **170**(5): p. 956-972 e23.

181. Ohsugi, M., et al., *Kid-mediated chromosome compaction ensures proper nuclear envelope formation.* Cell, 2008. **132**(5): p. 771-82.

182. Lindon, C. and J. Pines, *Ordered proteolysis in anaphase inactivates Plk1 to contribute to proper mitotic exit in human cells.* J Cell Biol, 2004. **164**(2): p. 233-41.

183. Taguchi, S., et al., *Degradation of human Aurora-A protein kinase is mediated by hCdh1.* FEBS Lett, 2002. **519**(1-3): p. 59-65.

184. Stewart, S. and G. Fang, *Anaphase-promoting complex/cyclosome controls the stability of TPX2 during mitotic exit.* Mol Cell Biol, 2005. **25**(23): p. 10516-27.

185. Stewart, S. and G. Fang, *Destruction box-dependent degradation of aurora B is mediated by the anaphase-promoting complex/cyclosome and Cdh1.* Cancer Res, 2005. **65**(19): p. 8730-5.

186. Janssens, V. and J. Goris, *Protein phosphatase 2A: a highly regulated family of serine/threonine phosphatases implicated in cell growth and signalling.* Biochem J, 2001. **353**(Pt 3): p. 417-39.

187. Bollen, M., et al., *The extended PP1 toolkit: designed to create specificity.* Trends Biochem Sci, 2010. **35**(8): p. 450-8.

188. Terrak, M., et al., *Structural basis of protein phosphatase 1 regulation.* Nature, 2004. **429**(6993): p. 780-4.

189. Liu, D., et al., *Regulated targeting of protein phosphatase 1 to the outer kinetochore by KNL1 opposes Aurora B kinase.* J Cell Biol, 2010. **188**(6): p. 809-20.

190. Kong, M., et al., *Alpha4 is an essential regulator of PP2A phosphatase activity.* Mol Cell, 2009. **36**(1): p. 51-60.

191. Xu, Y., et al., *Structure of the protein phosphatase 2A holoenzyme.* Cell, 2006. **127**(6): p. 1239-51.

192. Xu, Y., et al., *Structure of a protein phosphatase 2A holoenzyme: insights into B55-mediated Tau dephosphorylation.* Mol Cell, 2008. **31**(6): p. 873-85.

193. Wang, J., et al., *Crystal structure of a PP2A B56-BubR1 complex and its implications for PP2A substrate recruitment and localization.* Protein Cell, 2016. **7**(7): p. 516-26.

194. Xu, Z., et al., *Structure and function of the PP2A-shugoshin interaction.* Mol Cell, 2009. **35**(4): p. 426-41.

195. Hertz, E.P.T., et al., *A Conserved Motif Provides Binding Specificity to the PP2A-B56 Phosphatase.* Mol Cell, 2016. **63**(4): p. 686-695.

196. Ragusa, M.J., et al., *Spinophilin directs protein phosphatase 1 specificity by blocking substrate binding sites.* Nat Struct Mol Biol, 2010. **17**(4): p. 459-64.

197. Junttila, M.R., et al., *CIP2A inhibits PP2A in human malignancies.* Cell, 2007. **130**(1): p. 51-62.

198. Hurley, T.D., et al., *Structural basis for regulation of protein phosphatase 1 by inhibitor-2.* J Biol Chem, 2007. **282**(39): p. 28874-83.

199. Kwon, Y.G., et al., *Cell cycle-dependent phosphorylation of mammalian protein phosphatase 1 by cdc2 kinase.* Proc Natl Acad Sci U S A, 1997. **94**(6): p. 2168-73.

200. Mattison, C.P., et al., *Mps1 activation loop autophosphorylation enhances kinase activity.* J Biol Chem, 2007. **282**(42): p. 30553-61.

201. Bayliss, R., et al., *Structural basis of Aurora-A activation by TPX2 at the mitotic spindle.* Mol Cell, 2003. **12**(4): p. 851-62.

202. Kufer, T.A., et al., *Human TPX2 is required for targeting Aurora-A kinase to the spindle.* J Cell Biol, 2002. **158**(4): p. 617-23.

203. Sessa, F., et al., *Mechanism of Aurora B activation by INCENP and inhibition by hesperadin.* Mol Cell, 2005. **18**(3): p. 379-91.

204. Bayliss, R., et al., *Determinants for Aurora-A activation and Aurora-B discrimination by TPX2.* Cell Cycle, 2004. **3**(4): p. 404-7.

205. Fu, J., et al., *A single amino acid change converts Aurora-A into Aurora-B-like kinase in terms of partner specificity and cellular function.* Proc Natl Acad Sci U S A, 2009. **106**(17): p. 6939-44.

206. Seki, A., et al., *Bora and the kinase Aurora a cooperatively activate the kinase Plk1 and control mitotic entry.* Science, 2008. **320**(5883): p. 1655-8.

207. Chan, E.H., et al., *Plk1 regulates mitotic Aurora A function through betaTrCP-dependent degradation of hBora.* Chromosoma, 2008. **117**(5): p. 457-69.

208. Bruinsma, W., et al., *Bora and Aurora-A continue to activate Plk1 in mitosis.* J Cell Sci, 2014. **127**(Pt 4): p. 801-11.

209. Elia, A.E., L.C. Cantley, and M.B. Yaffe, *Proteomic screen finds pSer/pThr-binding domain localizing Plk1 to mitotic substrates.* Science, 2003. **299**(5610): p. 1228-31.

210. Elia, A.E., et al., *The molecular basis for phosphodependent substrate targeting and regulation of Plks by the Polo-box domain.* Cell, 2003. **115**(1): p. 83-95.

211. Yun, S.M., et al., *Structural and functional analyses of minimal phosphopeptides targeting the polo-box domain of polo-like kinase 1.* Nat Struct Mol Biol, 2009. **16**(8): p. 876-82.

212. Hanisch, A., et al., *Different Plk1 functions show distinct dependencies on Polo-Box domain-mediated targeting.* Mol Biol Cell, 2006. **17**(1): p. 448-59.

213. Hutterer, A., et al., *Mitotic activation of the kinase Aurora-A requires its binding partner Bora.* Dev Cell, 2006. **11**(2): p. 147-57.

214. Hammond, D., et al., *Melanoma-associated mutations in protein phosphatase 6 cause chromosome instability and DNA damage owing to dysregulated Aurora-A.* J Cell Sci, 2013. **126**(Pt 15): p. 3429-40.

215. Chen, M.J., J.E. Dixon, and G. Manning, *Genomics and evolution of protein phosphatases.* Sci Signal, 2017. **10**(474).

216. Kajino, T., et al., *Protein phosphatase 6 down-regulates TAK1 kinase activation in the IL-1 signaling pathway.* J Biol Chem, 2006. **281**(52): p. 39891-6.

217. Stefansson, B. and D.L. Brautigan, *Protein phosphatase 6 subunit with conserved Sit4-associated protein domain targets IkappaBepsilon.* J Biol Chem, 2006. **281**(32): p. 22624-34.

218. Stefansson, B., et al., *Protein phosphatase 6 regulatory subunits composed of ankyrin repeat domains.* Biochemistry, 2008. **47**(5): p. 1442-51.

219. Morales-Johansson, H., et al., *Human protein phosphatase PP6 regulatory subunits provide Sit4-dependent and rapamycin-sensitive sap function in Saccharomyces cerevisiae.* PLoS One, 2009. **4**(7): p. e6331.

220. Guergnon, J., et al., *Mapping of protein phosphatase-6 association with its SAPS domain regulatory subunit using a model of helical repeats.* BMC Biochem, 2009. **10**: p. 24.

221. Hosing, A.S., et al., *PP6 regulatory subunit R1 is bidentate anchor for targeting protein phosphatase-6 to DNA-dependent protein kinase.* J Biol Chem, 2012. **287**(12): p. 9230-9.

222. Golden, R.J., et al., *An Argonaute phosphorylation cycle promotes microRNA-mediated silencing.* Nature, 2017. **542**(7640): p. 197-202.

223. Douglas, P., et al., *Protein phosphatase 6 interacts with the DNA-dependent protein kinase catalytic subunit and dephosphorylates gamma-H2AX.* Mol Cell Biol, 2010. **30**(6): p. 1368-81.

224. Tan, P., et al., *Assembly of the WHIP-TRIM14-PPP6C Mitochondrial Complex Promotes RIG-I-Mediated Antiviral Signaling.* Mol Cell, 2017. **68**(2): p. 293-307 e5.

225. Vincent, A., et al., *BRCA1 affects protein phosphatase 6 signalling through its interaction with ANKRD28.* Biochem J, 2016. **473**(7): p. 949-60.

226. Rusin, S.F., et al., *Quantitative phosphoproteomics reveals new roles for the protein phosphatase PP6 in mitotic cells.* Sci Signal, 2015. **8**(398): p. rs12.

227. Bischoff, J.R., et al., *A homologue of Drosophila aurora kinase is oncogenic and amplified in human colorectal cancers.* EMBO J, 1998. **17**(11): p. 3052-65.

228. Landen, C.N., Jr., et al., *Overexpression of the centrosomal protein Aurora-A kinase is associated with poor prognosis in epithelial ovarian cancer patients.* Clin Cancer Res, 2007. **13**(14): p. 4098-104.

229. Zeng, B., et al., *Aurora-A is a novel predictor of poor prognosis in patients with resected lung adenocarcinoma.* Chin J Cancer Res, 2014. **26**(2): p. 166-73.

230. Bibby, R.A., et al., *A cancer-associated aurora A mutant is mislocalized and misregulated due to loss of interaction with TPX2.* J Biol Chem, 2009. **284**(48): p. 33177-84.

231. Gold, H.L., et al., *PP6C Hotspot Mutations in Melanoma Display Sensitivity to Aurora Kinase Inhibition.* Molecular Cancer Research, 2014. **12**(3): p. 433-439.

232. Goldenson, B. and J.D. Crispino, *The aurora kinases in cell cycle and leukemia.* Oncogene, 2015. **34**(5): p. 537-45.

233. Forbes, S.A., et al., *COSMIC: somatic cancer genetics at high-resolution.* Nucleic Acids Res, 2017. **45**(D1): p. D777-D783.

234. Perna, D., et al., *BRAF inhibitor resistance mediated by the AKT pathway in an oncogenic BRAF mouse melanoma model.* Proc Natl Acad Sci U S A, 2015. **112**(6): p. E536-45.

235. Andrews, P.D., *Aurora kinases: shining lights on the therapeutic horizon?* Oncogene, 2005. **24**(32): p. 5005-15.

236. Kelly, K.R., et al., *The novel Aurora A kinase inhibitor MLN8237 is active in resistant chronic myeloid leukaemia and significantly increases the efficacy of nilotinib.* J Cell Mol Med, 2011. **15**(10): p. 2057-70.

237. Carol, H., et al., *Efficacy and pharmacokinetic/pharmacodynamic evaluation of the Aurora kinase A inhibitor MLN8237 against preclinical models of pediatric cancer.* Cancer Chemother Pharmacol, 2011. **68**(5): p. 1291-304.

238. Bavetsias, V. and S. Linardopoulos, *Aurora Kinase Inhibitors: Current Status and Outlook.* Front Oncol, 2015. **5**: p. 278.

239. Huttlin, E.L., et al., *The BioPlex Network: A Systematic Exploration of the Human Interactome.* Cell, 2015. **162**(2): p. 425-440.

240. Couzens, A.L., et al., *MOB1 Mediated Phospho-recognition in the Core Mammalian Hippo Pathway.* Mol Cell Proteomics, 2017. **16**(6): p. 1098-1110.

241. Cheng, K.Y., et al., *The crystal structure of the human polo-like kinase-1 polo box domain and its phospho-peptide complex.* EMBO J, 2003. **22**(21): p. 5757-68.

242. Hodis, E., et al., *A Landscape of Driver Mutations in Melanoma.* Cell, 2012. **150**(2): p. 251-263.

243. Alfieri, C., L.F. Chang, and D. Barford, *Mechanism for remodelling of the cell cycle checkpoint protein MAD2 by the ATPase TRIP13.* Nature, 2018. **559**(7713): p. 274-+.

244. Guo, L., et al., *Nuclear-Import Receptors Reverse Aberrant Phase Transitions of RNA-Binding Proteins with Prion-like Domains.* Cell, 2018. **173**(3): p. 677-+.

245. Zhang, Z.C. and Y.M. Chook, *Structural and energetic basis of ALS-causing mutations in the atypical proline-tyrosine nuclear localization signal of the Fused in Sarcoma protein (FUS).* Proceedings of the National Academy of Sciences of the United States of America, 2012. **109**(30): p. 12017-12021.

246. Barros, T.P., et al., *Aurora A activates D-TACC-Msps complexes exclusively at centrosomes to stabilize centrosomal microtubules.* J Cell Biol, 2005. **170**(7): p. 1039-46.

247. Eyers, P.A., M.E. Churchill, and J.L. Maller, *The Aurora A and Aurora B protein kinases: a single amino acid difference controls intrinsic activity and activation by TPX2.* Cell Cycle, 2005. **4**(6): p. 784-9.

248. Barr, F.A., H.H. Sillje, and E.A. Nigg, *Polo-like kinases and the orchestration of cell division.* Nat Rev Mol Cell Biol, 2004. **5**(6): p. 429-40.

249. Habedanck, R., et al., *The Polo kinase Plk4 functions in centriole duplication.* Nat Cell Biol, 2005. **7**(11): p. 1140-6.

250. Holland, A.J., et al., *Polo-like kinase 4 kinase activity limits centrosome overduplication by autoregulating its own stability.* J Cell Biol, 2010. **188**(2): p. 191-8.

251. Kettenbach, A.N., et al., *Global assessment of its network dynamics reveals that the kinase Plk1 inhibits the phosphatase PP6 to promote Aurora A activity.* Sci Signal, 2018. **11**(530).

252. Dickinson, M.E., et al., *High-throughput discovery of novel developmental phenotypes.* Nature, 2016. **537**(7621): p. 508-514.

253. Douglas, P., et al., *Polo-like kinase 1 (PLK1) and protein phosphatase 6 (PP6) regulate DNA-dependent protein kinase catalytic subunit (DNA-PKcs) phosphorylation in mitosis.* Biosci Rep, 2014. **34**(3).

254. Bakkenist, C.J. and M.B. Kastan, *DNA damage activates ATM through intermolecular autophosphorylation and dimer dissociation.* Nature, 2003. **421**(6922): p. 499-506.

255. Freeman, A.K. and A.N. Monteiro, *Phosphatases in the cellular response to DNA damage.* Cell Commun Signal, 2010. **8**: p. 27.

256. Shaltiel, I.A., et al., *Distinct phosphatases antagonize the p53 response in different phases of the cell cycle.* Proc Natl Acad Sci U S A, 2014. **111**(20): p. 7313-8.

257. Neef, R., et al., *Phosphorylation of mitotic kinesin-like protein 2 by polo-like kinase 1 is required for cytokinesis.* Journal of Cell Biology, 2003. **162**(5): p. 863-875.

258. Wisniewski, J.R., et al., *Universal sample preparation method for proteome analysis.* Nat Methods, 2009. **6**(5): p. 359-62.

259. Cox, J., et al., *Andromeda: a peptide search engine integrated into the MaxQuant environment.* J Proteome Res, 2011. **10**(4): p. 1794-805.

260. Tyanova, S., et al., *The Perseus computational platform for comprehensive analysis of (prote)omics data.* Nat Methods, 2016. **13**(9): p. 731-40.

261. Sievers, F., et al., *Fast, scalable generation of high-quality protein multiple sequence alignments using Clustal Omega.* Mol Syst Biol, 2011. **7**: p. 539.

262. Waterhouse, A.M., et al., *Jalview Version 2--a multiple sequence alignment editor and analysis workbench.* Bioinformatics, 2009. **25**(9): p. 1189-91.